The uraemic microbiome
Oral and gut dysbiosis in experimental uraemia

Thesis submitted for the degree of Doctor of Philosophy

Dr David Randall, MA, MBBS, MRCP

Centre for Translational Medicine and Therapeutics

William Harvey Research Institute

Queen Mary University of London

Declaration

I, David William Randall, confirm that the research included within this thesis is my own work or that where it has been carried out in collaboration with, or supported by others, that this is duly acknowledged below and my contribution indicated. Previously published material is also acknowledged below.

I attest that I have exercised reasonable care to ensure that the work is original, and does not to the best of my knowledge break any UK law, infringe any third party's copyright or other Intellectual Property Right, or contain any confidential material.

I accept that the College has the right to use plagiarism detection software to check the electronic version of the thesis.

I confirm that this thesis has not been previously submitted for the award of a degree by this or any other university.

The copyright of this thesis rests with the author and no quotation from it or information derived from it may be published without the prior written consent of the author.

Signature: D. Randall

Date: 4th March 2022

Details of collaboration and publications: See appendix 1 and list of publication, p 27.

Acknowledgements

I am very grateful to my main PhD supervisor, Professor Magdi Yaqoob, for taking a punt on me as a fairly unpromising renal registrar and allowing me the opportunity to complete the work contained in this thesis. Thank you Magdi for your mentorship, guidance and insight, for sharing your vast knowledge of medicine and kidney disease, and for your personal support and encouragement through all stages of this work.

I am grateful to my second supervisor, Dr Kieran McCafferty, for helping me to navigate the complexities of academic research, for helping me to understand my data, for advice on how to get things done and for personal advice and guidance.

I was enormously helped by Professor Mike Curtis, who welcomed me into his lab group (initially at QMUL and subsequently at King's College London), shared protocols, wisdom and expertise, provided invaluable help with manuscript preparation and was very generous in his encouragement and guidance.

Thanks to Julius Kieswich, who expertly and reliably maintained all of the animal subjects described in this work. I could never have hoped to complete this project without his assistance, and I enjoyed our conversations during long days spent at the BSU.

Thanks to Dr Asil Alsam, who helped with much of the dental analysis reported in chapter three as well as proving a general friend and support.

Thanks to Dr Steve Harwood, who provided much guidance and practical help, and was always on hand with suggestions and amenable to my regular cries for assistance.

Abstract

Physiological and biochemical abnormalities present in patients with Chronic Kidney Disease (CKD) have been hypothesised to cause 'dysbiosis': pathological alterations to a host organism's resident populations of bacteria. It has been suggested that these microbiological changes may contribute to the progression of CKD. This thesis explores the nature of such dysbiotic changes in the oral and gut microbiota of animals with experimental uraemia, and considers whether modulation of the gut microbiota might be used therapeutically to improve the health of patients with kidney disease.

Part 1

Introduction: There is a high incidence of periodontal disease (PD) in patients with CKD, and it has been claimed that low-grade inflammation from PD may contribute to the progression of CKD. Here, it is hypothesised that actually the relationship may be the other way round, with CKD causing oral dysbiosis that subsequently leads to PD. **Results:** Using several rodent models, it is demonstrated that experimental uraemia reliably induces loss of periodontal alveolar bone height in both rats (mean -0.113mm, p<0.001) and mice (mean -0.02mm, p<0.001). Uraemic animals have a dysbiotic oral microbiome with increased alpha diversity (Simpson Index 0.82 vs 0.75, p=0.054), reduced total bacterial counts ($\log_{10}$ 5.80 vs 6.07 $\log_{10}$ cfu/ml, p=0.034), a decrease in health-associated taxa (phylum *Firmicutes*, $\log_{10}$ 5.43 vs 5.88 $\log_{10}$ cfu/ml, p=0.043, and genera *Streptococci* and *Rothia*) and an increase in gram-negative taxa (phylum *Proteobacteria* comprising 9.53% of isolates in uraemic animals vs 2.99% in controls,

p=0.003). Induced saliva from uraemic animals had a higher urea concentration than that from controls (3.73 vs 1.62mmol/L, p=0.007), and bacterial isolates which were under-represented in samples from uraemic animals showed reduced tolerance to higher urea concentrations during *in vitro* broth culture. Uraemic animals which were co-housed with healthy animals demonstrated significantly less bone loss than those housed with other uraemic animals (-0.109mm vs -0.149mm, p=0.038), and transfer of oral microbiota from uraemic animals induced more periodontal bone loss in healthy germ-free mice than transfer of oral microbiota from health animals (-0.042mm, p<0.001). **Conclusion:** Experimental uraemia causes loss of periodontal bone height. Although some of this may reflect the systemic effects of uraemia on bone, the demonstration of reproducible dysbiotic effects on the oral microbiome and the effects of co-housing and oral microbial transfer on periodontal phenotype suggest that uraemic dysbiosis plays a key role in the aetiology of PD in the setting of CKD.

Part 2

Introduction: Both bacterial generation of uraemic toxins and reduced generation of short-chain fatty acids have been suggested as possible metabolomic mechanisms that would implicate gut dysbiosis in the aetiology of CKD. We sought to characterise gut dysbiosis using rodent models of chronic uraemia. **Results:** Analysis of the gut microbiota of two identically treated cohorts of rats, obtained from the same supplier just a few weeks apart, revealed that batch effect far outweighed the effect of uraemia on the composition of the gut microbiota (batch effect accounting for 9.7% of variance, p=0.007; compared to 4.8% for uraemic vs control animals, p=0.227). These batch differences proved to be functionally significant, with the urinary

metabolome also showing far greater effects of batch than of uraemia (batch accounting for 66% of variance between samples, p=0.001, compared to 48% for uraemic vs control, p=0.007). Further cohorts of animals demonstrated similar large variations compared with previous cohorts, and urinary metabolomes between batches proved equally dissimilar, with no reproducible effect of uraemia. To understand this batch variability in the context of previous published work claiming a demonstrable effect of uraemia on gut bacterial populations, a meta-analysis was carried out of all publicly available NGS sequencing data investigating the effect of experimental uraemia on the gut microbiome of rodents. In this combined dataset, the leading determinants of variation were batch (69% of variance, p<0.001), primer type (23.9% of variation, p<0.001) and host species (rat vs mouse, 13.3% of variance, p<0.001). The presence of uraemia did influence sample clustering, but to a very limited extent (1.9% of variance, p=0.026). **Conclusion:** The effect of uraemia on the gut microbiome is minor, and is eclipsed by inter-batch variation, which makes it hard to state confidently that 'uraemic dysbiosis' occurs in the gut. The degree of variability between animals from different batches poses wider questions about the reproducibility of animal research in other settings. Alternative experimental strategies are discussed, such as longitudinal studies which explore how a given intervention affects the microbiota of the same animals over time, using animals as their own controls.

Part 3

Introduction: Fermentable dietary fibre, such as fructo-oligosaccharide (FOS), has been shown to induce significant generation of short-chain fatty acids by the gut microbiota, with a range of beneficial effects on health. We sought to establish whether such effects could be demonstrated

in experimental uraemia and might offer a microbiome-mediated therapeutic tool for patients with CKD. **Results:** FOS-supplemented diet produced similar and substantial effects on the gut microbiota of both control and uraemic animals. Whilst uraemia again accounted for minimal amounts of species-level variation between samples (2.4% of variance, p=0.75), diet was associated with a large degree of variance (46.3%, p<0.001), including large increases of the acetate producing genus *Bifidobacterium* (27.3% of reads vs 1.7%, p<0.001), and increases in propionate- and butyrate-producing taxa including *Bacteroidaceae* (23% vs 7.4% of reads, p=0.006), *Marvinbryantia* (4.5% vs 0.09%, p<0.001) and *Blautia* (1.8% vs 0.25%, p<0.001). Comparable changes were seen in the microbiota of both uraemic and control animals. Using whole genome sequencing metagenomics, the FOS-supplemented diet was associated with significant increases in the abundance of carbohydrate metabolism pathways (3.37×10^6 reads/sample in all FOS-treated animals vs 2.51×10^6 in all CELL-treated, p=0.029), including the bifid shunt and other bacterial glycolytic pathways, and in pathways involved in the initiation (2.26×10^5 vs 1.12×10^5 reads/sample, p<0.001) and elongation (4.20×10^4 vs 8.31×10^4 reads/sample, p=0.004) of short chain fatty acids. Animals fed the FOS-supplemented diet demonstrated substantial increases in caecal volume, and had significantly lower caecal pH, in keeping with the predicted increase in short chain fatty acid production. FOS administration was associated with beneficial effects on various aspects of the uraemic syndrome including a 51% reduction in serum urea concentrations (p=0.004), a 24% reduction in urine output (p=0.032) and a 0.6mmol/L reduction in serum potassium (p=0.02). **Conclusion:** Fermentable fibre produces substantial changes in the gut microbiome of both control and uraemic animals, associated with substantial improvements in several aspects of the uraemic syndrome. These results suggest that

fermentable fibre supplements may offer benefits to human subjects with CKD if the effects seen

in experimental animals can be translated into clinical practice.

Contents

Terminology and key concepts

The following section outlines a brief definition some of the key concepts in microbiome science which are used repeatedly in this thesis.

Microbiome and microbiota: These words are often used interchangeably to refer to all microorganisms present in a given ecological niche; for example, the oral cavity or the caecum. Although the vast majority of these will be bacteria (and often the terms are used to refer exclusively to bacteria), properly speaking a range of other organisms including fungi, archaea and viruses are also included. The work reported in this thesis concentrates only on bacteria. Used more precisely, microbiota refers to the organisms themselves, and microbiome to the genetic material in all of the genomes present.

Tools for studying the microbiome:

- *Bacterial culture* using traditional growth media (eg blood agar) and aerobic or non-aerobic incubation techniques was historically used to assess the composition of bacterial communities, and still has many advantages. Different bacterial isolates are identified by morphological differences between colonies on plates, and can then be grown to purity and identified using either phenotypic characteristics (eg microscopic appearance or metabolic behaviour using tests such as the coagulase or catalase tests) or by genetic

sequencing. This approach has many advantages (including robust identification of organisms at species or even strain level, and subsequent *in vitro* testing of organism function), but is labour intensive and risks excluding analysis of organisms that are difficult or impossible to culture. Culture of the oral microbiota of experimental animals is described in chapter three.

- *Amplicon sequencing* of DNA extracted from biological samples (eg oral swabs or stool) allows a comprehensive description of all organisms present in the sample. Marker genes are amplified using *polymerase chain reaction (PCR)* and amplicons are sequenced using pooled, high-throughput, *next generation sequencing (NGS)* with barcoded primers to assign sequences to individual samples. The most widely-used gene to study bacterial communities is the *16S rRNA gene*, which encodes the RNA scaffold for the small subunit of the bacterial ribosome: this gene is almost always unique to individual bacterial species. The results of NGS analysis of the oral and gut microbiome are presented in chapters three and four.

- *Whole genome sequencing (WGS) metagenomics* of DNA extracted from biological samples involves cutting DNA into fragments and then sequencing all of these fragments using NGS techniques and short, random primers. Sequencing is carried out repeatedly so that all DNA fragments are multiply sequenced; high-performance computing facilities are then required to reconstruct whole bacterial genomes from the sequenced fragments. This approach is known as *shotgun sequencing* and allows analysis not just of the composition of the bacterial microbiome, but also of all the genes it contains. Results of WGS metagenomics are presented in chapter five.

- *Metatranscriptomics* applies the techniques of WGS metagenomics to reverse-transcribed DNA created from RNA extracted from samples. It is used to describe the functional activity of bacteria. This thesis does not contain any metatranscriptomic work.

- *Metabolomics* describes the use of techniques from analytical chemistry such as *^{1}H-nuclear magnetic resonance (^{1}H-NMR) spectroscopy* to quantify metabolites in biological fluids such as serum or urine. It may be used to assess the functional contribution of bacteria to the host organism through generation of small molecules of biological significance, such as various **uraemic retention molecules** (which have been implicated in the aetiology of chronic kidney disease), or **short chain fatty acids** which have various beneficial effects on host health. Results of *^{1}H-NMR* metabolomics are presented in chapters three and four.

Statistical approaches to microbiome data

NGS analysis of bacterial samples produces a vast amount of data; for example, 16S amplicon sequencing of an oral or stool sample may yield thousands of reads of 250-350 base pair length. The following steps are use in the analysis of such data:

- *Pre-processing*: reads are assigned to individual samples, trimmed, and primer sequences are removed.

- *Binning*: sequences are clustered together on the basis of similarity. A range of approaches are used, which identify clusters of sequences that are termed either

Operational Taxonomic Units (OTUs) or *Amplicon Sequencing Variants (ASVs)*, and which are effectively proxies for individual bacterial species.

- *Assigning taxonomy*: OTUs/ASVs are compared with published databases to assign a taxonomic identity to each.

At the end of this process an abundance table is created, where for each biological specimen (eg an individual oral swab or stool sample), the abundance of several hundred or thousand individual species is listed. Various statistical approaches are then typically used to interrogate this data:

- *Alpha diversity* is a measure of intra-sample diversity, and may simply be thought of as the chance of obtaining the same type of organism if two are drawn at random from a sample. There are various ways of measuring alpha diversity, including the Simpson and Shannon indices.

- *Beta diversity* is a measure of how closely the ecology of two biological samples is related, and may be calculated using measures such as the Bray or Jaccard indices. Where a number of samples are compared, complex patterns of association are typically revealed; for example, sample A may be very similar to sample B, but quite different to sample C; however, sample B may share a number of similarities to sample C that are not shared with sample A. Various mathematical strategies have been employed to visually represent this clustering, often employing multi-dimensional modelling; the commonest of these is *Principal Coordinate Analysis (PCA)*. Data from PCA can be represented using ordination plots where individual samples are plotted on the first two axes from a multi-dimensional model; clustering reflects how similar or dissimilar they are to each

other and can be quantified by methods including Permutation Analysis of Variance (**PerMANOVA**) or Orthogonal Projection to Latent Squares Discriminant Analysis (**OPLS-DA**). Each axis can be evaluated for how much of the total diversity it describes and which individual species contribute heavily to distribution along that axis.

- The ***abundance of individual taxa*** can be compared between samples. This generates its own statistical challenges, both in reflecting the ***compositional nature of microbiome datasets*** and in correcting for ***multiple hypothesis testing***. Various statistical tools have been developed to address these, so that it can be said with confidence that a particular bacterial species is present in higher abundances in one group of samples than another.

Taxonomic classification

All living things can be classified based on similarity into a 'tree of life', at various taxonomic levels. The diagram below illustrates this tree with relevance to the analysis presented in this thesis.

Bacteria constitutes a ***kingdom*** within the ***domain Prokaryota***.

Phylum is the highest-level division with Bacteria, where key phenotypic differences between organisms begin to emerge (eg between the chiefly Gram-positive phylum *Firmicutes* and the chiefly Gram-negative phyla *Bacteroidota* and *Proteobacteria*).

Family (where names generally employ the suffix '*aceae*', eg *Enterobacteriaceae* or *Staphylococcaceae*) is the lowest level at which the taxonomic identity of an organism can be confidently assigned using the relatively short sequences generated by amplicon-based NGS

techniques, and has therefore been used as the lowest taxonomic rank for the meta-analysis comparison presented in chapter four.

Species identity can only generally be confidently assigned by full-length sequencing of the whole 16S gene (such as that performed on the cultured isolates as presented in chapter three).
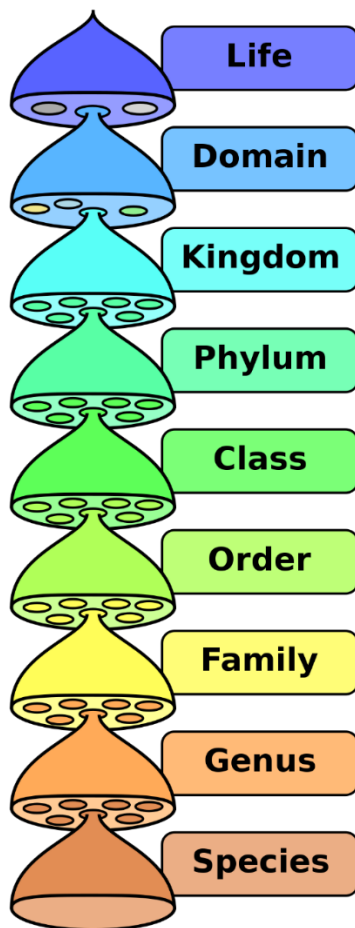
Reference figure: The hierarchy of the eight major taxonomic ranks used in modern biology. Halasz, P, 2007. Retrieved from https://en.wikipedia.org/wiki/Kingdom_(biology), accessed 17th January 2022.

List of figures

List of tables

List of commonly used abbreviations

^{1}H-NMR   Proton nuclear magnetic resonance (spectroscopy)

AIN   AIN-93M; a standard rodent diet from the American Institute of Nutrition

ASV   Amplicon sequencing variant

CELL   Cellulose-supplemented diet

CKD   Chronic kidney disease

FOS   Fructo-oligosaccharide supplemented diet

OPLS-DA   Orthogonal Projection to Latent Squares Discriminant Analysis

OTU   Operational Taxonomic Unit

PD   Periodontal disease

PCR   Polymerase chain reaction

SCFA   Short chain fatty acid

SNx   Subtotal nephrectomy

WGS   Whole genome sequencing

List of publications so far arising from this work

Randall, D.W., Kieswich, J., Swann, J. *et al.* Batch effect exerts a bigger influence on the rat urinary metabolome and gut microbiota than uraemia: a cautionary tale. *Microbiome* 7, 127 (2019). https://doi.org/10.1186/s40168-019-0738-y

Parsegian K, **Randall DW**, Curtis M, Ioannidou E. Association between periodontitis and chronic kidney disease. Periodontology 2000. 2022; in press.

Randall DW and Yaqoob MM. Oral Health in Chronic Kidney Disease. Austin Dent Sci. 2018; 3(1): 1018.

Presentation:

Randall DW, Alsam A, Kieswich JE, Joseph S, McCafferty K, Curtis M, Yaqoob MM. Uremic periodontitis: bacterial dysbiosis and immune dysfunction. American Society of Nephrology, 2018.

Chapter 1

Introduction: Bacteria and uraemia

Bacteria in kidney disease: friend of foe?

Bacteria are required for the normal development of mammalian kidneys. The kidneys of germ-free mice, housed in totally sterile conditions, are small and under-developed; a finding attributed to the role of the gut microbiota in producing short-chain fatty acids and metabolizing key amino-acids which are necessary for normal kidney development [1]. Bacteria are also necessary for renal health: germ-free mice have been shown to develop more severe long-term kidney damage after an episode of ischaemia-reperfusion injury, and to have an adverse inflammatory profile compared to normal, non-sterile animals [2].

Conversely, it was demonstrated decades ago that germ-free rats survive longer after bilateral nephrectomy than rats with normal gut microflora, and furthermore that rats mono-, di- or tetra-colonised with different species of bacteria have a progressive decrease in life expectancy when rendered anephric compared to those which remain germ-free. [3] Consistent with this, antibiotic treatment to deplete gut bacteria improves outcomes after reperfusion injury, and these effects are lost when the gut is re-populated with commensal microbiota. [4] A number of known uraemic toxins are bacterial metabolites [5] and absent in germ-free, [1] colon-free [5] and bacterially-depleted [6] hosts. Furthermore, it has been suggested that uraemia itself may alter the gut microbiome and increase the abundance of toxin-producing bacteria, leading to a worsening cycle of dysbiosis, toxin production and increasing renal fibrosis. [7, 8]

The relationship between gut microbes and kidney disease is complex: the complete absence of bacteria harms kidney development and worsens kidney injury in germ-free animals; but in conventional animals bacteria may contribute to renal injury. In this thesis I am to probe these contradictions and understand better the role of resident bacterial communities in the development of kidney disease, and in associated complications such as periodontal disease.

A brief history of medical microbiology

The human body provides a range of diverse habitats that are inhabited by a vast and complex array of microbes. Although the existence of such micro-organisms had been proposed by ancient and mediaeval scholars, it was the invention of the microscope by Antonie van Leeuwenhoek (1632-1723) that led to the first observations of bacteria – 'animalcules' – prompting speculation about their role in health and disease (Figure 1, p.41). Over the next three

and a half centuries, study of these microbial communities has proceeded at each stage in tandem with advances in scientific technology.

Developments in bacterial culture technique led to the 'golden age' of microbiology, with scientists such as Louis Pasteur (1822-95) and Robert Koch (1845-1910) helping to deduce key tenets of bacteriology. In the last two decades of the nineteenth century, the infectious agents responsible for major infectious diseases – diphtheria, typhoid, gonorrhoea, meningitis, leprosy, plague, tetanus, syphilis, whooping cough, pneumonia – were discovered at a rate or around one per year. [9] Koch's postulates, which tied individual diseases to specific pathogens, promoted the germ theory of disease in which bacteria were viewed as enemies: purveyors of disease and agents of decay.

Despite this, evidence was also emerging of how bacteria could exert beneficial effects. For example, in 1917, Professor Albert Nissle was able to confirm evidence that certain bacterial strains conferred health benefits by demonstrating that the one German solider in a military hospital who did not contract dysentery possessed a strain of *Eschericia coli* that provided colonisation resistance to Salmonella. [10] *E coli* strain Nissle 1917 has been described as the first recognised probiotic. The use of microbial products in the development of antibiotic medications provided further evidence of their potential benefits.

Further advances in understanding gut microbiology were made in the 1940s and 50s due to the development of anaerobic culture techniques, allowing the discovery of many species of bacteria that had previously not been studied under aerobic conditions. In the 1960s, work on germ-free mice revealed that normal bacteria communities were crucial for normal development and physiology, and these insights were employed in exciting new ways by the Gordon group in the

early 21st century by demonstrations that disease phenotypes such as obesity could be recreated by microbial transfer into otherwise healthy germ free mice. [11]

The advent of high-throughput genetic sequencing platforms in the late-1990s created the ability to survey accurately the large number of resident micro-organisms that are not easily cultured. Descriptive studies of bacterial populations, often using high-throughput sequencing of molecular identifiers (such as the 16S ribosomal gene which is specific to individual bacterial species), led to new interest in the large number of species resident within human hosts, and in particular:

- the variability of microbiota between different hosts, associating with various demographic variables such as age, ethnicity or diet,

- the association of different microbiota with health and disease states.

The term 'microbiome' was increasingly used to describe this newly-understood complexity, [12] and early research describing 'enterotypes' possessed by different members of the population, predisposing to different diseases, [13] captured the scientific and popular imagination, although descriptions were confined largely to association rather than clear patterns of causation. The human microbiome project was launched in 2007 to describe bacterial populations at a range of body sites in healthy and diseased individuals, using census data of the 16S gene alongside full metagenomic sequencing, and reported in 2012, [14] providing a helpful benchmark for subsequent work.

Whole genome sequencing based on 'shotgun' methods (where all DNA is particular samples is fragmented and then sequenced with short, random primers), was a technique developed in the

early part of the 21st century to allow assembly of entire metagenomes, effectively allowing the full metabolic machinery of entire communities of micro-organisms to be surveyed. This, coupled with other '-omics' approaches (such as meta-transcriptomics, proteomics and metabolomics), began to bridge the mechanistic gap between observing changes in bacterial populations and identifying how they might affect host phenotype.

Interventional studies have led to a deepening understanding of host-microbiome interaction, and have using methodologies including:

- creation of germ-free animals in sterile isolators, allowing study of host physiology and disease in the (albeit entirely unphysiological) complete absence of microbial activity.

- use of broad-spectrum antibiotics, which substantially reduce bacterial load and can help to determine the contribution made to complex biological processes by bacteria.

- inoculation experiments, where one or more individual bacterial strains are administered to host organisms to try to alter physiology (for example using 'probiotic' preparations of healthy commensal bacteria, present in fermented dairy products to treat obesity), [15] or to cause disease (for instance in experiments where *Fusobacterium nucleatum* has been implicated in the aetiology of bowel cancer [16]).

- feeding experiments, where altered diets (such as high-fibre 'prebiotic' diets) are used to try to manipulate microbial populations and increase the relative abundance of health-associated organisms, or increase bacterial production of beneficial metabolites;

- transfer experiments, where entire microbial communities are transferred into germ-free or antibiotic-treated hosts, to assess the transmissibility of microbiome-associated

phenotypes. Pioneering research transferring microbiota from malnourished Malawian children into germ-free mice demonstrated a key role for microbes in the development of the kwashiorkor variant of malnutrition, [17] whilst antibiotic-associated colitis associated with *Clostridium difficile* infection is now regarded as almost completely curable by transfer of healthy faecal microbiota. [18]

Interventional studies like these offer the only reliable way of assessing direct causality, and may also suggest therapeutic strategies where microbial communities can be restored, transferred, used or manipulated to improve health outcomes in the host organism.

Current understandings of the human microbiome

Each human organism plays host to trillions of microbes, including bacteria, fungi, protists, archaea and viruses. Resident bacterial cells alone outnumber host cells in an average human male by anything up to ten-fold ([19, 20]).

By far the largest numbers of bacteria are resident in the colon, followed by the mouth, distal small intestine, and skin, as described in Table 1, p. 42. [21] Bacterial populations also exist – and may influence health and disease – in other locations such as the vagina, the urinary tract and the upper respiratory tract.

There are significant compositional differences between the microbiota in different body sites, Figure 2, p. 41. For example, the microbiome of the healthy vagina is relatively simple, being dominated by *Lactobacillus* species that thrive in and contribute towards its acidic environment;

conversely, the microbial communities of the mouth and the gut are far more complex and possess organisms from a wider range of bacterial phyla.

Location-specific microbiota are adapted towards the physiological conditions encountered in any particular body site. For example, in the mouth, aerobic organisms are seen in high abundances, particularly on surfaces such as teeth which are regularly exposed to air. [22] In the gut obligate anaerobes outnumber facultative anaerobes and aerobes by a factor of 100:1. [23] The gut microbiota is dominated by bacteria from two phyla, *Firmicutes* and *Bacteroidetes*, although at species level it has been estimated the each individual may harbour up to 1000 different individual bacterial species. [24] Although intra-individual variation between different sampling points appears higher for the gut than for the oral microbiome (influenced by factors including diet, health status and antibiotic used amongst other things), overall it has been shown that inter-individual outweigh intra-individual variation. [25] There is significant geographic variation between species prevalent in different regions of the gut (for instance, with *Proteobacteria* and *Lactobacilli* being present in higher abundances in the small gut compared with the colon), and even within a particular gut segment the microbiota may be organised such that certain taxa predominate in ecological niches such as the villous crypts while others are found intra-luminally. [26]

A variety of functions for the gut microbiota have been demonstrated, including regulation [27] and development [28] of the immune system, extraction of energy from food, [29] regulation of host energy homeostasis, [30] micronutrient production [31] and maintaining resistance to pathogenic invasion. [32] On a functional level, as in the mouth it is believed that considerable

redundancy exists within the gut microbiome such that different species in separate hosts may provide similar metabolic functions, [14] as illustrated in Figure 3, p. 44.

Chronic kidney disease (CKD)

Chronic kidney disease (CKD) affects 9.1% of the world's population and contributed to 1.2 million deaths globally in 2017. [33] Just over 1 person in 1000 have stage 5 or 'end-stage' kidney disease, with around 3 million people dependent on renal replacement therapy (via haemodialysis, peritoneal dialysis or a kidney transplant) worldwide. [34] In the UK there are 60,000 patients dependent on renal replacement therapy.[35] The incidence of CKD is rising, [36] and the healthcare costs of treatment and especially of renal replacement therapy are substantial. [37]

In the early stages of CKD patients may be entirely asymptomatic and unaware of their diagnosis, but demonstrate proteinuria and reduced renal excretory function [38] and are exposed to significant risks of cardiovascular disease and other complications. [39]

The definition, staging and epidemiology of CKD

CKD is present when a patient has markers of kidney damage (including radiological abnormalities, proteinuria or reduced excretory function), present for more than three months. It is of particular clinical relevance when excretory function is reduced, measured in routine clinical practice using the estimated glomerular filtration rate or eGFR, derived from the serum

creatinine (or cystatin C) concentration. Individuals with an eGFR less than 60ml/min/1.73m^2 are diagnosed with stage 3 CKD; those with an eGFR <30ml/min with stage 4 CKD; and those with an eGFR <15ml/min with stage 5 or 'end-stage' CKD [38]. These categories are further augmented by adding a measure of albuminuria, since excretory dysfunction and albuminuria act independently to increase cardiovascular risk, Figure 4, p. 45.

An individual may develop CKD when the kidneys are damaged for any number of reasons, with the leading causes including diabetes mellitus, hypertension and glomerulonephritis. The result is a multi-system disease process characterised by fluid overload, anaemia, acidosis, blood electrolyte abnormalities, abnormal bone formation and retention of toxic waste products in blood; with widespread effects on endothelial cell function, immune system activity, cognition, appetite and mood. There is a high prevalence of cardiovascular disease, and the leading causes of death in patients with CKD are cardiovascular disease and infection. [40]

Kidney transplantation from either a live or cadaveric donor is the treatment of choice for most patients with end stage renal disease, offering survival, quality of life and health economic benefits compared to other forms of treatment. [41, 42] Where kidney transplantation is not possible, or whilst waiting for a suitable organ to become available, patients may be treated with maintenance haemodialysis (usually thrice weekly), peritoneal dialysis or with supportive (palliative) care.

Cardiovascular disease in CKD

Patients living with CKD have high rates of mortality and morbidity from cardiovascular disease [43], as illustrated in Figure 5, p. 46, which demonstrates that patients on dialysis in their third decade of life have similar yearly rates of cardiovascular mortality to adults in the general population in their eighth decade.

The histological features of cardiovascular disease in patients with CKD differ from those in the general population. Rather than developing discrete, lipid-rich, sub-endoethial deposits as in classic atherosclerotic cardiovascular disease, patients with CKD develop widespread medial hypertrophy associated with increased vessel stiffness, [44] medial calcification [45] and left ventricular hypertrophy. [46] Although traditional cardiovascular risk factors may play a role in this process, there are a number of CKD-specific risk factors [47] including salt and water overload [48] and dysregulated calcium and phosphate metabolism [49] that play key additional roles.

Much recent research on novel cardiovascular risk factors in CKD has focussed on the role of endothelial dysfunction in causing vessel wall disease. There are a number of potential causes of endothelial dysfunction in CKD, including shear stress caused by hypertension [50] and advanced glycation end-products in diabetic kidney disease [51]. However recent interest has focussed on three factors that link CKD directly to the microbiome:

- the toxic effects of some **uraemic retention molecules**.

- the effects of low grade, **chronic inflammation**.

- reduced production of **short chain fatty acids**.

Uraemic retention molecules (URMs) encompass a range of small and middle-sized molecules that accumulate in serum in patients with CKD as a result of impaired renal clearance; a number have been shown to be directly toxic to epithelium (being termed 'uraemic toxins'), [52] including several that are produced by bacterial metabolism of dietary protein (such as indoles, phenols and amines). The role of the microbiota in generating these toxins will be explored in chapter four of this thesis.

Chronic inflammation is a feature commonly seen in individuals with CKD, and may arise due to low level inflammatory disease in the gastrointestinal tract. For example, rats with induced uraemia have been shown to have impaired epithelial tight junction formation, [53] leading to what has been termed a 'leaky gut' with spillage of bacterial products such as endotoxin into the bloodstream, and activation of the innate immune system. [54] A further source of chronic inflammation is the mouth, and more specifically the periodontal crevice; and because periodontal disease reflects a direct interaction between resident microbial communities (in this case, the oral microbiome), and the host organism, I will examine the mechanisms of periodontal disease in chronic experimental uraemic in chapter three.

Short chain fatty acids are products of bacterial fermentation of dietary fibre, have been shown to have a number of immunomodulatory and anti-atherogenic properties. [55] Intervening with the gut microbiota to increase generation of these molecules may offer a mechanism to improve outcomes in CKD. These possibilities are explored in chapter five.

The hypothesis of this thesis

I have sought to investigate the hypothesis that a bi-directional relationship exists between uraemia and the body's bacterial communities, whereby uraemia may influence the composition and function of these resident microbial communities, and in reverse that these communities – perhaps themselves already altered by disease – may contribute to the disease phenotype of uraemia. This bi-directional hypothesis is conceptualised in Figure 6, p. 47.
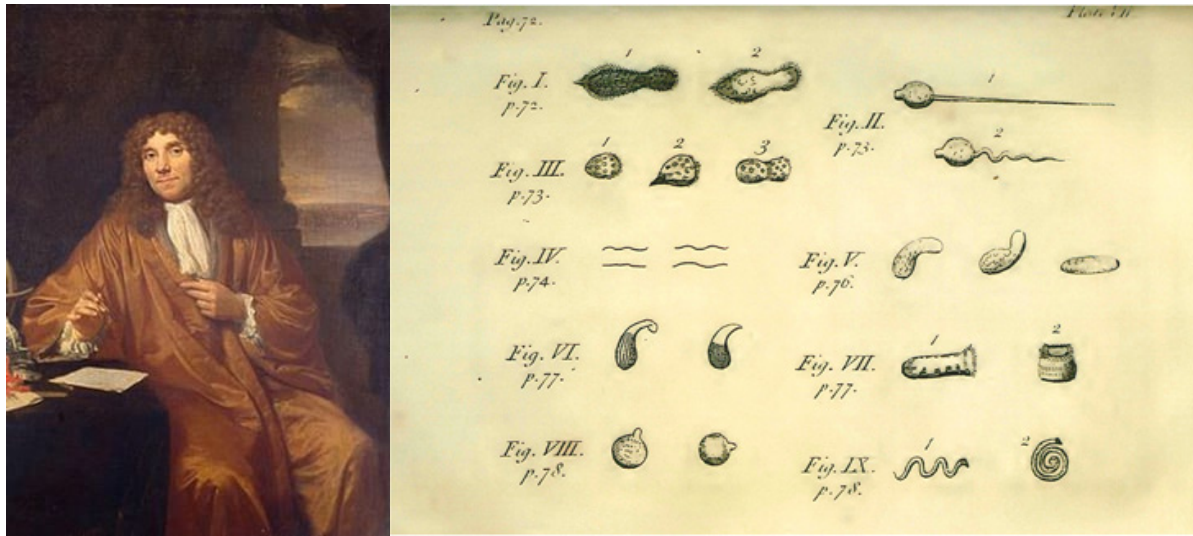
Figure 1: Antonie van Leeuwenhoek. *Left:* Portait by Jan Verkolje. *Right:* 1697 illustration of microscopic appearances of a drop of pepper water that had been left for three weeks on a shelf. Fig. IV is believed to be the first ever image of a bacterium produced in print. "I saw a great multitude of living creatures in one drop of water, amounting to no less than 8,000 or 10,000, and they appear to my eye through the microscope as common as sand does to the naked eye."

Location	Typical concentration of bacteria [1] (number/mL content)	Volume (mL)	Order of magnitude bound for bacteria number
Colon (large intestine)	10^{11}	400 [2]	10^{14}
Dental plaque	10^{11}	<10	10^{12}
Ileum (lower small intestine)	10^8	400 [5]	10^{11}
Saliva	10^9	<100	10^{11}
Skin	$<10^{11}$ per m^2 [3]	1.8 m^2 [4]	10^{11}
Stomach	$10^3–10^4$	250 [5]–900 [6]	10^7
Duodenum and Jejunum (upper small intestine)	$10^3–10^4$	400 [5]	10^7

[1] Except for skin, concentrations are according to [9]. For the skin, we used bacterial areal density and total skin surface to reach an upper bound.

[2] See derivation in section below.

[3] Skin surface bacteria density is taken from [11].

[4] Skin area calculated as inferred from standard formula by DuBois for the body surface area [12].

[5] Volume of the organs of the gastrointestinal tract is derived from weights taken from [13] by assuming content density of 1.04 g/mL [6].

[6] Higher value is given in [14].

Table 1: Estimate of total bacterial numbers at various body sites. Taken from Sender et al 2016 [20]
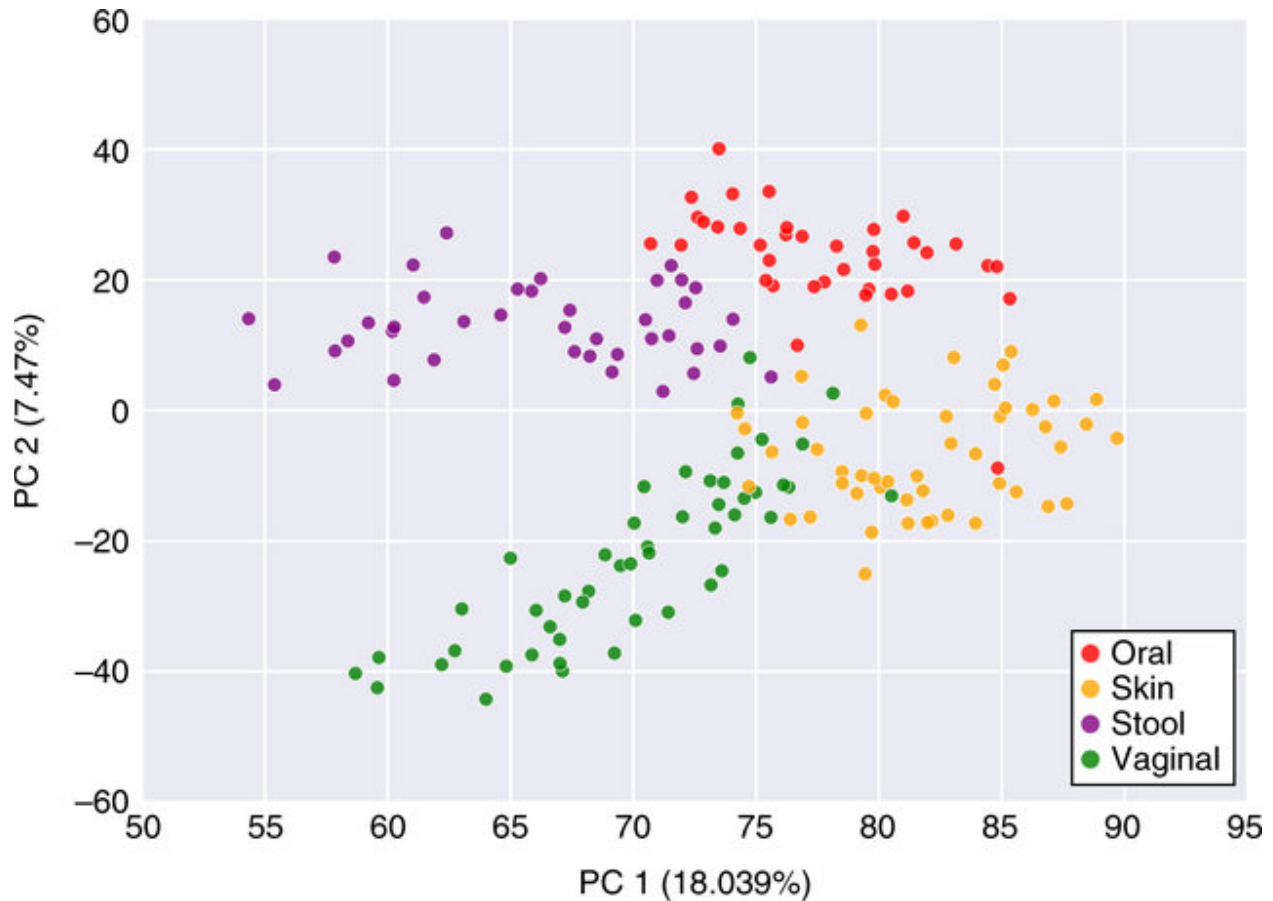
Figure 2: Principal Component Analysis of predicted metagenomes based on 175 biological samples taken from different body sites. Each point represents the predicted metagenome of a biological samples from the relevant body site of a particular subject, coloured according to body site. As this is a PCA plot, the distance between points is proportional to the similarity between samples, with the amount of total variance represented by each axis written on the axis label. In this case Principal Component 1 (PC1) accounts for 18.039% of the total variance in the dataset, and Principal Component 2 (PC2) accounts for 7.47%; relatively small proportions. In simpler datasets such as those of smaller numbers of experimental animals, a much higher proportion of variance may be captured with just the first two principal components. *Taken from Garza et al, Nature Microbiology. [56]*
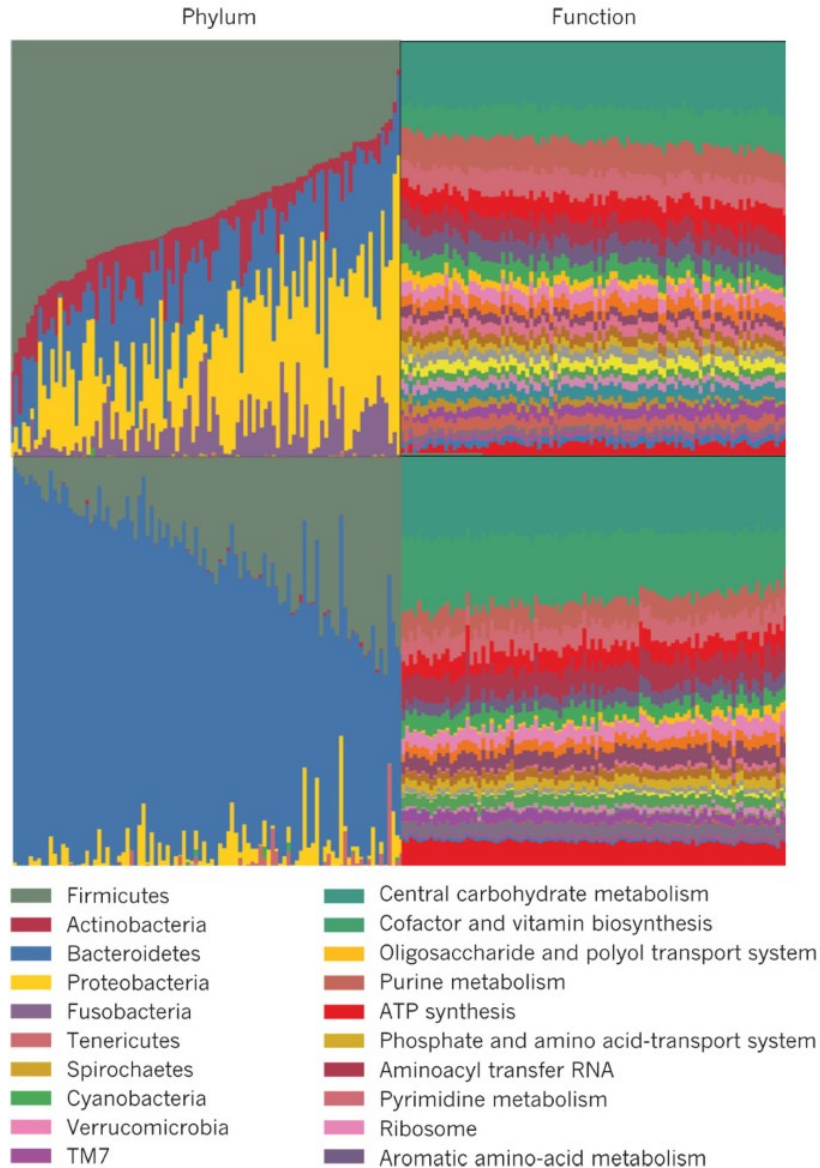
Figure 3: Functional redundancy in the human gut microbiome. Composition (panels on left) and function (panels on right) of the oral (top panels) and stool (bottom panels) microbiomes of experimental subjects, showing a basic functional redundancy despite compositional variation; very different populations at species level (panels on left) achieve a shared range of common biological functions (panels on right). Adapted from 'Structure, function and diversity of the healthy human microbiome', Nature, 2012 [14].

Classification of chronic kidney disease using GFR and ACR categories

GFR and ACR categories and risk of adverse outcomes			ACR categories (mg/mmol), description and range		
			<3 Normal to mildly increased	3–30 Moderately increased	>30 Severely increased
			A1	A2	A3
≥90 Normal and high	G1		No CKD in the absence of markers of kidney damage		
60–89 Mild reduction related to normal range for a young adult	G2				
45–59 Mild–moderate reduction	G3a[1]				
30–44 Moderate–severe reduction	G3b				
15–29 Severe reduction	G4				
<15 Kidney failure	G5				

GFR categories (ml/min/1.73 m²), description and range

Increasing risk

Increasing risk

[1] Consider using eGFRcystatinC for people with CKD G3aA1 (see recommendations 1.1.14 and 1.1.15)

Abbreviations: ACR, albumin:creatinine ratio; CKD, chronic kidney disease; GFR, glomerular filtration rate

Adapted with permission from Kidney Disease: Improving Global Outcomes (KDIGO) CKD Work Group (2013) KDIGO 2012 clinical practice guideline for the evaluation and management of chronic kidney disease. Kidney International (Suppl. 3): 1–150

Figure 4: Staging and cardiovascular risk in CKD. Taken from the Renal Association eCKD guide on CKD stages modified from the KDIGO staging [38], available at https://renal.org/information-resources/the-uk-eckd-guide/ckd-stages/ (accessed 13th January 2022).

Cardiovascular Mortality in the General Population (NCHS) and in ESRD Treated by Dialysis (USRDS)

Legend:
- GP Male
- GP Female
- GP Black
- GP White
- Dialysis Male
- Dialysis Female
- Dialysis Black
- Dialysis White

Y-axis: Annual Mortality (%)
X-axis: Age (years): 25-34, 35-44, 45-54, 55-64, 65-74, 75-84, >85
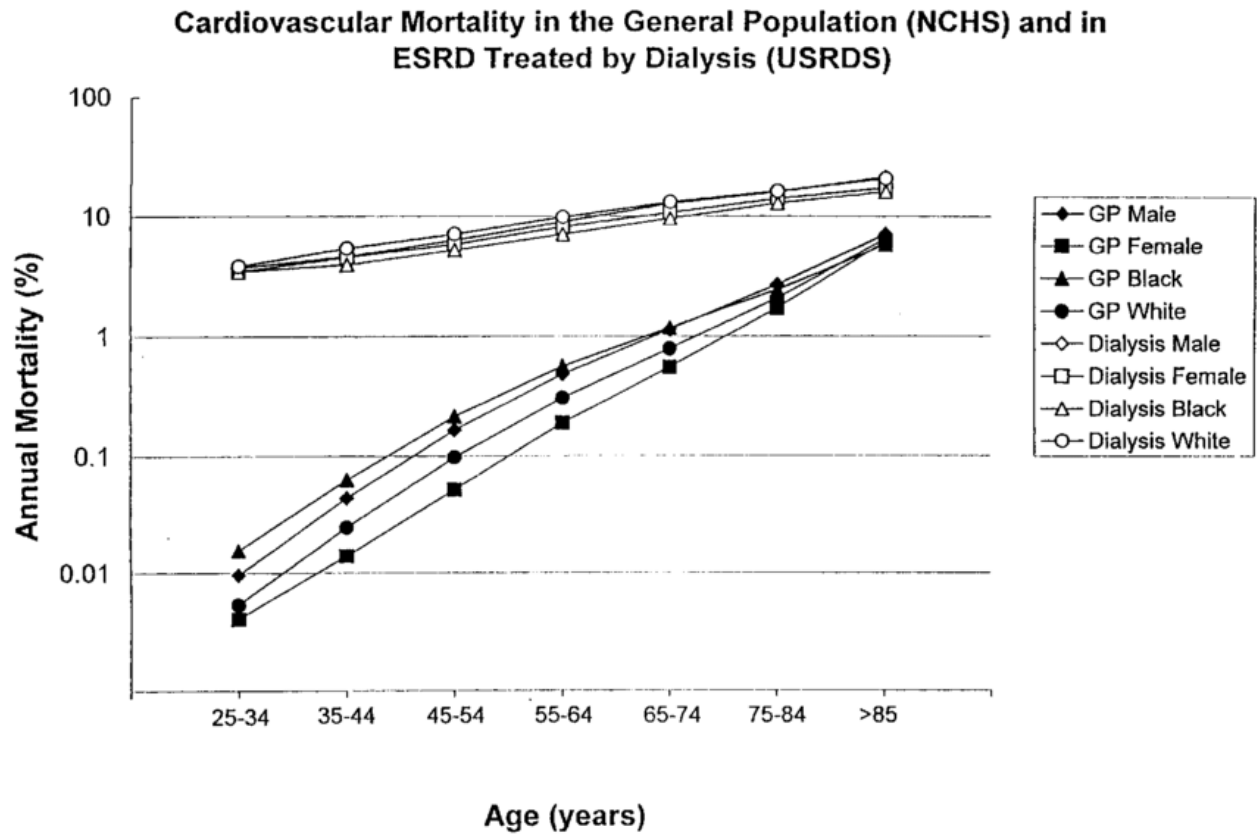
Figure 5: Increased rates of cardiovascular mortality in patients on haemodialysis compared to the general population (GP). From S Levey et al. 1999 [43].
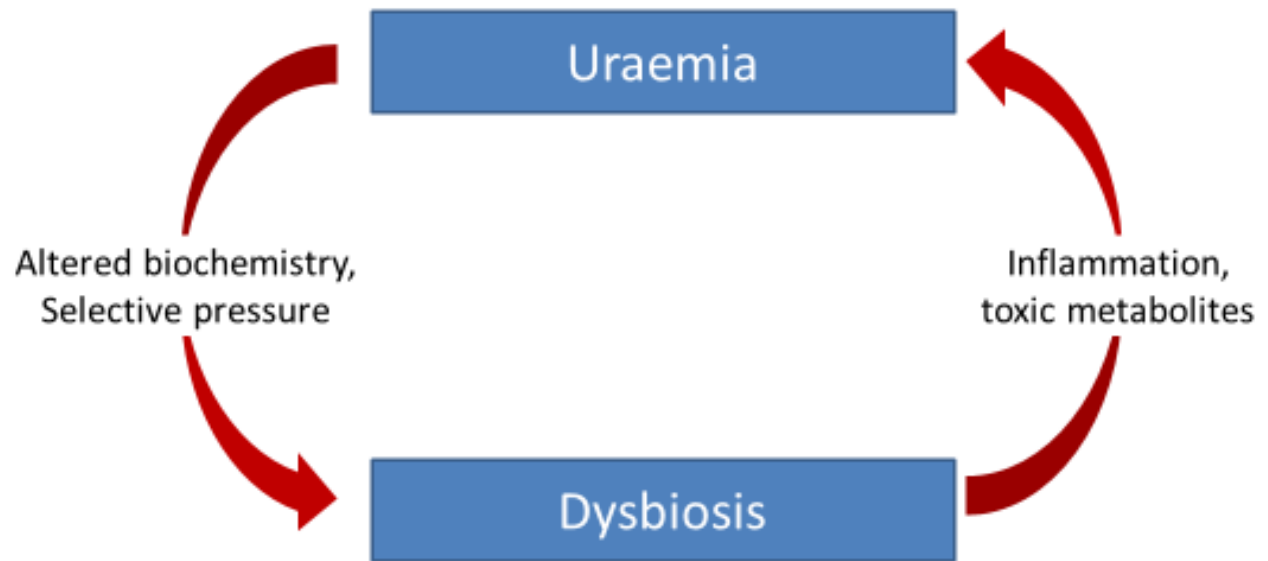
Figure 6: Potential interactions between chronic kidney disease and microbial communities.

Chapter 2

Core methods in microbiome research

*This chapter covers core methods applicable to each of the following chapters, including methods for the **induction of experimental uraemia**, culture and non culture-based methods for **assessing microbial communities** and **metabolomic techniques** for evaluating the function of the microbiota. Subsequent chapters describe additional techniques relevant to the subject matter of the chapter in question, for instance techniques to assess the microstructure of periodontal bone, or methods to measure whole body nitrogen balance. In addition, **appendix 2** contains detailed information on the full range of microbiological techniques used in the work presented in this thesis, which exceed the scope of this chapter.*

Induction of experimental uraemia

Chemically-induced uraemia

Attempts have been made to induce experimental uraemia in animals since at least as early as 1928. [57] Various chemicals have been used for this purpose including sodium tetrathionate, [58] lithium, [59] and acetaminophen, [60] however the most widely-used agent for the chemical induction of a uraemic phenotype is the nucleotide base adenine. [61, 62] Adenine is metabolised to 2,8-dihydroxyadenine in vivo which has been shown to cause a crystal-associated

tubulointerstitial nephritis, [63] mimicking a rare disease process seen in humans. [64] Although some have advocated twice daily oral adenine gavage as a way of reducing the variability found by using adenine-supplemented feed, [65] dietary adenine supplementation remains the most widespread method for chemical induction of uraemia. A variety of protocols can be used to achieve different levels of uraemia in both rats and mice, with mice typically only accepting lower concentrations of adenine that may produce a more chronic pattern of illness. [66, 67]

Surgically-induced uraemia

Surgical intervention has been shown to induce reproducible degrees of uraemia in rats depending on the amount of renal mass removed, from mild uraemia (one kidney removed), through moderate uraemia (80% of renal mass removed) to severe uraemia (88% of renal mass removed), compared to a sham operation. [68] The most widely accepted method for surgical induction of uraemia is five-sixth (or subtotal) nephrectomy (SNx), which reliably produces a model of progressive renal dysfunction, albeit with a not insignificant mortality. [69, 70]

Using a range of approaches

Different models of experimental uraemia produce different clinical syndromes that recreate aspects of human CKD. The different models each have strengths and weakness, meaning that using a combination of approaches may improve the robustness of research findings. For example, surgical induction of uraemia excludes the possibility of adenine-specific effects on the

microbiota (although limited published data suggests that adenine does not cause such effects, [71]), and allows co-caging of uraemic and control animals. Chemical induction of uraemia may produce more predictable and more significant degrees of uraemia than surgical methods, and eliminates perioperative mortality which is especially a feature of surgical models when used in mice. Furthermore, induction of chemically-induced uraemia is possible, although difficult, in germ-free conditions (through double-irradiation of adenine-containing feed, [1]), allowing comparison between germ-free and conventional uraemic animals.

The models we have elected to use in the studies reported here have included:

- *Chemically-induced uraemia in rats,* using a high concentration of adenine (0.75% of feed weight) for four weeks, followed by a four week washout period. This model generates rapidly progressive induction of uraemia followed by a period of recovery. At the time of sacrifice, kidneys in adenine-fed animals are grossly enlarged (Figure 7, p. 73) and histological examination reveals tubular adenine crystals with surrounding giant cell reactions and interstitial inflammation. [72]

- *Surgically-induced uraemia in rats,* using subtotal (five-sixths) nephrectomy, which causes steadily-progressive loss of renal mass due to hyperfiltration injury in the remaining glomeruli. [73, 74] This has been shown by our group to be a robust and reliable model of features of human CKD including myocardial bioenergetic dysfunction, [75] cardiovascular disease [76] and endothelial dysfunction. [77]

- *Chemical-induced uraemia in mice,* using relatively low-dose adenine in feed (0.15% by weight) over a long (18-20 week) period of administration. This has been shown to cause a slowly-progressive chronic uraemia with renal fibrosis and associated heart failure. [78]

Use of germ-free mice in microbiome research

The first colonies of germ-free animals, generally created by delivering newborn animals directly into sterile incubators by Caesarian section, were established in the 1940s. [79] The maintenance of such colonies is challenging and expensive, requiring dedicated facilities with complex filtering of air; sterilization of all equipment, feed and water by autoclaving and irradiation; employment of highly trained staff; elaborate and sophisticated maintenance protocols and regular monitoring to exclude accidental contamination. [80, 81]

Such totally sterile animals are deeply physiologically abnormal. The best described evidence of abnormal development is in the immune system, because early-life exposure to microbial communities has been shown to be crucial for 'training' immature immune cells. [82] Effects have also been shown in other organs, for instance kidneys from gnotobiotic mice have been shown to be small and underdeveloped compared to those of normal laboratory mice. [1]

Nevertheless, germ-free mice offer the opportunity to establish in absolute terms the relevance of bacteria to normal development (such as the implication from the poor development of kidneys in germ-free animals that bacterial products are required for normal organ growth). They also offer totally sterile hosts, albeit immunologically naïve and under-developed ones, into which

transfers of bacterial populations can be carried out without any effect of recent antibiotic exposure or the need for transplanted communities to compete with resident ones.

Practical techniques used

All animal experiments were conducted in accordance with the UK Home Office Animals (Scientific Procedures) Act 1986, with local ethical committee approval. All animal work was carried out in the Biological Services Units of Queen Mary University of London, at either Charterhouse Square or the Wingate Institute, Whitechapel; and complied fully with all relevant animal welfare guidance and legislation (UK Home Office Project License number PPL 70/8350 and P73DE7999).

All rats used in these experiments were male, outbred Wistar IGS rats obtained from Charles Rivers (Kent, UK) at 7 weeks of age.

All mice used for induction of uraemia were male, wild-type C57BL/6 mice, obtained from Charles Rivers at 7 weeks of age.

Germ-free mice of the same species were obtained from a colony maintained at the Biological Research Facility, St George's University of London, at 8 weeks of age.

All animals were housed in individually ventilated cages under 12 h light/dark cycles and were allowed unlimited access to feed and water.

Standard feed used for all animals was the RM1 rodent diet (Special Diet Services, Essex, UK). For certain intervention groups, the following other diets were used, also purchased from Special Diet Services:

- RM1 with 0.75% adenine for induction of uraemia in rats

- RM1 with 0.15% adenine for induction of uraemia in mice

- AIN-93M with 10% cellulose (CELL) as a low fermentable-fibre diet in rats

- AIN-93M with 10% fructo-oligosacchrides (FOS) as a high fermentable-fibre diet in rats

- Standard AIN-93M (AIN) for use in control groups to be compared with the fibre-supplemented AIN-93M feeds described above.

Chemically-induced uraemia in rats: After a week-long period of acclimatization, intervention rats were started on 0.75% adenine containing feed whilst control animals were maintained on standard RM1 control diet. The adenine-containing diet was continued for four weeks, followed by a washout period of four weeks when all animals received the control diet, after which the animals were sacrificed animals were sacrificed by lethal injection of sodium thiopentone (LINK Pharmaceuticals, Horsham, UK). Animals were placed in metabolism cages to allow for 24h urine collection and faecal pellet collection immediately prior to sacrifice. Other tissues were retrieved after sacrifice as described subsequently.

Surgically-induced uraemia in rats: After a week-long period of acclimatization, rats underwent a two-stage surgical procedure involving either subtotal nephrectomy (SNx) or a sham procedure. SNx involved exteriorisation of the left kidney with decapsulation and removal of the upper and lower poles and subsequent replacement of the middle pole only, followed by total right nephrectomy two weeks later. Sham procedures involved exteriorisation, decapsulation and replacement of the left kidney, followed by the same procedure on the right kidney two weeks later. Animals were culled eight weeks after the second stage of surgery animals by lethal injection of sodium thiopentone (LINK Pharmaceuticals, Horsham, UK). Collection of biological specimens occurred as detailed in subsequent chapters.

Chemically-induced uraemia in mice: After a week-long period of acclimatization, intervention animals were placed on a modified diet (RM1 with 0.15% adenine), whilst control animals remained on standard RM1 diet. Mice were weighed weekly. 24h urine and stool collections occurred in the week prior to sacrifice. Sacrifice occurred after 18 weeks on the experimental diet by lethal injection of sodium thiopentone (LINK Pharmaceuticals, Horsham, UK), with a variety of tissues being preserved for subsequent analysis.

Microbial transfer experiments: Fifteen germ-free C57BL/6 mice were transferred direct from their sterile isolator at the Biological Research Facility, St George's University of London, to the Biological Services Unit at Charterhouse Square using a clean but non-sterile specialist animal transfer company (Impex, UK) in three separate batches (one batch of seven for receipt of

microbiota from control donors, two batches of four each for receipt of microbiota from uraemic donors).

On arrival, each mouse received an oral microbial transfer (OMT) by oral gavage of oral swabs previously taken from uraemic or control donor animals. Each donor swab was used to transfer into two (or in one case, one) recipient(s); seven were designated control recipients and eight, uraemic recipients. Gavage was carried out using a sterile swab thoroughly immersed in transport medium that had been inoculated with donor microbiota and frozen since the time of sampling, and agitating the swab in the mouth of the recipient mouth for 15 seconds and encouraging them to suck on it. After receiving the OMT, the mice were placed in cages containing cage contents from the donor animals, which had been frozen at -80º until the time of use, to permit ongoing microbial transfer by coprophagy.

Animals were then maintained in ordinary individually-ventilated cages in an open area of the Biological Services Unit, with standard 12h light/dark cycles. They had unlimited access to standard RM-1 diet and tap water. Oral swabs were taken to assess the efficacy and durability of bacterial transfer at 3-weeks and 9-weeks after transfer in all animals, and all animals were then culled, after a 24-hour urine collection, at 18 weeks of age (10 weeks after transfer).

Evaluation of the degree of experimental uraemia

Physiological assessment: All animals were weighed weekly and underwent 24h urine collections in the final week of life. Both weight loss and polyuria are signs of clinical uraemia.

Biochemical assessment: Blood samples were obtained by thoracotomy and cardiac puncture at the time of sacrifice, and spun down directly to isolate serum which was frozen at -80º until the time of analysis. Quantification of serum urea, creatinine, calcium and phosphate concentrations was done by IDEXX Bioresearch, Ludwigsberg, Germany.

Clinical uraemia in rats

Uraemic animals generated by both the chemically-induced and surgically-induced uraemic protocols demonstrated an expected phenotype including elevation of serum urea and creatinine, weight loss and polyuria (Figure 8, p. 74).

The chemically-induced uraemia protocol generated a more severe uraemic phenotype, with greater elevations of serum urea and creatinine, lower weight and more polyuria. The higher urinary volumes may additionally represent the 'tubular' phenotype of adenine-fed animals (resulting in a defect in urinary concentrating ability). There were no differences between the control animals in the two protocol groups.

Clinical uraemia in mice

Whilst control animals showed steady weight gain through the experimental period, weights of uraemic mice rapidly tailed off and then began to fall after 8-10 weeks of adenine-containing diet (Figure 9, p. 75). Uraemic mice developed polyuria, passing an average of 7.72ml urine per 24 hours compared to 1.22ml in controls, $p<0.0001$ (Figure 10, p. 76). Compared to control mice, at

the end of the 18-week period of adenine administration, uraemic animals developed severe abnormalities of serum urea and creatinine, Table 4, p. 169.

Analysis of microbiota

Bacterial culture

Traditionally, the composition of a bacterial community was determined by culturing a sample taken from the community on a broad-based culture medium such as blood agar. This allows a determination of total bacterial abundance, and by counting colonies according to morphology type, and subsequently growing each different colony to purity and identifying the organism (by combinations of traditional tests such as catalase, coagulase or urease; or by sequencing identifier genes), a measure of community composition can be obtained.

There are a number of advantages of culture-based techniques (leading to recent renewed research interest in these approaches, to complement newer culture-independent techniques) [83]: firstly, they allow robust estimation of the abundance of viable bacteria (measured as colony forming units per millilitre, or cfu/ml); secondly, they allow confidence species-level identification of isolates; thirdly, they allow *in vitro* testing of bacterial isolates to explore their functional potential; and fourthly, they allow organisms to be used in further experimental procedures, for example, to test the ability of a potential pathogen to cause disease.

The great disadvantage of culture-based methods of determining bacterial community structure is that many organisms are difficult or even impossible to culture *in vitro*, with laboratory-based culture imposing a selective pressure that may distort the true relative abundances of different members of a community in the host organism. [84] The advent of high-throughput next-generation amplicon sequencing of bacterial genes allowed the discovery of many previously uncultured species, and with it the accurate determination of bacterial populations based on what bacteria are actually present in a sample rather than which organisms will grow in *in vitro* culture. For example, the recent discovery of Candidate Division TM7 (or *Saccharibacteria*) was made first through molecular sequencing, before eventually it was possible to grow the first such organisms through intensive culturing using epibiont species parasitized by TM7 bacteria [85]. A recent metagenomic study of human gut samples identified 1,952 new uncultured candidate bacterial species, increasing the known phylogenetic complexity of the human gut microbiome by 281% [86].

Identification of cultured bacterial isolates

The traditional microbiological methods of identifying organisms used gram staining supplemented by catalase, coagulase, urease and other functional tests. These may be combined into 'Analytical Profile Index' (API) kits, which may still be superior to molecular analysis in differentiating subspecies that are closely genetically related and which differ more by phenotype than by genotype.

However, in academic study these in-vitro tests of bacterial have now been largely superseded by genetic sequencing of markers genes, or alternatively by spectroscopic tests such as Matrix-Assisted Laser Desorption/Ionisation Time Of Flight mass-spectroscopy (MALDI-TOF). [87]

In this study, all cultured isolates were identified using amplification of the whole 16S rRNA gene, using the widely-used 27F/1492R primer pair. Genetic sequencing of the whole of the 16S gene has been shown to have greater precision than traditional phenotypic methods. [88] Further description of the role of the 16S gene is provided below.

Amplicon sequencing

High-throughput next-generation sequencing of amplified sections of identified genes offers a rapid way of describing the total bacterial population in a given sample, without the technical challenges and selective pressure exerted by bacterial culture.

The most widely-used identifier gene is the 16S ribosomal RNA gene, which was first studied in the 1970s and developed for robust identification of cultured bacteria in the 1980s. [89] Indeed, analysis of variation between ribosomal RNA was critical in helping to define the evolutionary lineages of different kingdoms in the 'tree of life'. [90]

The prokaryotic ribosome (with a total sedimentation coefficient of 70S) comprises 50S and 30S subunits, the smaller 30S subunit comprising a 16S rRNA molecule and 21 associated ribosomal proteins. The 16S rRNA provides the scaffold allowing correct assembly of its associated proteins, as well as containing the anti-Shine Dalgarno sequence which binds template

messenger RNA from which the larger 50S subunit assembles amino acids in the process of translation.

The 16S gene has a number of properties that make it ideal for use in studying bacterial populations such as those in the mammalian colon:

- It is constitutively expressed as a 'housekeeping' gene in all bacterial cells.

- It is not present in eukaryotic cells, allowing the evaluation of bacterial and archaeal populations in the presence of host DNA.

- It has a number of highly conserved regions, allowing the use of universal primers that cover all (or almost all) bacterial and archaeal species,

- It contains nine hypervariable regions that differ significantly between bacterial and archaeal taxa.

The whole gene is approximately 1500bp long, with the nine hypervariable regions (named V1 to V9) interspersed along its length. Figure 11 (p. 77) shows a schematic of the gene and its hypervariable regions, along with the various points along the gene at which common primer sets bind to generate amplicons for different types of sequencing [91].

Choice of primer pairs for sequencing depends upon the appropriateness of the amplicons generated for the required sequencing modality, versus the amount of information contained within the amplicon to allow for full identification to genus or species level [92].

For full identification of an individual bacterial isolate, PCR carried out using the (F27, R1492) primer pair allows amplification of almost the whole gene, yielding amplicons suitable for

Sanger sequencing. This is usually suitable for identification of an organism to species level, however closely related species (for instance within the *Enterobacteriaceae* family), may have 16S genes differing only in one or two base pairs in the V4 variable region, or may even have identical 16S gene sequences, requiring additional tests (either culture-dependent techniques such as Analytical Protocol Index (API) or culture-independent techniques such as whole-genome sequencing), to allow species-level identification.

However, for high-throughput/low-cost sequencing strategies such as next-generation sequencing using the Illumina MiSeq or older Roche 454 pyrosequencing platforms, shorter DNA amplicons (150-500bp) are sequenced, covering one or more of the hypervariable regions of the gene. These allow comparisons of amplicon sequence variants (ASVs) or operational taxonomic units (OTUs), allowing the composition of populations to be assessed once such variants are assigned a probable taxonomic identity on the basis of comparison with a reference dataset, such as the Silva reference dataset [93, 94], Greengenes [95] or NCBI BLAST [96]. Confident identification on the basis of these shorter amplicons may only be possibly at genus or family level.

Studies have revealed that choice of both primer pairs and sequencing platform can affect the ability of sequencing runs to detect different types of bacteria, introducing potential bias into experimental datasets. [91, 97, 98] Reassuringly, the more modern Illumina MiSeq platform seems to produce higher quality data than the older 454 pyrosequencing platform, and bias introduced by primer pair selection seems to affect measures of beta diversity to a lesser extent that it does the relative abundances of individual taxa. [99]

Functional studies and metagenomics

Studies of population composition yield only a certain amount of information. In the context of an experimental intervention, they can allow the effect of the intervention on the relative abundance of different taxa to be established, but they can at best only allow an inference to be made about the possible functional consequences of such changes. Tools such as PICRUSt [100] and piphillin [101] construct predicted metagenomes based on 16S abundance data using the published genomes of organisms detected by sequencing, but are limited by the range of published genomes available and the difficulty of attributing precise taxonomic identities to organisms on the basis of short 16S reads.

A more robust measure of the functional capacity of a bacterial population can be made by performing whole genome sequencing metagenomics on extracted DNA. Such methods rely on shotgun sequencing, where genomic DNA is sheared into randomly-sized lengths (typically 2-150kbp), which are roughly sorted according to size and then cloned into vectors and sequenced from both ends from known primer sites, or using short, random primers [102]. These mate pairs (which do not generally overlap, but are known to run in opposite directions at an approximate distance apart), are then clustered into contigs and eventually assembled into a whole (or multiple) individual genomes, or are assembled against known reference genomes, Figure 12, p. 78. The process of assembly of reads requires a large amount of computing power, generally necessitating access to high-performance computing facilities. As with all genetic techniques, the sequencing quality of the original reads determines the quality of the final product. A population can then be assessed on the abundance of genes it possesses within different functional

categories, or from different metabolic pathways, allowing questions of population function to be determined and compared between groups.

Statistical considerations in microbiome research

Data gathered from microbiome analysis is quite different from data types commonly seen in other areas of health science. Indeed, the best comparison is with datatypes gathered from environmental surveys in ecological science, and many of the statistical techniques used to analyse microbiome data have been borrowed directly from ecology. [103, 104]

Typically, analysis of the microbiome will yield data in the form of an abundance table, where the abundance of (often hundreds) of individual bacterial species are recorded in each of the samples tested. There are several features of this type of data that make it challenging to analyse using conventional statistical techniques. For example, if a conservationist was surveying different areas of jungle, they may end up with data that is:

- sparse, with lots of zeroes (ie, in any particular area of jungle they may not discover any examples of particular species which are found in other areas);

- noisy, with biological replicates from similar regions displaying high degrees of heterogeneity, even where experimental technique is excellent;

- difficult to interpret in terms of relevance to research questions; for instance, a jungle may have only a handful of tigers, but they may each be of far more importance than hundreds of beetles;

- influenced by many different variables; for example, environmental factors influencing the proportion of species present at a given jungle location may include temperature, humidity, time of day, presence of environmental pollutants, proximity to water, recency of forest fires, etc;

- significantly redundant: the presence of one species may heavily influence the presence of another.

A key method developed in ecology for analysing such datasets is ordination, with various techniques available depending on whether the data is quantitative (principal component analysis, PCA; correspondence analysis; redundancy analysis), or qualitative (principal coordinate analysis, PCoA; non-metric multidimensional scaling, NMDS).

Each techniques allows the key determinants of variation to be extracted and visualised; typically by creating a complex, multidimensional statistical model (with the number of dimensions typically being 1 minus the sample number). Samples can then be plotted in two dimensions using the first two axes from the statistical model, allowing visual representation of sample clustering, identification of outliers and demonstration of key trends.

Detailed description of experimental technique

Appendix 2 (p. 344) describes in detail the practical basis for the microbiological work presented in the rest of this thesis, including:

- descriptions of bacterial culture techniques and organism identification,

- description of extra in vitro bacteriology carried out, including assessing urease activity and urea tolerance of individual isolates,

- methods used for DNA extraction and processing,

- details of polymerase chain reaction (PCR),

- details of 16S sequencing using barcoded primers,

- details of whole-genome metagenomics and subsequent genome assembly and data analysis,

- a note on specific statistical approaches used.

Metabolomics

Metabolomics describes the scientific study of metabolites – small molecules used and produced in the biochemical processes of living things – in biological tissues and fluids. Since the primary interactions between gut microbiota and host organisms with relevance to health and disease are purported to be mediated through such metabolites, the science of metabolomics fits hand in glove with the study of microbial populations in understanding the functional implications of this complex relationship.

Although a variety of techniques can be used in metabolomic studies, there are broadly two forms of analysis:

- *Untargeted analyses* use techniques such as proton nuclear magnetic resonance (^{1}H-NMR) spectroscopy to study all small metabolites in a biofluid or tissue. These studies

are often hypothesis-generating, offering relative quantification of substances between different samples across a broad range of molecular classes.

- *Targeted analyses* use biological standards and techniques such as gas chromatography/mass spectroscopy (GC/MS) to measure absolute quantities of known molecules of interest. These techniques are typically used for confirmation of known hypotheses.

Chapters three and four both detail untargeted ^{1}H-NMR spectroscopy, used to evaluate broad changes in the rat salivary metabolome in uraemic in chapter three and in the rodent urinary metabolome in uraemia in chapter four; this technique is briefly explored here.

NMR Spectroscopy

NMR spectroscopy is a technique that allows identification of the constituent components of a chemical mixture by determination of the magnetic fields around individual atomic nuclei. It was developed in 1930s New York and won the 1944 Nobel Prize in physics for its pioneer, Isidor Isaac Rabi (1898-1988). [105] NMR spectroscopy represents an excellent method for identification and relative quantification of small organic molecules in mixed biological solutions (such as serum or urine), [106] as well as having other applications including determination of the 3-dimensional structure of complex molecules such as proteins.

The principles of NMR

In quantum mechanics, spin is an intrinsic property of elementary particles that is best thought of as the vector of angular momentum – the 'direction' in which the magnetic field around the particle, generated by spin, is 'pointing'. In essence, such particles behave like small magnets. When an external magnetic field is applied to substances in solution, particles in low energy states align to the external magnetic field. Application of energy to these particles, using radiofrequency radiation at a frequency particular to the particle in question, causes the particle to move to a higher energy state and line up against the external magnetic field (this is rather like using a finger to apply energy to the needle of a compass, so that it lines up pointing south). This causes energy to be absorbed, which is subsequently released when the particle returns to its original, lower, energy state (like removing the finger from the compass needle, so that it swings back to north). Sensitive radio receivers can detect these absorbances and releases of energy, and the energy absorbance at different radiofrequencies can be plotted to produce an NMR spectrum.

Chemical shift

NMR-spectroscopy can be carried out for any atomic nuclei possessing the property of spin (typically those with an odd atomic mass), but most often is carried out either for either ^{1}H ('proton-NMR'), or ^{13}C.

The amount of energy required to shift particles from low to high energy levels (ie resonance; altering their spin states), is proportion to two things: the strength of the external magnetic force (which is determined by the settings of the NMR spectroscope), and the local magnetic moment

around the particle in question. This in turn my be affected by various local factors, which are related to the chemical microenvironment surrounding the nucleus in question.

NMR spectra

NMR spectra are typically plotted on axes where:

- The y-axis represents the absorption and subsequent release of energy (radiofrequency radiation) – termed the 'free induction delay', typically averaged over several measurements because the signal is small.

- The x-axis represents the strength of magnetic field needed to produce resonance. This is expressed in 'parts per million' (ppm), relative to the strength of field required to produce resonance in the ^{1}H nuclei of tetramethylsylene (TMS, Figure 13, p. 79).

TMS is used as the reference substance because it has 12 ^{1}H nuclei in exactly the same electrical environments (methyl groups bound to silicon), producing a strong peak, and because the electrons in the hydrogen bonds are closer to the ^{1}H nuclei in TMS than in almost all other biological substances, meaning the field strength required to achieve resonance is greater than for almost all other substances, so TMS is always on the right hand end of NMR spectra.

The local environment of ^{1}H nuclei – determined by the chemical structure of the substance they form part of – influences the frequency at which resonance occurs. Structural factors combine to give substances unique spectral signatures, with different peaks being formed by ^{1}H nuclei in difference chemical environments, reflecting the following principles:

- ^{1}H number – the number of protons in an identical environment is directly proportional to the area under the curve of the peak height in question, so the three ^{1}H nuclei in a methyl group (-CH3) would have an area under the curve three times that of the one in a hydroxyl group (-OH).

- Shielding – the effect of the external magnetic field is exerted more strongly on nuclei with less electron density around them, than on those with more electron density, requiring less field strength (lower ppm) to achieve resonance than in those more heavily shielded. This depends on the relative electrical charge of other atoms near to the ^{1}H nuclei in question, and the extent to which they attract shared electrons away from the ^{1}H nucleus.

- Splitting – if a given group of ^{1}H nuclei is exposed to other nearby ^{1}H nuclei, their magnetic fields will interact with the ^{1}H nuclei in question and split this peak into n+1 subpeaks: a neighbouring -CH2 group will result in a triplet, and a neighbouring -CH group will result in a doublet.

These principles are illustrated in Figure 14 for the NMR spectrum of ethanol, where the three different types of ^{1}H nuclei return peaks that can be differentiated by area, shielding and splitting.

Practical NMR technique

Modern NMR spectroscopes incorporate extremely strong superconducting magnets cooled by liquid helium, to generate extremely strong magnetic fields of up to 20 Tesla (by contrast, the earth's magnetic field is around 0.0001T, and a typical fridge magnet might generate a magnetic field of 0.01T).

Biological samples including urine and saliva underwent prolonged centrifugation to remove protein, and were then diluted in D_2O solvent containing a pH regulator and TSP (deutritium has a very different NMR resonance frequency to ^{1}H, hence using D_2O rather than H_2O). Some samples were diluted further if volumes (particularly for mouse saliva and serum) were inadequate.

A 600 MHz Avance III NMR spectrometer (Bruker Biospin Ltd.) was used for the analysis, including a BBI 600 MHz 5-mm Z gradient probe and automated tuning and matching (ATMA unit) NMR detector (Bruker Biospin Ltd.). The Nuclear Overhauser Effect Spectroscopy (NOESY) method was used to generate 2D NMR spectra.

The NMR spectral profiles gained were digitised and imported into Matlab (Mathworks) using in-house scripts. The raw spectra were adjusted for 24-h urine volumes by multiplying all NMR absorbance values by the urine or salivary volume in millilitres. The peaks for water, TSP and urea were excised from the raw NMR spectra, which were then aligned to adjust for variation in peak shift due to pH differences. Further normalisation was carried out using the probabilistic quotient method between samples in order to ensure comparable baselines between samples.

Unsupervised PCA was used to identify sources of variation in the metabolic data. This was followed by supervised OPLS-DA analysis to assess differences according to group – for instance, uraemic vs control. In-house-developed scripts were used to perform these multivariate statistical analyses.

Positive identification of various metabolites was achieved by identifying their spectral profiles and confirming this using Chenomx NMR Suite 8.3 evaluation version (Chenomx, Edmonton, Canada), and peak integrals were calculated from metabolite peaks. Comparisons between these integrals were used to calculate differences in relative abundance using Microsoft Excel, with the Student's *t*-test and Welch's correction used to assess significance.

All raw NMR data has been uploaded to the Metabolights online repository [107] (https://ebi.ac.uk/metabolights/) using the study identifier **MTBLS1833**.

Figure 7: Representative photographs of kidneys from adenine-fed (left) and control (right) animals.
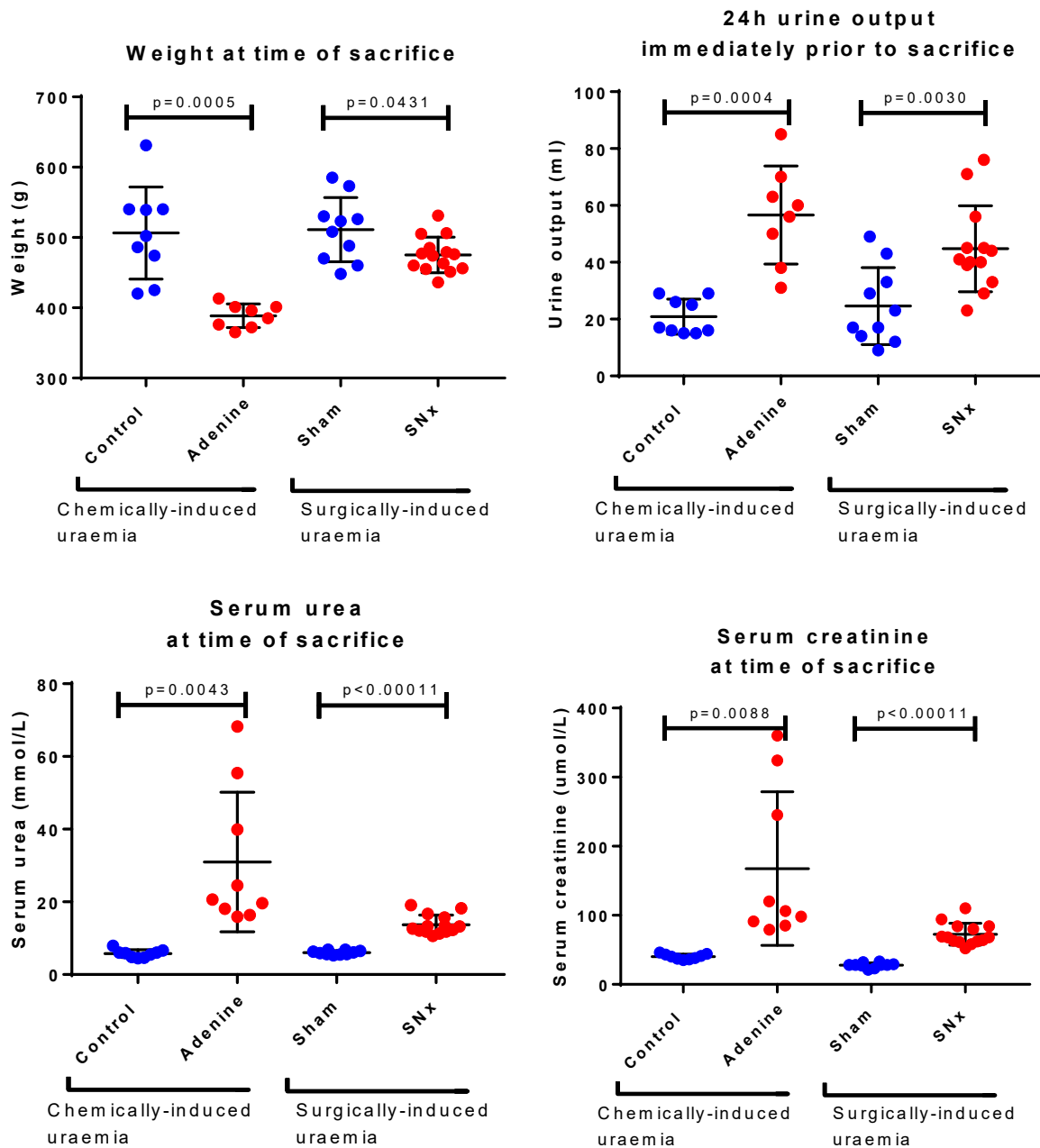
Figure 8: Evaluation of the degree of clinical uraemia in experimental rats. P values in each graph are calculated by Student's t-test with Welch's correction for unequal variances. SNx, subtotal nephrectomy.
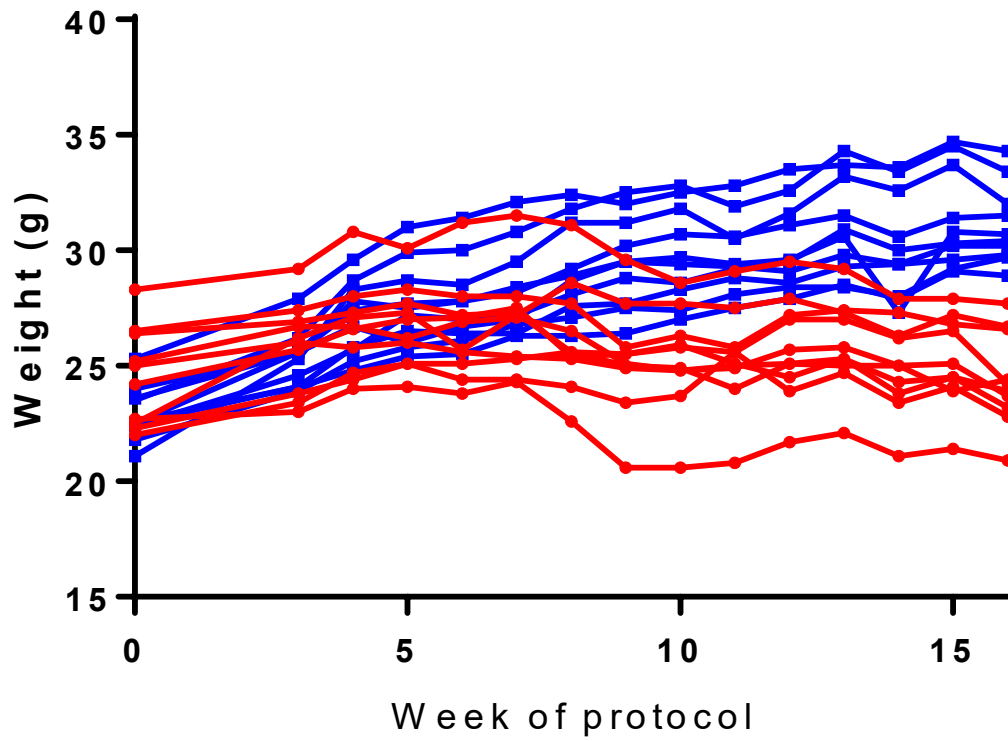
Figure 9: Weekly weights of experimental mice. Control animals are shown in blue and uraemic animals in red.
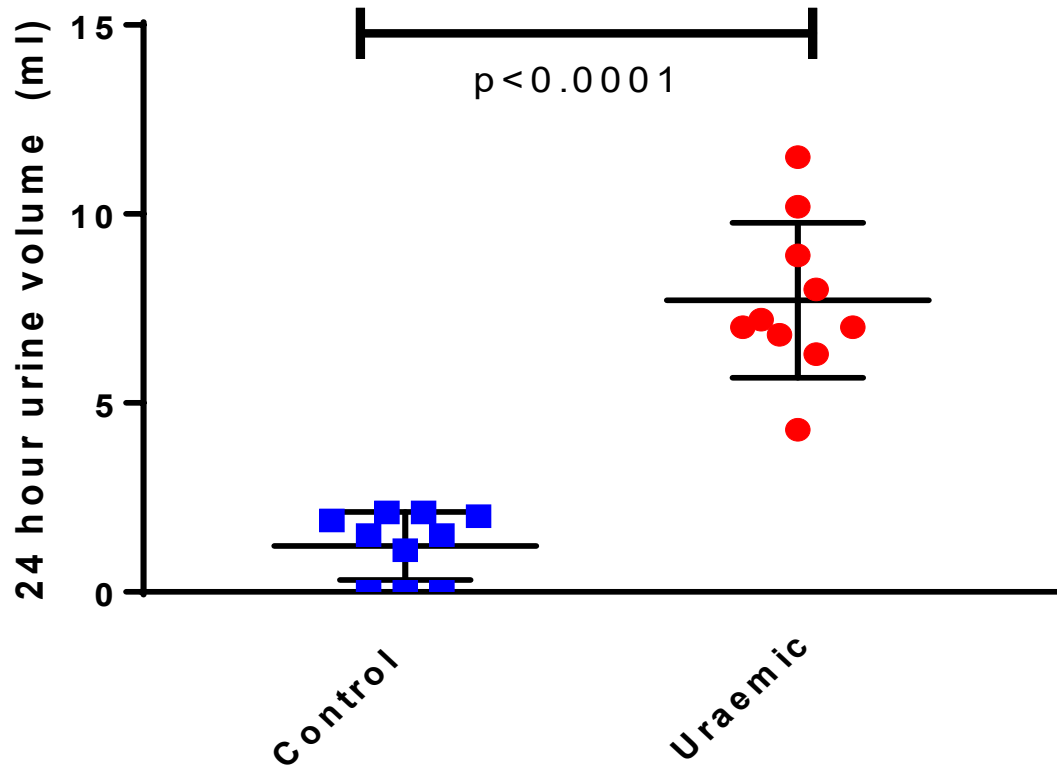
Figure 10: 24h urine output of experimental mice. Significance is assessed using Student's t-test with Welch's correction for unequal variance.
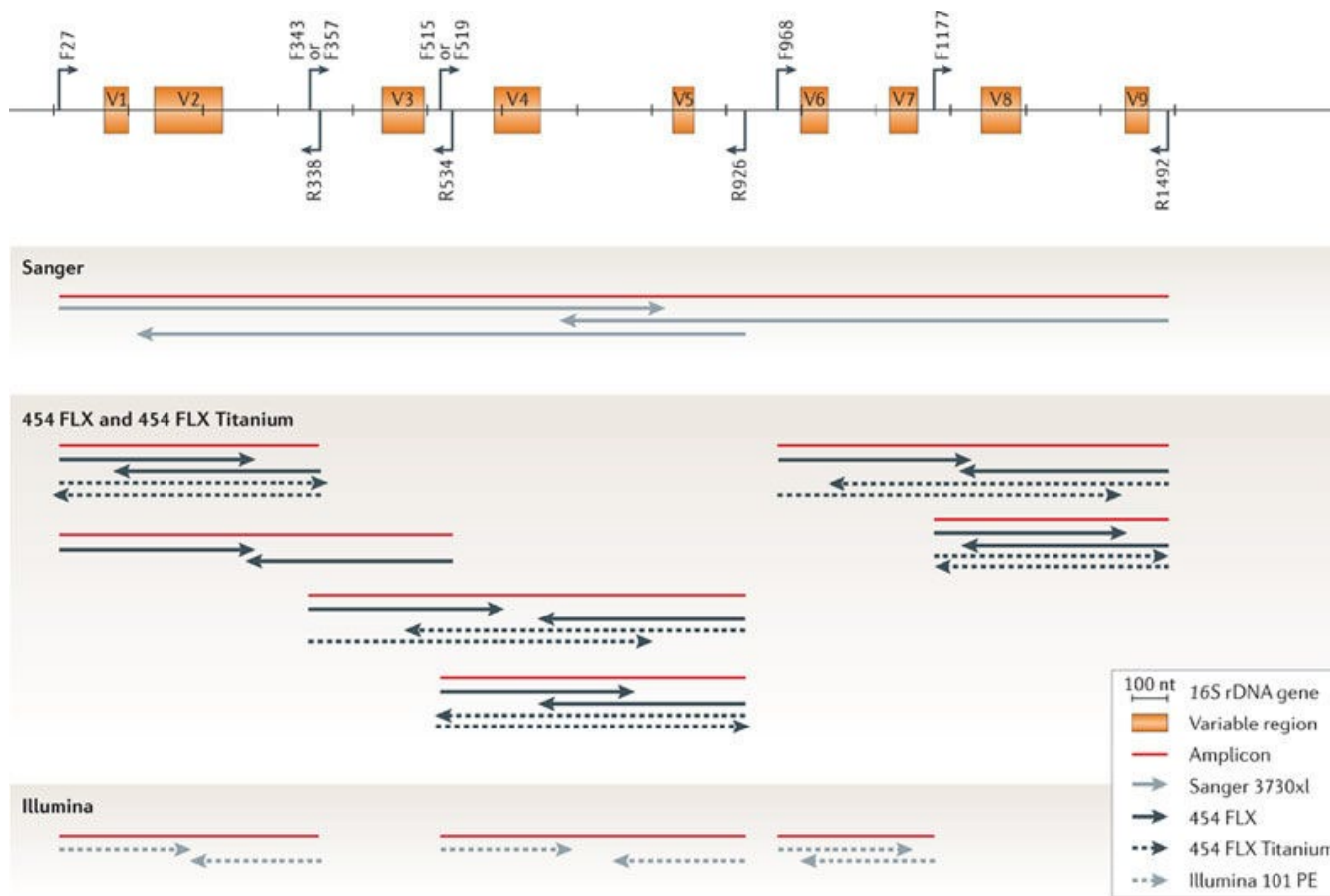
Figure 11: Schematic of the 16S rRNA gene. The nine hypervariable regions and common primer binding sites are shown. For the oral microbiome work presented in this thesis, the 27F/1492R primer set were used to sequence the whole 16S gene for identification of cultured isolates, and the 27F/338R (V1/2) primer sets for next generation sequencing. Taken from Kuczynski et al, 2011 [91]
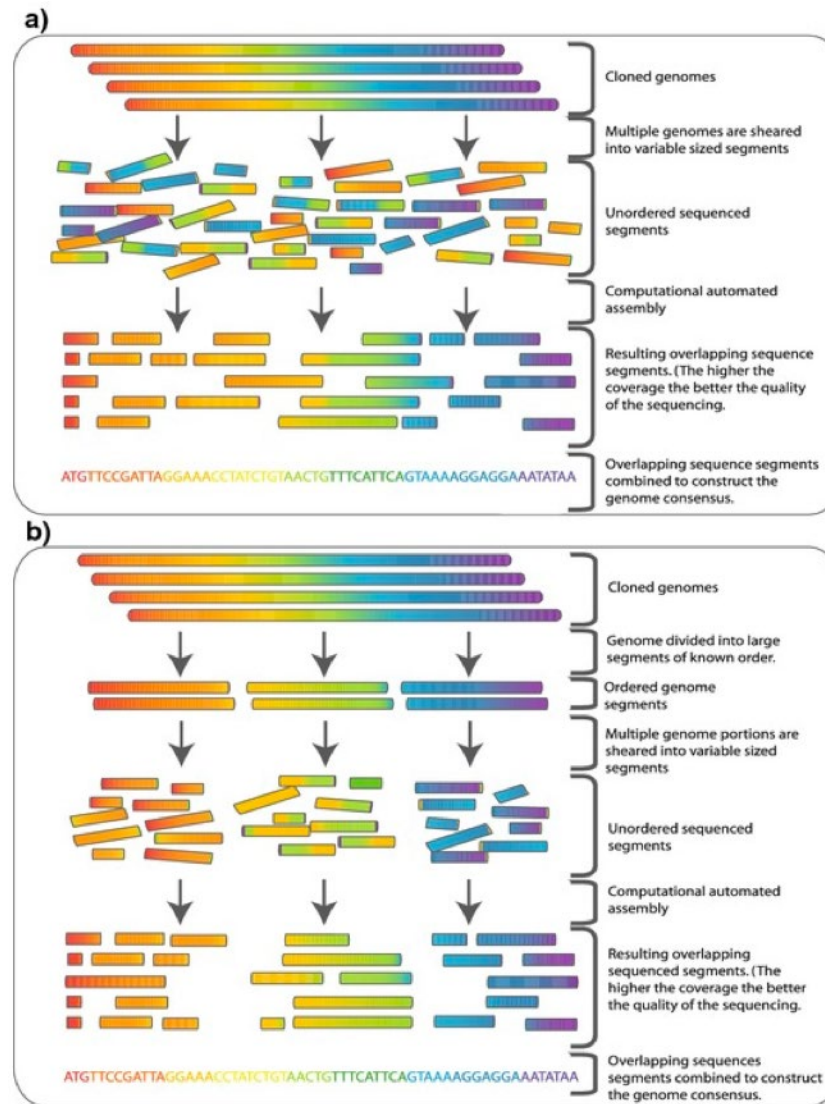
Figure 12: Principles of sequence assembly in shotgun metagenomic sequencing. Adapted from Commins, J. et al (2009) [108]
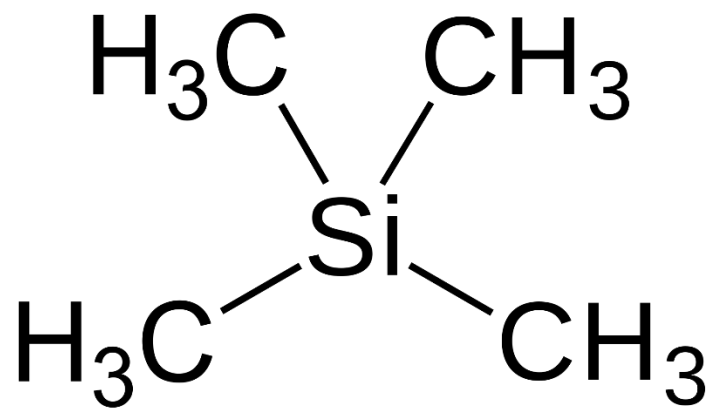
Figure 13: Molecular structure of tetramethylsylene (TMS). Taken from Jynto (talk), https://en.wikipedia.org/wiki/Tetramethylsilane#/media/File:Tetramethylsilane_2D_flat.svg, retrieved on 1st February 2022.
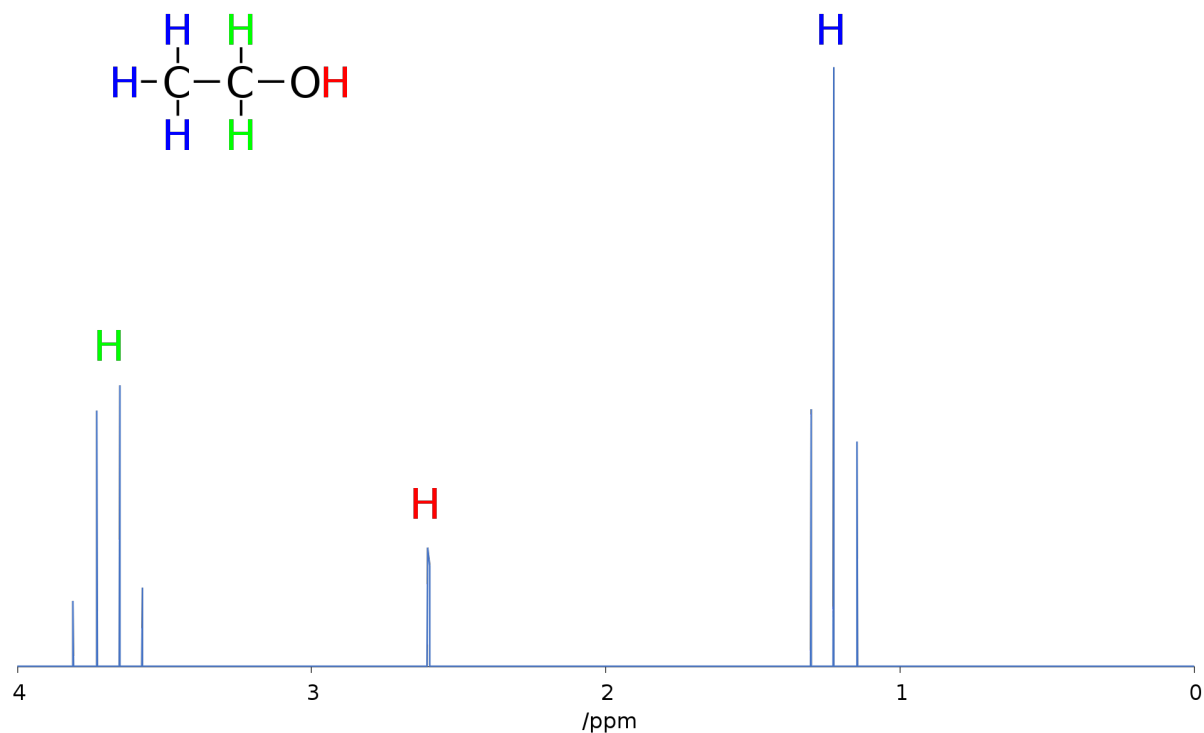
Figure 14: Example ^{1}H-NMR spectrum of ethanol, plotted as signal intensity vs. chemical shift. There are three different types of H atoms in ethanol regarding NMR. The hydrogen (H) on the -OH group (red) is not coupling with the other H atoms and appears as a singlet, but the CH_3- (blue) and the -CH_2- (green) hydrogens are coupling with each other, resulting in a triplet and quartet respectively. Taken from: Andel, own work, data from SDBSWeb: https://sdbs.db.aist.go.jp/sdbs/cgi-bin/landingpage?sdbsno=1300 (National Institute of Advanced Industrial Science and Technology, accessed 3rd August 2019)

Chapter three

The oral microbiome and periodontal disease

Introduction

Periodontal disease (PD) is a complex pathological process in which a bacterial challenge presented by a dysbiotic microbial community in subgingival dental plaque [109] drives a deregulated immune and inflammatory response which ultimately causes osteoclastic resorption of alveolar bone and eventual loss of teeth. [110]

There is a high prevalence of PD in patients with CKD, and given the close relationship between the aetiology of PD and bacterial dysbiosis, we sought to establish whether disruption of the oral microbiota caused by chronic uraemia might be the mechanism that explains this.

The aetiology of periodontal disease

Clinical periodontitis is always proceeded by gingivitis: inflammation of gingival soft tissue without evidence of alveolar bone destruction. Both gingivitis and PD are preceded by build-up of dental plaque, which represents a complex microbial biofilm that may calcify (tartar) and thus allow a protected niche for pathological, anaerobic gram-negative organisms to flourish (Figure 15, p. 114). [111, 112]

Bacteria which are implicated in the development of periodontitis possess numerous virulence factors which allow evasion of immune surveillance. [113, 114] The immune reaction to these persistent microbial insults causes soft-tissue inflammation, destruction of bone and ultimately loss of teeth; as well as chronic, low-grade, systemic inflammation. [115-117]

Epidemiology of PD in the general population

Observational studies suggest that the population prevalence of moderate to severe periodontal disease is between 15-30% in high income countries, [118-120] with some evidence that the prevalence might be higher in low or middle income countries (LMICs). [121] A review of several large cohort studies with long follow-up periods in widely separated geopolitical regions identified factors associated with faster progression of periodontal pathology, including:

- increasing age,

- presence of diabetes,

- cigarette smoking,

- poor oral hygiene routines and dental care,

- individual genetic factors.

Genetic defects associated with periodontitis include mutations of genes associated with immune modulation and especially of proteins involved in the resolution of inflammation, suggesting that hosts that are unable to successfully switch off gingival inflammation may be at particular risk of progressing to full-blown PD. [122] Some forms of PD may even demonstrate Mendelian inheritance patterns and associations with particular genetic polymorphisms. [123-125]

The oral microbiome

The Human Oral Microbiome Database collates taxonomic information, including 16S rRNA sequences, for all described human oral bacteria. There are estimated to be 700 species resident within the human oral cavity and related spaces (eg the pharynx and oeseophagus), with up to a third still identified only by 16S genetic analysis and awaiting full taxonomic description. Six phyla (*Firmicutes*, *Actinobacteria*, *Proteobacteria*, *Bacteroidetes*, *Spirochetes* and *Fusobacteria*), make up 96% of the total, with a further seven phyla comprising the remaining 4% of organisms. [126] In one study, in which nine oral sites were swabbed in five healthy volunteers, a total of 141 different bacterial species were identified across six different phyla, with different oral sites harbouring significantly different bacterial populations. [127]

The human oral microbiome is known to differ significantly at species level between individuals, but to be significantly conserved over time within individuals. There appears to be a large amount of functional redundancy in the oral microbiome, and it has been suggested that looking

for functional differences between individuals (for instance, between diseased and healthy experimental subjects), may be more relevant than concentrating on species level variation. [128] To this end, recent interest has developed in using metagenomic and metatranscriptomic approaches to explore the functional activity of bacterial populations in health and disease. [129]

The role of bacteria in the development of periodontitis

Periodontitis is a complex disease resulting from interactions between oral bacterial communities and host defences. Several hypotheses have been advanced to explain the role of bacterial communities (present as the oral biofilm plaque) in its aetiology. The categorisation below is adapted from Bartold and Van Dyke, 2000 [115]:

- *The non-specific plaque hypotheses*, which was first advanced in the 1950s, holds that it is simply the burden of plaque present that causes gingivitis and then periodontitis, regardless of the particular composition of the bacterial species present. [130] Host defences are able to cope with low volumes of bacteria, but in the context of high-volume plaque lesions, are overwhelmed by pro-inflammatory bacterial products and inflammation ensues.

  This hypothesis was increasingly questioned in the face of mounting evidence that the presence of specific bacterial species, rather than simple bacterial burden, seemed to be the trigger predisposing to development of periodontal inflammation.

- *The specific plaque hypothesis*, advanced in the 1970s, was based on the notion that plaque samples from patients with periodontal disease demonstrated different microbiology from plaque samples taken from healthy controls, with relative decreases in Gram-positive bacteria and an increase in Gram-negative phyla such as *Proteobacteria*. The influential concept of red and orange complex bacteria (associated with periodontitis, as opposed to the 'early colonisers' of the blue, green, purple and yellow complexes, Figure 16, p. 115, [131]), was based on this hypotheses, and yet proved insufficient to explain fully the aetiology of the disease, since these bacteria are often present at low levels and without causing disease in healthy individuals.

- *The ecological plaque hypothesis*, advanced in the 1990s, focused on the role of the oral environment in the development of periodontitis. [132] For long periods a healthy equilibrium may exist between bacterial communities and host defences, but this could be upset by a variety of environmental stresses: build-up of plaque due to lapsed oral hygiene, smoking, development of diabetes, stress or immunosuppression. The host may respond to local inflammation by producing protein-rich gingiva-crevicular fluid, which hands a selective advantage to proteolytic Gram-negative bacteria, which then leads to worse periodontal inflammation and destruction of bony tissue.

The concept of oral dysbiosis

The Polymicrobial Synergy and Dysbiosis (PSD) model, builds on the notion that particular organisms acting alone may cause periodontitis. However, it suggests that particular 'keystone

pathogens' may orchestrate wider changes in other bacterial phenotypes, transforming healthy oral microbial populations into pathological populations; for instance by conferring the ability to evade immune detection and cause persistent and tissue-destructive inflammation. [109] A key exemplar of this model is periodontitis associated with *Porphyromonas gingivalis* colonisation. *P. gingivalis* is a Gram-negative organism from phylum *Bacteroidota*, which was once thought to be a direct cause of periodontitis, after its introduction into non-human primates led directly to the development of disease. [133] However, it has since been demonstrated to be introduced into organisms without causing disease, for example into complement-deficient animals, [113] or into germ-free animals as a mono-culture without other bacterial species being present. [127] As a keystone pathogen, *P. gingivalis* does not cause disease itself, but possesses virulence factors to disrupt host defences and coerce otherwise 'beneficial' bacteria to induce periodontal inflammation.

A number of changes have been noted in sequenced bacterial populations from individuals with periodontitis compared to those from individuals with healthy periodontal tissues: an increase in alpha diversity, reduction in health-associated taxa (such as *Rothia* and *Veillonella* species), and an increase in pathogenic species including from phyla *Proteobacteria* and *Actinobacteria* [134, 135]. Together these changes have been termed dysbiosis, a concept which has generated public interest and entered the Oxford English Dictionary in 2018 defined as "an imbalance between the types of organism present in a person's natural microflora, especially that of the gut, thought to contribute to a range of conditions of ill health". [136]

Periodontal disease in CKD

The relationship of CKD and oral health is varied and complex. Many patients with CKD, particularly in advanced disease, complain of a range of oral symptoms including altered (often metallic) taste, halitosis, stomatitis and xerostomia. [137] Such oral symptoms may have implications for the quality of life, nutritional status and the general health of patients living with CKD. [138] Objectively, both in patients and experimental models, CKD has been shown to reduce salivary flow rates and alter salivary biochemistry, with increased concentrations of urea and creatinine and high oral pH. [139-141] Furthermore, some research suggests that patients with CKD may have limited access to dental care, and have poor oral hygiene routines. [142, 143]

CKD and periodontal disease

The most robust evidence available associates CKD with a high prevalence of gingival disease and periodontitis. One meta-analysis suggested that roughly 20% of dialysis patients have no teeth, and rates of PD were 56.8% in patients with stage 5 CKD and 31.8% in patients with milder forms of CKD. [137] Another meta-analysis found a similar, consistent association between CKD and periodontitis with an odds ratio of 1.65 compared to the general population. [144] Data from the Renal Impairment In Secondary Care (RIISC) cohort of 932 patients in the UK found that CKD patients had an odds ratio of 4.0 compared to community-matched controls for all forms of periodontitis and 3.9 for the severest form of the disease. [145] In the large National Health And Nutrition Examination Survey (NHANES) III dataset from the US, subjects

with all stages of CKD had a combined prevalence of periodontitis of 12.9% compared to 7.5% in subjects without CKD, and a trend was seen towards a dose-dependent increase in periodontitis rates in more severe stages of CKD that reached statistical significance in non-white populations. [146]

Association with cardiovascular mortality

There are well described associations in the general population between periodontitis and both cardiovascular disease and all-cause mortality. [147, 148] This association holds true in CKD, as CKD patients with periodontitis have an increased mortality compared to CKD patients without periodontitis, a deleterious effect similar in size to the effect of having diabetes as a comorbidity. [149] A similar increase in mortality in CKD patients with periodontitis compared to those without was found in a recent meta-analysis, although in this study, researchers did not establish a link with cardiovascular disease. [150] Furthermore, CKD patients with periodontitis have been shown to have higher levels of systemic inflammation and malnutrition compared to those with better oral health, [151, 152] and this systemic inflammatory milieu, driven by periodontal inflammation, oxidative stress and endothelial dysfunction, may account for some of the excess cardiovascular disease seen in the CKD patient population.

Potential mechanisms underlying the association between CKD and PD

Periodontal disease may arise in any patient due to a complex interaction between ***host factors, environmental and behavioural factors***, and ***bacteriological factors***. [115, 135] Each of these domains can be affected when an individual develops CKD, and each may drive the subsequent development or progression of periodontitis.

Host factors

Effects of uraemia on the oral environment

The flow rate and chemical composition of saliva play crucial roles in determining the oral microenvironment. Patients with CKD produce less saliva than controls with normal renal function, with an increase in salivary concentrations of both nitrogenous waste products (such as urea and creatinine) and electrolytes (including sodium, potassium, and phosphate), likely reflecting an overall increase in osmolality in keeping with a reduction in flow rate. [139] These changes have also been demonstrated in experimental models of uraemia. [141] Indeed, it has been suggested that salivary abnormalities including high pH and increased levels of urea and phosphate may protect patients with CKD against caries whilst predisposing them towards developing periodontal breakdown. [138, 153, 154]

Uraemia leads to increased urea levels in gingival crevicular fluid and significant increases in the salivary pH both in patients with moderate CKD [155, 156] and in those with advanced disease who are undergoing in-centre haemodialysis. [156-158] As an alkaline pH environment provides more favourable growth conditions for several periodontal pathogens (such as *Porphyromonas*

90

gingivalis, *Prevotella intermedia*, and *Fusobacterium nucleatum* [159]), these organisms may have an ecological advantage in the periodontal pockets of patients with CKD/ESRD. This conclusion is indirectly supported by the higher levels of salivary urea in patients with severe periodontal breakdown. [160]

Effects on bone

CKD - mineral and bone disorder (CKD-MBD) is the term used to describe a spectrum of skeletal, biochemical and extra-skeletal calcific abnormalities seen in the presence of CKD. [161] Key to the pathogenesis of the disorder is the inability of the failing kidney to hydroxylate inactive vitamin D (25-hydroxyvitamin D) into its active form calcitriol (1,25-dihydroxycholecalciferol). [162] This, along with impairment of renal phosphate excretion, systemic ionic hypocalcaemia and skeletal resistance to parathyroid hormone trigger homeostatic hormonal responses including elevation of parathyroid hormone (PTH), which is associated with increased bone turnover. PTH secretion can, over time, become autonomous, escaping normal negative feedback control. Fibroblast growth factor 23, which rises early in CKD, presumably in response to hyperphosphataemia, is a potent hypophosphaturic agent that causes loss of phosphate from bone, and also antagonises bone mineralisation. [163, 164] Bone tissue biopsies are rarely performed in routine clinical practice, with the management of CKD-MBD being based around maintaining serum calcium, phosphate, vitamin D, and PTH levels within target ranges. [165, 166] However, when biopsies are performed, high-turnover lesions with poor-quality bone mineralisation are the most common abnormalities seen in untreated patients; [167]

and low-turnover lesions associated with suppressed serum PTH levels being especially associated with aggressive treatment of elevated PTH. [168]

Several animal models of chronic uraemia have been optimized over a prolonged experimental period to allow the development of associated hyperparathyroidism to mimic human CKD-MBD. In these studies, periodontitis-associated loss of alveolar bone height and volume relative to controls was partially improved when dietary calcium was given to reduce PTH, suggesting that PTH may be involved in the aetiology of the alveolar bone loss. [169] Using a mouse model of chronic uraemia (induced by partial renal ablation), one study demonstrated a significant reduction in cortical alveolar bone height compared to sham controls; these changes were exacerbated by a high phosphate diet that drove up serum PTH. [170] Although human data on whether CKD-MBD affects the development of periodontal breakdown are sparse, a small study of 20 patients with CKD reported that hyperparathyroidism was associated with the enlarged facial bones in both women and men, possibly due to increased bone turnover. [171]

Effects on immune system function

Host immunity plays a crucial role in the development of periodontal breakdown, [172, 173] and abnormal immune system function underlies the familial associations of PD. Systemic uraemia affects the immune system by several mechanisms including (i) abnormal neutrophil activity, [173-175] (ii) increased oxidative stress, [176] (iii) impaired development and maturation of immune cells, [173] dysregulated cytokine release [177, 178] and defective barrier immunity. [53, 179]   This contributes to what has been described as "maladaptive, uncontrolled and persistent" inflammation in patients living with CKD, [180] who have been described as

simultaneously immunosuppressed (with infectious diseases being a key cause of morbidity and mortality) and systemically inflamed (which may contribute to chronic cardiovascular risk). [181]

In the specific context of periodontitis, the ability of neutrophils to enter gingival tissues to counter bacterial invasion has been well described as an important factor in maintaining gingival health, and patients with leukocyte adhesion deficiency-1 disease (which impairs neutrophil migration) develop aggressive and early-onset periodontal breakdown. [182] Similar changes in neutrophil function have been described in patients with CKD, with the effect of FGF23 being demonstrated to prevent neutrophil recruitment into inflamed tissue. [174] This suggests that similar defective immune responses may partially underlie the development of PD in patients with CKD.

Comorbidity

The leading cause of CKD globally is diabetes mellitus, which itself is strongly associated with the development of PD. [183] The relationship is complex, with poor diabetic control predicting increased risk of periodontitis, perhaps through impaired immune function; and treatment of PD causing improvement in glycaemic control, suggesting a bidirectional relationship. [184]

Hypertension can be a primary cause of CKD as well as being a secondary complication of disordered sodium homeostasis in patients with CKD from other causes. Hypertension has a complex association with PD, with a suggestion that microcirculatory changes in the gum that are present in hypertension may cause PD, alongside evidence that PD itself may cause hypertension as chronic inflammation leads to endothelial dysfunction and atherosclerosis. [185]

The treatment of CKD comorbidities may also cause PD, such as when inflammatory diseases of the kidney are treated with corticosteroids or other immunosuppressant medications which have been linked to increased incidence of PD. [186] Nutrition has also been linked to the aetiology of PD, [187] and with many patients with CKD following tightly controlled dietary advice to limit sodium, phosphate and potassium intake, it is possible that nutritional deficiency may also explain some of the excess rates of PD in the CKD population.

Environmental and behavioural factors

Social deprivation has been shown to associate with CKD, [188, 189] and similar factors have been shown to associate with poor oral health and the development of PD. [190, 191] Patients with CKD may struggle to maintain good oral hygiene routines, with one systematic review suggesting that a quarter of haemodialysis patients across a number of studies never brush their teeth. [137] The fact that patients on maintenance haemodialysis will generally attend the dialysis unit three times per week may limit their ability to engage with dental care.

Bacteriological factors

Alterations in the flow rate and composition of saliva in patients with CKD may impose a strong selective pressure on the oral microbiome and induce changes in community structure that may drive the development of periodontitis. Several studies have demonstrated abnormal oral bacterial communities in patients with CKD. A study that involved 77 U.S. participants (18 patients with CKD and 59 non-renal controls) has shown that CKD was associated with lower

abundances of health-associated taxa *Streptococcus* and *Veillonella* and increased abundance of the gram-negative taxon *Neisseria*; this, in turn, correlated with increased blood concentration of pro-inflammatory cytokines, such as IL-18. [192] Similarly, patients undergoing in-centre haemodialysis demonstrated increased bacterial diversity, higher abundances of disease-associated taxa (including genus *Neisseria* and the 'red complex' pathogen *Porphyromonas gingivalis*), and a reduction in some health-associated taxa, including *Rothia*, compared to non-renal controls. [193]

Hypothesis

Patients living with CKD have a high prevalence of PD [144, 145, 194], and it has been suggested by some that the association is explained by the chronic, low-level inflammation caused by PD driving progressive renal fibrosis. [149, 195]

However, there are several reasons to support the reverse view, that CKD may directly cause PD. Patients with CKD have abnormalities in the flow rate and biochemical composition of saliva [139, 140] which may alter the oral microenvironment and exert selective pressure on the oral microbiome. Furthermore, patients with CKD have marked abnormalities of bone metabolism [196] and immune system function [197] which may also be relevant to the development of PD.

We hypothesized that CKD may be a cause of PD, challenging current understandings of the association between these conditions, and that induction of dysbiosis of the oral microbiota may be a critical mechanism in this process.

Specific methods

Animal work

Chemically-induced uraemia in rats

The total cohort size was 18 rats. After a week-long period of acclimatisation, nine rats were started on the adenine-containing intervention diet whilst another nine were maintained on standard control diet. This diet was continued for four weeks, followed by a washout period of four weeks when all animals received the control diet, after which the animals were sacrificed. Oral swabs were taken from all animals at the point of maximal uraemia for those receiving the intervention diet (at the end of the 4-week period of adenine administration).

Surgically-induced uraemia in rats

The total cohort size was 24 rats. After a week-long period of acclimatization, fourteen underwent subtotal nephrectomy (SNx) and ten underwent sham procedures. Oral swabs to assess the microbiota were taken four weeks after the second stage of the surgical procedure, to parallel those taken in the chemically-induced uraemia protocol.

Additional rats for histological and salivary analysis

Thirteen additional rats were used to obtain saliva samples for subsequent analysis, and to undertake bone staining to assess the bone formation rate. These rats underwent SNx or sham

procedures as outlined above (n=6 sham surgery, n=7 SNx), and were otherwise housed identically to those in the 'Surgically induced uraemia in rats' protocol above. In their final week of life, 500µg calcein green (approximately 1mg/kg) was injected intravenously three times at 48h intervals. The following week induced saliva collection was carried out under terminal anaesthesia with ketamine/xylocaine. After full induction of anaesthesia, 1mg pilocarpine was injected into the peritoneum, with a further 1mg administered 5 minutes later if there was no salivary response. Saliva was then collected over the following 8 minutes using a 100mL pipette and 1.5ml Eppendorf tubes. Salivary volume was directly assessed by weighing the filled tubes and subtracting the weight of the tube itself. Salivary pH was directly measured using a pH meter and narrow-gauge probe (Mettler Toledo, Leicester, UK), before saliva was snap frozen in liquid nitrogen and transferred to a -80º freezer until the time of analysis.

Chemically-induced uraemia in mice

The total cohort size was 20 mice. After a week-long period of acclimatization, ten animals were placed on an intervention diet (RM1 with 0.15% adenine), whilst ten remained on standard RM1 diet. Oral swabs to assess changes in microbiota were obtained prior to starting the experimental protocol, and at 2 weeks, 6 weeks, 10 weeks, 14 weeks and 18 weeks after starting it. All mice were sacrificed 18 weeks after the start of the experimental protocol (at 26 weeks of age), after a 24-hour urine collection. Additional orals swabs were obtained prior to the time of sacrifice from four 'donor' animals in each group, for using in the 'oral microbial transfer' experiment described below. Additionally, soiled cage contents including bedding and droppings from the cages in which these donor animals were housed were frozen for further use as described below.

Oral microbial transfer in mice

Oral microbial transfer was carried out as described in chapter 2.

Animals were then maintained in ordinary individually-ventilated cages in an open area of the Biological Services Unit, with standard 12h light/dark cycles. They had unlimited access to standard RM-1 diet and tap water. Oral swabs were taken to assess the efficacy and durability of bacterial transfer at 3-weeks and 9-weeks after transfer in all animals, and all animals were then culled, after a 24-hour urine collection, at 18 weeks of age (10 weeks after transfer).

Laboratory methods

Measurement of alveolar bone height

Heads were removed and jaw specimens obtained from all animals using a guillotine and sharp dissection with scissors. Alveolar bone height was measured using a morphometric method previously demonstrated to have equal reliability to radiological [198] and histological techniques. [199] After any samples (typically mandibles) required for conventional histology, micro-CT or scanning electron microscopy were removed, skulls were chemically defleshed by incubation in the protease-based detergent Terg-a-zyme ® (Sigma-Aldrich, UK), for 48 hours at 55°C, with remaining soft tissue being removed mechanically after this. Photographs were obtained using a 20x magnification dissecting microscope, and multiple measurements were made of the distance between the cemento-enamel junction and the alveolar bone crest using

ImageJ software, [200] as outlined by Baker and colleagues, [201] although without the use of blue dye. Bone height was measured over the lingual and buccal surfaces of molar roots, and a composite measurement for each animal was calculated. These figures are expressed relative to the average bone height in control animals, with significance assessed using Student's t-test with Welch's correction for unequal variances.

Light microscopy

Tissues removed prior to de-fleshing were fixed in formalin, decalcified using 10% formic acid and then embedded in paraffin. Each jaw was sectioned in frontal buccolingual orientation using a microtome (5 mm) and mounted on charged glass slides. Every tenth section was stained by haematoxylin and eosin using an automated slide processor, and then photographed using a Nikon Eclipse 80i Stereology microscope using 4/0.13 and 10/0.45 objective lenses.

Immunohistochemistry

Neutrophils and IL-17 were detected using primary antibodies (Abcam, Cambridge, UK) and anti-rabbit (PK-6101) secondary antibody (Maravai LifeSciences, San Diego, US). Sections were then viewed and photographed using the same microscope and lens as used for light microscopy of the H&E stained slides.

Scanning electron microscopy

This was used to assess for qualitative differences in the growing surface of periodontal bone between control and uraemic animals. Samples were transported in 70% ethanol to the Dental Physical Sciences unit at the Mile End Campus, QMUL. Samples were rendered totally anorganic by treatment with 7% available chlorine sodium hypochlorite bleach for 3 weeks to remove all residual soft tissue. This treatment completely removes the periodontal ligament so that the teeth could by removed manually to expose the surface of the alveolar bone. All SEM imaging was done using 20kV accelerating voltage and a solid state backscattered electron (BSE) detector, using a chamber pressure of 50Pa.

Confocal scanning light microscopy

Samples in 70% ethanol from calcein-injected animals were embedded in polymethyl methacrylate (PMMA), and blocks were cut and polished to produce flat surfaces before being used for confocal scanning light microscopy (CSLM). This was carried out at the Rockefeller Building, Division of Biosciences, University College London using a Leica SPE confocal system with an inverted microscope. The PMMA blocks were cover-slipped with glycerol. Objectives used were 10/0.45, 20/0.75 and 63/1.3 oil. Images were analysed using ImageJ software and a measure of the daily rate of dentine and bone formation calculated at the incisor root and lower mandibular border, respectively. The bone formation rate (BFR) was calculated using the formula BFR = MAR * (MS/BS) as suggested by the ASBMR Histomorphometry Nomenclature Committee [202], where the Mineral Apposition Rate (MAR) was calculated by

dividing the distance between the innermost and outermost calcein bands (given 96h apart) by 4, and the Mineralizing Surface (MS) and Bone Surface (BS) were measured directly using ImageJ.

Micro CT

This was carried out on samples embedded in PMMA, to assess bone mineralisation and the quality of bone produced between control and uraemic rats. Samples were scanned on the MuCAT2 micro-CT system designed and operating in the Dental Physical Sciences unit at the Mile End Campus, QMUL. The samples were scanned at 90kV & 180uA at 20 or 22um voxel size. Reconstruction was performed with GPU accelerated filtered Feldkamp back-projection algorithm and the grey-level data was calibrated to linear attenuation coefficient at 40 keV using a multi-material calibration carousel and X-ray modelling software. [203] Quantification of bone mineral density was carried out by assessing the mean linear attenuation coefficient of 20 tagged regions with a radius of three pixels in three dimensions at each tagged location and a calibration voltage of 27.5keV.

Analysis of microbiota

This was carried out using both culture and non-culture dependent methods, as described previously. Additional in vitro culture work to determine the urease activity and urea tolerance of all cultured organisms was carried out as described in appendix 2 (from p. 351). Statistical methods for culture and sequencing data are as described in appendix 2 (from p. 348).

Quantification of salivary urea

A colorimetric detection kit for urea nitrogen (ThermoFisher Scientific) was used according to the manufacturer's instructions. Samples of saliva were processed at 1:2 and 1:20 dilutions and the mean concentration using both dilutions in duplicate was accepted. Corresponding serum samples were analysed using the same kit but at 1:20 and 1:40 dilutions to allow comparison.

NMR spectroscopy of saliva

Saliva samples were diluted with buffer containing trimethylsilylpropanoic acid (TSP) and analysed on an NMR spectrometer (Bruker) operating at 600.22 MHz ^{1}H frequency at Imperial College London as per the experimental and statistical methods described in chapter 2.

Specific statistical methods

Statistical analysis of bone height data

All data for loss of periodontal bone height was found to be normally distributed when assessed by the Shapiro-Wilk test. All testing for significance of difference between two groups was carried out using Student's t-test with Welch's correction for unequal variances, in GraphPad Prism or Microsoft Excel.

Analysis of effect of housing on microbiology and bone height

Two-way ANOVA was carried out in GraphPad Prism to define the significance of the different levels of bone loss (dependent variable), according to both housing and treatment class (independent variables) in the surgically-induced uraemia experiment. No comparable analysis was carried out for the chemically-induced uraemia protocol because it was impossible to vary the housing since all animals in a single cage received the same diet.

Analysis of urea tolerance

Figure 36 (p. 135) plots the proportional increased average growth per sample in uraemic vs control animals, calculated as (mean growth in uraemic animals / mean growth in controls) where the mean growth in uraemic animals was higher than that in controls; and as (mean growth in controls / mean growth in uraemic animals) where the mean growth in controls was higher. Linear regression was used to draw a line of best fit between the mean inhibitory concentration of urea and the relative competitiveness of different isolates in control vs uraemic animals; standard settings in GraphPad Prism were used to accomplish this and Prism software was used to calculate the slope and the significance of its gradient.

Data availability

Raw sequencing data from all samples has been uploaded to the Sequence Read Archive (SRA) of the National Centre for Biotechnology Information (NCBI,

Results

Experimental uraemia causes periodontal bone loss in rats

Chronic uraemia was induced in male Wistar rats using two protocols: chemically-induced uraemia (using adenine-containing feed) and surgically-induced uraemia (using subtotal nephrectomy, SNx). Examination of de-fleshed heads revealed that uraemic animals generated using both experimental protocols displayed significantly more periodontal bone loss than controls after an eight-week period of uraemia (an average of 0.113mm less alveolar bone height relative to controls, $p<0.0001$, Figure 17, p. 116, supplementary Table 11, p. 397 in appendix 5). Representative images from defleshed jaws reveal that whilst control animals had some degree of periodontal bone loss, in the uraemic animal this was so severe that it was actually possible to see a clear gap between the bottom of the tooth and the alveolar crest (Figure 18, p. 117).

Histological examination of representative samples confirmed a greater distance between cemento-enamel junction and alveolar bone ridge in the uraemic than control. Despite this, there was only modest evidence of overt inflammatory change, in contrast to periodontal disease seen in humans. Higher magnification images in the uraemic specimen revealed subtle changes in keeping with inflammatory periodontal disease, including an aggregation of neutrophils and early migration of the junctional epithelium compared to images from the control animal (Figure 19, p. 118).

Immunohistochemistry revealed significant staining for IL-17 which co-localized with staining for neutrophils in areas deep within the alveolar bone in uremic specimens, (Figure 20, p. 119) suggesting their possible involvement in reabsorption of bone.

Micro-computed tomography demonstrated abnormalities of bone formation in uraemic specimens, with a non-significant trend towards reduced mineral density (the linear attenuation coefficient in bone just below the alveolar bone crest was $1.604cm^{-1}$ in controls and $1.547cm^{-1}$ in uraemic animals, p=0.069; and at sites deeper within the mandibular bone was $1.658cm^{-1}$ in controls and $1.621cm^{-1}$ in uraemic animals, p=0.271, Figure 21, p. 120).

Scanning electron microscopy of the surface of alveolar bone facing the periodontal ligament revealed a smooth surface almost bereft of Sharpey's fibres in uraemic animals, in contrast to the normal, 'spiky' bone appearance in controls, suggestive of a failure of bone growth at this surface in uraemic specimens (Figure 22, p. 121).

To evaluate systemic features of chronic uraemia that may affect periodontal bone formation, we measured serum concentrations of parathyroid hormone (PTH), calcium and phosphate. There was no difference in serum PTH concentrations between control and uraemic animals (serum

PTH 16.95pg/ml in controls vs 12.37 in uraemic animals, p=0.251, Figure 23, p. 122), or in serum calcium (2.58mmol/L in controls vs 2.586 in uraemic animals, p=0.841) or phosphate (2.19mmol/L in controls vs 2.107 in uraemic animals, p=0.254, Figure 24, p. 123).

To assess global rates of bone and tooth formation, samples from animals injected with three doses of 1mg/kg calcein green at 48 hour intervals the week prior to sacrifice were assessed by confocal microscopy to calculate the daily rate of bone and tooth formation (Figure 25, p. 124). There were no differences between groups in the rate of dentine formation in the incisor root ($14.78\mu m^3/\mu m^2/d$ in sham operated controls vs $15.69\ \mu m^3/\mu m^2/d$ in SNx, p=0.517), or of bone formation at the lower mandibular border ($4.249\mu m^3/\mu m^2/d$ in controls vs $3.562\mu m^3/\mu m^2/d$ in SNx, p=0.397), Figure 26, p. 125.

Uraemia is associated with oral dysbiosis

Oral swabs were assessed using both bacterial culture and next generation sequencing of the 16S rRNA gene amplicon to assess the effect of experimental uraemia on the oral microbiota. The parallel use of these complementary techniques allowed for evaluation of total bacterial abundance, in vitro testing of individual bacterial isolates for their tolerance of high-urea environments as well as completing a thorough survey all members of the oral microbiota, and not just those which are readily cultured.

Lower total bacterial counts after 48 hours of incubation under both aerobic and anaerobic conditions were seen in samples from uraemic animals ($\log_{10}$ 6.07 cfu/ml transport medium in controls vs 5.80 in uraemic animals, p=0.034, Figure 27, p. 126); partly accounted for by

substantially reduced total counts of the most abundant phylum, *Firmicutes* ($\log_{10}$ 5.88 cfu/ml in controls vs 5.42 in uraemic animals, p=0.043).

Conversely, absolute counts of Gram-negative phylum *Proteobacteria* were non-significantly higher in uraemic animals than in controls ($\log_{10}$ 4.12 cfu/ml in controls vs 4.55 in uraemic animals, p=0.151), which in the context of reduced overall counts in these animals meant that these uraemic animals had significantly higher proportional abundances of *Proteobacteria* (9.53% vs 2.99% of total cultured bacteria, p=0.003, Figure 28, p. 127).

At genus level, uraemic animals demonstrated lower counts of both the most abundant genus *Streptococcus* ($\log_{10}$ 5.56 cfu/ml in controls vs 5.05 in uraemic animals, p=0.017), and the second most abundant genus *Rothia* ($\log_{10}$ 5.56 cfu/ml in controls vs 5.23 in uraemic animals, p=0.022). Conversely, samples from uraemic animals displayed higher growth of a number of minor taxa compared to control samples, which reached significance for the genus *Acinetobacteria* ($\log_{10}$ 3.79cfu/ml in uraemic animals, absent in controls, p=0.006, Figure 29, p. 128).

Next-generation sequencing of the 16S rRNA gene amplicon was used to confirm the pattern seen in the cultural analysis. Proportional abundances of different phyla plotted for each sample showed a similar decrease in *Firmicutes* and an increase in Gram negative phyla *Proteobacteria* and *Bacteroidetes* in samples from uraemic animals, with *Proteobacteria* accounting for 22.6% of reads in uraemic animals vs 12.5% in controls, p=0.002. Corresponding to the described reductions in major taxa and increases in minor ones in uraemic animals, oral communities from uraemic animals were found to have higher alpha diversity (signifying more diverse oral

communities) than in control animals when measured using the Simpson Index (0.75 in controls vs 0.82 in uraemic animals, p=0.045, Figure 30, p. 129).

Ordination plots for all samples revealed that the most significant source of variation was between shipment batches (different batches from the same vendor were used in each experiment). However, when ordination for each experiment was plotted separately, there was indeed differential clustering between control and uraemic animals, with Permutational Analysis Of Variation (PerMANOVA) assessing the significance of separation according to uraemia proving significant for the surgically-induced uraemic protocol (R_2=0.147, p=0.012) but not in the chemically-induced uraemia protocol (R_2=0.112, p=0.184, Figure 31, p. 130).

Co-housing alters bacterial communities and affects the severity of periodontal disease

The surgically-induced uraemia protocol allowed us to investigate the influence of either housing uraemic rats singly (with uraemic animals), or in mixed cages (uraemic animals with healthy, sham-operated, controls). The caging strategy is illustrated in Figure 32, p. 131.

The uraemic animals that were housed in mixed cages alongside controls developed less periodontal bone loss than those housed only with other uraemic animals. Two-way ANOVA confirmed that whilst treatment class had the biggest effect on bone loss in these animals (accounting for 77% of variance, p=0.001), the contribution of housing also proved significant (6.7% of variance, p=0.014). A simple t-test comparing the degree of bone loss between co-housed and singly housed uraemic animals confirmed that the mixed-cage uraemic animals had

significantly less bone loss than those that were singly housed with other uraemic animals (mean bone height -0.149mm compared to mean of control animals in those that were singly housed, and -0.109mm in those that were mixed-housed, p=0.038), Figure 33, p. 132.

An ordination plot based on 16S gene sequencing demonstrated that mixed-housed animals had an intermediate microbial profile between the singly-housed control and uraemic groups. Two-way ANOVA carried out for the first two principal components revealed that housing significantly affected clustering in component 2 (19.86% of variance, p=0.043), although to a lesser extent than treatment class (25.84% of variance, p=0.024). Only treatment class significantly affected principal component 1 (treatment 28.48% of variance, p=0.0196; housing 0.02% of variance, p=0.94, Figure 34, p. 133).

Uraemia alters salivary biochemistry in rats which may explain the observed oral dysbiosis

To assess whether alterations in saliva following the induction of uraemia might be responsible for the differences in oral microbiology, induced saliva samples were obtained using pilocarpine administration to rats under terminal anaesthesia.

There were no differences in either the flow rate or pH of induced saliva (supplementary Table 12, p. 398, appendix 5), however uraemic animals were found to have significantly higher concentrations of salivary urea (in proportion to an increase in serum urea) when measured by colorimetric analysis (1.62mmol/l in controls vs 3.73mmol/l in uraemic animals, p=0.007, Figure 35, p. 134).

Untargeted proton Nuclear Magnetic Resonance spectroscopy (^{1}H-NMR) was performed to characterize biochemical perturbations associated with uraemia and assess the functionality of the altered microbiota. Salivary concentrations of acetate were 27% lower in uraemic animals compared to controls (122.19 relative units in controls vs 89.11 in uraemic animals, p=0.013), and concentrations of lactate 47% lower (although this did not reach significance, 116.81 vs 61.35 relative units, p = 0.056). Results for other salivary metabolites are listed in supplementary Table 13, p. 399, appendix 5.

In vitro testing was carried out on all bacterial isolates from the cultured analysis, that had been deep frozen in pure colonies after initial isolation and identification. There was a positive association between the observed growth of an isolate in uraemic animals relative to controls and the mean inhibitory concentration of the isolate for urea. Linear regression was used to calculate a line of best fit, which proved to be significantly different from horizontal (slope 0.34, p=0.046), confirming a positive correlation between urea tolerance and the observed abundance of the isolate in uraemic animals relative to controls, Figure 36, p. 135.

Using Christensen's urea agar we demonstrated that urease producing organisms were better-represented among urea-tolerant groups, a trend which did not prove significant (urease positive organisms accounting for 14.1% of bacterial growth in uraemic animals and 8.6% in controls, p=0.32).

Uraemia induces periodontal bone loss and progressive oral dysbiosis in mice

In order to ensure that these results were not rodent species-specific, experimental uraemia was induced in wild-type male C57BL/6 mice using a slowly progressive model of chemically-induced uraemia. As in rats, uraemic mice displayed increased periodontal bone loss (-0.02mm relative to the mean of controls, p=0.0005, Figure 37, p. 136; supplementary Table 14, p. 401, appendix 5).

Oral swabs were taken every four weeks during the experimental period, and next generation sequencing of the 16S rRNA gene amplicon revealed progressive changes in samples from uraemic animals, characterized by increased heterogeneity between samples, and progressively differential clustering on principal component analysis. Significant differences in clustering as measured by PerMANOVA emerged between control and uraemic microbiotas at 10 weeks into the experimental period (roughly co-incident with the development of significant differences between control and uraemic animals in weight, suggestive of clinical uraemia, which first became apparent at 9 weeks into the experimental period). These changes persisted at 14 weeks, but after 18 weeks of experimental diet, uraemic animals exhibited such significant within-group differences meaning that although there was still a marked separation between the clustering of uraemic vs control samples on visual inspection of PCA plots, this did not quite reach significance when assessed using PerMANOVA (R^2 = 0.134, p=0.066). Quantification of population variances using permutational analysis of multivariate dispersions (PERMDISP) confirmed that samples from uraemic animals became progressively heterogeneous as uraemia increased (average distances to median being 6.78 in controls and 18.31 in uraemic animals by 18 weeks, p=0.012, Figure 38, p. 137).

The ANalysis of Composition of Microbiomes (ANCOM) methodology was used to identify amplicon sequencing variants (ASVs) that were differentially abundant between groups after correction for multiple hypothesis testing. All ASVs more abundant in controls were from the dominant phylum *Firmicutes*, whilst those increased in uraemic animals represented a diverse range of organisms from phyla including *Actinobacteria* and *Proteobacteria*, and included ASVs representing organisms (such as from genus *Psychrobacter*) that have previously being implicated in the development of PD in animals [204].

Periodontal disease can be transmitted by oral microbial transfer into healthy germ-free mice

We assessed the causative role of bacterial dysbiosis in PD by carrying out oral microbial transfer (OMT) from control and uraemic donor mice into germ-free animals. The design of this experiment is described in Figure 39, p. 138.

Germ-free mice receiving OMT from uraemic mice developed substantially more periodontal bone loss than those receiving OMT from control mice (-0.042mm to the mean in control recipients, p<0.001, Figure 40, p. 139; supplementary Table 15, p. 402, appendix 5).

The success of OMT was formally assessed by differential clustering on an ordination plot, Figure 41, p. 140, and using PerMANOVA. This revealed that transfer of the uraemic microbiota accurately established the donor microbiota in recipient animals (non-significant differences between donors and recipients, $R^2 = 0.12$, p = 0.158); that although control recipients visually clustered with control donors, there did exist significant differences between these groups ($R^2 =$

0.196, p = 0.023); but that by far the largest differences existed between uraemic and control recipient microbiotas, similar to the difference between uraemic and control donors (R^2 = 0.233, p <0.001).

Recipients of oral microbial transfer were found to have stable microbial communities that persisted at three and nine weeks after transfer, and which appeared to represent exaggerations of the features of the control and uraemic microbiota seen in both the donor mice and in the previously described rat and mouse experiments. Thus, at 9 weeks, recipients of uraemic microbiota demonstrated reduced bacterial counts ($\log_{10}$ 6.2cfu/ml in control recipients vs $\log_{10}$ 5.32 in uraemic recipients, p<0.001), markedly increased alpha diversity (Simpson Index 0.24 in control recipients vs 0.94 in uraemic recipients, p<0.0001), and differential clustering on ordination plots, in a similar but more extreme direction to the donor communities.

Microbiotas from control recipients were heavily dominated by bacteria from phylum *Firmicutes*, whilst microbiotas from uraemic recipients displayed heterogenous oral microbial communities including high prevalence of various phyla including *Firmicutes*, *Actinobacteria*, *Proteobacteria*, *Bacteroidetes* and *Cyanobacteria* (Figure 42, p. 141).
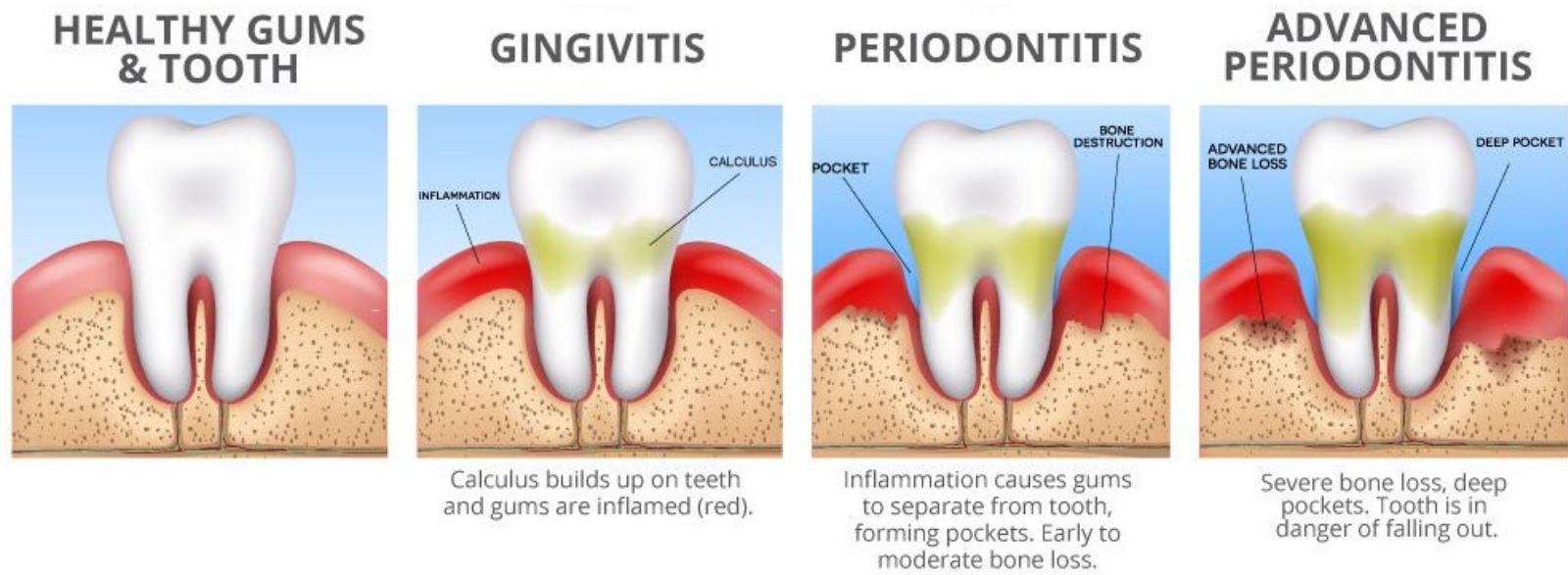
Figure 15: The stages of gum disease. Taken from https://dentalclinicraipur.com/periodontal-disease-gum-disease-2, accessed 19th January 2022.
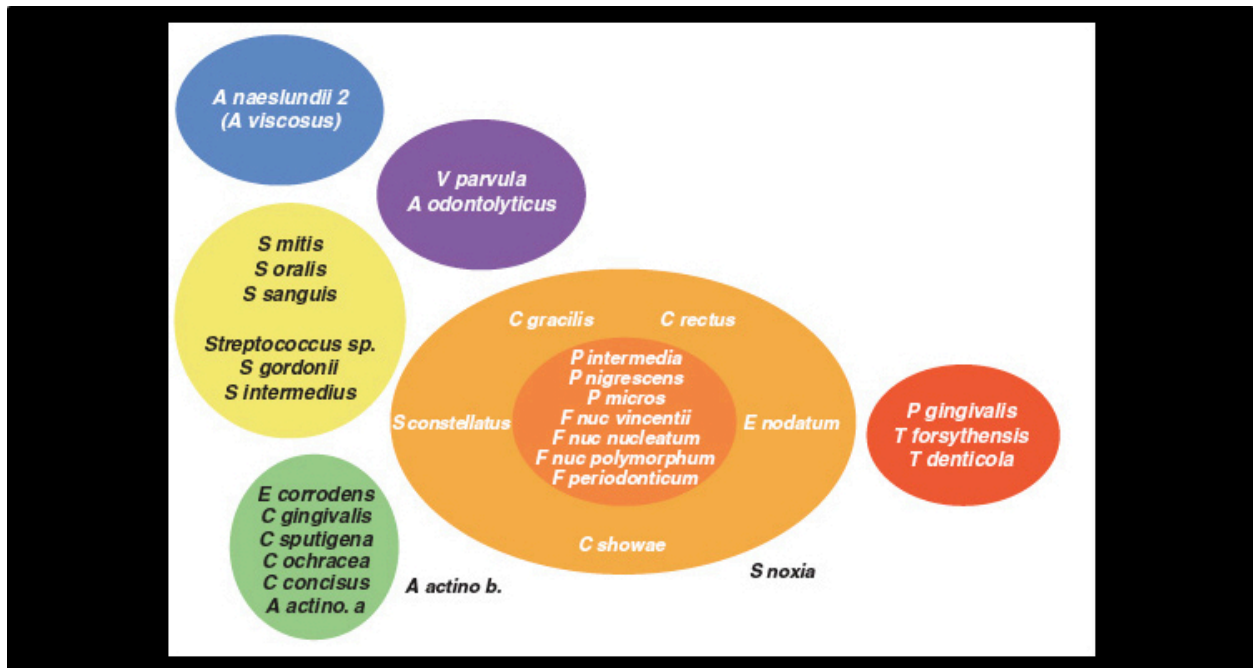
Figure 16: Microbial complexes in subgingival biofilm. Organisms in the red and orange complexes have been particularly associated with the development of periodontal disease. Adapted from Socransky et al, 1998, [131].
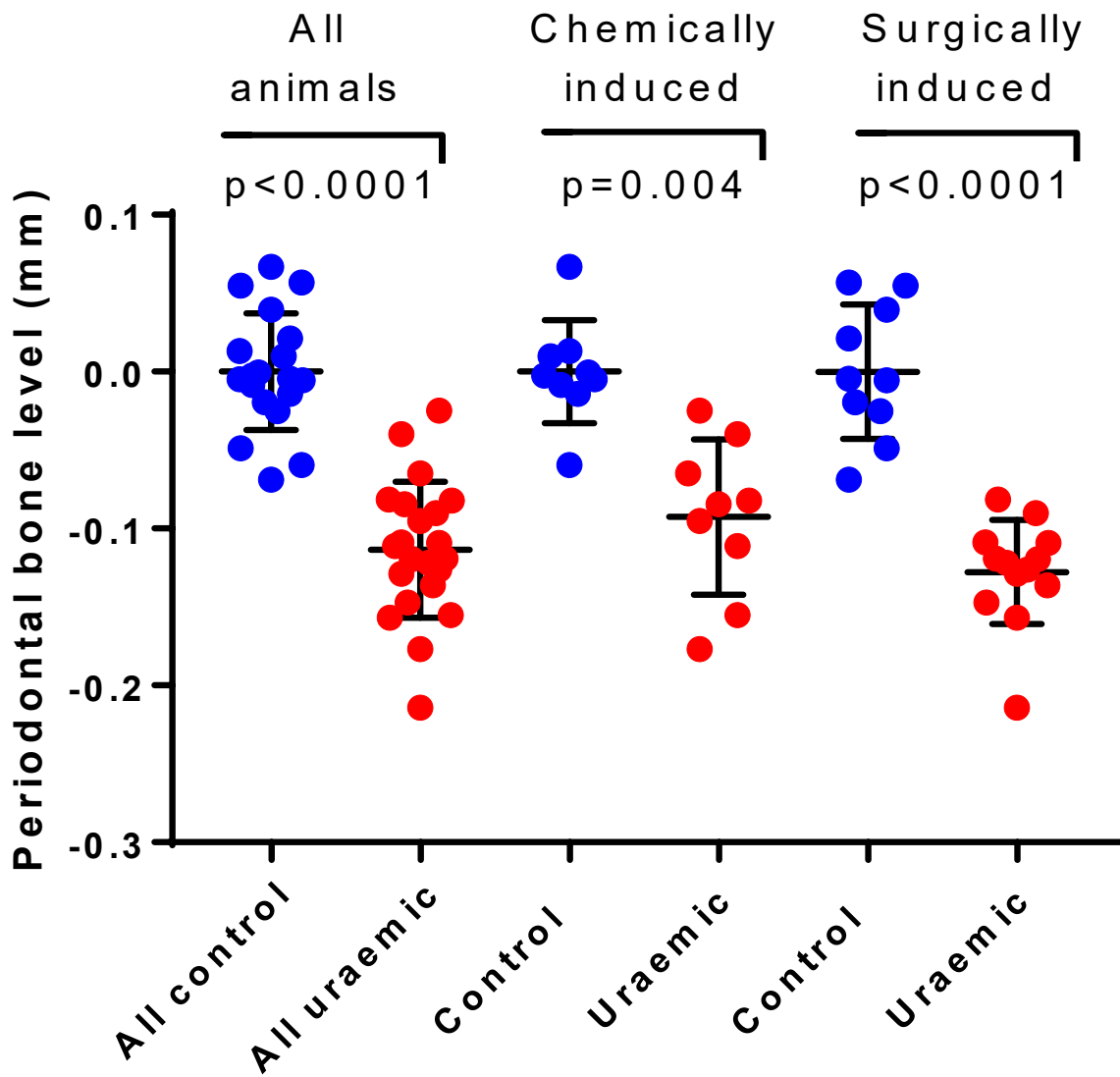
Figure 17: Distance between the cemento-enamel junction and alveolar bone crest measured using a dissecting microscope. Each point represents the average of multiple measurements over the buccal and lingual surfaces of all molar roots in a single rat, expressed relative to the average amount of bone loss in all control animals.
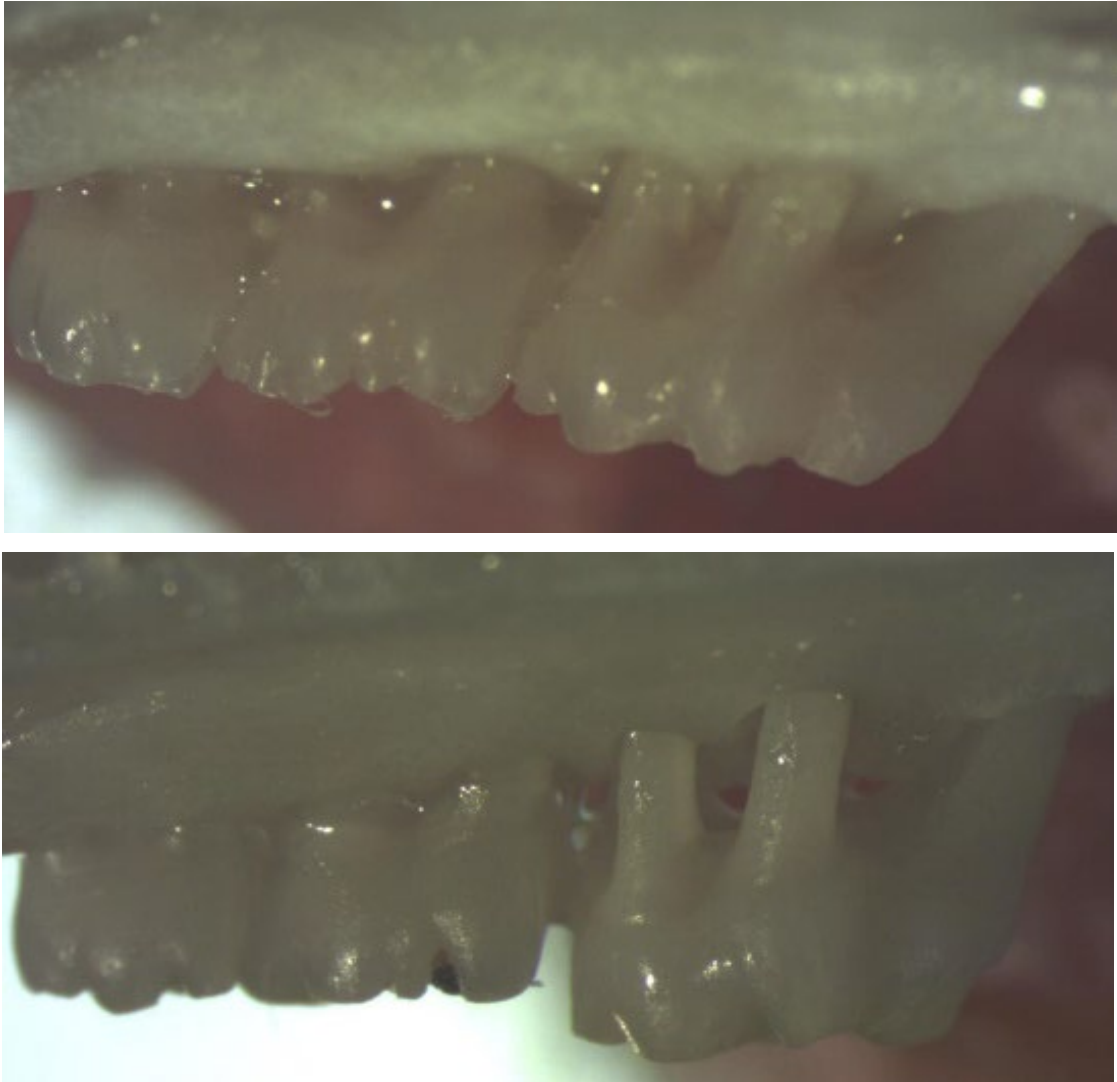
Figure 18: Representative images showing greater loss of maxillary alveolar bone in a uraemic animal (bottom) compared with a control animal (top), visualised using a dissecting microscope at 20x magnification. The loss of alveolar bone is so significant in the uraemic animal that a clear gap can be seen between the underside of the tooth and the bone crest between some of the roots.

CONTROL   **URAEMIC**
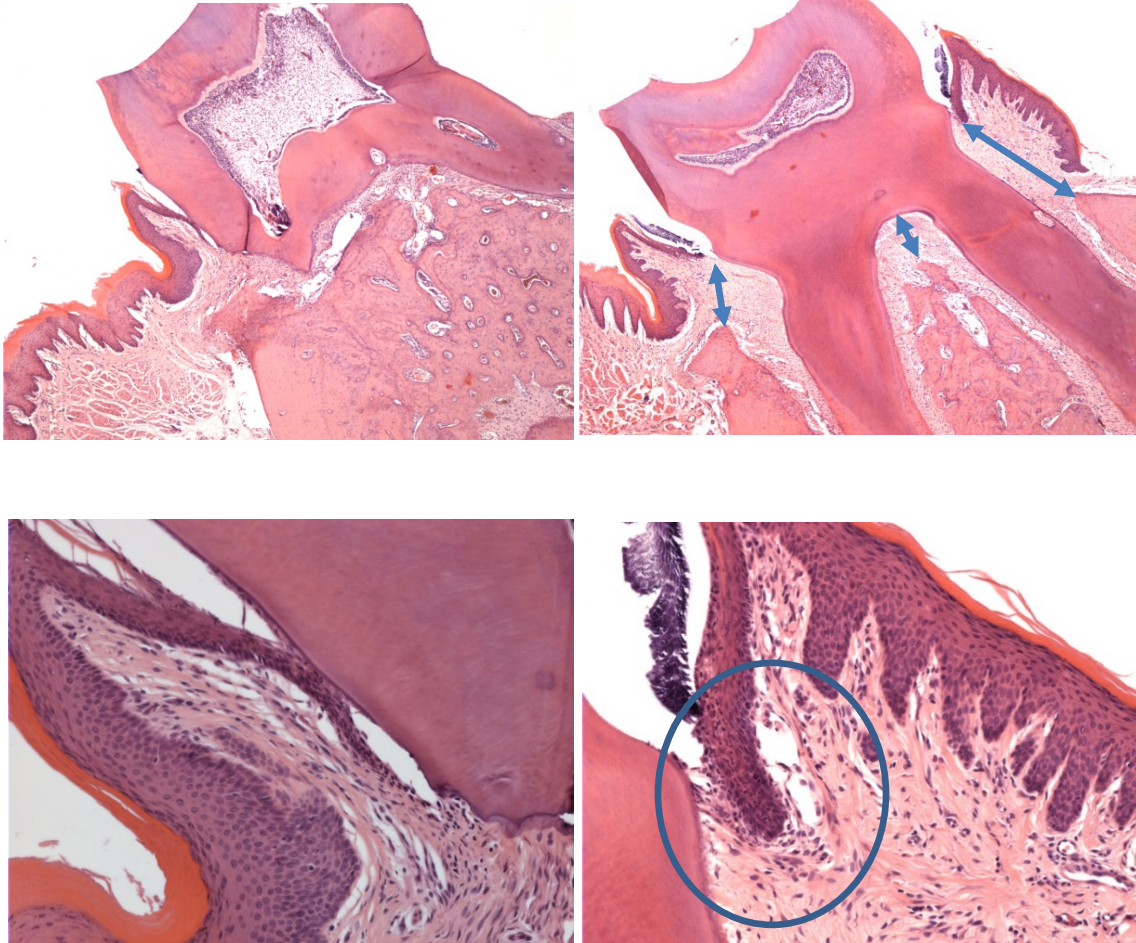
Figure 19: Light microscopy of haematoxylin and eosin (H&E) stained slides of periodontal tissue. Top panels: using a 4x objective lens. The blue arrows indicate the loss of bone height in the uraemic specimen. Bottom panels: using a 40x objective lens. The highlighted region in the uraemic specimen reveals neutrophil aggregation and early downwards migration of the junctional epithelium.

Control

Uremic

Uremic

Uremic
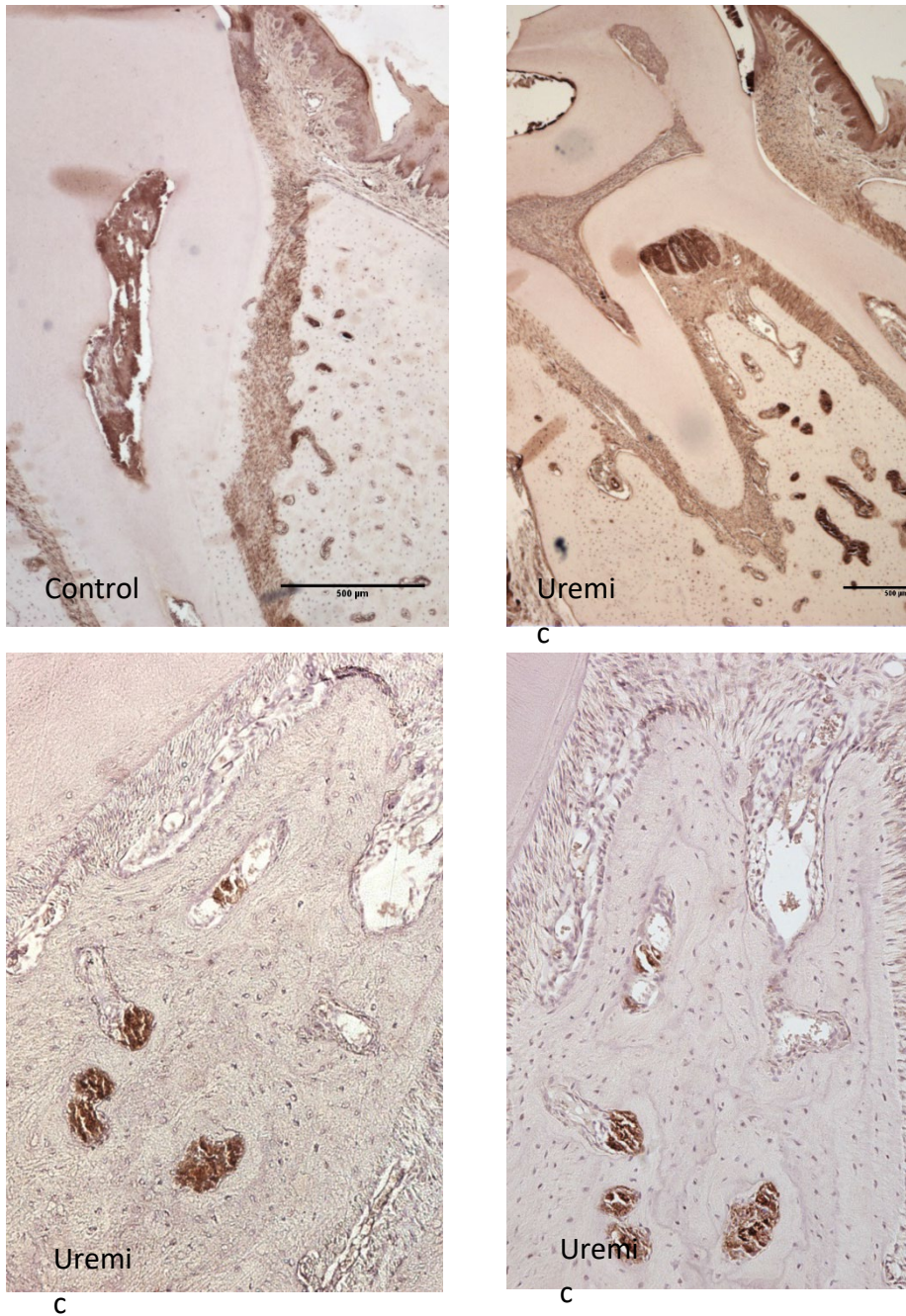
Figure 20: Immunohistochemistry of rat mandible. Top panels: staining against IL-17 is increased in the mucosa and in regions of reabsorption deep within the periodontal bone in the uraemic sample; 4x objective lens. Bottom panels: staining against IL-17 (left) and neutrophil defensin 4 (right) in the uraemic specimen shows co-localisation of these antigens in areas of bony reabsorption; 40x objective lens.
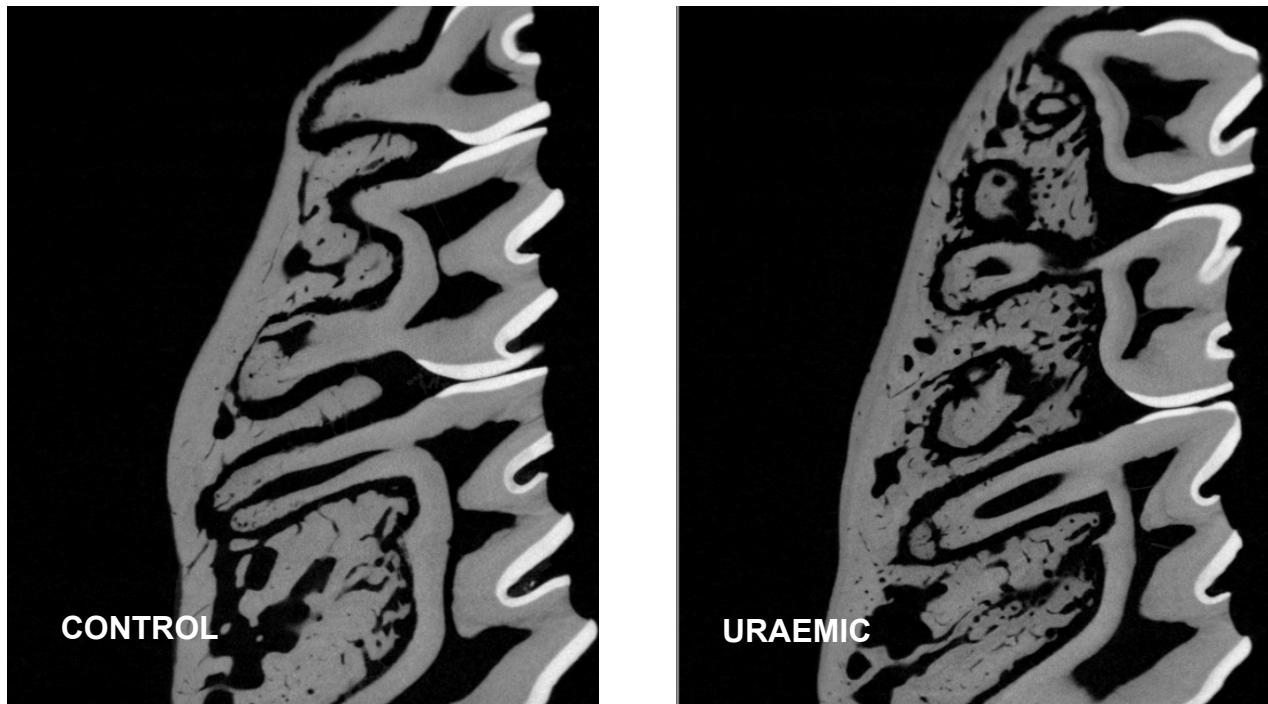
Figure 21: Micro-computed tomography in the para-sagittal plane through the molar roots. There is a paucity of mandibular bone mineralisation and ragged bone edge in the uraemic specimen. Analysis was carried out of the bone mineral density at a selection of sites within the deep and superficial periodontal bone; there was a trend towards reduced mineralisation in uraemic animals which did not reach significance.
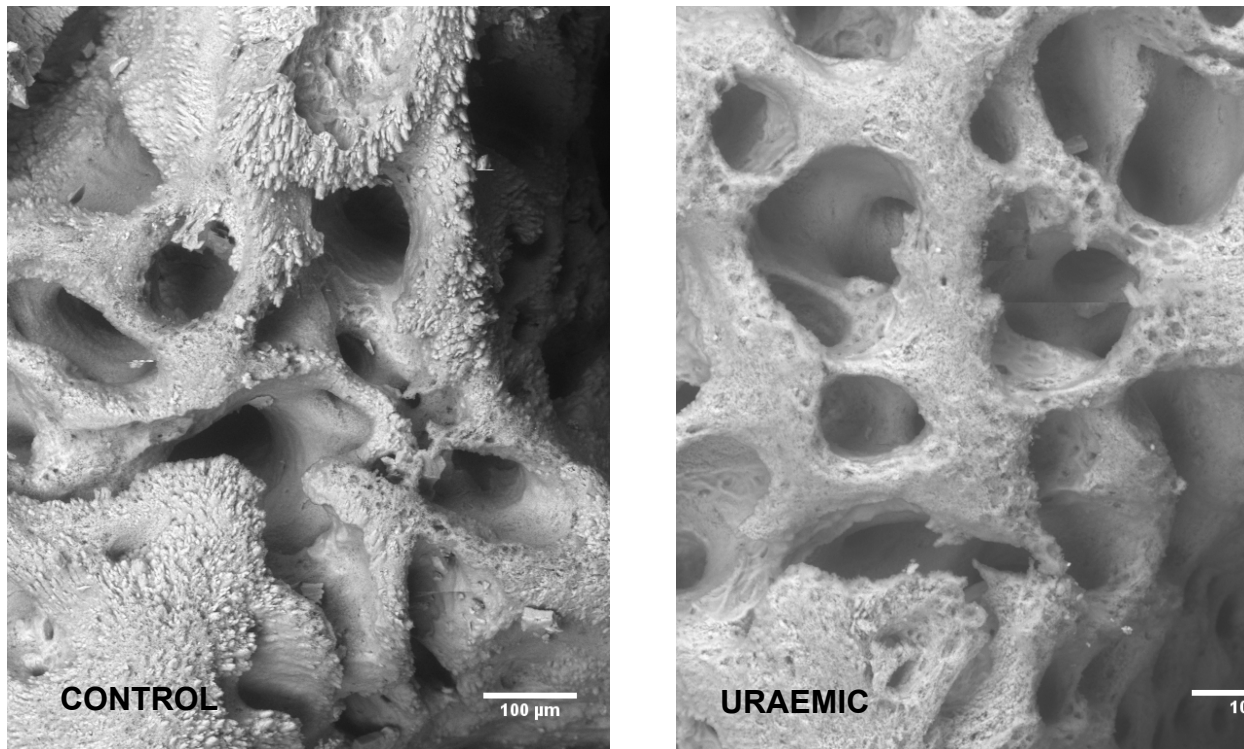
Figure 22: Scanning electron microgram of the surface of alveolar bone facing the periodontal ligament and tooth roots in macerated specimens. The smoother appearance of the bone surface in the uraemic animals reflects reduced mineralisation in Sharpey fibres (composed of type III collagen) at the growing surface of the bone.
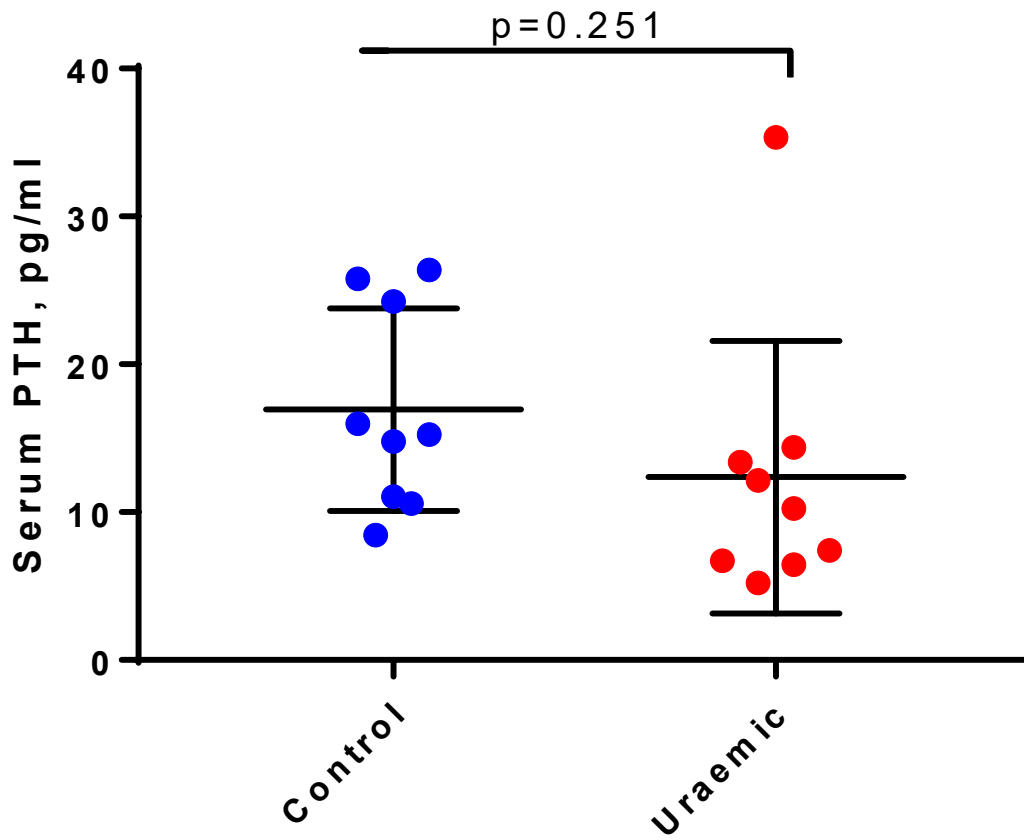
Figure 23: Serum parathyroid hormone (PTH) concentration in control and uraemic rats at the time of sacrifice using the chemically-induced uraemia protocol. Significance is assessed using Student's t-test with Welch's correction.
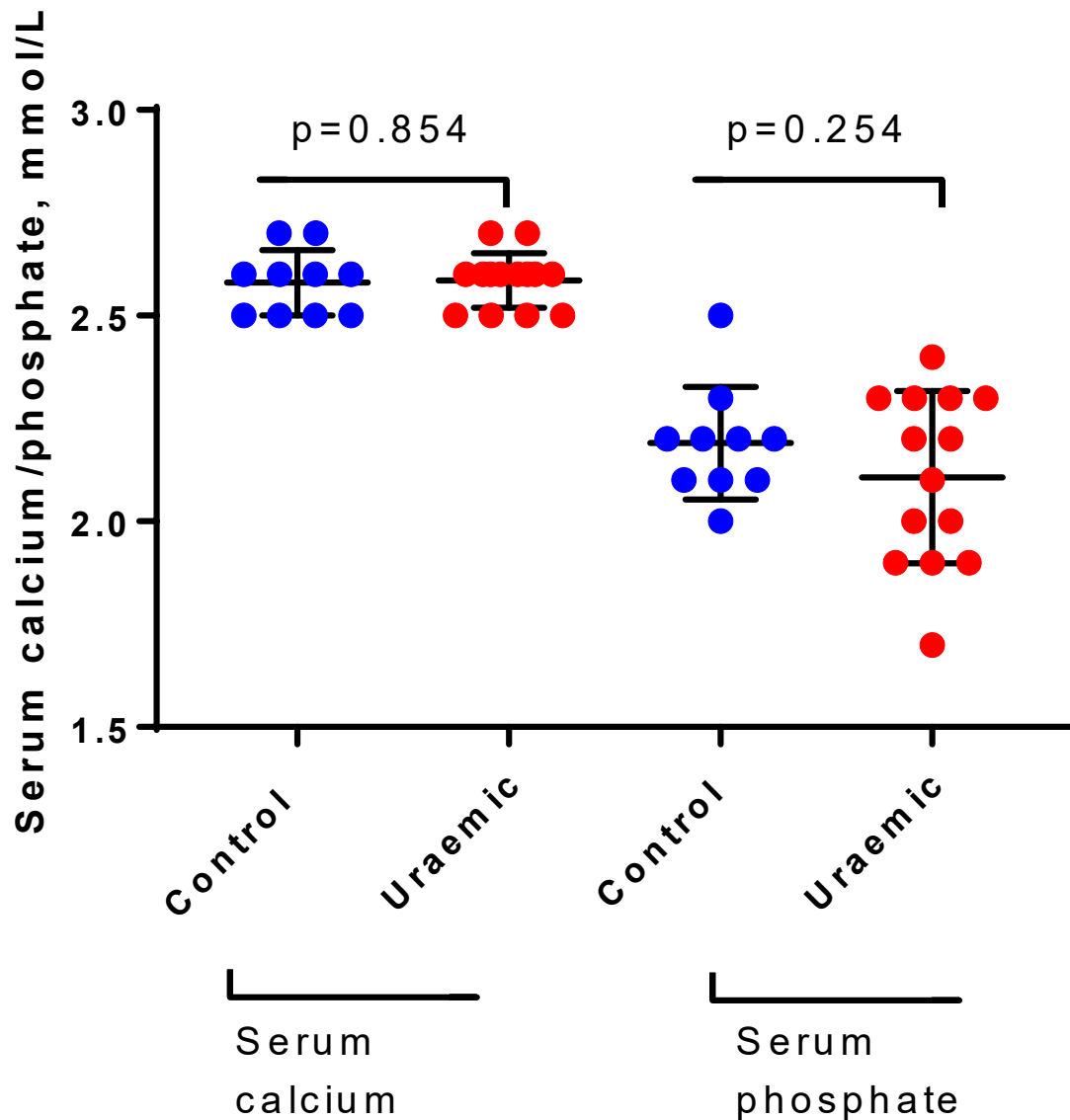
Figure 24: Serum calcium (left) and phosphate (right) in control and uraemic rats at time of sacrifice according to the surgically-induced uraemia protocol. Significance is assessed using Student's t-test with Welch's correction.
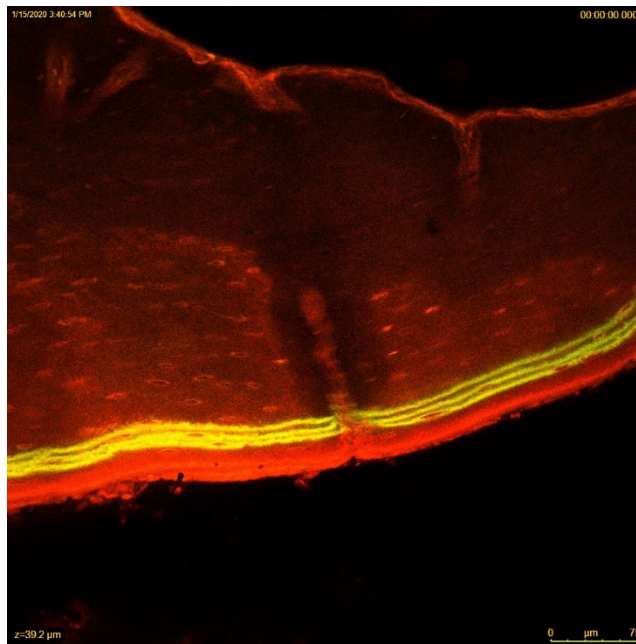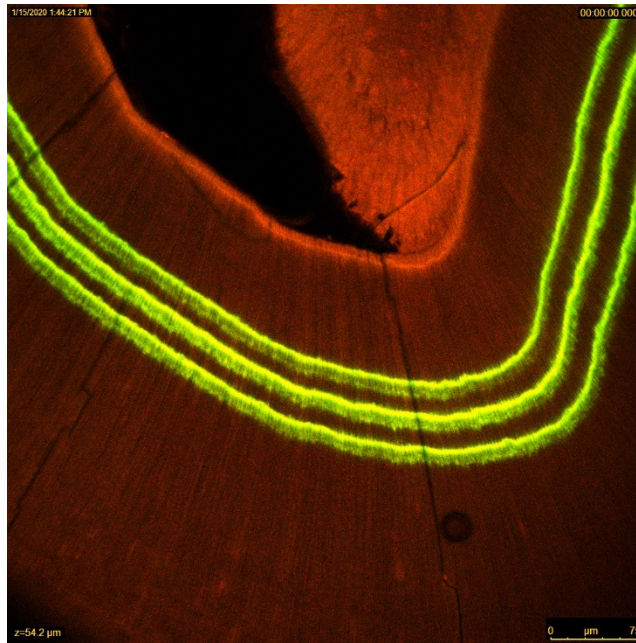
Figure 25: Confocal scanning light micrographs of calcein-green injected rats, used to calculate incisor dentine formation rate and bone formation rate at the insicor root (top) and lower mandibular border (bottom).
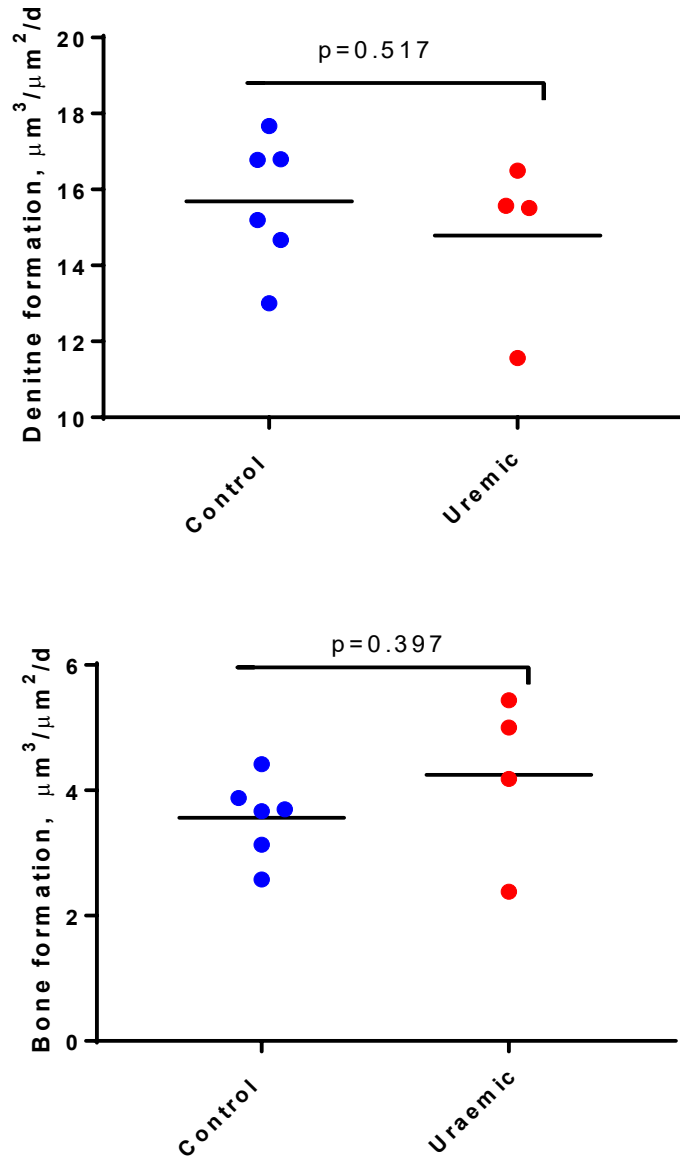
Figure 26: Rates of incisor dentine formation (top) and bone formation at the lower mandibular edge (bottom) in control and uraemic rats, as assessed by measurement of calcein green staining of bone based on a dosing frequency of 48 hours. Significance is assessed by Student's t-test with Welch's correction.
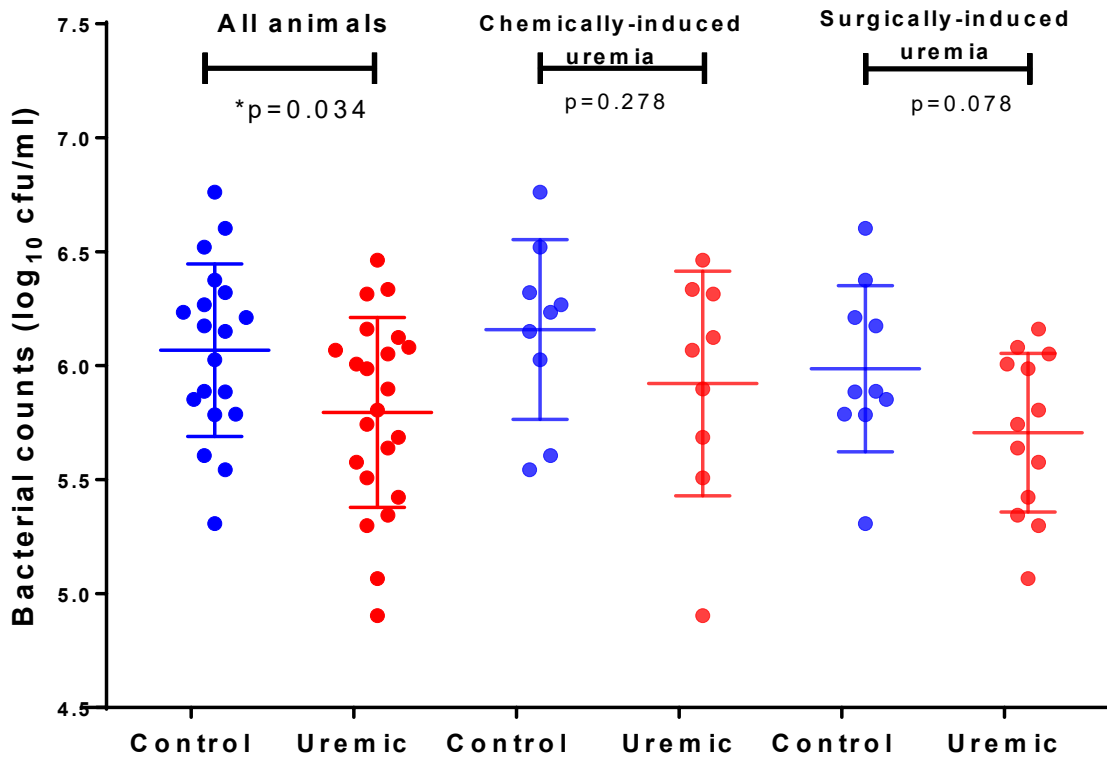
Figure 27: Total bacterial counts (colony forming units/ml) measured by summing colonies counted on blood agar plates grown in aerobic and anaerobic conditions for 48h. Significance is assessed using Student's T-test with Welch's correction for both separate experimental protocols as well as the combined dataset.

Control

Uremic

Phylum *Firmicutes*
- Streptococcus
- Staphylococcus
- Lactobacillus
- Aerococcus
- Enterococcus

Phylum *Actinobacteria*
- Rothia
- Micrococcus
- Corynebacterium

Phylum *Bacteroidetes*
- Empedobacter

Phylum *Proteobacteria*
- Acinetobacter
- Pasturellaceae
- Enterobacter
- Haemophilus
- Klebsiella
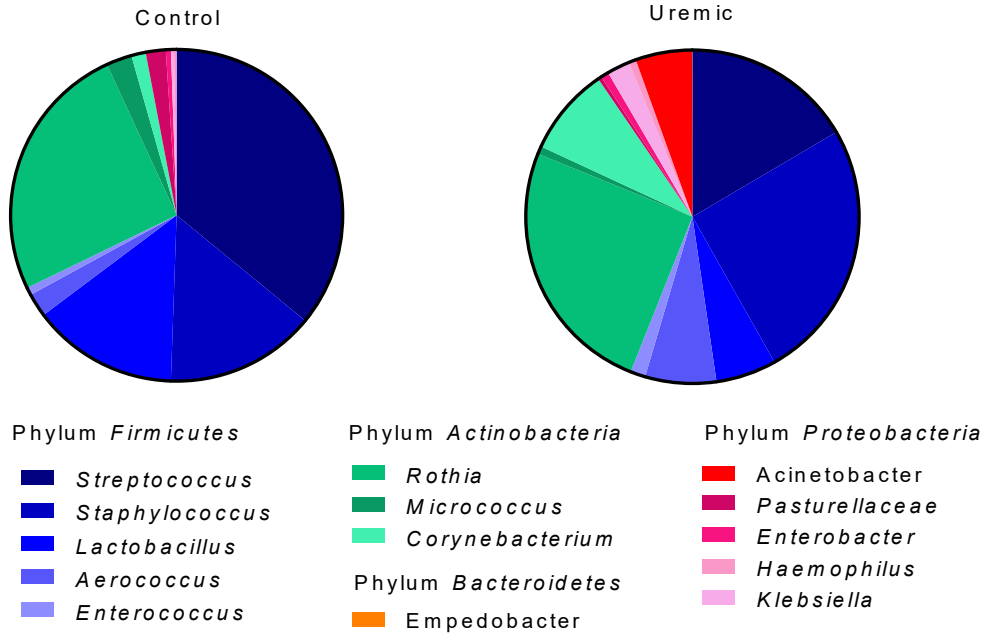
Figure 28: Community composition of the oral microbiota determined by culture in control and uraemic rats. All cultured isolates are included, agglomerated to genus level and expressed in terms of their mean percentage contribution to the oral microbial community of each rat.
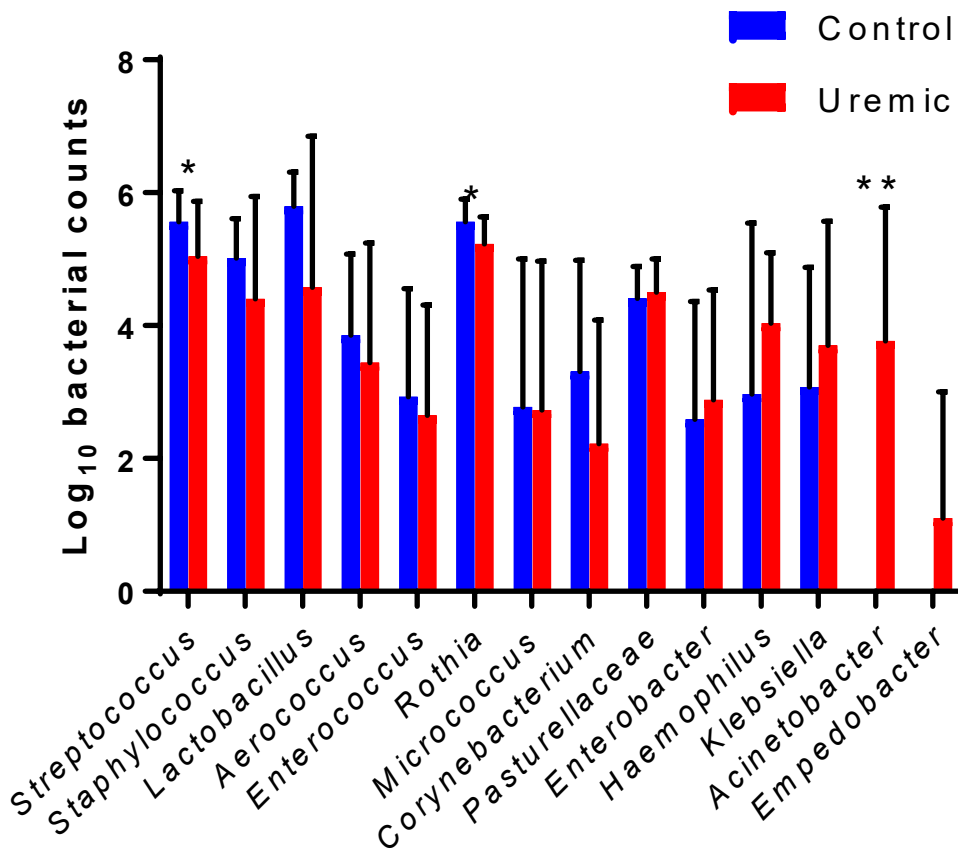
Figure 29: Absolute abundances of each cultured isolate (log10 cfu/ml). Bars show mean and standard error for all control and all uraemic animals, significance where shown was calculated using the T-test with Welch's correction. * p<0.05; ** p<0.01.
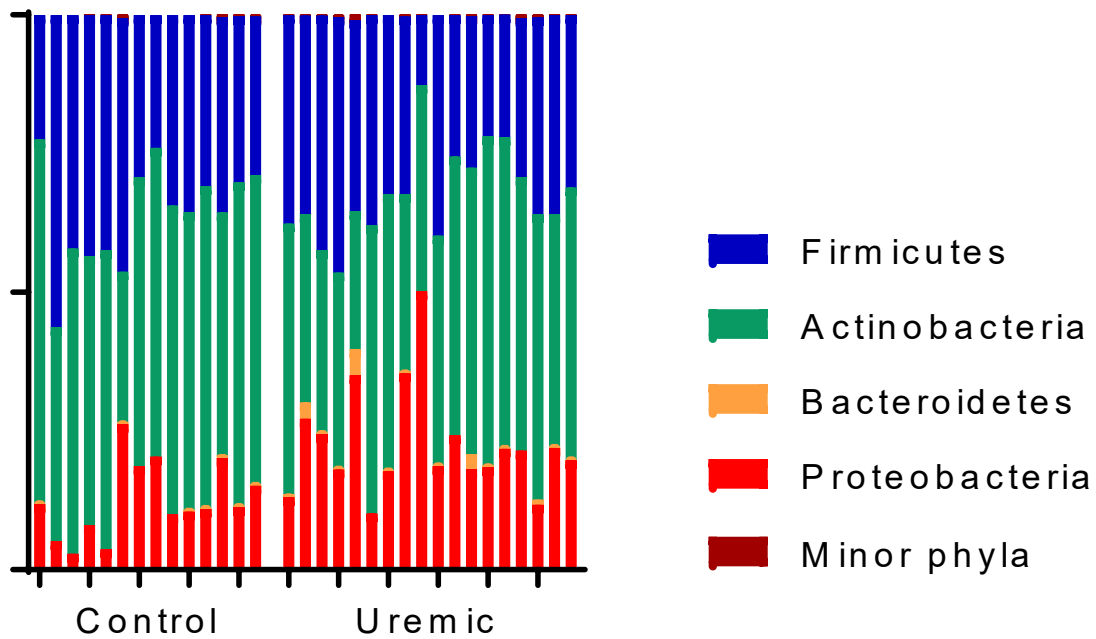
Figure 30: Community composition of the oral microbiota of rats assessed by next generation sequencing of the 16S amplicon. Each vertical bar represents the total microbial community for a single animal, grouped according to experimental conditions (control vs uraemic), colour is applied according to assigned taxonomy at phylum level. Overall, *Proteobacteria* accounted for 22.6% of reads in uraemic animals vs 12.5% in controls, p=0.002.
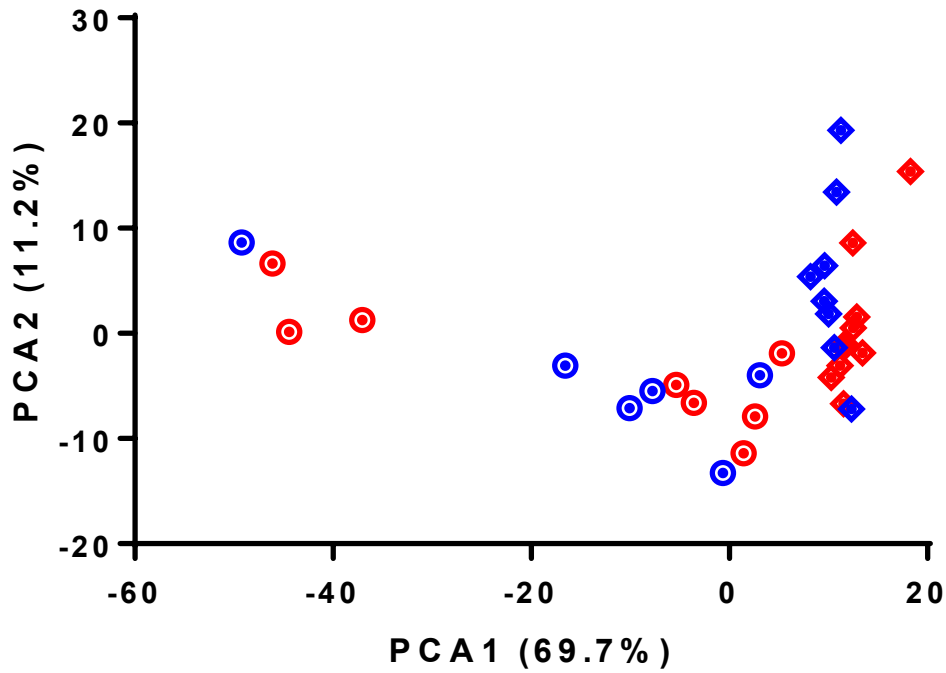
Figure 31: Principal coordinate plot showing distance between oral communities assessed by next generation sequencing of the 16S amplicon. Each point represents the oral community of an individual rat, with symbol shape representing the two experiments performed, which used separate batches of animals (circles denote the chemically-induced uraemia experiment, diamonds surgically-induced uraemia).
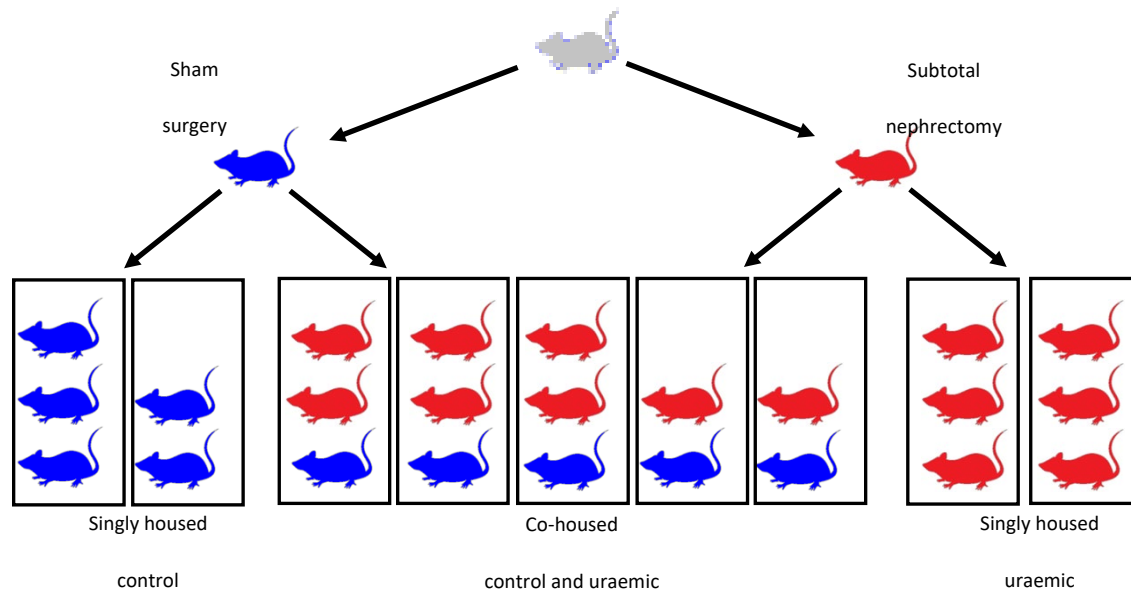
Figure 32: Housing of animals in the surgically-induced uraemia arm of the experiment. Of the fourteen uraemic rats (red), six were singly housed with other uraemic animals (the two cages represented on the right), and eight were mixed-housed with control animals in the same cage (the five cages in the middle).
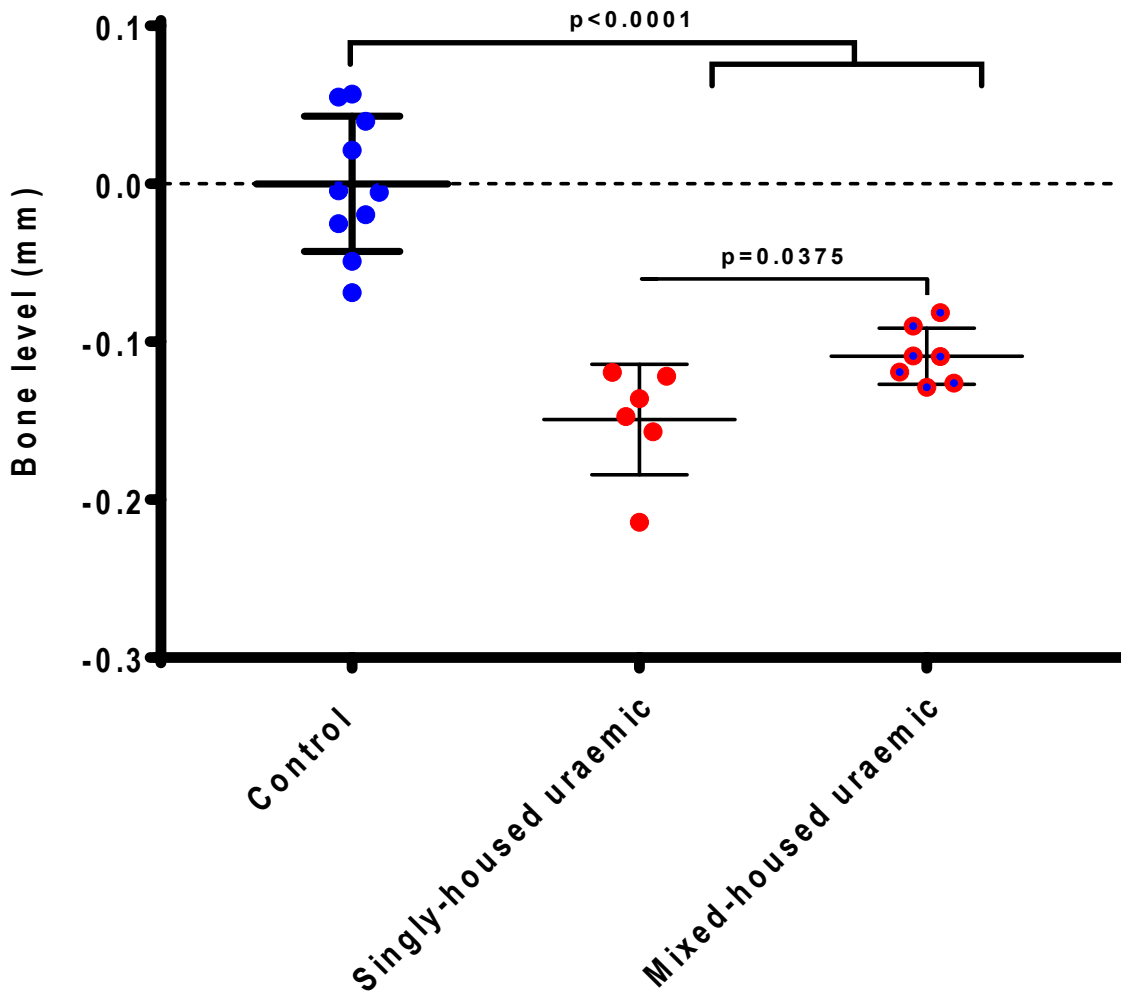
Figure 33: Periodontal bone loss, measured and presented as previously, according to housing, for animals in the surgically-induced uraemia experiment. Significance between different groups as shown were calculated by the T-test with Welch's correction; analysis by 2-way ANOVA is presented in the main text. Singly-housed uraemic animals were those undergoing subtotal nephrectomy that were housed with other animals that had undergone subtotal nephrectomy; they had more periodontal bone loss than mixed-housed uraemic animals which had undergone subtotal nephrectomy but were housed with sham-operated (control) animals (p=0.0375).
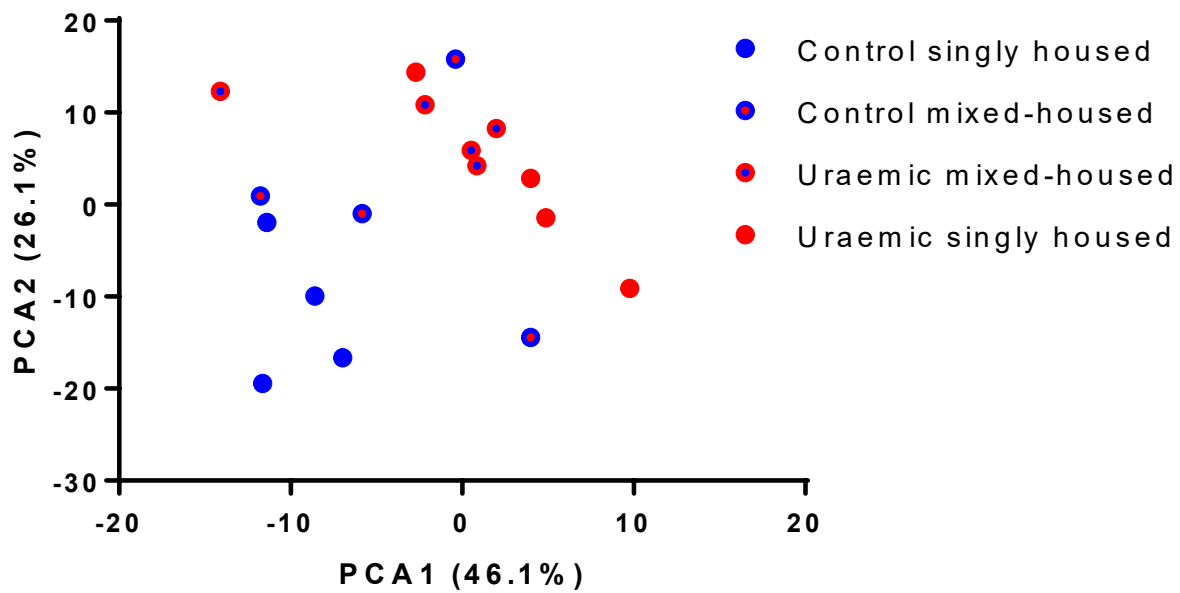
Figure 34: PCA plot of sequencing data of the oral microbiota of rats in the surgically-induced uraemia experiment. Each point represents the oral microbial community from a single animal, identified according to treatment class and caging. Mixed-housed animals (two-colour symbols), whether control or uraemic, tended to develop an intermediate microbial profile, clustering somewhere between the singly-house control and uraemic samples.
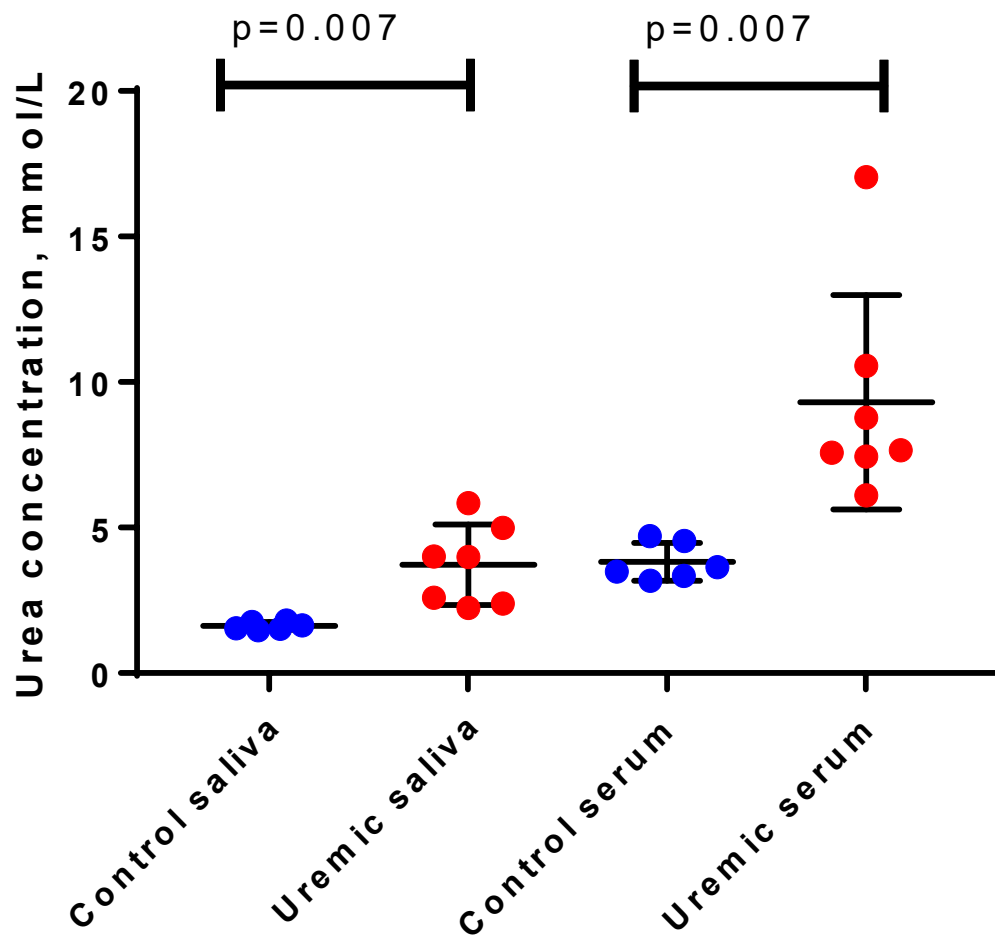
Figure 35: Urea concentration (mmol/L) in induced saliva and serum samples taken at the time of sacrifice in rats after either subtotal nephrectomy or sham surgery. Urea concentration was assessed by colourimetric assay and significance was assessed using the T-test with Welch's correction.
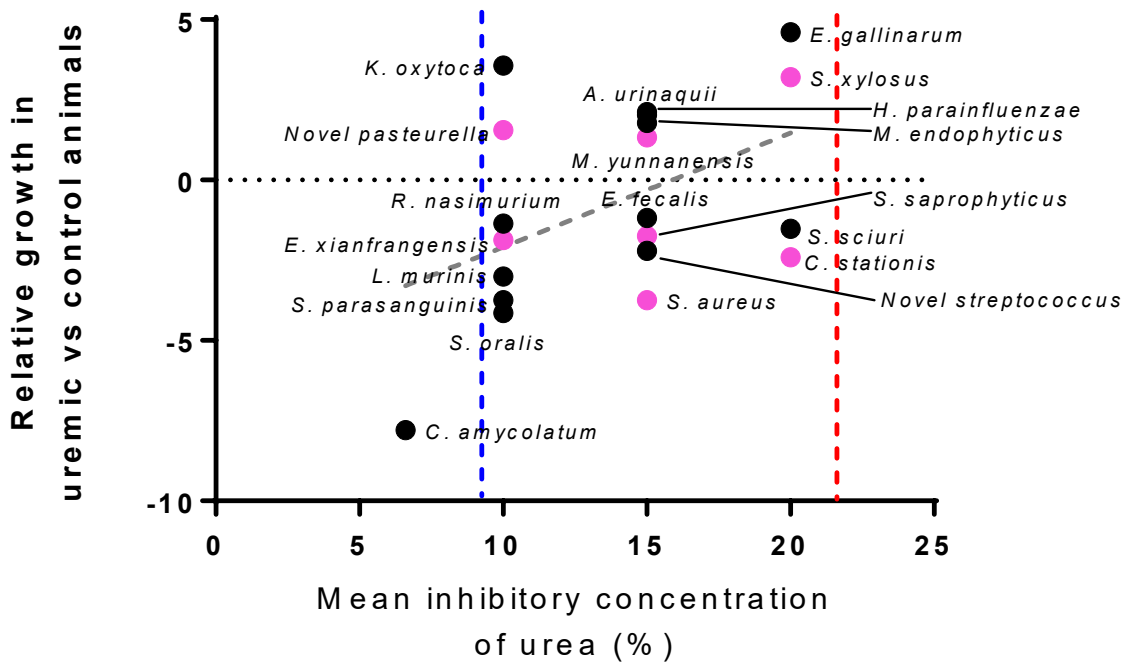
Figure 36: The mean inhibitory concentration of urea for all cultured isolates from the oral microbiota of rats, plotted against their relative observed growth in uraemic vs control animals. Each point represents the bacterial species labelled, and the y-axis represents the proportional increase in the observed mean growth of that species in uraemic over control animals; zero on the y-axis would represent equal growth in control and uraemic animals, positive values represent increased abundance in uraemic animals compared to controls and negative values increased growth in controls compared to uraemics. Species demonstrating *in vitro* urease activity are shown in pink. The blue and red dotted lines indicate the mean salivary urea concentrations in control (blue) and uraemic (red) animals, for comparison purposes. Overall there is a positive association (line of best fit) between urea tolerance and increased abundance in uraemic animals.
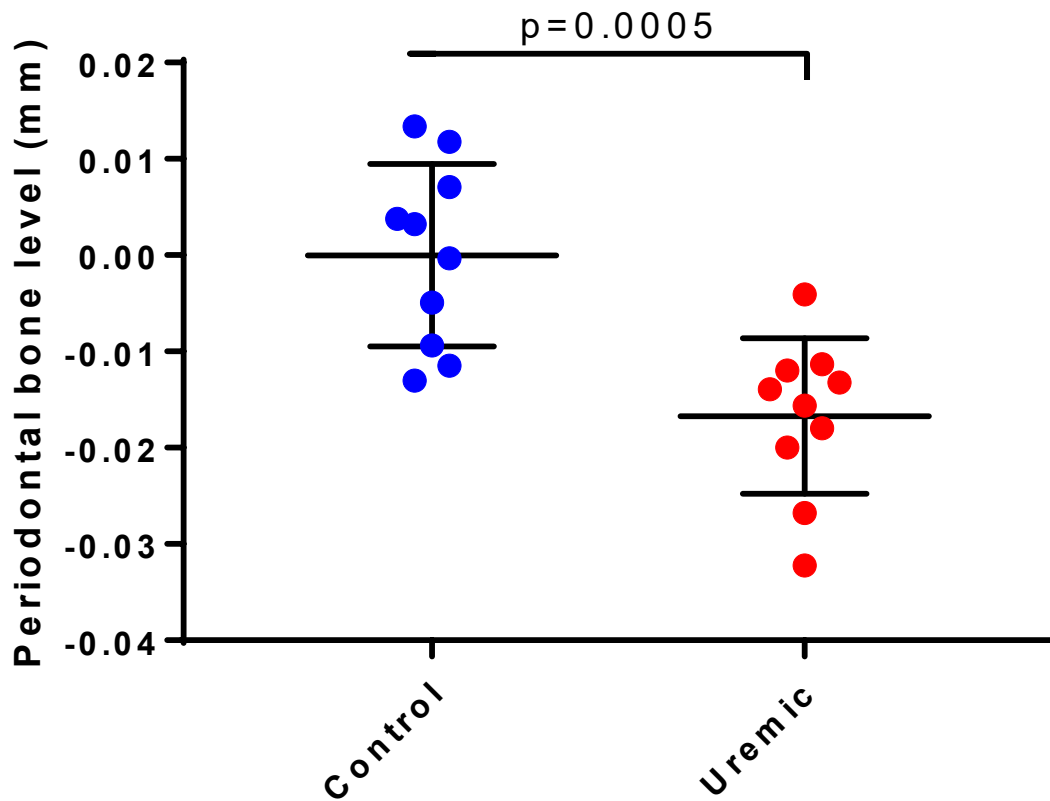
Figure 37: Distance between the cemento-enamel junction and alveolar bone crest measured using a dissecting microscope in mice. Each point represents the average of multiple measurements over the buccal and lingual surfaces of all molar roots in a single mouse, expressed relative to the average amount of bone loss in all control animals. Significance is assessed using Student's t-test with Welch's correction.

Pre-treatment

PERMANOVA p=0.111
PERMDISP p=0.964

2w

PERMANOVA p=0.344
PERMDISP p=0.049

6w

PERMANOVA p=0.876
PERMDISP p=0.206

10w

PERMANOVA p=0.021
PERMDISP p=0.015

14w

PERMANOVA p=0.001
PERMDISP p=0.004

18w

PERMANOVA p=0.066
PERMDISP p=0.012
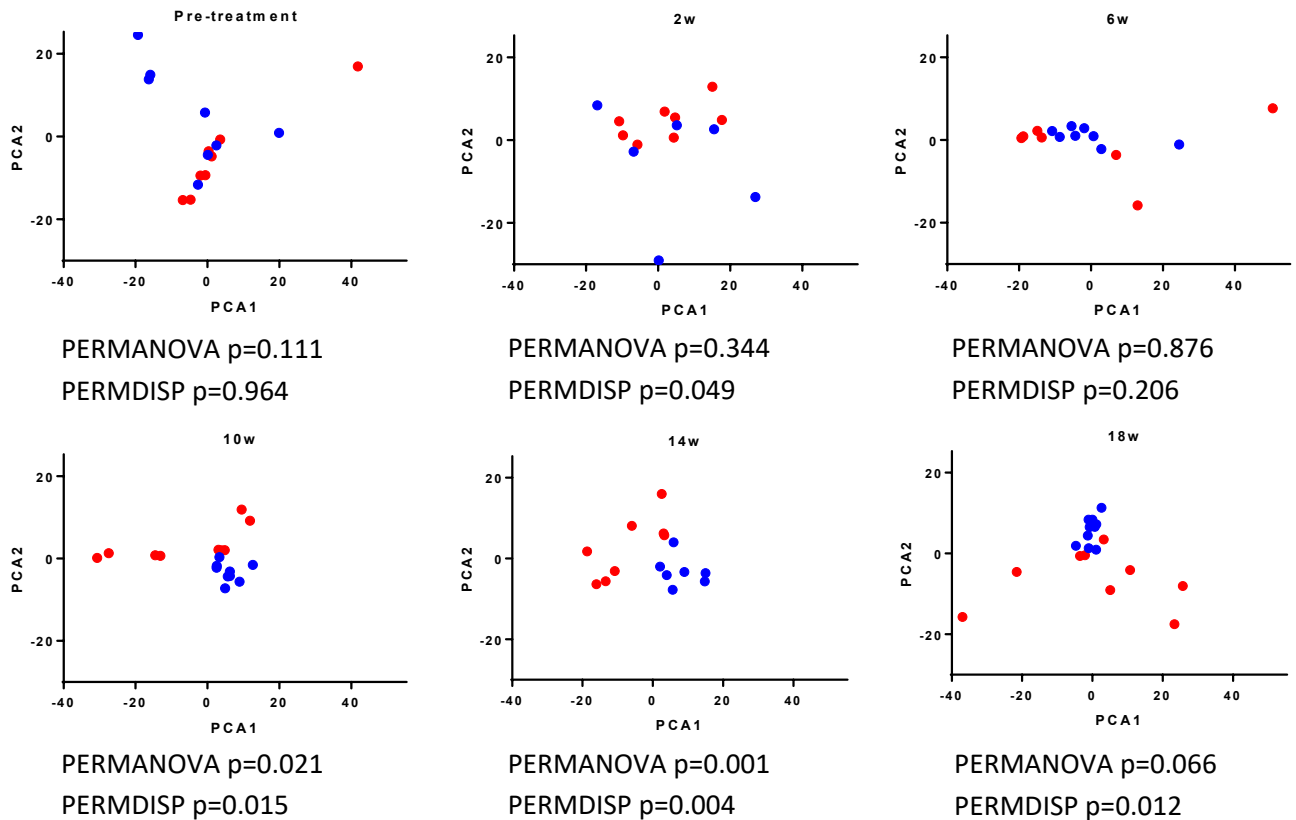
Figure 38: Uraemia induces progressive oral dysbiosis in mice. Principal component analysis plots of oral microbial communities assessed at four weekly intervals prior to and after commencing an adenine containing diet, by next-generation sequencing of the 16S rRNA gene amplicon. Samples from control animals are shown in blue and those from uraemic animals in red. For each plot the significance is shown for differential clustering (assessed by PerMANOVA) and heterogeneity of variance (assessed by PERMDISP).

Control donors, n=4   Uraemic donors, n=4
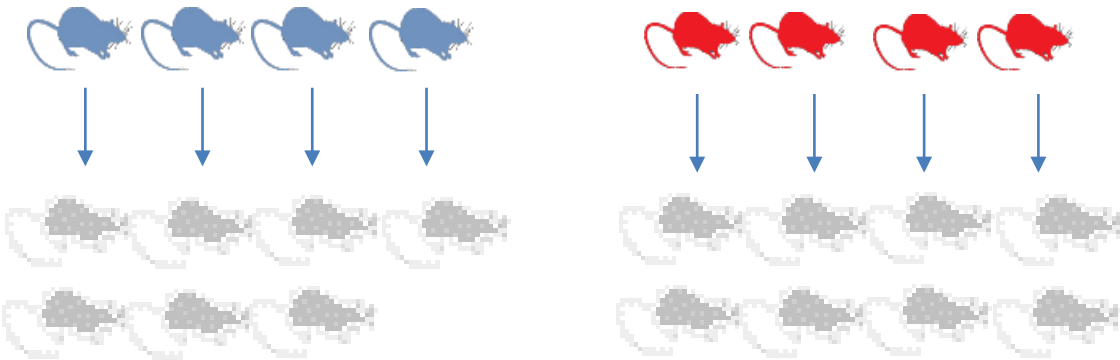
Control recipients, n=7   Uraemic recipients, n=8

Figure 39: Experimental design for oral microbial transfer experiment. Oral microbial communities from four control and four uraemic donor animals were frozen at the time of sampling and then transferred into germ-free animals at eight weeks of age. These animals were then conventionally housed, and oral microbial communities were sampled three and nine weeks after transfer, before animals were culled ten weeks after transfer, at eighteen weeks of age.
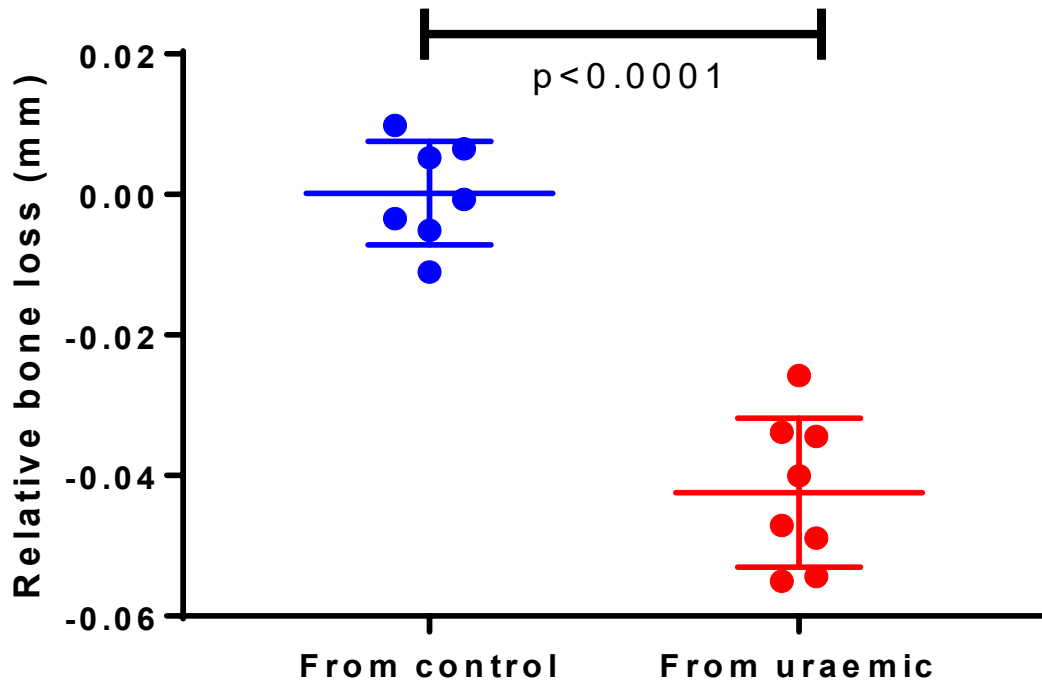
Figure 40: Periodontal bone height in recipients of control and uraemic microbiota. Recipients of oral microbiota from uraemic donors demonstrated significantly more periodontal bone loss than recipients of microbiota from control animals. Each point represents the average periodontal bone loss in a single animal as described previously.
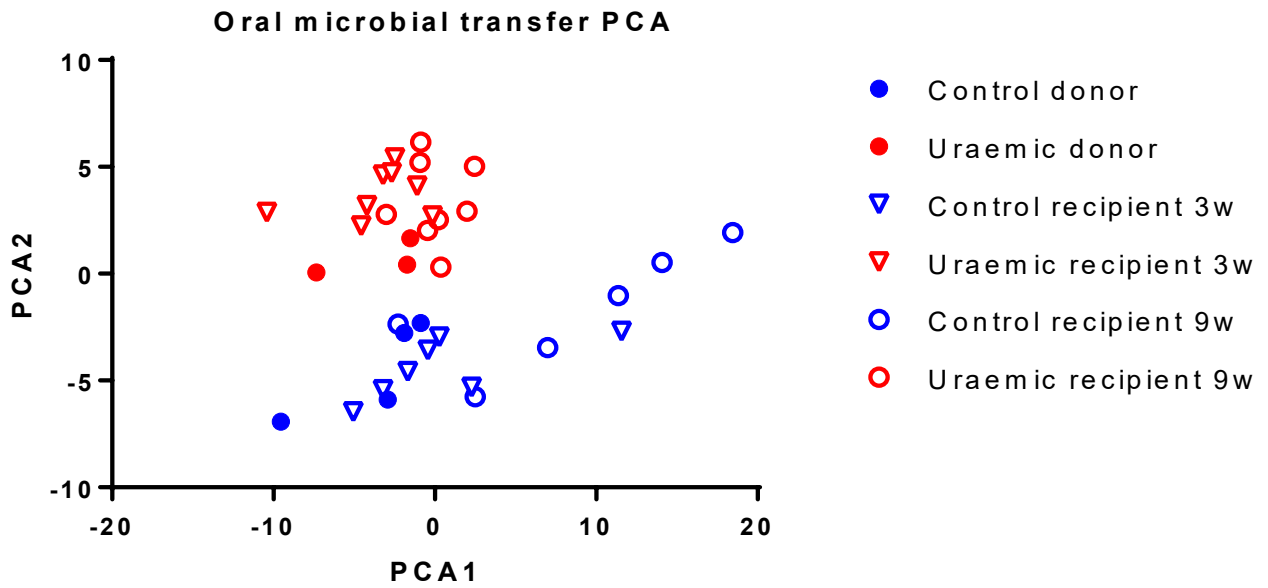
Figure 41: Principal component analysis from donor and recipient oral communities. The solid symbols represent the original donor communities; empty symbols represent recipient samples at either three weeks post transfer (triangles) or 9 weeks post transfer (circles).
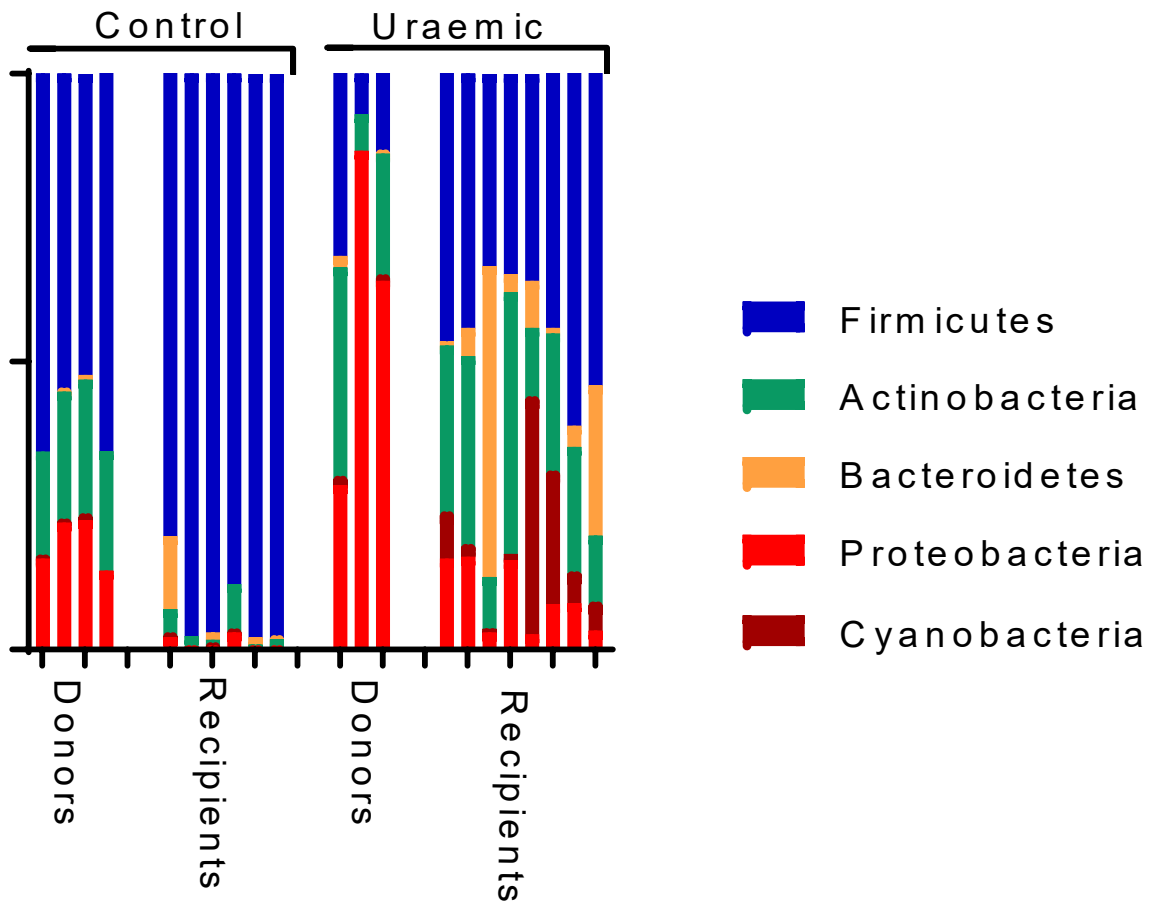
Figure 42: Community composition of recipients of oral communities from control and uraemic donors. The microbiomes are assessed by next-generation sequencing of the 16S amplicon at nine weeks after microbial transfer, or in donors using the same technique on samples taken just before the time of transfer.

Discussion

The results in this chapter demonstrate that experimental uraemia causes periodontal bone loss in rodents, as displayed using three separate experimental models in two different host species. Uraemic animals from each of these models demonstrated significant greater loss of periodontal bone height compared to controls. This phenotype was ameliorated by co-housing uraemic animals with control animals, and was reliably transferred into germ-free mice after oral microbial transfer, along with stable but dysbiotic oral microbiota.

The histological changes caused by uraemia showed some similarities with those caused by other forms of periodontal disease, including replacement of specialized junctional epithelium [205] with proliferating epithelium with sulcal folds, which appears similar to the pocket epithelium seen in humans with periodontal disease. [117, 206] There is also evidence of aberrant bone formation in the alveolar bone crest adjacent to inflamed periodontal structures, and immunohistochemical evidence of immune system activation localized to areas of bone destruction.

However, overall, the significant loss of bone height in uraemic animals was not accompanied by a florid periodontal inflammatory response as is commonly seen in other forms of PD. This may represent a different, more muted inflammatory phenotype being present in the context of uraemic periodontitis. For example, a failure of neutrophil migration has been shown to be a primary cause of severe IL-17 driven periodontitis in patients with Leucocyte Adhesion Deficiency-1 (LAD-1) disease, [207] and similarly deficient neutrophil activation and migration has been described in CKD, [174] along with a tendency to increased inflammatory bone loss. [208] Perhaps the lack of overt, neutrophil-rich inflammation in these samples represents an

inadequate immune response to oral bacteria, but which may still contribute to the reabsorption of periodontal bone via osteoclast activation.

Alternatively, other systemic features that affect bone growth in kidney disease may be affecting periodontal bone formation independently of any effects mediated by the oral microbiota. Against this hypothesis, the uraemic animals did not show overt evidence of renal bone disease or hyperparathyroidism; this is consistent with other studies which demonstrate that a high phosphorus diet in addition to SNx is required to induce frank hyperparathyroidism in rats. [209] However, the electron micrographs displaying a lack of Sharpey formation and active bone growth at the periodontal crest may suggest that the observed loss of bone height may be attributable as much due to a failure of bone growth as it is to an active process of reabsorption – there were no obvious reabsorptive lesions. The micro-CT imaging suggested aberrant bone formation even deeper in bone, away from the periodontal crest, which may suggest systemic effects outweigh local ones mediated by inflammation. However, the transmission of periodontal bone loss into otherwise healthy germ free mice through oral microbial transfer as well as the reduction in bone loss in co-housed uraemic animals suggests that dysbiotic oral microbiota nevertheless have an important causative role, and the calcein-stained samples did not reveal obvious deficiencies in the bone formation rate in uraemic samples.

It is probably too early to define with confidence, on the basis of the data presented here, the exact mechanisms behind the reduced periodontal bone height in uraemic animals that has been reproducibly demonstrated here, and further experimental work may be helpful in this regard. It may be that systemic and local inflammatory factors both contribute to the uraemic periodontal disease seen.

The loss of alveolar bone height demonstrated in uraemic animals was significant less severe than that seen in ligature-induced models of periodontitis in both rats [199] and mice, [210] but similar to that seen in periodontitis models employing oral gavage with disease-causing micro-organisms such as *Porphyromonas gingivalis* (which variably causes up to 0.03mm bone loss in the C57/BL6 mice we used, comparable to the 0.02mm we described, despite C57/BL6 mice being known to be relatively resistant to periodontitis). [201, 210]

The results in each experimental model suggested a common signature of the effects of uraemia on oral bacterial communities, consisting of a reduction in overall bacterial counts; an increase in alpha diversity; depletion of taxa such as *Streptococcus* and *Rothia* which are key components of healthy oral microbiotas; [211, 212] and an increase in bacteria (typically non-oral Gram-negative rods) that have previously been associated with PD. [116, 213]

Although few studies in humans have described the oral microbiota in the context of uraemia, those that have reveal a strikingly similar microbial signature to that observed here. In particular, Hu et al. demonstrated significant changes in oral microbial communities in CKD patients when compared with healthy controls, with an increase in the phylum *Proteobacteria*, at the relative expense, in proportional terms, of taxa in the *Firmicutes* phylum, including *Streptococcus* and *Veillonella.* [192] Kidney transplant recipients with poor graft function [214] and haemodialysis patients [215] have likewise been demonstrated to have dysbiotic oral microbiota, consistent with our assertion that uraemia itself induces dysbiosis.

Increased salivary urea is a possible mechanism driving these changes: the composition of saliva uniquely determines the selective pressures on the oral microbiota, and (notwithstanding the

limited correlation of bacterial behaviour in liquid culture compared to *in vivo* biofilms) there was a correlation between urea tolerance and increased abundance in uraemic animals. Notably, *Streptococcus* and *Rothia* isolates, which were present at reduced abundances in uraemic animals, did not display *in vitro* urease activity and showed reduced tolerance of higher urea concentrations in broth culture.

The oral microbial signature of uraemia described here was seen in an exaggerated but stable form when microbiota from control and uraemic animals were transferred into previously germ-free mice. The ability of abnormal microbial communities to stably establish themselves and cause PD after transfer into germ-free mice has been previously described, [216, 217] and the high degree of periodontal bone loss demonstrated in these animals shows the relevance of oral dysbiosis in the aetiology of periodontal disease.

In rats, co-housing with healthy animals seemed to lessen some of the dysbiotic changes seen in uraemic animals, and to ameliorate the associated PD phenotype. It has long been known that co-housing can affect oral microbiology, [218] and in work recently published by Abusleme et al. it has been shown that healthier microbiota may outcompete and even fully replace more dysbiotic communities. [219]

In this study, uraemia was not accompanied by a reduction in salivary flow rates and an increase in salivary pH, as shown elsewhere in rodent models of uraemia. [141] This is likely to be a consequence of the mechanism we used to induce saliva. Pilocarpine administration overrides physiological control of salivary flow rates, and if the mechanism by which high salivary urea increases pH is dependent on bacterial hydrolysis of urea to ammonium, it is possible that the immediate removal of saliva by pipetting prevented these bacterial effects from taking place.

Reduced concentrations of acetic and lactic acid in control samples is consistent with the reduction in *Streptococcus* and *Lactobacillus* which are known to digest sugars and produce a range of organic acids. [220]

Use of animal subjects excludes confounding factors, such as co-morbidity and dental hygiene habits, which may serve as alternative explanations for the high level of PD in human subjects with CKD. [138, 221] Use of only male animals (as is common in studies of experimental uraemia) may limit generalisability to the whole human CKD population, although population data suggests women with CKD suffer a similar incidence of PD as men. [149]

Additional research could consider the extent to which periodontal bone loss is a result of a normal immune reaction to a dysbiotic bacterial burden, or whether the periodontal immune reaction in uraemic animals is, in itself, abnormal. More broadly, given that these results demonstrate a causative role for uraemia and the aetiology of PD, further research could assess whether periodontal inflammation, once established, contributes to renal fibrosis and cardiovascular disease, and whether there is a role for dental screening and treatment to improve renal and cardiovascular outcomes in individuals with CKD.

It is proposed that uraemic periodontal disease should be regarded as a novel complication of CKD, and that dysbiotic change in oral bacterial communities induced by uraemia plays a crucial mechanistic role.

Summary:

- **Experimental uraemia reliably induces loss of alveolar bone height in both rats and mice.**

- **Uraemic animals had a dysbiotic oral microbiome with increased alpha diversity, reduced total bacterial counts, a decrease in health-associated taxa and an increase in disease-associated Gram-negative taxa.**

- **Induced saliva from uraemic animals had a higher urea concentration than that from controls.**

- **Bacterial isolates which were under-represented in samples from uraemic animals showed reduced tolerance to higher urea concentrations during *in vitro* broth culture.**

- **Uraemic animals which were co-housed with healthy animals demonstrated significantly less bone loss than those housed with other uraemic animals.**

- **Transfer of oral microbiota from uraemic animals induced more periodontal bone loss in healthy germ-free mice than transfer of oral microbiota from health animals, along with transference of a stable, dysbiotic oral microbiota.**

Conclusion: uraemia induces oral dysbiosis that may subsequently affect bone formation at the alveolar bone ridge, causing periodontal disease.

Chapter 4:

Batch effect, reproducibility and the effect of uraemia on the gut microbiome

Introduction: our initial hypothesis

Uraemic toxins have been shown to be produced by bacterial metabolism of dietary protein in the large intestine, [1, 5] leading to interest in the gut microbiome as a potential therapeutic target to reduce the cardiovascular morbidity of patients with CKD. [222] Furthermore, the absence of bacterially-produced short chain fatty acids (SCFA) has been suggested as a contributary factor in the aetiology of the disease. [1]

We hypothesized, as suggested by Wang et al [7] in an in-silico study based on the results of Vaziri et al's early molecular study of the gut microbiota in uraemia, [223] that uraemia may

induce dysbiosis of gut bacterial communities leading to a contraction of beneficial species, especially those that produce SCFA, and an expansion of pathogenic, toxin-producing taxa.

Specific methods

24 wild-type outbred Wistar International Genetic Standard (IGS) rats were obtained from a single supplier (Charles Rivers, Kent, UK). For logistical reasons (based on the capacity of surgical facilities at the Charterhouse Square Biological Services Unit), the rats were purchased in two separate shipment batches. Fourteen were rendered uraemic by undergoing a two-stage subtotal (five-sixth) nephrectomy (8 from batch 1, 6 from batch 2), whilst 10 underwent sham procedures (6 from batch 1, 4 from batch 2, Figure 43, p. 160).

There were no differences in animal husbandry or diet between batches. At the time of sacrifice 8 weeks later, the urinary metabolome was assessed by untargeted proton nuclear magnetic resonance (^{1}H-NMR) spectroscopy, and composition of the gut microbiota was assessed by sequencing 16S rRNA gene amplicons.

Results part 1: Metagenomic and metabolomic batch effects outweigh effects of uraemia

All animals undergoing subtotal nephrectomy developed an expected uraemic phenotype, including elevations in serum urea and creatinine, weight loss and polyuria compared to sham-

operated controls, and there were no gross phenotypic differences between animals from different batches (Figure 44, p. 161).

Batch effects outweigh those of uraemia in untargeted analysis of urinary metabolomics

Principal component analysis (PCA) of normalized and aligned urinary NMR spectral profiles identified that shipment batch was responsible for the largest source of variance in the biochemical data, seen chiefly in principal component 1, which accounted for 38% of variance. Surgical treatment accounted for a smaller but nonetheless definite source of variance, with these differences being seen chiefly in the second principal component, which accounted for 17.7% of total variance (Figure 45, p. 162).

Separate orthogonal projection to latent structures discriminant analysis (OPLS-DA) models were constructed to elucidate biochemical variation associated with shipment batch and treatment class, Figure 46, p.163. The model built using shipment batch had a stronger predictive power (Q^2Y=0.66, p=0.001) than the model built using treatment class (Q^2Y=0.48, p=0.007). Discriminatory metabolites between the two shipment batches were identified from the OPLS-DA model, and their relative abundances were calculated from integration of the relevant regions of the aligned spectral profiles.

Animals in batch 1 excreted significantly greater amounts of glycine (141.5 vs 68.5 relative units, Benjamini-Hochberg adjusted *p*<0.001), alanine (29.3 vs 18.0 units, *p*<0.001) and glucose (43.9 vs 19.7 units, *p*=0.006) than animals in batch 2. They also excreted higher amounts of the

potential gut bacterial products acetate (a short-chain fatty acid, 192.2 vs 105.2 units, p=0.003), succinate (a bacterial metabolic product of dietary fibre digestion, 97.9 vs 72.6 units, p=0.017), and lactate (571.7 vs 188.3 units, p=0.001), compared with those in batch 2. Hippurate was almost completely absent from the urine of batch 1 animals but present in urine from all animals in batch 2 (6.6 vs 34.5 units, p=0.003). Correspondingly, benzoate, a gut microbially-derived precursor of hippurate, was lower in the urine of batch 2 animals compared to those in batch 1 (111.0 vs 52.1 units, p<0.001, Table 2, p. 164).

Whilst a high degree of between sample variation meant the batch effect did not reach overall significance, on review of individual sample NMR spectra many animals had no detectable trimethylamine (TMA), a product of bacterial protein metabolism, including almost all of those in batch 1, whereas others (predominantly those in batch 2) had clearly detectable concentrations.

To determine whether these substantial batch variations could have led to erroneous conclusions about the effect of uraemia on the urinary metabolome, an OPLS-DA model was built for each shipment batch separately using surgical treatment class (subtotal nephrectomy vs sham) as the response variable. The model built on the batch 1 profiles was not found to be significant (Q^2Y=0.265, pQ^2Y=0.120), leading to the potential conclusion that the urinary metabolome is not influenced by uraemia in these animals. However, a significant predictive model was obtained using profiles from batch 2 (Q^2Y=0.543, pQ^2Y=0.049), despite small sample numbers, suggesting that conversely, in these animals, uraemia does indeed determine urinary phenotype.

Batch effects outweigh those of uraemia on analysis of the gut microbiome

To assess whether differences in the gut microbiota between shipment batches and treatment classes might underlie these trends in the metabolomic data, sequencing of the V3 hypervariable region of the amplified 16S rRNA gene in DNA extracted from caecal fluid was carried out. Sequence abundance data underwent isometric log-ratio transformation to allow compositional analysis of the different microbial communities.

Unsupervised PCA of the compositional data revealed that shipment batch had a larger impact on sample clustering than did treatment class. Consistent with this, permutational multivariate analysis of variance (PerMANOVA) was performed using an ADONIS analysis of a Euclidean distance matrix, and confirmed that batch had a small but significant effect on the gut microbiome ($R^2 = 0.097$, p = 0.001), whilst treatment class did not ($R^2 = 0.048$, p = 0.227, Figure 47, p. 165). This was further confirmed by showing that a valid predictive OPLS-DA model could be built using shipment batch as the response variable ($Q^2Y = 0.573$, $p < 0.05$), but not when using treatment class ($Q^2Y = 0.206$, $p = 0.2$).

The gut microbiotas of animals differed significantly in community structure between batches, with samples taken from animals in batch 2 displaying higher alpha diversity than those from animals in batch 1, across a range of measures including the Inverse Simpson (40.7 vs 58.5, p=0.043) and Shannon indices (4.53 vs 4.81, p=0.046). Conversely, there was no difference in alpha diversity between uraemic and control animals (Figure 48, p. 166).

To explore these differences more closely, populations were assessed on the basis of taxonomic assignments of OTUs at phylum, order, class, family and genus levels. Microbiotas in all animals

were dominated by phyla *Firmicutes* (accounting for 83.1% of total reads) and *Bacteroidetes* (14.5%), with all other phyla (*Verrucomicrobia*, *Tenericutes*, *Proteobacteria*, *Actinobacteria*, *Saccharibacteria* and *Deferribacteres*) together representing less than 2.5% of total sequences when normalized across samples (Figure 49, p. 167).

Differences in the abundances of OTUs and higher taxonomic groupings were analysed between shipment batches and treatment classes using the Analysis of Composition of Microbiomes (ANCOM) framework, based on isometrically log-ratio transformed abundance data and Benjamini-Hochberg adjustment for multiple hypothesis testing. Differential abundances between samples taken from animals in different shipment batches were apparent as high as at class level, with animals in batch 2 having higher relative abundances of *Pseudomonadales* in phylum *Proteobacteria*. No higher order differences were demonstrated between uraemic and control animals.

On further analysis at OTU level it became clear that it was primarily the less abundant OTUs which showed significant differences between batches, while OTUs differing significantly between uraemic and control animals were generally more abundant. Thus, whilst the relative abundance of 33/1110 OTUs (2.97% on the total) differed significantly between shipment batches, these represented only 3.80% of total sequences when analysed by the abundance of each OTU. However, the six OTUs which differed significantly between treatment classes (0.54% of the total) accounted for 5.13% of total sequences when adjusted for abundance.

These six OTUs showing significant abundance differences between uraemic and control animals were all from the family *Lachnospiraceae*; five from the NK4A136 group and one from

the UCG-001 group. All but one showed significant decreases in relative abundance in uraemic animals, including the third most abundant OTU overall.

The 33 OTUs showing significant compositional differences between batches were drawn from five different phyla. In keeping with the higher alpha diversity seen in samples from batch 2 animals, 30/33 differentially abundant OTU between batches were seen in higher abundances in animals from this batch. Interestingly bacterial genera known to possess significant metabolic potential were prominently represented amongst these differentially-abundant organisms, including a number of producers of short-chain fatty acids (*Roseburia*, *Butyricicoccus*, *Butyrivibrio* and *Acetomaculum*), and three from the phylum *Proteobacteria* (Table 3, p. 168).

Results part 2: These effects persist despite adding additional cohorts

The findings from the previous work indicated that additional cohorts of animals would be required to establish how the differential effects between batches and between experimental groups (uraemic and control) were manifested. A further cohort of rats was added, as were two batches of C57/BL6 mice – one large batch (20 animals, 10 rendered uraemic using adenine containing feed and 10 lefts as controls), and a smaller batch of only five animals; three uraemic and two control, included to see if similar batch effects apply in mice. In this third rat cohort, during the week prior to surgery rats were moved regularly between cages to see if this homogenised bacterial populations.

Thus a total of 39 outbred IGS Wistar rats, purchased in three separate shipment cohorts; and 25 C57/BL6 mice, purchased in two separate cohorts were re-analysed together, all of which had been obtained from the same supplier (Charles Rivers, Kent, UK) at 7 weeks of age.

Cohort effects again outweigh those of uraemia on the gut microbiome

As previously described, to enable a direct comparison of bacterial composition between samples from all cohorts, amplicon sequencing variants (ASVs) were assigned a taxonomic identity using the SILVA database and aggregated at family level (the lowest taxonomic level at which all sequences were confidently assigned).

Ordination of log-ratio transformed abundance data identified that whilst rat cohorts 1 and 2 clustered closely together (those previously described in this chapter), rat cohort 3 was quite distinct from these. This pattern mirrored phenotypic differences between these rat cohorts: whilst within each animal cohort, there were significant phenotypical differences between control and uraemic animals; nevertheless rats from cohort 3 were heavier and displayed higher levels of serum urea and creatinine than those in cohorts 1 and 2 (Table 4, p. 169).

Principal coordinate analysis revealed that the two mouse cohorts clustered distinctly from each other and from the rat samples (Figure 50, p. 170). Although it appears in Figure 45 that rat cohorts 1 and 2 cluster together, Permutational Analysis of Variance (PerMANOVA) confirmed that significant differences between these groups existed in a reduced dataset containing only these samples (although explaining only 12.2% of variance, p=0.003, Figure 51, p. 171).

PerMANOVA confirmed that uraemia itself did not affect clustering in the combined dataset of all samples (explaining only 2.33% of variance, p=0.196), whilst cohort and species strongly did (explaining 27.5% of variance, p<0.001; and 29.6% or variance, p<0.001; respectively).

Major differences in composition occur between cohorts

Comparison of cohorts at phylum level revealed that all microbial profiles were dominated by the phyla *Firmicutes* and *Bacteroidota*, which accounted for an average of 72.8% and 26% of bacterial abundance, respectively, across all samples (98.8% of total reads, results that mirror findings in other studies of rodent microbiota). Differential abundance at phylum level was most pronounced between microbiotas from hosts of different species, with five of eight bacterial phyla present showing significant relative abundance differences between rat and mouse samples (including the second-most abundant phylum overall, *Bacteroidota*, which represented 46.2% of sequences from mice, but only 19.4% of those from rats, difference in log-ratios between groups p<0.001, Figure 52, p. 172).

Cohort differences were also prominent across the dataset, with samples from rat cohort 3 displaying lower relative abundances of *Firmicutes* (70.9% in cohort 3 vs 83.6% in cohorts 1 and 2, p<0.001 between log-ratio transformed values), higher relative abundances of *Bacteroidota* (28.9% in cohort 3 vs 14.7% in cohorts 1 and 2, p<0.001), and also significant differences in relative abundances of minor phyla including *Verrucomicrobiota*, *Deferribacterota*, *Desulfobacterota*, and *Patescibacteria* compared to samples from rat cohorts 1 and 2.

In contrast to species and cohort effects, across the whole dataset there were no significant differences between the log-ratio transformed relative abundances of any of the phyla represented between uraemic and control animals (Figure 53, p. 173).

Detailed analysis to determine individual taxa which were differentially abundant between control and uraemic animals in different cohorts

The *ANCOM* [224] and *Phylofactor* [225] packages in *R* were used to conduct a detailed analysis of each individual experimental cohort for taxa displaying differential abundances between uraemic and control microbiotas at each taxonomic level between species and phylum. The results of these analyses are shown in Appendix 3, p. 374.

Briefly, the outcomes were mixed. In some cohorts (eg rat cohort 2 and mouse cohort 1) there were a number of taxa showing differential abundances between experimental groups, sometimes at relatively high taxonomic levels; in other cohorts there were absolutely no differentially abundant taxa. There was no consistent pattern seen across all cohorts.

The effect of uraemia on the 24-hour urinary excretion of common bacterial metabolites is similarly inconsistent between cohorts

[1]H nuclear magnetic resonance (NMR) spectroscopy was performed on 24-hour urine samples from all animals except those in mouse cohort 2. Peak integrals were calculated for ten metabolites associated with the gut microbiota. These included acetate, propionate, butyrate,

lactate, acetoin, trimethylamine, trimethylamine-*N*-oxide (TMAO), indoxyl-sulphate (IS), benzoate, and hippurate, with abundance being expressed as a ratio to the abundance of urinary creatinine.

Clear species differences were evident between rat and mouse samples for many of the metabolites. However, even when mouse samples were excluded from the analysis, cohort differences proved more significant than the effect of uraemia for all metabolites except IS, propionate and butyrate.

In the whole dataset, the only metabolite to be significantly affected by uraemia was the well-described uraemic toxin IS, excretion of which was increased in uraemic animals. However, this overall increase in IS excretion was driven by animals in rat cohort 3 and mouse cohort 1; in rat cohorts 1 and 2 no difference in daily IS excretion was noted between the control and uraemic animals. Rats in cohort 3 had greater elevation of serum urea and creatinine than those in the other rat cohorts; it is possible that this may have explained the difference, although it remains problematic that different cohorts, treated identically, develop different degrees of uraemia. Species-dependent differences were seen in TMAO excretion with uraemia: this uraemic toxin was excreted in excess amounts by uraemic rats compared to control rats but the opposite pattern was seen in the mice.

Modest and only partially consistent results were seen in the excretion of short-chain fatty acids. Uraemic mice excreted reduced amounts of butyrate compared with control mice, whilst uraemic rats excreted less acetate but more propionate than controls (

Figure 54, p. 174, supplementary Table 16, p. 404, appendix 5).
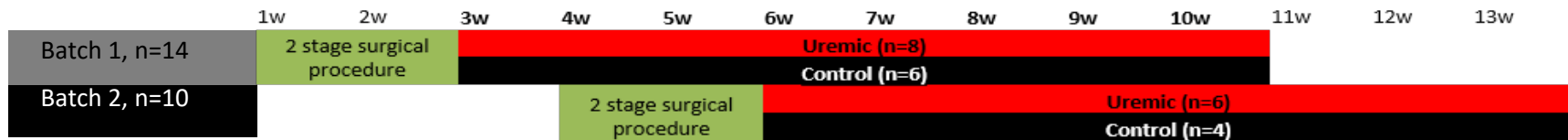
Figure 43: Outline of experimental procedures. Time in weeks is shown along the top of the figure. Animals arrived in two batches, three weeks apart, at age 7 weeks, and after a week-long acclimatisation period, underwent a 2-stage subtotal nephrectomy or sham procedure. 8 weeks after the second stage of this procedure, after a 24-hour urine collection, they were sacrificed and samples of serum and caecal fluid collected.
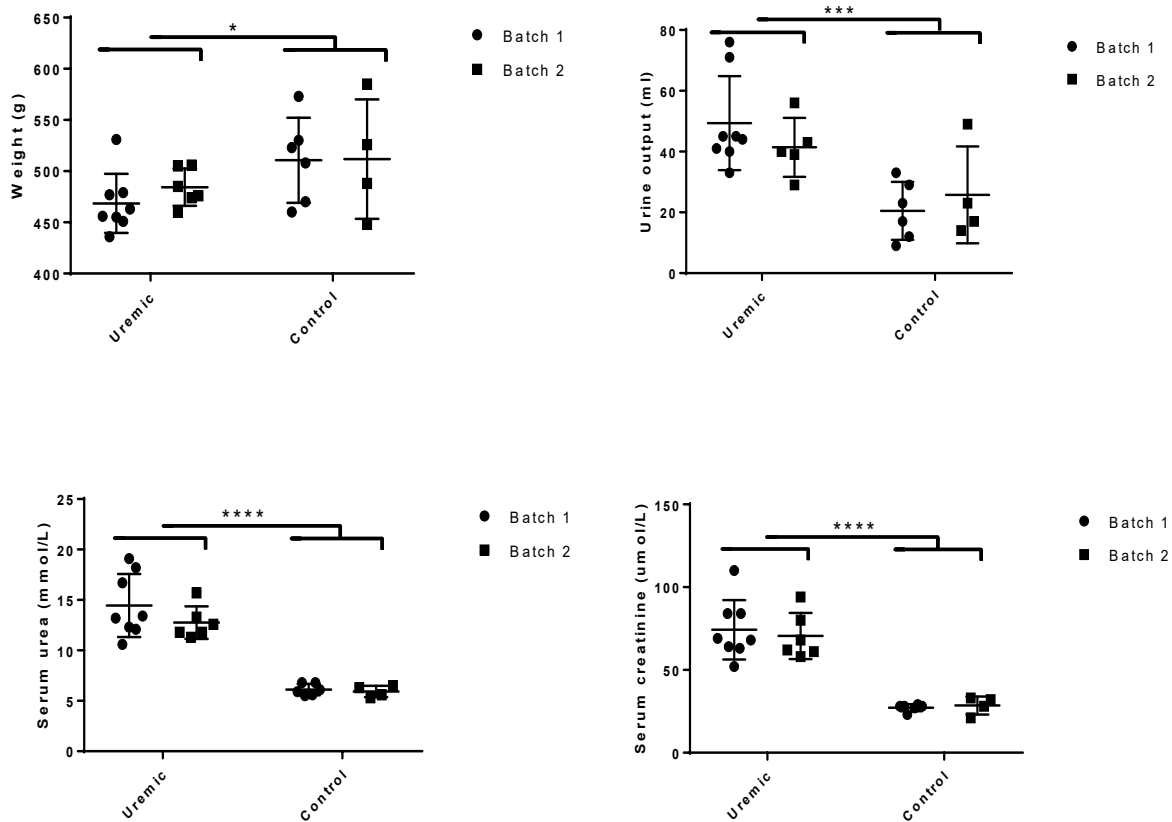
Figure 44: Animal data at the time of sacrifice. Differences were seen for each parameter between uraemic and control animals, but not been similarly treated animals in different patches. Significance was assessed for each parameter by 2-way ANOVA by treatment and by batch: Weight at time of sacrifice (p=0.033 for treatment, p=0.586 for batch, by 2-way ANOVA); 24h urine volumes immediately before sacrifice (p=0.0009 for treatment, p=0.256 for batch, by 2-way ANOVA); serum urea at time of sacrifice (p<0.0001 for treatment, p=0.392 for batch, by 2-way ANOVA); serum creatinine at time of sacrifice (p<0.0001 for treatment, p=0.645 for batch, by 2-way ANOVA).
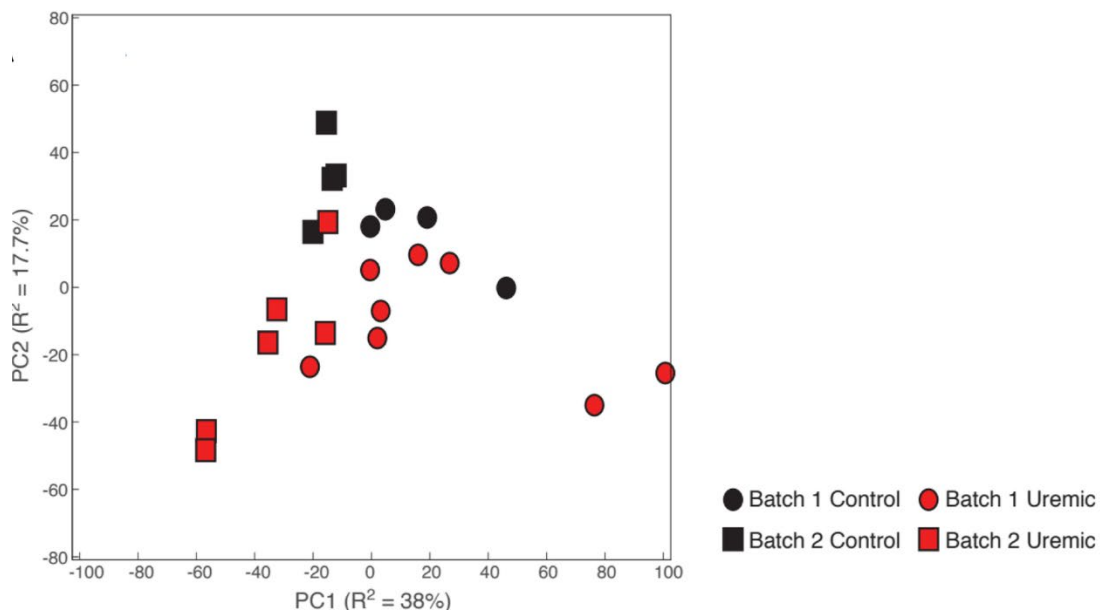
Figure 45: Ordination plot of principle component analysis (PCA) of normalised and aligned NMR spectra from untargeted 1H-NMR spectroscopy of 24 hour rat urine collections. Samples separated when analysed by batch chiefly in the first principal component, which accounted for 38% of total variance; and separated when analysed by surgical treatment chiefly in the second principal component, which accounted for 17.7% of variance.
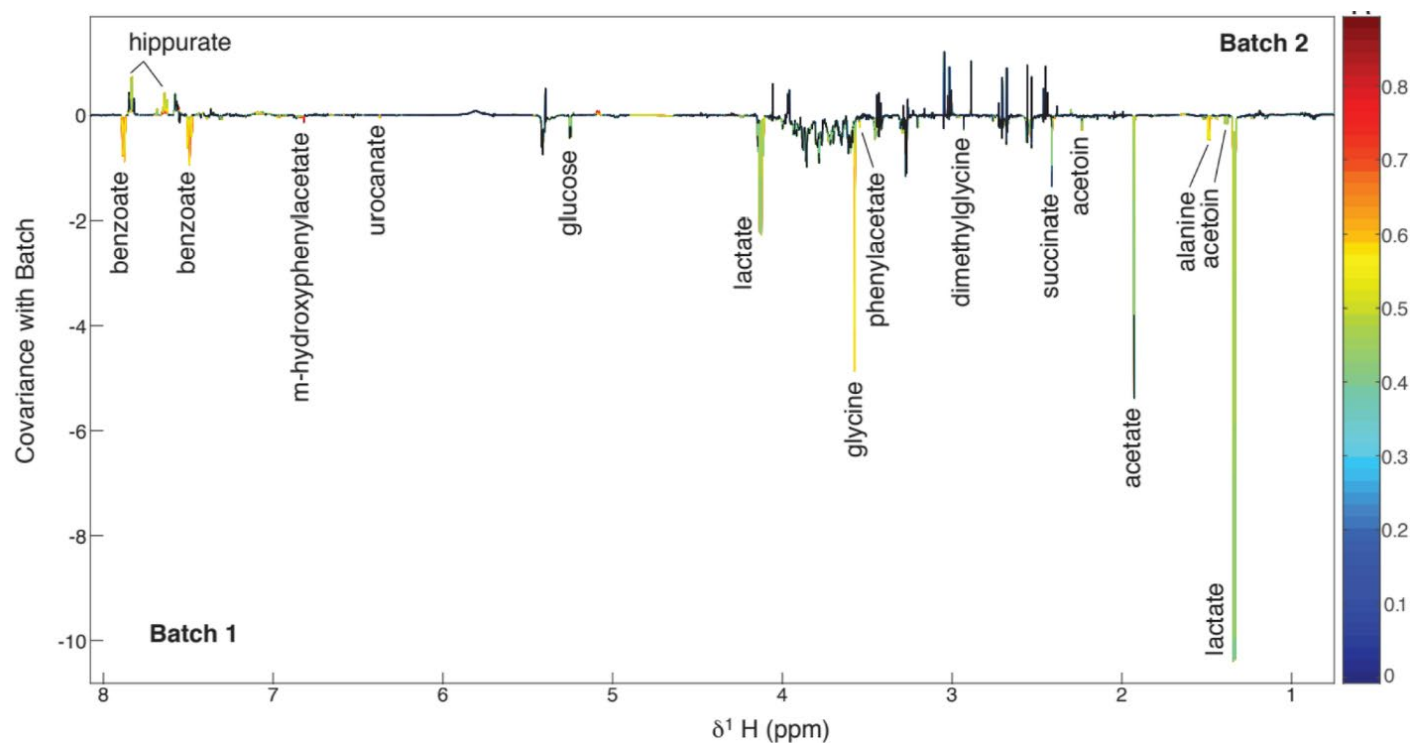
Figure 46: Untargeted 1H-NMR spectroscopy of 24 hour rat urine collections. Loadings plot from an orthogonal projection to latent squares discriminant analysis (OPLS-DA) model built using shipment batch as the response variable, back-plotted as an NMR spectrum with peak height indicating covariance with batch (downwards deflections indicate substances more abundant in animal urine from batch 1; upwards deflections indicate substances more abundant in animal urine from batch 2). The line is coloured according to the significance of the association, adjusted for multiple testing using the Benjamini-Hochberg method; black indicates non-significance between groups. Peaks are labelled with the identity of the responsible substance.

Substance	Batch 1	Batch 2	p‡	Uraemic	Control	p‡
Acetamide	28.803	28.126	0.930	24.867	34.845	**0.001**
Acetate	192.187	105.217	**0.010**	160.957	138.128	0.776
Acetoin	9.593	8.767	0.192	8.957	9.674	0.188
Alanine	29.330	18.013	**0.001**	23.765	24.923	0.809
Allantoin	28.996	29.158	0.967	25.391	35.508	0.054
Benzoate	110.964	52.071	**<0.001**	82.269	87.564	0.809
Betaine	55.595	39.399	0.129	47.318	49.834	0.809
Citrate	119.823	112.407	0.752	126.188	99.414	0.127
Creatinine	140.283	152.104	0.642	131.066	171.189	**0.027**
Dimethylamine	21.667	21.548	0.967	19.390	25.504	**0.054**
Dimethylglycine	15.669	12.643	0.124	14.725	13.538	0.677
Formate	2.873	3.007	0.967	1.995	4.575	0.127
Glucose	43.856	19.678	**0.018**	34.385	30.208	0.809
Glycine	141.491	68.457	**<0.001**	105.888	112.505	0.809
Hippurate	6.559	34.509	**0.010**	14.556	27.501	0.533
Lactate	571.659	188.265	**0.005**	402.362	388.686	0.922
m-hydroxyphenylacetate	7.086	5.944	0.827	5.387	8.632	0.600
2-oxoglutarate	167.931	182.841	0.642	183.945	158.543	0.533
Phenylacetate	13.308	8.148	**0.001**	10.380	11.982	0.600
Pyruvate	5.064	6.344	0.659	4.855	7.028	0.600
Succinate	97.877	72.642	**0.044**	85.106	88.682	0.809
Taurine	37.782	29.758	0.573	23.957	51.946	**0.009**
Trimethylamine	5.214	16.793	0.124	13.864	4.549	0.159
Trimethylamine-N-oxide	42.391	32.387	0.253	34.013	44.547	0.267
Trigonelline	-0.013	-0.024	0.218	-0.023	-0.009	0.059
Urocanate	2.764	1.001	**<0.001**	2.056	1.799	0.776

Table 2: Normalised relative concentrations of selected urinary metabolites (relative units). ‡ P values calculated using Student's *t*-test with Welch's correction for unequal variances, subsequently adjusted to limit the false discovery rate to 0.15 using the Benjamini-Hochberg procedure. Values in bold are significant at this level.
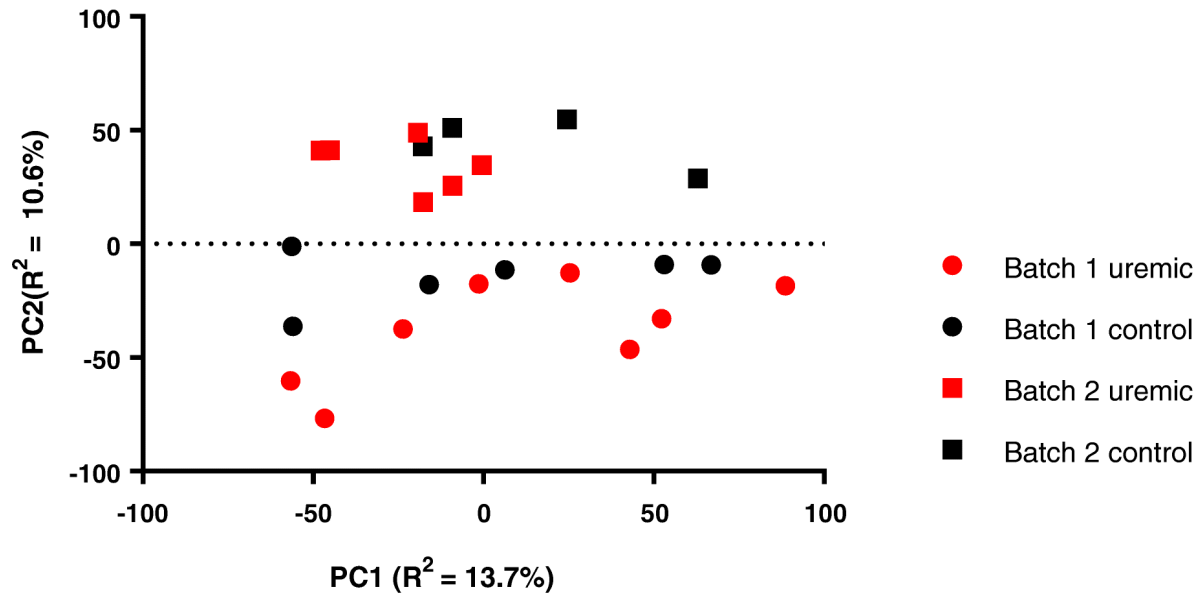
Figure 47: Next generation sequencing of the 16S rRNA gene amplicon from caecal fluid. Untargeted principal component analysis of log-ratio transformed species (OTU) abundance by sample, showing closer clustering associated with shipment batch than with treatment class.
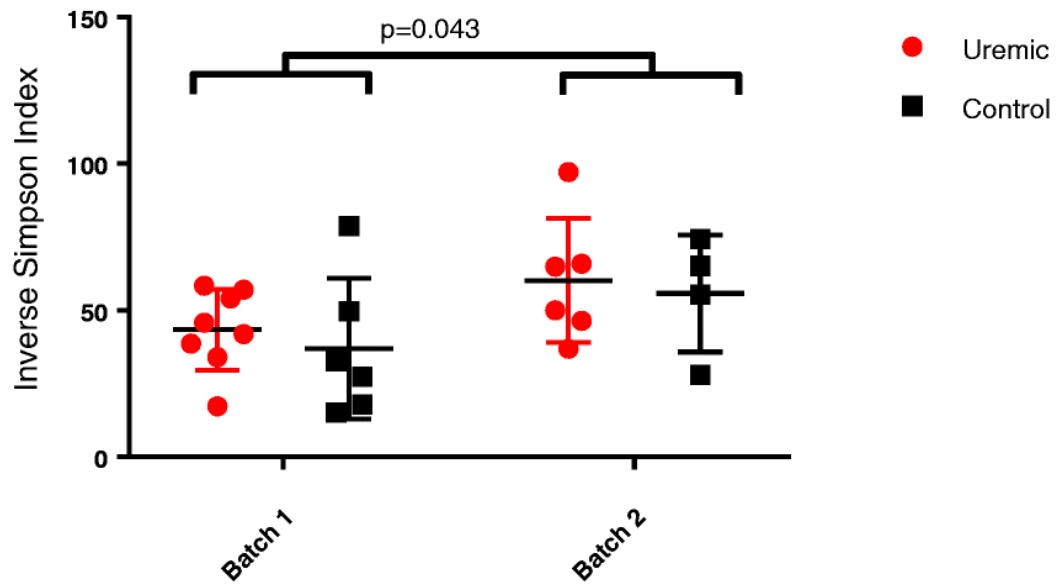
Figure 48: Alpha diversity of gut bacterial communities. Alpha diversity was higher in batch 2 than batch 1 when analysed by the Inverse Simpson Index (40.7 vs 58.5, p=0.043 by Student's T-test with Welch's correction).
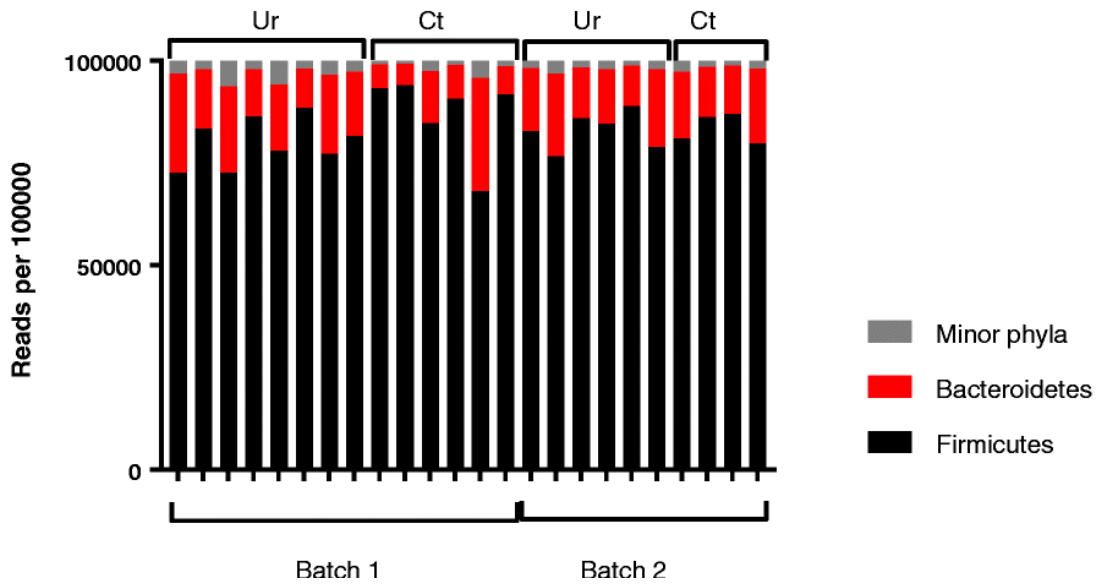
Figure 49: Relative abundances of major phyla in each sample. Each sample is represented by a vertical bar; grouped by batch and treatment group. There were no significant differences when analysed by batch or by treatment groups.

OTUs showing composition differences between batches (1 vs 2) by genus	
Increased in batch 1	**Increased in batch 2**
Ruminoclostridium (2)	Lachnospiraceae (10)
Citrobacter	Ruminoclostridium (4)
	Anaerococcus (2)
	Roseburia (2)
	Bacteroides (2)
	Subdoligranulum
	Butyricicoccus
	Butyrivibrio
	Ruminococcus
	Acetomaculum
	Lactobacillus
	Pasteurella
	Pseudomonas
	Enterohabdus
	Mollicutes sp
OTUs showing composition differences between treatment classes (uraemic vs control)	
Increased in uraemia	**Increased in control**
Lachnospiraceae	Lachnospiraceae (5)

Table 3: Taxonomic attributions of OTUs differentially abundant when analysed by shipment batch and treatment class. Differential abundance was assessed using the Analysis of Composition of Microbiomes (ANCOM) framework with alpha set at 0.05 and a cutoff value of 0.6.

	Rat cohort 1			Rat cohort 2			Rat cohort 3		
	Ct	Ur	p	Ct	Ur	p	Ct	Ur	p
Weight	510.66	468.5	0.063	511.8	484.3	0.422	537.8	525.1	0.482
24h urine output	23.83	49.3	0.006	25.8	37.4	0.28	24.2	53.2	<0.001
Serum urea	6.11	14.4	<0.001	5.9	12.8	<0.001	8.3	24.9	<0.001
Serum creatinine	27.16	74.2	<0.001	28.5	70.5	<0.001	32.5	96.3	<0.001

	Mouse cohort 1			Mouse cohort 2		
	Ct	Ur	p	Ct	Ur	p
Weight	31.09	24.4	<0.001	36.1	21.4	<0.001
24h urine output	1.22	7.7	<0.001	1.6	4.1	0.169
Serum urea				9.2	68.2	0.081
Serum creatinine				27	115.7	0.059

Table 4: Characteristics of animal cohorts. Mice in cohort 1 were not bled, but were managed exactly the same as those in cohort 2.
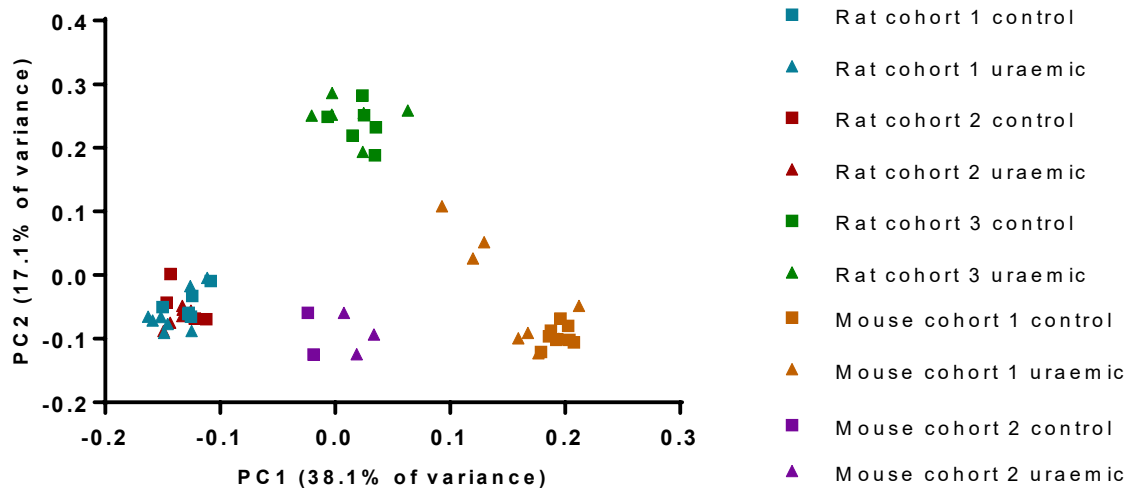
Figure 50: Principal component analysis of all mature gut microbiota samples in the dataset. Each point represents the gut microbiota of a single experimental animal, coloured according to cohort with squares representing control and triangles representing uraemic animals.
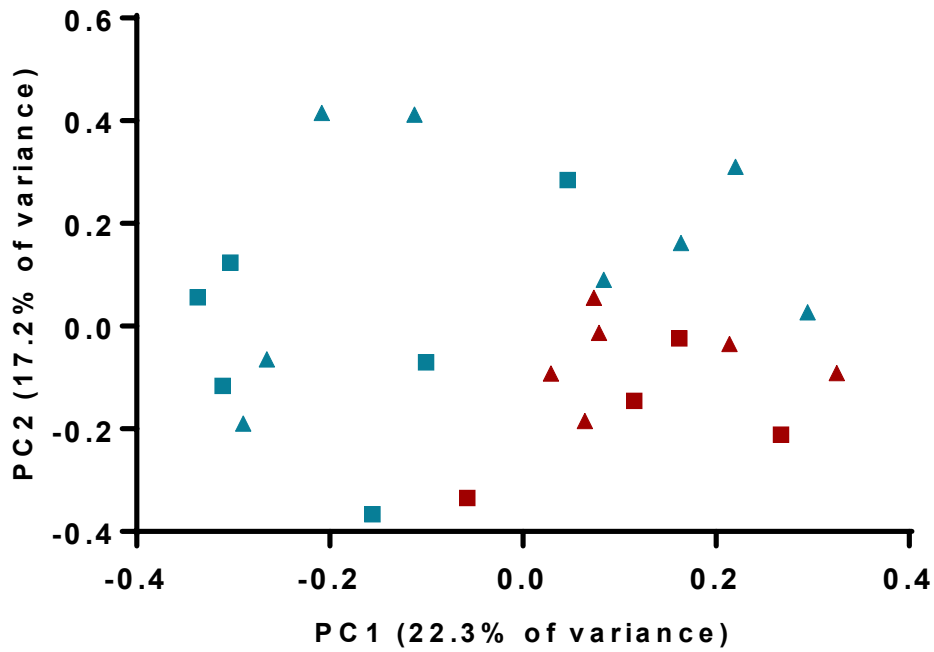
Figure 51: Principal component analysis of a reduced dataset containing only rat cohorts 1 and 2 from the full dataset. Colouring and shapes are the same as in the previous figure. Although in the previous figure these cohorts seemed to cluster together, here it can see that the microbiotas of animals in different cohorts were largely separate.
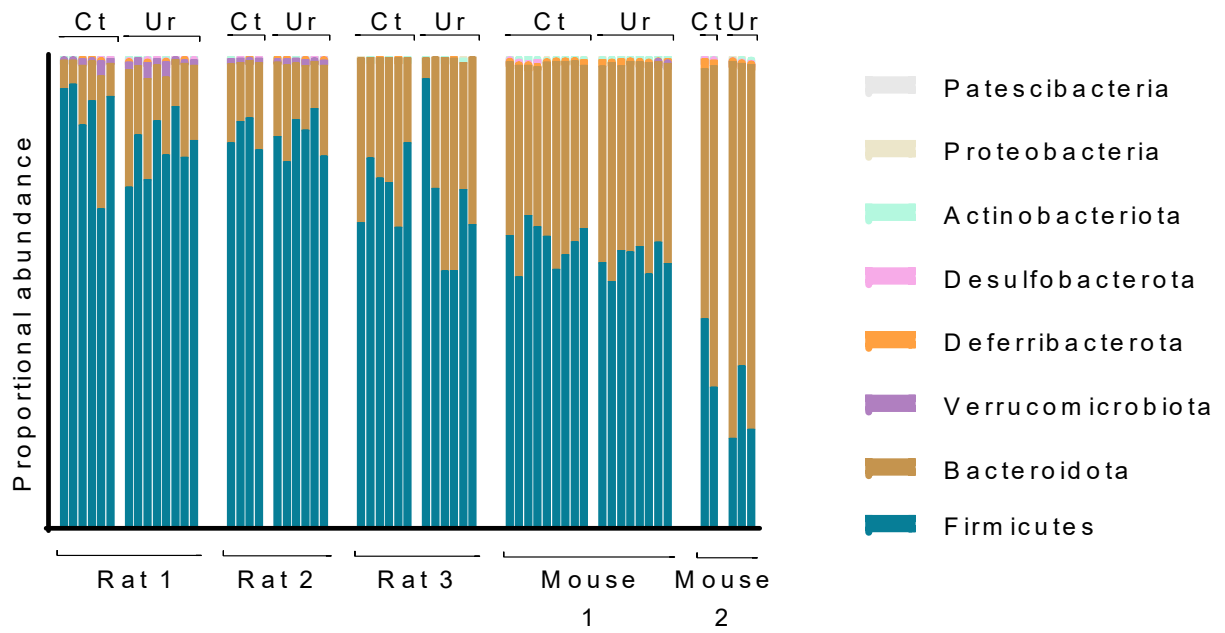
Figure 52: Relative abundance data aggregated to phylum level for all samples. Each bar represents the sequenced microbiota of a single animal, which are clustered according to cohort and treatment class (control vs uraemic).
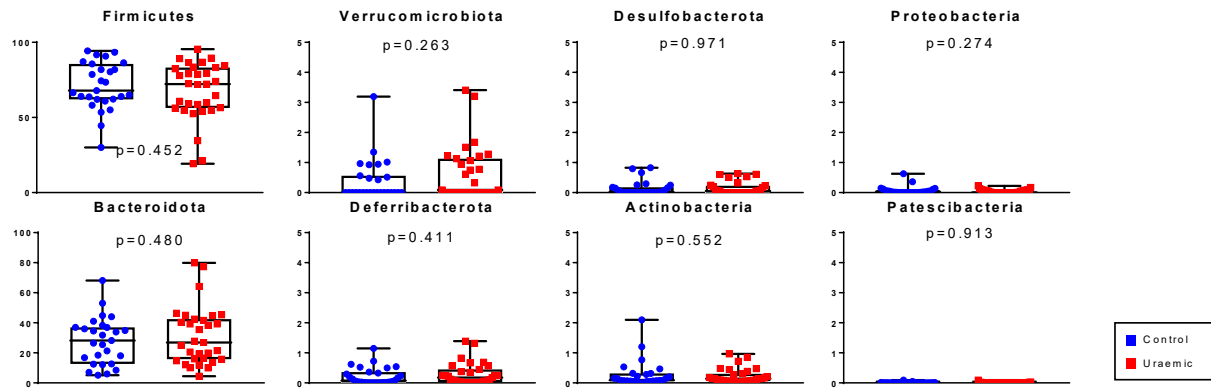
Figure 53: Relative contributions towards microbial composition of each bacterial phylum represented in the dataset, grouped according to treatment class. The y-axis measures relative abundance (percent); p-values are calculated using Welch's t-test based on log-ratio transformed relative abundance data.
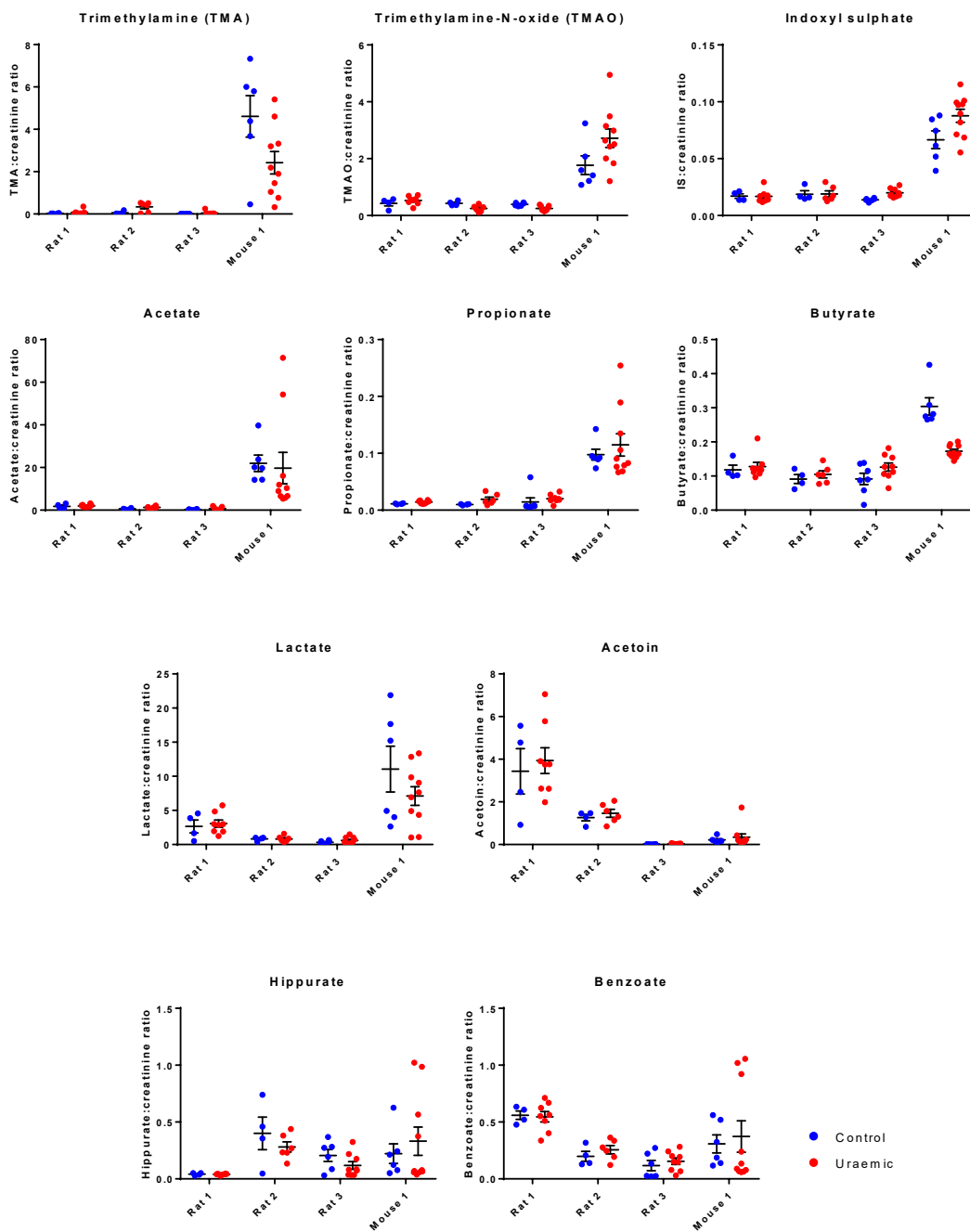
Figure 54: The effect of experimental uraemia on the urinary excretion of common bacterial metabolites. The metabolite:creatinine ratio for each metabolite based on integration of peak heights from NMR spectral profiles generated from analysis of 24-hour urine samples is shown, alongside the mean and standard error.

Results part 3: a meta-analysis of published datasets

The data presented so far in this chapter, which suggests that the effect of uraemia is minor, inconsistent and far less important than batch effects in predicting gut microbiota, are at odds with previously published data which have promoted the idea of 'uraemic dysbiosis' being a significant phenomenon.

Most notably, Vaziri et al demonstrated that 175 operational taxonomic units were differentially abundant in the gut microbiota of rats following either subtotal nephrectomy or sham surgery, concluding that uraemia profoundly affects the gut microbiota. [223] This study has proved influential on numerous review articles that have propagated the idea of 'uraemic dysbiosis'. [226-231] However, the Vaziri study comprised only a small number of animal subjects (five control and six uraemic rats, from a single cohort), and other animal studies have yielded contrasting and sometimes conflicting results. [71, 232, 233]

As each of these published animal studies employed only a single, small cohort of animals, it is challenging to disentangle the biological effect of uraemia from simple cage effects. Wide variations in sequencing strategies and bioinformatic techniques risk further amplifying artefactual differences and obscuring real biological effects.

To seek to assess the extent of batch variation across the published literature, and to seek trends which may exist but fail to reach significance in individual studies because of small sample sizes, a meta-analysis was conducted in which publicly available gut microbiome data from two online repositories were re-analysed, comprising a total of 127 rodents across ten experimental cohorts

in seven published studies, to attempt to find common microbial signatures seen across different experimental groups that may be confidently attributed to the effect of uraemia.

Meta-analysis methodology

The Short Reads Archive (SRA) operated by the National Centre for Biotechnology Information (NCBI) was searched for relevant studies, using the search term (uraemia OR uremia OR kidney OR renal) AND (microbiome OR microbiota) AND (rodent OR rat OR mouse OR mice). This search returned gut microbiome data from 412 samples across fourteen separate studies, which were assessed for suitability for inclusion using the Run Selector facility. Eligibility criteria were: use of rodent subjects, use of experimental techniques to induce chronic (>2 weeks) uraemia, and the use of non-culture dependent, DNA-based tools to assess the gut microbiota. Exclusion criteria included the use of experimental interventions, other than the induction of uraemia; however, in some studies employing a four-group design (eg, control, control plus intervention, uraemic, uraemic plus intervention), data from animals in the non-intervention control and uraemia groups were included.

Eight studies were excluded: three because there was no induction of uraemia, two which used RNA rather than DNA sequencing; one which employed an acute kidney injury rather than a chronic kidney disease model; one which studied kidney tissue rather than gut samples, and one which included only human samples.

The remaining six studies were included [71, 179, 232-235], including published results reported in the previous chapter (Randall 2019) which comprised data from two cohorts of animals (termed Randall2019a and Randall2019b). Each of these studies have been published in a peer-reviewed journal.

One of these studies (Al-Asmakh2020, [235]) included sequencing samples from the ileum, caecum, and colon for each animal; we elected to include only caecal samples in this analysis to match the majority of the samples from other rat cohorts.

Data was also included from two further cohorts (Randall 2021a and Randall 2021b) which were described earlier in this chapter (as rat cohort 3 and mouse cohort 1); and are also publicly available via the SRA.

Finally, phylochip microbiome data from the older, Greengenes repository, was obtained for a final study, Vaziri 2013, [223] which was the first major study to claim to show the effect of uraemia on the gut microbiome. All other phylochip datasets in the Greengenes repository were screened for eligibility using the criteria above but none were suitable.

The full design of the meta-analysis is documented in Figure 55, p. 187.

Results

Of the seven published studies included in the meta-analysis, three were designed to investigate bacterial production of uraemic toxins, [179, 233, 234] three to investigate gut-acting

medications for the improvement of the uraemic syndrome (only samples from non-intervention animals were included), [71, 232, 235] and one was primarily to investigate the effect of uraemia on the gut microbiome itself. [223] Full details about the experimental conditions used in each experiment are available in the published experimental write-ups, and are summarised in Table 5, p. 188.

In total, data was included from 127 animals; 73 rats across six cohorts (33 control and 40 uraemic) and 54 mice across four cohorts (28 controls and 26 uraemic). There were significant differences between these datasets in the methods used to induce uraemia, the age of animals at the time of sacrifice, the sample types studied, and in the methods of DNA analysis, primer pairs and sequencing depths used.

Data were downloaded from the online repositories; raw sequencing data were re-analysed using the DADA2 pipelines and taxonomic identities assigned using the Silva reference database. There was a broad but non-significant positive correlation between sequencing depth (mean reads per sample) and observed species richness (amplicon sequencing variants, ASVs, per sample); Spearman rank coefficient 0.55, p=0.133.

Cohort and host species are the key drivers of variation across all datasets

Sequencing data from different cohorts were agglomerated at family level (the lowest taxonomic level at which all ASVs were assigned a clear identity) and combined to allow broad trends in variation to be visualized across all datasets. After centred log-ratio transformation, redundancy

analysis revealed clustering to be most significantly influenced by cohort, with the Al-Asmakh2020 and Kikuchi2017 cohorts clustering completely apart from other samples and only the Randall2019a and Randall2019b cohorts, which comprised animals obtained a few weeks apart from the same supplier, displaying broadly overlapping ordination Figure 56, p. 174.

Permutational analysis of variance (PerMANOVA) of the log-ratio transformed datasets was used to establish how much variation could be attributed to different independent experimental variables; this revealed that cohort accounted for the largest amount of variation (69% of variance, $p<0.001$), with host species (rat vs mouse) accounting for 13.3% of variance ($p<0.001$).

Other significant associations were found between clustering and primer type (V1/V2 vs V3 vs V3/V4, 23.9% of variation, $p<0.001$), method of inducing uraemia (surgery vs adenine feed, 13.2% of variation, $p<0.001$), sequencing methodology (454 pyrosequencing vs Illumina, 9.7% of variance, $p<0.001$) and sample type (faeces vs caecal fluid, 6.7% of variance, $p<0.001$); although many of these variables were closely associated with cohort.

Treatment effect (control vs uraemic) did influence sample clustering, but to a much lesser extent (1.9% of variance, $p=0.026$).

Certain community shifts between control and uraemic samples may be shared between cohorts

To understand what aspects of sample variance may allow control and uraemic samples to be separated across all cohorts, scores and loadings from the redundancy analysis were interrogated.

This revealed that whilst control and uraemic samples were not significantly separated in axes 1 and 2, when the redundancy analysis model was further explored, it was discovered that there was a significant shift between control and uraemic samples in both axes 3 and 4 directions (axis 3 represented 14.3% of total variance and axis 4 represented 6.7%, Figure 57, p. 190). Overall there was a vector of [-0.035,-0.046] between the spatial mean of all uraemic samples compared to the spatial mean of all control samples (p=0.045 and p=0.009, respectively); furthermore there were uniform negative vectors of movement in both axes between the spatial mean of uraemic and control samples within each individual cohort, implying the same microbial shifts are occurring in all datasets.

Loadings for these axes were compared to establish which particular taxa were responsible for the observed trends (Table 6, p. 191). Samples associated with a downwards ('uraemic') deflection on axis 4, the more strongly correlated with treatment class, displayed increased relative abundances of families including *Peptostreptococcaceae*, *Clostridiaceae* and *Prevotellaceae*; and reduced abundances of families *Akkermansiaceae* and two highly abundant taxa, *Lactobacillaceae* and *Oscillospiraceae*. A 'uraemic' deflection along axis 3 was also associated with an increase in *Prevotellaceae* and *Christenellaceae*, which had both also been increased in axis 4. *Peptococcaceae* and *Akkermansiaceae* were associated with opposite deflection in the two axes, likely reflecting different effects in different cohorts.

Significant compositional differences exist between experimental cohorts

Each experimental dataset was agglomerated at phylum level, and community composition was plotted for each sample to allow comparison between cohorts (Figure 58, p. 192).

Significant differences were evident between rat and mouse sequencing cohorts, with the dominant phylum in rats being *Firmicutes*, accounting for 76% of reads in rat samples vs 40% in mouse samples (p<0.001), whilst in mouse samples the most abundant phylum was *Bacteroidetes* (58.7% of sequencing reads in mouse samples but only 9.9% in rat samples; p<0.001). Mouse samples were generally simpler than those from rats, with the contribution of these major taxa accounting for an average of 98.4% of reads in mice, but only 84% in rats (p<0.001).

The Al-Asmakh2020 and Kikuchi2017 appeared to be outliers compared to other rat cohorts. In the Al-Asmakh2020 cohort there was a very substantial increase in taxa that were represented at a lower abundance overall, especially *Proteobacteria* and *Actinobacteria*, in uraemic animals, accounting for an average of 39.9% and 9.4% of reads, respectively, in this group. Conversely samples in the Kikuchi2017 cohort were very simple, with reads from the phylum *Firmicutes* accounting for 98.5% of reads across all samples and uraemia having little discernible effect.

The Vaziri2013 dataset was analysed differently from the others because of the differences between phylochip and sequencing data. The phylochip system records mean fluouroscopic intensities for 4255 probes across 43 separate taxa, and the assigned taxonomies did not always align with the more modern Silva taxonomy used for sequencing reads in the other datasets.

Furthermore the reported values per phylum reflect as much the composition of the phylochip itself as necessarily the relative abundances in the bacterial DNA. Because of this, only the top 12 phyla were included in the bar chart analysis in Figure 58, representing a slightly different range of taxa than the twelve phyla seen in the other cohorts. Notwithstanding this, a similar picture emerged to other rat samples, with the *Firmicutes* phylum being predominant. The relatively high abundances of minor phyla in the Vaziri2013 samples may reflect increased prominence of these probes in the design of the phylochip.

Uraemia may increase alpha diversity in rats, but effects are inconsistent across cohorts

Alpha diversity using a variety of measures (observed ASVs per sample and the Chao1, ACE, Shannon, Simpson, Inverse Simpson and Fisher indices) was calculated in all cohorts using raw sequencing abundance data (the Vaziri2013 cohort was not included in this analysis because the nature of the phylochip analysis makes the results incomparable directly with sequencing methodologies), supplementary Table 17, p. 406, appendix 5.

When all samples were analysed together, there were no significant differences in alpha diversity between control and uraemic animals. However, samples from rats were found to have higher alpha diversity than samples from mice across most measures, significantly so for observed ASVs per sample (338 in rats vs 232 in mice, p=0.006), and the related Chao1 and ACE indices.

Among rat samples, those from uraemic animals showed higher alpha diversity than those from controls across all measures; significantly so for the Shannon (4.135 in control vs 4.656 in uraemic, p=0.011), Simpson (9.952 vs 9.975, p=0.01) and Inverse Simpson (40.74 vs 62.59, p=0.012) indices. Although this was chiefly driven by the highly diverse uraemic samples in the Al-Asmakh2020 cohort, a trend towards increased alpha diversity was seen universally across all measures of diversity in every rat sequencing cohort.

A far less obvious picture was seen in mouse samples, with no measures of alpha diversity showing significant differences between control and uraemic samples. There were no convincing patterns of association on the level of individual cohorts, with some showing increased diversity in controls (eg Kikuchi2019) and some increased diversity in uraemic animals (eg Randall2021b).

Beta dispersion was assessed in control and uraemic groups within each cohort to test the hypothesis that uraemia increases the heterogeneity of gut communities. Rat samples were significantly more heterogeneous than mouse communities overall (average distances of individual points to group median 0.399 vs 0.312, p<0.001), however uraemic animals did not demonstrate increased beta dispersion compared control animals either in the whole dataset (0.352 in controls vs 0.364 in uraemic animals, p=0.53); or at species level analysis (in either rats or mice); only in the Al-Asmakh2020 cohort was there a significant difference between diversity (with uraemic animals displaying increased heterogeneity of dispersion, 0.22 vs 0.44, p=0.003). This association was not significant in any other cohort and in a number, the trend was reversed with uraemic samples being less heterogenous than controls.

Samples from control and uraemic animals cluster apart in most cohorts

Plots of redundancy analysis ordination for log-ratio transformed datasets at the level of individual ASVs were constructed for all cohorts (Figure 59, p. 193). Samples from uraemic animals clustered separately from those from control animals in most cohorts, and this was confirmed using PerMANOVA which quantified significant between-group differences associated with uraemia in seven of the ten cohorts. Nevertheless, significantly divergent clustering attributable to cage effects was seen in a number of cohorts; perhaps especially affecting control samples, in the Mishima2015, Nanto-Hara2020, Randall2019a and Randall2021b cohorts.

In some cohorts, uraemia may affect the relative abundances of health and disease-associated taxa

The ANCOM methodology was used to assess differential abundances of all bacterial subtaxa between control and uraemic samples in all cohorts, at each taxonomic level between individual ASVs and phyla. These results are summarised in supplementary Table 18, p. 410, appendix 5.

In two cohorts (Al-Asmakh2020 and Vaziri2013), a classically dysbiotic picture emerged with reductions in health-associated, gram-positive taxa (prominently genus *Lactobacillus*, also *Bacteroides* and *Akkermansia*), and an increase in gram-negative bacteria (including families

from the class *Gammaproteobacteria*, such as *Enterobacteriaceae* and *Pseudomonadaceae*; and subtaxa from class *Actinobacteria* including *Corynebacteriaceae* and *Bifidobacteriaceae*).

These changes were not seen universally, and in some cohorts – including notably two of the cohorts which did not show significantly differential clustering in ordination plots and PerMANOVA (Randall2019a and Kikuchi2017) – there were no differentially abundant taxa between control and uraemic groups at any taxonomic level after adjustment for multiple-hypothesis testing. In other cohorts, conflicting results were seen, such as in the two mouse cohorts Mishima2015 and Nanto-Hara2020, where some *Lactobacillus* species were actually seen to increase in abundance in samples from uraemic animals.

To assess whether similar trends were seen across multiple groups, but perhaps not reaching statistical significance because of small samples sizes, the mean relative abundance of all families was calculated in control and uraemic samples in all cohorts except Vaziri2013, where the use of Phylochip molecular identification makes proportional abundances unreliable. Results for the five most abundant taxa, and three others representing taxa previously identified by ANCOM as potentially influenced by uraemia, are presented in Figure 60, p. 194.

There were no families for which uraemia caused uniform changes in all cohorts. However, two highly prevalent taxa showed a trend to reduced abundances in uraemic animals (eg *Lactobacillaceae*, the second most abundant family overall, which had at least slightly lower relative abundances in 7/8 cohorts where it was detected, and *Lachnospiraceae*, fifth most abundant family overall, which had lower relative abundances in 7/9 cohorts). A number of taxa showed relatively uniform increases in uraemic animals, including several families from the

phylum *Firmicutes* (*Clostridiaceae*, increased in 9/10 cohorts; *Erysipeltrichaceae*, increased in 7/9 cohorts; *Peptostreptococcaceae*, increased in 6/7 cohorts), two from phylum *Bacteroidota* (including the second most abundant family overall, *Muribaculaceae*, increased in 6/8 cohorts, and *Tannerella*, increased in 6/7 cohorts); and two from phylum *Actinobacterota* (*Eggerthella*, increased in 7/9 cohorts; and *Bifidobacteriaceae*, increased in 4/4 cohorts). Other highly abundant families (eg *Oscillospiraceae* or *Ruminococcaceae*) did not show anything approaching a uniform association with uraemia.

Search of NCBI SRA database for using search terms: (uraemia OR uraemia OR kidney OR renal) AND (microbiome OR microbiota) AND (rodent OR rat OR mouse OR mice)

- 412 individual samples
- In 14 published studies

Added two further experimental cohorts, one of mice and one of rats, which were previously unpublished but which are available on the SRA database.

- 17 mice
- 12 rats

Added a further rat cohort which was publicly available in the older Greengenes repository.

- 11 rats

Excluded 8 studies (296 samples):

- Three did not include generation of experimental uraemia
- Two featured RNA not DNA sequencing
- One studied acute uraemia
- One studied kidney samples (not microbiome)
- One studied human microbiota

- 127 samples
  - 73 rats in six cohorts
  - 54 mice in four cohorts
- Across seven published studies

Figure 55: Consort diagram of meta-analysis.

Cohort	Host species	Number (control/uraemic)	Method for induction of uraemia	Age at time of sacrifice	Sample type	Molecular study method	16S region studied	Sequencing depth (mean reads/sample)	Assigned ASVs in dataset
Al-Asmakh2020	Rat	12 (6/6)	0.75% adenine feed	14w	Cecal fluid	Illumina	V3/V4	182,389	2,453
Kikuchi2017	Rat	13 (6/7)	5/6 nephrectomy	42w	Feces	454 pyrosequencing	V1/V2	3,000	550
Kikuchi2019	Mouse	10 (5/5)	0.2% adenine feed	16w	Feces	Illumina	V1/V2	34,366	369
Mishima2015	Mouse	12 (6/6)	0.2% adenine feed	15w	Feces	454 pyrosequencing	V1/V2	8,297	1,022
Nanto-Hara2020	Mouse	15 (8/7)	0.2% adenine feed	16w	Feces	Illumina	V1/V2	30,890	631
Randall2019a	Rat	14 (6/9)	5/6 nephrectomy	18w	Cecal fluid	Illumina	V3	175,607	1,331
Randall2019b	Rat	10 (4/6)	5/6 nephrectomy	18w	Cecal fluid	Illumina	V3	193,520	1,228
Randall2021a	Rat	12 (6/6)	5/6 nephrectomy	18w	Cecal fluid	Illumina	V1/V2	12,481	712
Randall2021b	Mouse	17 (9/8)	0.15% adenine feed	26w	Cecal fluid	Illumina	V1/V2	19,393	983
Vaziri2013	Rat	11 (5/6)	5/6 nephrectomy	16w	Feces	Phylochip	All	NA*	NA*

Table 5: Protocols for animal cohorts and techniques used for molecular characterisation of gut microbiota in the datasets included in this study. * The publicly available phylochip data from the Vaziri2013 [223] dataset consists of mean fluouroscopic intensity data from 4,522 probes each consisting of a 25bp DNA strand against a portion of the 16S gene unique to one bacterial taxon. Each of these probes was treated as a separate ASV for the purposes of *phyloseq* analysis.
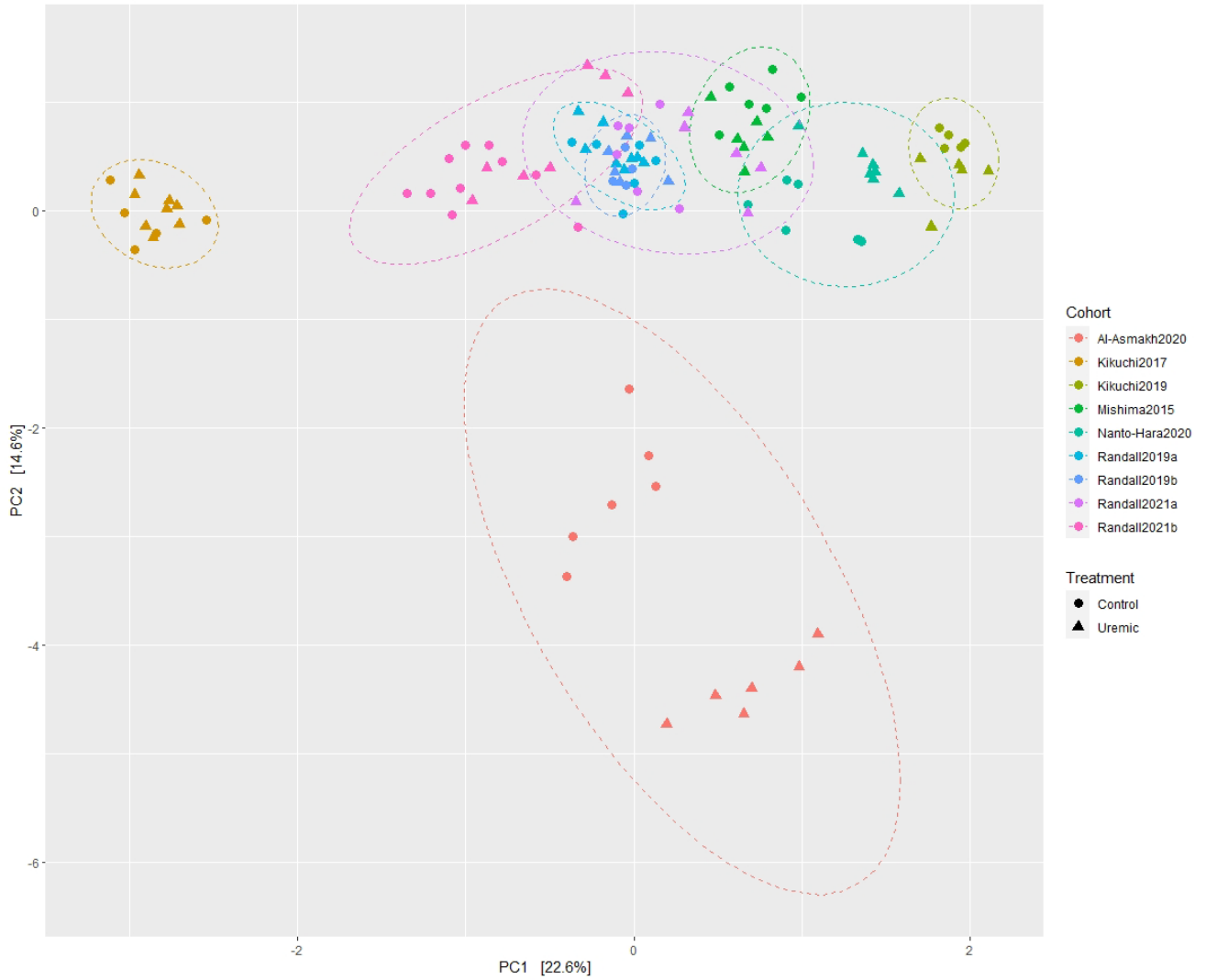
Figure 56: Ordination plot of redundancy analysis of combined, log-ratio transformed data from all sequencing samples, agglomerated at family level. Each point represents an individual sample; circles represent samples from control animals and triangles samples from uraemic animals; colours represent samples from different cohorts.

189
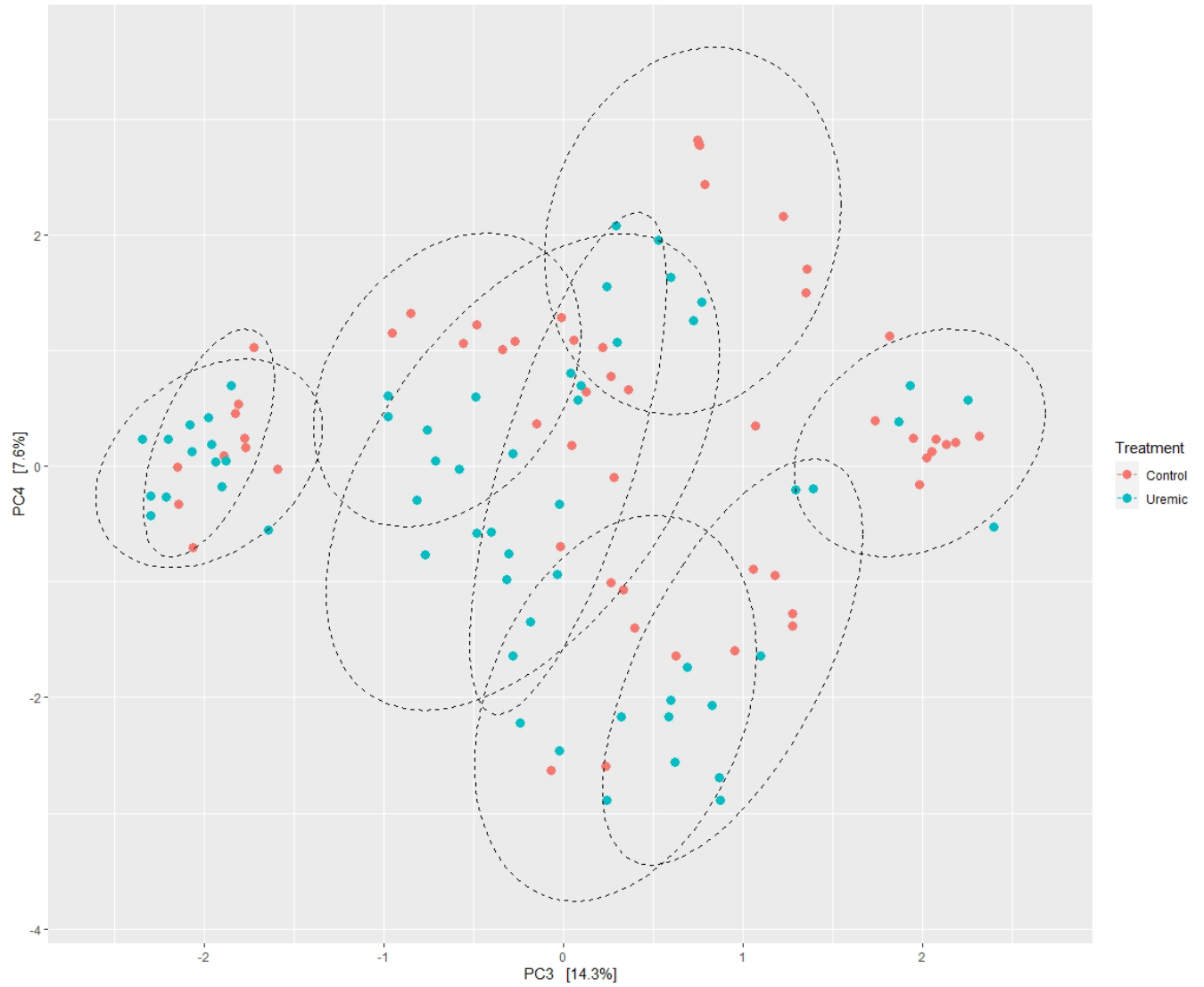
Figure 57: Ordination plot showing axes 3 and 4 from the RDA model of all samples. Each point represents an individual sample, coloured according to treatment. Ellipses represent different cohorts.

	Axis 3; 14.3% of variance		Axis 4; 6.7% of variance	
	Family	Loading	Family	Loading
Increased in uraemia	*Peptococcaceae*	0.337	*Peptostreptococcaceae*	0.51
	Prevotellaceae	0.285	*Clostridiaceae*	0.416
	Christenellaceae	0.272	*Erysipelatoclostridiaceae*	0.251
	Akkermansiaceae	0.244	*Prevotellaceae*	0.198
	Peptostreptococcaceae	0.235	*Christenellaceae*	0.11
Decreased in uraemia	*Eggerthellaceae*	-0.115	*Peptococcaceae*	-0.11
	Erysipellaceae	-0.137	*Oscillospiraceae*	-0.112
	Muribaculaceae	-0.162	*Lactobacillaceae*	-0.236
	Streptococcaceae	-0.185	*Rikenellaceae*	-0.249
	Erysipelatoclostridiaceae	-0.23	*Akkermansiaceae*	-0.262

Table 6: Loadings for axes 3 and 4 in the RDA model. These axes showed significant associations with the shift in spatial means between control and uraemic samples (p=0.045 and p=0.009, respectively). The five families most positively and negatively associated with each axis are listed along with their respective contributions to the model.
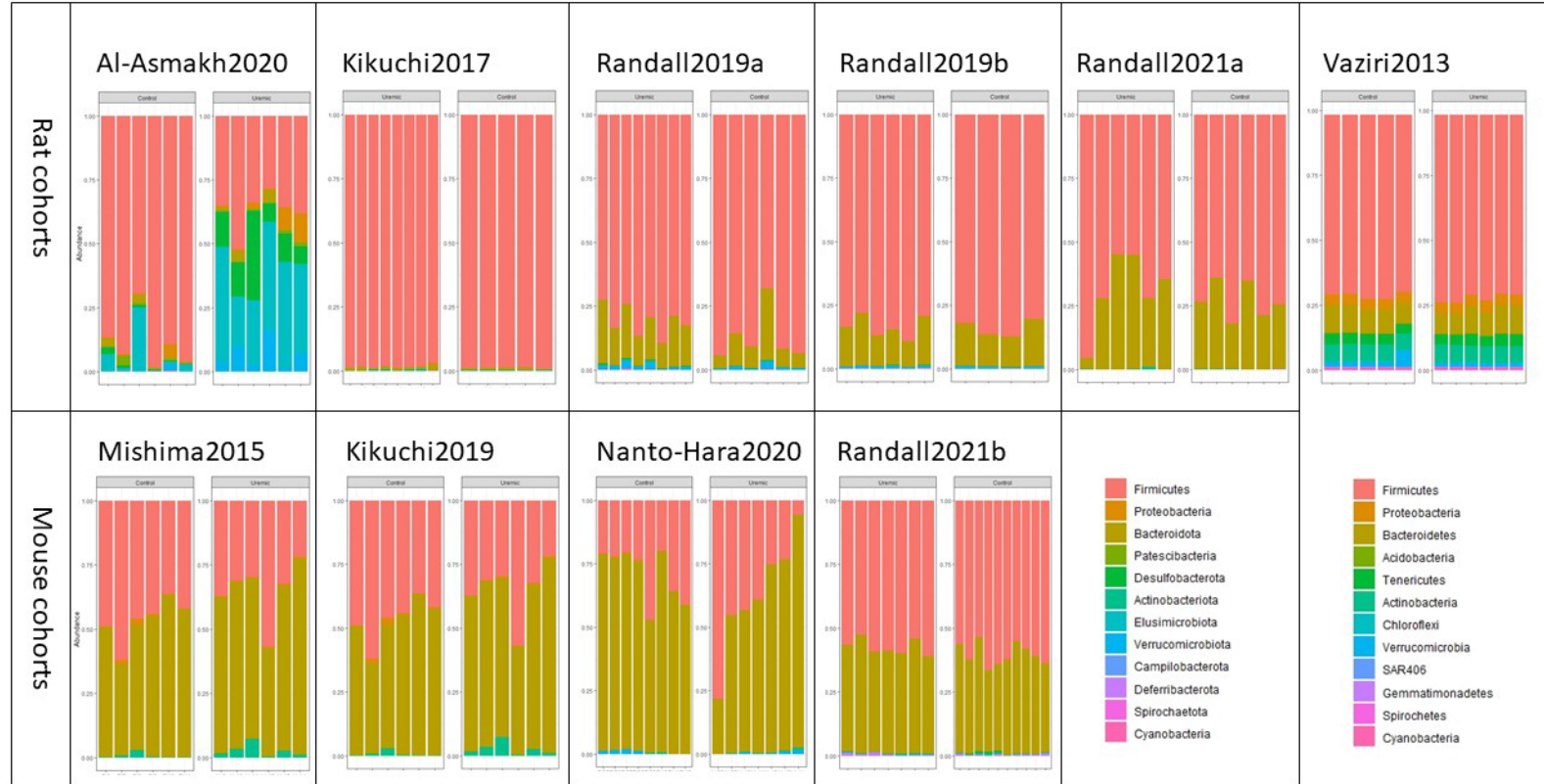
Figure 58: Proportional community bacterial abundances at phylum level in all experimental cohorts. Rat cohorts are on the top row and mouse cohorts below. Each vertical bar represents a sample from a single animal, grouped within cohorts with control samples on the left and uraemic samples on the right. Because of the nature of phylochip analysis, the Vaziri2013 cohort included data for 43 cohorts including many making negligible contributions to the overall population; for the Vaziri2013 cohort only the 12 most abundant cohorts are shown and a different legend is provided to reflect the different taxonomy used in phylochip analysis compared to more taxonomic assignments.
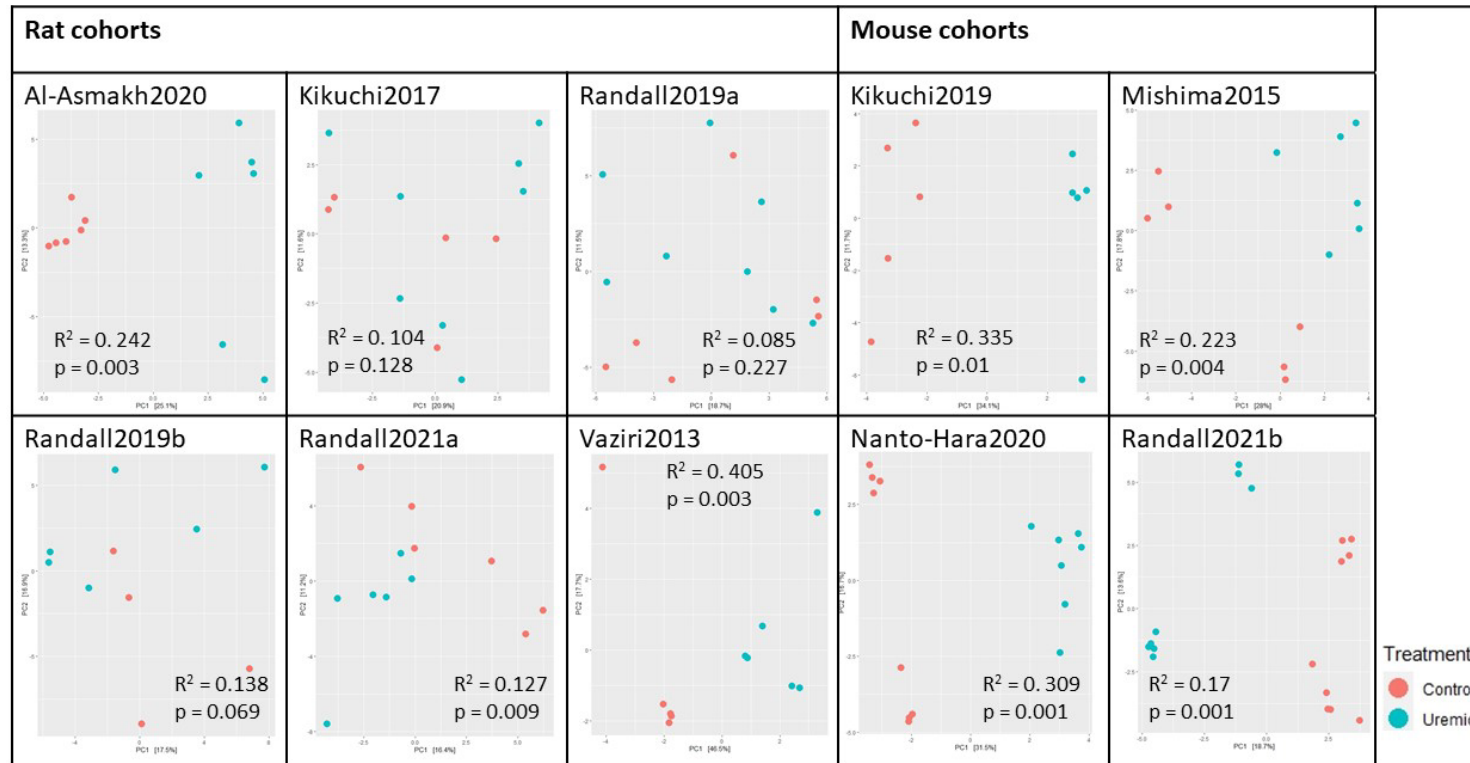
Figure 59: Ordination plots of composition-transformed data for all cohorts at the level of individual ASVs. Each point represents a sample from an individual animal, coloured according to treatment (control vs uraemic). R^2 and p-values from PerMANOVA analysis of the same data are superimposed on each plot. Divergent clusters between similarly treated animals seen in the Mishima2015, Nanto-Hara2020, Randall2019a and Randall2021b are attributed to caging effects.
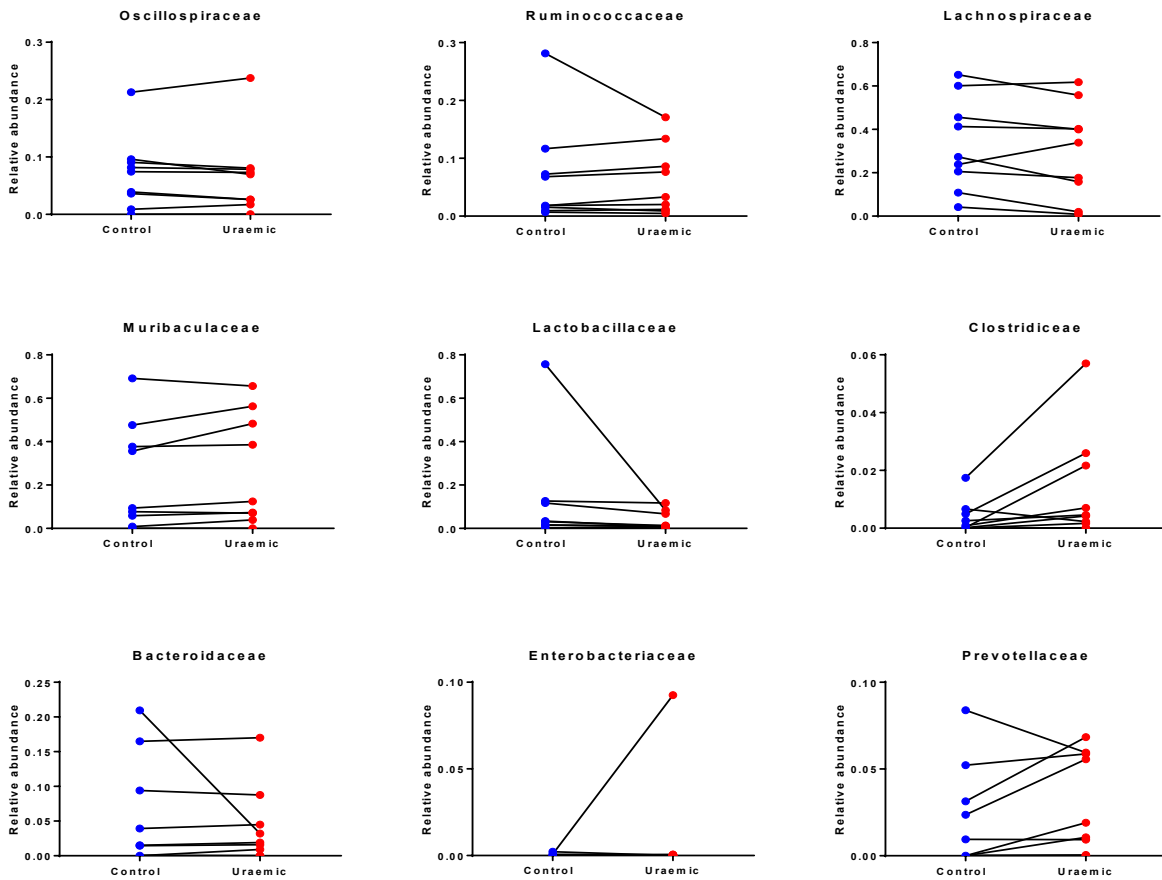
Figure 60: Relative abundances of different families of the most abundant bacterial families in control vs uraemic animals within different experimental cohorts. Each point represents the mean relative abundance of that family of bacteria in samples from either control or uraemic animals from an individual cohort of animals, and the lines connect control and uraemic animals in the same cohort. None of the average differences in means shown were significant at an alpha of 0.05.

Discussion

Lack of reproducibility in pre-clinical animal research remains a major challenge in experimental biology, [236] and is at least partially explained by variation between animal microbiomes. [237] Animal research has been based on the assumption that whilst experimental animals in different facilities may have differences at species level between their gut microbiota, [238] at a population level, in healthy laboratory animals on identical diets, these diverse collections of microorganisms achieve a shared set of basic metabolic functions – an assumption supported by evidence of significant functional redundancy within gut microbial communities [239]. The work presented in this chapter suggests these assumptions may not be valid.

Sequencing and metabolomic data

In the first half of this chapter, the data presented confirms that significant batch variations exist between the gut microbiota of laboratory animals, and associates them with multiple, major variations in a range of urinary metabolites, with the potential for significant downstream effects on wider areas of host phenotype.

For example, circulating hippurate has been suggested as a biomarker for gut microbial diversity, associating with the risk of metabolic syndrome; [240] however, these results suggest it may be totally absent in the urine of experimental animals based on shipment batch. Likewise the biological relevance of dietary amines has been demonstrated through the association of trimethylamine (TMA) and its metabolite trimethylamine-N-oxide (TMAO) with cardiovascular

disease, [241, 242] including in patients with chronic kidney disease. [243] However, these results suggest that rats purchased from the same supplier in different shipment batches may metabolize dietary amines in quite different ways, potentially questioning the generalisability of research based on individual batches of animal subjects.

Since the diet of animals in each group was identical, differences in bacterial metabolic pathways are likely to underlie these differences in the urinary metabolome. Certainly, a number of bacterial taxa which we demonstrated to be differentially abundant between cohorts are known to have metabolic significance, including several that are major sources of short chain fatty acids and associated with beneficial health outcomes, [244-246] and several from the phylum *Proteobacteria* that has recently been shown to contribute significantly to functional variation between gut metagenomes. [247]

These results are also broadly consistent with recent work suggesting that in CKD, concentrations of known uraemic toxins rise in plasma because of impaired urinary excretion, rather than an increase in gut production of these toxins. [248] Although we demonstrated a modest increase in the 24-hour urinary excretion of IS across all samples (p=0.04), this was driven by results in rat cohort 3 and mouse cohort 1. Thus, as well as failing to demonstrate any gross shifts in gut microbiota in uraemia, we have also provided additional evidence against the idea that an altered microbiota might be driving the progression of uraemia through increased gut biosynthesis of toxins, popularised in notions of a 'gut-kidney axis'. [227, 249]

The rodent gut microbiome is a complex community of several hundred different bacterial species that possesses significant metabolic potential of immense relevance to the host organism.

It has previously been demonstrated that this community differs according to a variety of factors including host age [250] and genetics. [251, 252] caging arrangements, [250, 252, 253] bedding material and water sterilization technique [254] and vendor shipment batch. [251] Xiao et al generated a catalogue of the mouse metagenome by sequencing faecal material from 184 mice, and found that vendor was a prime determinant in variation at a genetic and function level. [255] We have provided further evidence to validate the findings of significant differences between cohorts and have shown by NMR metabolomics that these changes have significant functional implications.

Meta-analysis

The use of a meta-analysis to apply the insights around batch variation to repository data from other published animal studies is relatively novel. In clinical research, the use of meta-analyses is common, and when correctly performed, such studies are often considered to constitute the highest form of evidence. [256, 257] Conversely, whilst in basis sciences research, narrative reviews of published data are common, attempts to synthesis and re-analyse data from disparate studies using meta-analysis tools are rare. [258, 259] This is regrettable, since as we demonstrate, standardised datasets (eg 16S gene amplicon sequencing results) allow data from different studies to be compared easily, resulting in far larger experimental groups and allowing genuine trends in data to be uncovered which transcend batch variation and may be obscured in studies of small sample size.

In this meta-analysis, we re-analysed and compared all datasets available in public repositories that describe the effects of chronic experimental uraemia on the gut microbiome of rodents. The overwhelming picture that emerged was of between-cohort differences which eclipsed the effect of experimental intervention in explaining the observed variation between samples. Although it is possible that differences in experimental technique and sequencing methodologies may account for some of these cohort differences, we suggest that the majority is likely to be accounted for by baseline differences in the gut microbiome of animals raised in different animal facilities. The fact that there was significant heterogeneity between cohorts in the effect (or lack of effect) caused by experimental uraemia (for instance, between the Al-Asmakh2020 and Vaziri2013 cohorts, where large effects were associated with uraemia, and the Kikuchi2017 and Randall2019a datasets where there was very little observable effect), poses significant questions about the generalizability of rodent research in any biological experiments where the gut microbiota might play a significant physiological or pathological role.

Significant differences between rat and mouse samples illustrate how gut microbiota adapt closely to different host environments and suggests that effects seen in one species may not generalise to others. This also implies that extra caution should be used in extrapolating findings from rodent microbiome research to humans.

However, a few broad effects of uraemia on the gut microbiome emerged from comparing different cohorts together. None of these trends were seen in all cohorts, implying there is no distinct and reproducible signature of uraemia on the gut microbiome; however each of the following features were seen in the majority of cohorts, implying that the common factor of

uraemia may be causative: increased alpha diversity (in samples from rats), an increase in opportunistic taxa less commonly seen in gut communities, including subtaxa from phyla *Firmicutes*, *Bacteroidota* and *Actinobacterota,* and in the Al-Asmakh2020 and Vaziri2013 cohorts, from class *Gammaproteobacteria*; and a decrease in core, health-associated taxa, particularly *Lactobacillus* and *Lachnospiraceae*.

The fact that shared cross-cohort effects were so hard to describe despite control and uraemic samples clustering separately in most cohorts highlights that cage effect represents a major source of experimental bias in microbiome research. In the experimental cohorts included in this meta-analysis, caging was according to treatment class in almost all (ie control animals housed with other controls, and uraemic animals with other uraemic animals), often because the practicalities of administering a modified feed or performing surgery required that control and uraemic animals were housed apart. The consequence of separate housing is that when samples are analysed, it becomes impossible to distinguish the effects of uraemia on the microbiota from the diverging effects that would be seen between any two groups of animals housed in separate cages. Profound cage effects were seen between different groups of similarly-treated animals in a number of the cohorts analysed (Mishima2015, Nanto-Hara2020, Randall2019a and Randall2021b), and in several of the cohorts there were ASVs present in high abundance in one experimental group but totally absent in the other group, which are highly likely to reflect cage effects rather than the biological effect of uraemia. Interestingly, the fewest changes seen between control and uraemic groups were seen in cohorts where attempts had been made to reduce caging effects, either by moving animals between cages prior to the initiation of surgery to homogenize microbial populations (Randall2021a), by housing control and uraemic animals

together after post-operative recovery (Randall2019a and Randall2019b), or by housing all animals in individual cages (Kikuchi2017).

Reassuringly, the effects described in each experimental cohort are broadly the same as those reported by the authors in the original descriptions of their research. They also broadly reflect findings in human cohorts, where common findings in patients with CKD compared to healthy controls have included an increase in *Clostridia*, [260-263] *Bifidobacteria*, [264] and *Gammaproteobacteria*; [230, 260, 261, 265-267] and a decrease in *Lactobacillus[265]* and different species from the family *Lachnospiraceae*. [230, 261, 263, 264, 267, 268] However, results between human cohorts appear just as contradictory as for rodent cohorts, with results from a number of studies diverging from the trends we have reported for most of the taxa mentioned above, including *Clostridia*, [265, 267] *Bifidobacteria [260, 265]* and *Lactobacillus*. [260, 262] Although many human cohorts reported a reduction in alpha diversity in patients with CKD, [261, 263-265] others have reported in line with our findings in rats that alpha diversity rises in uraemia. [8, 269, 270] It is possible that the dietary restrictions encouraged for human subjects with CKD, rather than the effect of uraemia itself, causes these conflicting results.

The broad trends that emerged of the effect of uraemia on the gut microbiome are biologically plausible and may suggest that the gut microbiome has a contributary role in the development of CKD. Reductions in core microbial communities may reflect the changing biochemical environment of the gut, as nitrogenous waste and changes in pH may alter selective pressures and allow opportunistic organisms to multiply at the expense of usual microflora. The two major taxa to show reduced abundances in uraemic animals – *Lactobacillaceae* and *Lachnospiraceae* –

are both highly metabolically active and associated with production of short chain fatty acids which have a variety of beneficial health outcomes. [55, 271] Reductions of both taxa have been described in a pattern of 'dysbiosis' associated with other diseases, [228, 272, 273] as have increases in *Gammaproteobacteria* [274, 275] which we have shown to be variably increased in the gut microbiota of uraemic animals. These latter organisms possess the metabolic potential for production of toxic molecules from metabolism of dietary protein [52, 247] and so their increased abundance in uraemic animals may directly contribute to adverse renal and cardiovascular outcomes.

Limitations of this research

Interpretation of the significance of the microbial trends reported here is limited by the relatively short reads produced by high-throughput amplicon sequencing, with many ASVs being identified confidently only at genus or family level. For example, in the Nanto-Hara2020 cohort, fifteen ASVs from the genus *Muribaculaceae* were present at increased abundances in uraemic animals whilst nine were present at reduced abundances in controls; these differentially expressed ASVs accounted for a total of 39.3% of all sequencing reads in this cohort. It is not clear why some of these species increased in uraemic animals whilst other decreased, and it is possible that functional differences at species level are responsible, especially since *Muribaculaceae* are known to possess significant metabolic potential. [276] Although prediction of functional properties on the basis of published whole genome sequencing has been suggested as a possible low-cost solution to this problem (using packages such as PICRUSt [100] and piphillin [101]),

such packages are only as good as the range of published genomes available, and for families such as *Muribaculaceae* which are predominantly described in mice, coverage is currently much scantier than for organisms that commonly colonize humans. After trial runs which matched a disappointingly small proportion of ASVs to published genomes, we felt that proceeding with such an approach with the data presented here would introduce an unacceptable degree of unreliability.

Our results are of limited generalisability to humans with uraemia, because CKD in humans is far more complex than experimental uraemia in rodents. It is plausible that a range of other factors in human populations (for example, dietary restrictions recommended to control serum potassium and phosphate concentrations, or the effects of comorbidities like diabetes, obesity, hypertension, cardiovascular diseases or oral medications used to treat these conditions), may lead to significant changes in the gut microbiota of patients with CKD compared to healthy controls. These results do, however, question the extent to which any observed gut microbial changes may be attributable solely to uraemia.

Further research

Future research should focus on the following unanswered questions: Firstly, microbiological studies, to try to determine what features of organisms, or consortia of organisms, make them particularly susceptible to the effects of uraemia, or to possess the adaptability to survive within a uraemic milieu. Longitudinal studies showing how communities evolve over time as a host

organism becomes uraemic may be helpful in this regard, as may *in vitro* testing of urea tolerance by batch culture. Secondly, functional studies using different -omics techniques (metagenomics, metatranscriptomics and metabolomics) may determine ways in which bacterial metabolic potential may differ in uraemic versus control microbiomes, and suggest how this may affect the host organism. Thirdly, therapeutic studies may consider whether seeking to manipulate the gut microbiome in uraemia carries the potential to reduce progression of kidney disease and prevent its complications. Rather than viewing the gut microbiota as purely a problem, there is the potential that successful manipulation of the metabolic machinery it contains may evoke benefit for the host organism.

Conclusions

These results challenge the assumption that in healthy organisms, different microbial communities achieve a common set of basic metabolic functions despite variation in the individual species present [14, 277]. It can no longer be assumed that healthy laboratory animals, purchased from the same supplier, are metabolically similar. The inherent microbial dissimilarity and associated metabolic differences between animals in different batches provides a significant source of experimental variation. Many products from bacterial metabolism in the gut are known to have beneficial effects (such as the short chain fatty acids), or deleterious ones (eg 'uraemic toxins' such as amines, phenols and indoles), and if different batches of animals possess microbiota that produce such substances in greater or lesser amounts, the phenotype of the host organisms may be significantly different.

This also highlights the need for single-centre trials to be confirmed by multi-centre studies in clinical research. There is substantial evidence that human microbiota vary by ethnicity, diet and geographical location, and that these differences are linked to metabolic differences in the host organisms; [278-280] drugs showing benefit in one group of individuals cannot be assumed to do so universally until they have been shown to do so.

Such batch variations could easily lead to spurious positive results. For example, a group that demonstrates an effect in response to an experimental intervention with a small group of animals may decide to increase the number of animals in order to publish their findings; they purchase new animals from the same supplier, but fail to reproduce their earlier results because the new additions have significantly different microbial metabolic potential. Even worse, they may have carried out interventional procedures on one batch of animals, and then used animals from a different batch as controls, with exaggerated differences between groups reflecting underlying differences in microbiomes rather than any effect of the experimental procedure. The alternative in each case – to re-run the whole experiment with animals purchased in a new, single batch – may be prohibitively expensive, may fail to reproduce the initial results, and seems to stand against the second of the 'Three R's' governing ethical use of animals in research: the reduction of the number of animals used [281].

An alternative to using multiple batches of experimental animals would be to run longitudinal studies, in which each animal serves as its own control, before and after an experimental intervention. This gets around the problem of their being no clearly identified, objective 'normal' control microbiome across experimental units, and goes some way to suggesting mechanistic

associations (eg if one bacterial species rises in proportional abundance after the induction of uraemia compared to before it, whilst another falls in proportional abundance, it may reasonably be supposed that the former is better adapted to a uraemic environment than the latter). However, such longitudinal studies reduce, but do not abolish, batch effects; and may also risk conflating the effects of increasing age with those of the experimental intervention.

Summary

- **Comparison of two identically treated cohorts of rats, obtained from the same supplier just a few weeks apart, revealed that batch effect far outweighed the effect of uraemia on the composition of the gut microbiota.**

- **These batch differences were functionally significant, with the urinary metabolome also showing far greater effects of batch than of uraemia.**

- **Addition of extra batches of animals revealed even wider batch effects among rats, and that similar batch effects are also seen in C57/BL6 mice.**

- **In a meta-analysis carried out of all publicly available NGS sequencing data, the leading determinants of variation were batch primer type, host species (rat vs mouse and method of inducing uraemia. Intervention effect (control vs uraemic) did influence sample clustering, but to a much lesser extent.**

- **Across all datasets there was the suggestion that abundances of certain taxa may be affected by experimental uraemia, with uraemia often being associated with a reduction in abundances of *Lactobacillus* and *Lachnospiraceae*, and increases in *Clostridiaceae* and *Proteobacteria*.**

Conclusions:

- **Contrary to what has been widely asserted, there is limited evidence that uraemia disrupts the composition of the gut microbiota, and gut dysbiosis caused directly by uraemia probably does not play a major role in the aetiology of CKD.**

206

- **Evidence of a high degree of variability between the gut microbiomes of animals from different experimental batches poses major challenges to a wide range of animal research and may underlie the difficulties sometimes experienced in reproducing experimental research.**

Chapter 5

Modulating the gut microbiome to ameliorate uraemia

Introduction

The gut microbiome has been proposed as a potential mechanistic factor in explaining the different patterns of diseases between traditional African and modern Western populations for many years. Denis Burkitt (1911-1993) popularised the notion that many diseases common in Western populations shared a common aetiology in the absence of fibre in Western diets heavy in processed food, [282-284] a hypothesis that earned him the nickname 'fibre man' (Figure 61, p. 245).

Burkitt's hypothesis chiefly concerned the bulking effects of dietary fibre, because far less was known at the time about the detailed composition of the gut microbiota and its metabolic potential than has been discovered since.

The impact of diet on the gut microbiota was underlined by a series of seminal studies in the modern microbiome era. In 2010 *De Filippo et al* published a detailed analysis of the stool microbiota of children living in mud huts in Burkina Faso compared to Western children in the European Union; there were substantial differences in microbiota with the African children having far higher proportions of *Bacteroidetes* (including the hitherto unknown genus *Xylanibacter*) and Western children having far higher abundances of *Firmicutes*, including taxa such as *Clostridia*. Correspondingly, the African children had significantly higher faecal levels of short chain fatty acids (Figure 62, p. 246). [278]

Similar patterns of association between individuals eating traditional, plant-based diets and those eating Western diets higher in animal fats and protein have been demonstrated between African and Amerindian populations and Americans, [285] between Bangladeshi and American children, [279] and between Africans living in Africa and African Americans eating a Western diet. [280] In the latter study, metabolomic analysis revealed that a Western diet was associated with higher stool bile acid concentrations whilst an agrarian African diet was associated with higher levels of short chain fatty acids.

Similarly, several animal studies have demonstrated that similar changes can be induced in experimental animals fed diets of different compositions. Turnbaugh et al demonstrated that the gut microbiota of germ-free mice which had been 'humanised' by inoculation with human gut

contents could be manipulated by a switch between a plant-based and a high fat diet; subsequently they demonstrated that these communities could be successfully transferred into other germ-free mice. [286] Devkota et al showed that a switch from a plant-based to a milk-based diet led to altered gut microbiota, with an increase in species tolerant to bile acids that were associated with colitis. [287] Martinez-Medina et al similarly demonstrated that a Western diet encouraged overgrowth of pathological species and disrupted epithelial tight-junctions, leading to increased gut inflammation. [288]

Short chain fatty acids

Short chain fatty acids are aliphatic open-chain carboxylic acids. The most important biological species are acetate, propionate and butyrate, which have 2, 3 and 4 carbon backbones, respectively; Figure 63, p. 247.

Production of SCFAs

SCFA are produced by a range of metabolic pathways present in different bacteria, with metabolic cross-talk between bacterial species with cooperative metabolic machinery adding to the complexity. [289-292] Although SCFA production is possible from non-carbohydrate sources (including fats, proteins and longer polypeptides), species with this potential have been estimated to account for less than 1% of the gut microbiota, and fermentable carbohydrate,

broken down by bacterial glycosyl hydrolases, remain the main substrate for gut SCFA production. [293]

Below is an outline of the more common metabolic pathways for production of the three commonest SCFA:

Acetate: Acetic acid is present, pre-formed, in many foods (for instance, vinegar is 4-8% acetic acid, and dietary acetic acid has been linked to a number of positive health outcomes, [294]). However much of the body's absorbed acetate arises as a result of bacterial fibre fermentation, and the metabolic pathways for this are widely distributed among a range of different anaerobic bacterial taxa, through the action of pyruvate oxidase on pyruvate generated by glycolysis of simple sugars broken down from complex dietary fibres by microbial hydrolysis. [293, 295]

Propionate: In contrast to acetate production, production of propionate and butyrate is only achieved by certain bacterial taxa and may involve different pathways in different bacterial species. Propionate metabolism may be achieved in *Bacteroidetes* and *Negativicutes* via the succinate pathway (some *Negativicutes* may also use the acrylate pathway to produce propionate from lactate), and by the propanediol direct from deoxy-hexose in *Lachnospiraceae*. [296]

Butyrate: Butyrate production begins with the combination of two acetyl-CoA molecules to form acetoacetyl-CoA, which is then reduced to butyryl-CoA. To reduce butyryl-CoA to butyrate, there are two major bacterial pathways. In *Faecalibacterium prausnitzii* (part of the family *Ruminococcaceae*), and *Eubacterium rectale, Roseburia spp* and other

Lachnospiraceae, the enzyme butyryl-CoA:acetate CoA-transferase consumes further acetate to produce butyrate; [297] in other bacterial species such as *Coprococcus* (f. *Lachnospiraceae*) and some species from family *Clostridiaceae*, the enzyme butyrate kinase achieves this reduction. Overall, the ability to produce butyrate is highly variable in these families with highly closely-related species possessing or not possessing the necessary enzymes. [298]

These pathways are described in Figure 64, p. 248. Considerable metabolic cross-talk occurs between organisms with different metabolic activity, sometimes characterised as an interaction between 'primary degraders' such as *Bifidobacteria, Bacteroides* species and *Ruminococcus bromii*, which are involved in the initial steps of metabolising complex carbohydrate fibre into simple sugars and SCFAs including acetate and propionate, and secondary fermenters (typically *Firmicutes*) which utilise these simple sugars and acetate to produce butyrate, Figure 65, p. 249. [299] *In vitro* batch fermentation experiments have shown that the gut pH may also be a major factor in influencing the activity of different pathways, with a lower pH (5-6) favouring the secondary fermenters and increased butyrate production, and a higher pH (6-6.5) favouring the primary fermenters and acetate and propionate production. [300, 301]

Concentration and distribution of SCFAs

Key post-mortem studies have shown that the principal site of SCFA production in humans is the caecum, where levels are around tenfold higher than in the distal small gut. SCFA, being acids,

lead to a significant decrease in intra-luminal pH in the caecum, and along the rest of the colon, as SCFA concentrations fall, the pH rises. In humans, the proportional production of the three principal SCFA are 60:20:20 between acetate, propionate and butyrate when measured in colonic samples. Concentrations are a thousand-fold lower in portal blood compared with colonic fluid. [302] It has since been shown that the liver effectively removes all butyrate produced in the gut on first pass metabolism, with none reaching the peripheral circulation, and only acetate produced in the gut achieving measurable concentrations in the systemic circulation. [303, 304] Urinary excretion of SCFA in humans has been estimated to be around tenfold lower for propionate than for acetate, and around tenfold lower for butyrate than for propionate, with acetate representing around 95% of urinary SCFA. [305, 306]

Cellular effects of SCFAs

SCFAs interact with cells by two primary mechanisms:

- By entry into cells through cell surface transporters: both the monocarboxylate transporter MCT1 (which transports monocarboxylates including pyruvate and lactate into cells in symport with protons), and the sodium-coupled monocarboxylate transporter SMCT1 (which transports a similar range of molecules in symport with sodium) have been demonstrated also to transport SCFAs into colonocytes. [307, 308] Butyrate may also enter cells by direct diffusion in its undissociated, lipid soluble form.

- By the G-protein couple receptors, such as the GPR109A on the cell surface of colonocytes, which primarily responds to nicotinate but which also demonstrates affinity for butyrate, [309] or GPRs 41 and 43 which are widely expressed and previously viewed as orphaned, but have now been demonstrated to possess SCFAs as primary ligands. [310]

They have been demonstrated to have a variety of effects on a wide range of cells:

- *Maintaining gut barrier functions*: SCFAs have been shown to enhance the barrier function of the colon, both through increased mucus secretion [311] and through improved colonocyte tight junctions. [312]

- *An energy source:* Butyrate is the preferred energy source of colonocytes, contributing around 75% of their energy needs. [313, 314] Any butyrate absorbed into the portal blood is then removed by the liver, and along with the significant amount of absorbed propionate, is used for gluconeogenesis; it is estimated that SCFAs together contribute around 10% of the body's energy needs. [315, 316] Further positive metabolic effects may include SCFAs reducing insulin resistance (partly through inducing intestinal gluconeogenesis both directly and via neurohormonal mechanisms involving GPR41), and improved lipid homeostasis. [317]

- *Regulation of appetite:* Acetate, the only SCFA reaching significant levels in the systemic circulation, has shown to be a powerful regulator of appetite. In rodent studies this has been shown to be due to direct effects on the hypothalamus, [318] and this has

been suggested in human studies to be a key mechanistic link between observed alterations in the microbiome and the population prevalence of obesity. [319]

- *Neuropsychiatric effects:* In animals models of depression and anxiety, depressed animals have been shown to have bacterial dysbiosis associated with reduced production of SCFA, [320] and to respond positively to administration of exogenous preparations of SCFA. [321] Humans with major depressive disorders have likewise been shown to demonstrate low levels of SCFA and depleted levels of bacterial species involved in SCFA production. [322-325] SCFA have been identified as one aspect (along with other gut generated molecules such as neurotransmitters) of a broad 'gut-brain' axis that has the potential to offer new insights and therapeutic options in human psychiatric disease. [326, 327]

- *Reducing gut inflammation and malignancy* through several mechanisms:

  o Inhibition of histone deacetylases: Histones are large proteins with numerous alkaline amino acid side chains (usually lysine or arginine), that allow them to bind and wind up DNA strands to prevent them from becoming tangled or damaged. This ability to bind DNA tightly is compromised when histones are acetylated; a class of molecules called histone deacetylases (HDAC) removes these acetyl residues thus allowing DNA to be more tightly bound to histones and be less liable to damage. [328] These molecules also make DNA less open to transcription, and so affect cellular function. Intracellular butyrate has been shown to be a powerful inhibitor of HDACs, with the potential for improved colonocyte

function by a range of constitutive gene expression. [329, 330] HDAC inhibition also allows for increased transcription of glutathione-s-transferases (GSTs) which reduce oxidative stress and inflammatory drive.

- o Inhibition of nuclear factor kappa beta (NFkB): Butyrate acts via GPR109A on colonocytes to inhibit NFkB. Unchecked, this can, under pro-inflammatory conditions migrate into the cell nucleus and cause transcription of a range of inflammatory mediators leading to gut inflammation.

- o Activation of p53: Butyrate has been shown to activate p53, a prominent tumour suppressor gene that acts as a transcription factor for various other genes such as p21, with the anti-proliferative and pro-apoptotic effects. [331, 332]

- *Wider immunomodulatory effects:* These effects occur typically through activation of GPR41 and 43, which have been shown to have important chemotactic properties. Mice not expressing these receptors in intestinal tissues struggle to clear bacterial intestinal infections, [333] whilst activation of these receptors leads to IL-10 driven, tolerant TH1 responses, maintaining intestinal homeostasis, reducing colitis and promoting tolerance of commensal gut bacteria. [334] SCFA have also been shown, via both GPR41 and 43, but also high HDAC inhibition, to reduce production of the inflammatory cytokines IL-6 and IL-8, and to reduce vascular inflammation when stimulated by lipopolysaccharide or tumour necrosis factor alpha [335] and induce B and T regulatory cells. [336, 337]

Modulating the gut microbiome

The task of improving human health by manipulating the gut microbiome has been attempted for over a century, since Cheplin and Rettger used live preparations of *Bacillus acidophilus* (now known as *Lactobacillus*) to transform the microbiota of experimental subjects. [338] The accumulating evidence of association between plant-based diets and healthy outcomes, along with a growing appreciation of the wide range of positive physiological effects caused by short-chain fatty acids has led to many modern attempts to manipulate the microbiome.

Broadly, two approaches have been tried, for which consensus definitions are provided below:

- *Probiotics* describe 'live microorganisms which when administered in adequate amounts confer a health benefit on the host'. (The International Scientific Association for Probiotics and Prebiotics (ISAPP) consensus statement on the definition and scope of prebiotics, Nature Reviews Gastroenterology and Hepatology, 2017). [339]

- *Prebiotics* describe 'substrates that are selectively utilized by host microorganisms conferring a health benefit'. (Food and Agriculture Organization and World Health Organization Expert Consultation on health and nutritional properties of powder milk and lactic acid bacteria, 2001). [340]

In addition, numerous other constituents of food may have physiologically active components confering benefits to health, including fish oils, vitamins, flavonoids, polyphenols and neurotransmitters; many have contributed to the growth of interest in 'functional foods'. [341]

Various studies have shown that *probiotic* preparations can alter gut microbial communities and confer benefits to health in a number of different areas of medicine, often when administered alongside prebiotics in preparations that have been termed 'symbiotic'. For example, Perraudeau et al recently demonstrated improvements in glycaemic control in type two diabetics using a preparation of five different anaerobic bacteria and inulin, a classic prebiotic. [342] However, the challenges of culturing, storing and finding stable preparations of live bacteria for distribution and administration provide a challenge in turning experimental success into real-world clinical interventions. [343]

Prebiotics and dietary fibre

Prebiotic preparations, in contrast, are generally stable compounds that are easily stored and transported. They may prove more acceptable to patients because many are natural parts of plant-based foods. Furthermore, because they offer significant amounts of metabolic substrate, they may also prove effective in driving the generation of beneficial metabolites such as short chain fatty acids in addition to effects they may exert in manipulating the community composition of the microbiome.

The use of the term 'prebiotic' overlaps significantly with the term 'dietary fibre': both terms describe indigestible molecules that pass through the upper gastrointestinal tract intact and act by selectively stimulating particular species of bacteria in the colon. However, there are prebiotics that are not fibre (such as dietary polyphenols [344] or polyunsaturated fats [345]), and various

types of dietary fibre – especially insoluble forms such as cellulose or lignins – which do not exert prebiotic effects, Figure 66, p. 250. [339]

The best studied prebiotics are all types of dietary fibre:

- *Fructo-oligosaccharides* are short chain polysaccharides (with a degree of polymerisation of between 3 and 10 monosaccharide units), mostly of the form Glu-Fru(n); where Glu represents glucose and Fru represents fructose. Fructose molecules are linked by beta (2-1) bonds, with most molecules including a terminal, alpha-linked glucose molecule. [346] They can be extracted from a number of foodstuffs including onions, leeks and chicory, with the highest known concentrations occurring in the Jerusalem artichoke and the blue agave plant. They are somewhat sweet and used extensively in the food industry because of their flavour and lack of calories.

- *Galacto-oligosaccharides* are similarly sized polymers made up of galactose and glucose subunits, they are typically produced by fermentation of milk products, such as in the popular fermented milk drink keffir, [347] as well as being produced synthetically from lactose using yeast enzymes. [348]

- *Inulins* are fructose polymers of longer chain lengths than fructooligosaccharides; with degrees of polymerisation between 10 and 60 subunits. Chain length has been linked to both the speed of fermentation [349] and to the types of bacteria which preferentially metabolise different types of fibre. [350]

- *Lactulose* is perhaps the simplest form of fibre that exists, being a simple disaccharide of fructose and galactose. It is discussed further below, along with previous evidence for its effectiveness in liver and renal disease as well as its probiotic effects.

- *Other oligosacchrarides* including xylooligosaccharides, [351, 352] isomaltosaccharides [353] and yeast-based mannan oligosaccharides [351] have each been shown to have beneficial prebiotic effects in humans and animals.

- *Human breast milk oligosaccharides* have been extensively studied, because they represent the third biggest chemical component of human breast milk, and yet are entirely non-absorbable by the human neonate and serve instead to allow a healthy gut microbiome to develop, dominated by the genus *Bifidobacterium*. [354] This has been shown to produce colonisation resistance to bacterial and viral infections [355] as well as a range of immunological and metabolic benefits. [356]

Additional benefits of fermentable fibre in CKD: removal of nitrogenous waste

As well as their beneficial metabolic and immunological properties, short chain fatty acids are also potentially of benefit in the context of renal impairment by simple virtue of their acidity. Significant generation of SCFA in the caecum has the effect of lowering the luminal pH, with the potential to lead to significant increases in gut excretion of nitrogenous waste.

Much of our knowledge about these potential effects of SCFA production comes from the widespread clinical use of lactulose (which as discussed above is the simplest form of fermentable fibre and has potent prebiotic effects), in the treatment of hepatic encephalopathy. [357, 358] This is a condition sharing with CKD a primary causative role for retained nitrogenous waste; in the case of hepatic encephalopathy, ammonia; which is not converted into urea because of defective hepatic urea cycle activity, and may accumulate in individuals with decompensated liver disease leading to impaired consciousness and coma.

Lactulose is a synthetic disaccharide formed from the basic sugars galactose and fructose. It is produced commercially by the isomerisation of lactose, but is also produced in normal milk during heat treatment so that small amounts are present in pasteurised milk (Figure 67, p. 251).

Lactulose cannot be metabolised by mammals, [359] and although a very small fraction of oral intake is absorbed and excreted unchanged by the kidney, [360] the majority passes intact to the large gut where it is hydrolysed by bacteria into lactate and acetate. [361] This lowers gut pH [362, 363]. It has been shown that lactulose administration increases the nitrogen content of stool (principally through increased incorporation of nitrogen in bacterial protein, although also through ammonium dissolved in the soluble fraction of stool), with an attendant 23% reduction in the urea generation rate. [364] The explanation of this 'nitrogen fixing' effect of lactulose relates to the effect of a more acidic gut pH on the ratio of the ammonium ion (NH_4^+) to ammonia (NH_3). The pKa of ammonia is 8.9 at 37°, [365] meaning that at a normal blood pH of 7.4, the majority of ammonia exists in NH_3 form, although some is present as ammonium (NH_4^+). The gut lining is relatively impermeable to NH_4^+, but freely permeable to NH_3, meaning that in

the presence of an acidic gut environment, a strong pH gradient causes freely permeable NH_3 ammonia to diffuse into the gut, where it is ionised into NH_4^+ ammonium which cannot diffuse back into the blood, and which may then be incorporated into bacteria or excreted in solution in the liquid component of stool. It has been shown that in dogs, at a caecal pH of <6.0, the normal flow of ammonia from gut to blood is reversed, and the colon actually becomes an organ of nitrogen excretion. [366]

Other beneficial effects of lactulose and other forms of fermentable fibre:

- Lactulose may provide a beneficial selective pressure for acidophilic bacteria such as members of the phylum *Firmicutes*, at the expense of other phyla such as *Proteobacteria*, which have been associated with disease. Although some clinical studies have failed to demonstrate significant changes in the gut microbiota associated with lactulose administration, [367] others have shown positive effects, [368] as have a number of animal studies. [369, 370] Such a change may reduce the burden of proteolytic digestion and production of a range of harmful products such as indoles, amines and cresols.

- Lactulose produces osmotic laxative effects contributing to reduced intestinal transit time, as well as to excretion of water, sodium, potassium, creatinine and hydrogen ions. Since constipation is a common problem in patients with CKD, these effects may be of clinical relevance and may be shared with other forms of fermentable dietary fibre [346, 353, 371, 372].

The range of effects of lactulose are summarised in Figure 68, p. 252. Lactulose has previously been trialled as a therapy in CKD with promising results, [373-376] although studies have been limited by short duration and a limited amount of clinical data collected.

Hypothesis

We sought to establish whether a high-fibre, prebiotic diet in animals with experimental uraemia might lead to successful manipulation of the gut microbiome in both control and uraemic animals, leading to potential health benefits including:

- removal of nitrogenous waste from the body through the gut

- a reduction in renal injury through the anti-inflammatory effects of short-chain fatty acids.

Pilot data: using lactulose to improve outcomes in experimental uraemia

An initial attempt was made to study these effects through administration of lactulose to rats with experimental uraemia. These attempts were unsatisfactory because of methodological difficulties in administering lactulose to rats, and although there were positive outcomes in terms of successful manipulation of the gut microbiome (with significant increases in SCFA producing bacteria) and a reduction in serum urea, the validity of these results were compromised by

overall loss in weight and reduced oral water intake in the rats administered lactulose, likely due to bacterial contamination of the lactulose solutions. Results from these experiments are summarised in Appendix 4.

Main experiment: using fructo-oligosaccharide to improve outcomes in experimental uraemia

Introduction

Fructo-oligosaccharides consist of short-chain length fructose polymers, generally with a terminal glucose molecule, as represented in

Figure 69, p. 253. Commercial preparations of FOS consist primarily of the GF2, GF3 and GF4 molecules, and the same molecules lacking the terminal glucose, termed inuobiose (F2), inulotriose (F3) and inulotetraose (F4). The latter molecules are generally produced in production techniques involving the enzymatic degradation of longer chain inulins extracted from plant sources such as chicory root, the former by fructofunanosidation of sucrose. [377]

FOS preparations have previously been demonstrated to have significant effects on the rodent microbiome, including especially increasing relative abundances of primary fibre degraders *Bifidobacterium*. [378, 379] Although there is some suggestion that high dose FOS supplementation may decrease butyrate producing organisms, [380] there is evidence that in the longer term they cause increased production of gut butyrate [381] and that a number of specialist

butyrate producing organisms (including *Roseburia* species and *Faecalibacterium prausnitzii*) grow well in FOS-supplemented growth media. [382] FOS preparations have been shown to cause increased production of all SCFA fractions in several *in vivo* experiments. [349, 383-385]

Cellulose was chosen as a suitable control diet to compare with addition of FOS to rodent feed. The need for an additional, non- (or less-) fermentable form of dietary fibre was felt to be necessary in assessing the effect of FOS of rodent diets for two reasons:

- Since the energy present in the fibre fraction of food is not readily available to mammalian hosts (except by virtue of bacterial fermentation), an animal consuming a certain quantity of a standard rodent diet with the addition of say 10% FOS would be consuming less energy that an animal consuming the same amount of an unaltered diet.

- All forms of dietary fibre are expected to have bulking effects in addition to any effects exerted through bacterial metabolic products; using cellulose-added diets as a control for FOS-added diets offered a way of getting around these confounders to isolate the metabolic effects of FOS.

Cellulose is the most abundant organic polymer on earth, being the chief constituent of plant cell walls and contributing to almost 60% of the biomass of wood. It has the chemical formula $(C_6H_{10}O_5)_n$, consisting of up to thousands of β-linked (1-4) molecules of D-glucose, as shown in Figure 70, p. 254.

Cellulose is well tolerated in rodent diets, and associated with significant increases in stool volume. [386] Although there is evidence of limited bacterial metabolism of cellulose in rats,

[387, 388] nevertheless it has been shown to be much more resistant to fermentation than other forms of fibre (such as FOS) in a number of studies. [389-392] Thus it was felt to be a suitable control which was relatively resistant to bacterial fermentation and not associated with significant SCFA production.

Methods

Generation of experimental diets

The experimental diet AIN-93M is a well-established rodent diet that was derived by the American Institute of Nutrition in order to supply in standardised and reliable forms all of the nutritional needs of laboratory rats. It contains 5% fibre in the form of cellulose. [393] It was used as the basis for generation of experimental diets, ordered from Special Diet Services, Essex, UK; based on standard pelleted AIN-93M. These two diets were:

- 90% standard AIN-93M plus 10% powdered cellulose (hereafter referred to as the CELL diet)

- 90% standard AIN-93M plus 10% powdered fructo-oligosaccharide, derived from chicory root (hereafter referred to as the FOS diet).

Animal work

A total of 97 wild-type outbred Wistar IGS rats were purchased in four separate batches from Charles Rivers, Kent, UK. They were used in two main experiments, to investigate the effects of the FOS-containing diet on:

- Chemically-induced uraemia, cohorts 1 and 2

- Surgically-induced uraemia, cohorts 3 and 4

The use of two cohorts of animals for each experiment, and two models of chronic uraemia, was to reduce the chance that the batch effects described previously would compromise the validity experimental findings. The different cohorts are described in Table 7, p. 255.

All rats arrived at 7 weeks of age, and during a week-long acclimatisation period were moved between cages at least twice to allow gut microbial communities to homogenise.

For the first experiment (chemically-induced uraemia), rats were rendered uraemic as described in chapter 2, using a four-week course of 0.75% adenine containing RM1 diet, with control animals receiving control diet (standard RM1). Animals were then randomised to receive experimental diets according to the proportions in Table 7 and sacrificed with collection of samples after 24 urinary and stool collection four weeks later.

For the second experiment (surgically-induced uraemia), subtotal nephrectomy or sham procedures were carried out as detailed in chapter 2. Four weeks after the second stage of surgery, animals began to receive experimental diets according to the proportions in Table 7. Animals in cohort 3 were sacrificed with collection of samples after 24 urinary and stool

collection four weeks later. Caecal samples from this cohort were used to whole-genome metagenomic sequencing as detailed later. Animals in cohort 4 underwent 24-hour urine and stool sampling at the same stage as those in cohort 3, but then received broad spectrum antibiotic treatment with neomycin 0.5mg/kg/d and vancomycin 1mg/kg/d administered in drinking water for 10 days. After this period they underwent repeat 24-hour stool and urinary collection and then were sacrificed with collection of other samples.

The experimental protocols for all animals are summarised in Table 8, p. 256.

Calculation of total urine, stool and feed nitrogen

Total nitrogen content of urine, stool and diet was measured using elemental analysers at the Department of Geography, Queen Mary University of London, Mile End Campus.

Stool and feed:

The wet weight of samples was accurately measured before the samples were freeze dried, the dry weight measured, and the samples were crushed. 11.66% cysteine and 46.65% urea were used as standards, and two random replicates were run for each sample. Analysis was carried out using a Thermo Flash Elemental Analyser 1112. After purging of air, a twin furnace protocol was used, with oxidation catalyst in the left-hand column and reduced copper in the quartz column. After the furnace columns were two inline scrubbers; the first 20% silica gel and 80% soda lime to remove excess water, and the second 100% soda lime to remove carbon. A final magnesium perchlorate filter was used to remove any residual water. A standard CHNS

separation column was then used before total nitrogen was quantified using a Thermal Conductivity Detector.

Urine:

Due to the extremely high nitrogen content, samples were diluted 1:250 in deionised water with a resistivity of >10MΩ. Standards of potassium nitrate at varying concentrations were used as standards, and two replicates were run for each sample. Analysis was then run using standard protocols on a Skalar Formacs HT TN (ND25) elemental analyser.

Whole genome metagenomic sequencing of the gut microbiome

Faecal samples from the surgically-induced uraemic cohort were used for whole-genome sequencing (WGS) metagenomic analysis of the gut microbiota. Samples from this cohort were chosen for this analysis instead of samples from one of the chemically-induced uraemia cohorts in order to avoid any influence of orally-administered adenine on gut bacteria.

DNA was extracted using the Qiagen PowerSoil kit, as described previously, and sent for WGS using the Illumina Novaseq 4000 system, with the library prepared using the TruSeq Nano DNA kit, via Macrogen, Seoul, South Korea. Subsequent genome assembly was carried out by a collaborator (Professor Lesley Hoyles) at Nottingham Trent University, before analysis of abundance tables for organisms (according to 16S sequencing identities), COG functional classes, CAZy carbohydrate pathways and KEGG modules were analysed in house using the ALDEx2 package in R. [394]

Results

Diets with added fibre were well tolerated by both control and uraemic rats

For animals in cohort 1, weekly weights for all adenine-fed animals were static throughout the period of adenine administration, while weight in control animals rose rapidly during this period. After transfer to the experimental diet (AIN-93M, CELL or FOS), there was a period of fast catch-up growth in all uraemic animals with no differences between animals taking different diets. At the time of sacrifice, control animals were substantially heavier than other animals (mean 550g compared to means of 438g, 425g and 424g in the AIN, CELL and FOS groups respectively; p<0.001 by one-way ANOVA), with no differences between uraemic groups on different diets, Figure 71, Figure 72; p. 257 & 258.

Animals receiving the FOS diet consumed less diet than animals in other groups. Significance was seen only when the FOS diet was compared to uraemic animals receiving AIN diet (mean FOS consumption 25.3g vs mean AIN consumption 31.23g, p=0.039 by Tukey's post-hoc analysis), Figure 73, p. 259.

These results were validated in the second adenine cohort; and in surgically-induced uraemia, cohort 3. In both of these cohorts, control animals were heavier than their uraemic counterparts; overall the animals in the chemically-induced cohort were lighter than those in the surgically-induced group because the animals were two weeks younger at the time of sacrifice (because of

the additional 2-weeks required between the stages of surgery), and because the degree of uraemia is greater in the chemically-induced model, Figure 74, p. 260.

The FOS diet significantly affected the macroscopic appearance of the lower gut, its contents, and stool

Fibre supplementation using the CELL diet, but not the FOS diet, increased stool weight in uraemic animals compared to AIN diet, Figure 75, p. 261. Stool pellets from CELL animals had a notable paler and drier appearance than those from the other two groups, Figure 76, p. 262.

There was a marked discrepancy between the appearance of colons and caeca at the time of sacrifice between FOS treated animals and all other groups. Animals being administered the FOS diet had much heavier caeca than other groups (7.188g compared to 3.625g, 4.238g and 4.013g in control, AIN and CELL groups, $p<0.0001$ for all comparisons, Figure 77, p. 263). Their caecal contents were liquid and contained gas, whereas the caecal contents from other groups had a viscous consistency, similar to putty, Figure 78, Figure 79; p. 264 & 265.

The pH of caecal fluid was assessed directly after sacrifice using a calibrated pH probe. The mean pH in FOS treated animals was 6.451; significantly lower than in control (pH 7.178, $p=0.0002$), AIN fed (pH 7.34, $p<0.0001$) and CELL fed (pH 7.5, $p<0.0001$) animals (significance between groups assessed by post-hoc Tukey test after one-way ANOVA). The differences between other groups were not significant, Figure 80, p. 266.

These results, again, were validated in the confirmatory rat cohorts. In both control and uraemic animals in both the chemically-induced and surgically-induced cohorts, FOS treated animals had significantly heavier caeca than CELL treated animals, and the caecal pH was lower in animals on the FOS diet than in those receiving the CELL diet, Figure 81, Figure 82; p. 267 & 268.

The FOS diet significantly reduced serum urea through increased gut clearance of nitrogenous waste

Serum urea in FOS-fed uraemic animals in cohort 1 was more than 50% lower than serum urea in uraemic animals receiving AIN diet, (mean serum urea 10.7mmol/L in FOS-fed vs 22.2mmol/L in AIN-fed animals, p=0.004 by Tukey's post-hoc test following one-way ANOVA), Figure 83, p. 269.

In the confirmatory cohorts, similar finds were seen in the chemically induced cohort: serum urea was 25.81 and 14.08mmol/L in the CELL and FOS groups respectively, a 45.4% reduction in the FOS treated group, p<0.001). Across both surgically-induced uraemia cohorts, which resulted in a milder uraemic phenotype, there was nevertheless a significant 18.1% fall in serum urea from 12.96 to 9.84mmol/L in FOS treated animals (p=0.001), Figure 84, p. 270.

By contrast, FOS feeding did not affect either serum creatinine or creatinine clearance in any of the cohorts; results from cohort 1 are shown in Figure 85, p. 271.

Total nitrogen balance was calculated in the surgically-induced cohort. The FOS diet led, in uraemic animals, to a significant increase in stool nitrogen excretion (p=0.002), coupled to a

decrease in urinary nitrogen excretion. There were no differences between groups in total nitrogen intake, Figure 86, p. 272.

Antibiotic treatment abolishes the urea-lowering effect of the FOS diet

Animals from cohort 4 were bled eight weeks after the second stage of surgery, and then administered broad spectrum antibiotics (neomycin and vancomycin to target both gram positive and gram-negative organisms) for ten days before sacrifice.

Whereas before antibiotic treatment, the FOS-fed animals had lower serum urea than those fed the CELL diet, after antibiotics this difference between groups was abolished, Figure 87, p. 273.

Fermentable fibre lowers serum potassium

Across both adenine treated cohorts, rats treated with FOS diet had lower serum potassium concentrations than those fed with both CELL and AIN diets (mean serum potassium in FOS fed animals was 4.6mmol/L, lower than means serum potassium in CELL fed animals of 5.2mmol/L, p=0.026; and in AIN-fed animals of 5.4mmol/L, p=0.02). In control animals, both CELL and FOS diets non-significantly decreased serum potassium compared to AIN, Figure 88, p. 274.

Fermentable fibre reduces polyuria and increases stool water content

Both FOS-fed and CELL-fed animals were less polyuric than AIN-fed uraemic animals, passing on average 38.3ml and 40.1ml of urine per 24 hours, compared with 51.1ml in AIN-fed animals ($p=0.032$ for FOS-fed and $p=0.058$ for CELL-fed compared to AIN-fed). Correspondingly, they were less polydipsic, with FOS-fed animals drinking an average of 62.1ml and CELL-fed animals an average of 66.9mls compared to 75.5ml in AIN-fed uraemic animals ($p=0.001$ for FOS-fed and $p=0.14$ for CELL-fed compared to AIN-fed), Figure 89, p. 275.

The reduction in polyuria is likely to be partially attributable to increased water clearance in stool. In uraemic animals, those fed FOS diet had a higher liquid fraction of stool (46%) than those fed CELL (35.6%, $p=0.0025$ by Sidak's multiple comparison test after 2-way ANOVA), Figure 90, p. 276.

Fermentable fibre, but not induction of experimental uraemia, has significant effects on composition of the gut microbiota

Metagenomic data assembled from the whole-genome sequencing run of DNA extracted from the caecal fluid of animals in cohort 3 (surgically-induced uraemia) was used to determine the composition of the caecal bacterial community at species and higher taxonomic levels. The gut microbiota of twenty-four animals was compared:

- Subtotal nephrectomy, CELL diet, n=6
- Subtotal nephrectomy, FOS diet, n=6

- Sham surgery, CELL diet, n=6

- Sham surgery, FOS diet, n=6

Each sample contained a very similar total of observed species, implying that the sequencing depth was perfectly adequate and additional depth would be unlikely to yield any further compositional information, Figure 91, p. 277.

Alpha diversity was assessed by a number of standard measures including the Shannon, Simpson and Inverse Simpson indices. Diet proved a significant source of variation in alpha diversity between samples (two-way ANOVA p=0.0027 by Shannon, p=0.0041 by Simpson and p=0.0037 by Inverse Simpson indices); the FOS diet was in each case being associated with reduced alpha diversity, Figure 92, p. 278.

Principal coordinate analysis confirmed that the main determinant for clustering between samples was diet, and that intervention class (uraemic vs control) caused minimal effect. Confirming this, Permutation Analysis of Variance (PerMANOVA) revealed that 46.3% of variance could be attributed to diet (p<0.001) whilst only 2.4% could be attributed to intervention class (p=0.75), Figure 93, p. 279.

Sequencing reads were assigned taxonomic identities on the basis of k-mers using the GTDB classifier (https://gtdb.ecogenomic.org/), one of the most accurate and extensive genome-based databases available, curated by the University of Queensland. The 853 species represented 529 genera, 223 families and 48 phyla.

Bacterial composition was plotted at phylum level and confirmed earlier observations, that microbiota were similar between samples taken from animals on the same diet, regardless of intervention type. Microbiotas in the CELL groups had high abundances of phyla *Firmicutes*, *Bacteroidetes* and *Verrucomicrobiota* (these consisted largely of genus *Akkermansia*); whereas microbiotas in the FOS fed group had far lower relative abundances of *Verrucomicrobiota* and *Firmicutes* and instead high proportional abundances, more than 50% in some cases, of phylum *Actinobacteria*, which consisted largely of genus *Bifidobacteria*. These organisms were present at only very low levels in CELL fed animals, Figure 94, p. 280.

The ALDEx2 package in R was then used to determine at the level of phylum, family, genus and class which taxa were differentially abundant between groups according to intervention class or diet. Effect plots were constructed at species level to visualise the degree to which changes in differential abundance of different organisms could be attributed either to intervention class or diet. These revealed no species differentially abundant based on intervention class, but multiple species differing in abundance between CELL and FOS treated groups, Figure 95, p. 281.

At each of these taxonomic levels, the ALDEx2 'aldex.kw' and 'aldex.ttest' functions were used to perform firstly a one way ANOVA to determine differences in means before groups, before-post-hoc Dunn tests were carried out to determine differences between individual groups and the t-test to determine differences according to diet and intervention class. All were adjusted for multiple hypothesis testing using the Benjamini-Hochberg method.

As suggested by the dispersion plot above, there were virtually no differences between control and uraemic groups receiving the same diet type as defined by post-hoc Dunn's tests, or between control and uraemic groups in the whole cohort determined by the T-test, at any taxonomic level.

By contrast, diet caused extensive changes in bacterial composition: of the 48 phyla detected, 14 were over-represented in CELL treated animals and 3 in those receiving FOS; these differentially abundant taxa were some of the most abundant taxa in the dataset, representing 63.6% of all organisms (44.6% of organisms belong to phyla significantly over-represented in CELL fed animals, 19% to phyla significantly over-represented in FOS fed animals.)

There were numerous, high-level differences between the microbiota of animals fed FOS- or CELL supplemented diets. Broken down by phylum these included:

- Within the most abundant phylum overall, *Firmicutes*:

    o Class *Clostridia*, which were the most abundant class overall and classified within the GTDB as subphylum *Firmicutes_A*, one of the two principal constituent classes within the phylum, were significantly over-represented in samples from CELL-fed animals accounting for 52.3% on reads in CELL-fed animals vs 31.9% in FOS-fed, p=0.0002).

    o Accordingly, the major family within this class, *Lachnospiraceae,* were likewise over-represented in CELL-fed rather than FOS-fed animals (41.8% vs 26.8% of total reads, p=0.005); however, at genus level a mixed pattern emerged:

- A number of genera within the family *Lachnospiraceae* were significantly increased in FOS-fed rather than CELL-fed samples, including a number of well-documented SCFA-producers such as *Marvinbryantia* (4.5% of reads in FOS-fed animals vs 0.09% in CELL-fed, P<0.0001), *Blautia* (1.8% of reads in FOS-fed samples vs 0.25% in CELL-fed, p<0.0001) and *Dorea* (0.98% of reads in FOS-fed vs 0.81% in CELL-fed, p=0.009)

- Families within the family *Lachnospiraceae* showing increased abundance in CELL-fed animals were largely less-described organisms, uncultured and lacking a specific name. These included uncultured genus *CAG-95* (representing 10.2% of reads in CELL-fed samples vs 0.07% in FOS-fed, p<0.0001), uncultured genus *UBA2882* (8.8% of reads in CELL-fed samples vs 0.05% in FOS-fed, p=0.0004), uncultured genus *UBA3282* (2.8% of reads in CELL-fed samples vs 0.12% in FOS-fed, p<0.0001), uncultured genus *CAG-110* (2.4% of reads in CELL-fed samples vs 0.04% in FOS-fed, p<0.0001) and uncultured genus *CAG-56* (1.8% of reads in CELL-fed samples vs 0.08% in FOS-fed, p<0.0001). Some known SCFA producers did increase in cell-fed animals, including genus *Kineothrix* (2.2% of reads in CELL-fed samples vs 0.09% in FOS-fed, p<0.0001) and subgenera from genus *Eubacteria* including *Eubacterium_F* (5.2% of reads in CELL-fed samples vs 0.07% in FOS-fed, p=0.0002), *Eubacterium_J* (0.23% of reads in CELL-fed samples vs 0.023% in FOS-

fed, p<0.0001) and *Eubacterium_R* (0.4% of reads in CELL-fed samples vs 0.01% in FOS-fed, p=0.0002).

These results are summarised in Figure 96, p. 283.

- o Class *Bacilli*, classified in the GTDB database under subphylum undifferentiated *Firmicutes*, were substantially over-represented in FOS-treated animals (6.4% of reads in FOS treated organisms compared to 2.6% in CELL treated, p<0.0001), although this was driven almost entirely by two outlier samples which as discussed in the legends to Figure 93 had high abundances of otherwise poorly represented organisms from the order *Erysipelotrichales* (including genera *Absiella* and *Turicibacter*). and from the order *Lactobacillales* (including genera *Lactobacillus* and *Enterococcus*).

- Phylum *Bacteroidota* was the second best represented phylum overall, accounting for an average of 27.1% of total reads across all samples, with no abundance difference between groups according to diet. However, the two most abundant divisions within it showed significant differences between FOS-fed and CELL-fed animals:

  - o In FOS-fed animals, family *Bacteroidaceae* accounted for 23% of all bacterial reads compared to 7.4% in CELL fed animals (p=0.006). This was accounted for almost entirely by a number of species from genus *Bacteroides*, including *B. uniformis* (13% of reads in FOS-fed vs 1.99% in CELL fed, p=0.002), *B. salyersiae* (3.55% vs 0.47%, p=0.005) and *B. ovatus* (3.54% vs 0.17%, p<0.0001), although the difference was chiefly driven by increases in a subset of

animals and were not seen universally. Conversely, *B. intenstinalis* was present at higher abundances in CELL-fed animals (2.8% in CELL-fed vs 0.17% in FOS-fed animals, p=0.02).

- o The other major subtaxa of phylum *Bacteroidota* to be represented in this dataset was family *Rikenellenceae*, which represented 10.1% of reads in CELL-fed animals but only 0.38% in FOS-fed (p=0.002). Almost all of this was accounted for by unnamed species sp002358415 from genus *Alistipes* (10.% of reads in CELL-fed vs <0.001% of reads in FOS-fed, p<0.0001).

  Results for phylum *Bacteroidota* are summarised in Figure 97, p. 284.

- The phylum *Actinobacteriota* was massively over-represented in FOS-fed animals (27.3% of reads in FOS treated organisms compared to 1.7% in CELL treated, p<0.0001), caused entirely by significant increased in a number of species from genus *Bifidobacterium*, including *B. animalis* (by far the most abundant, accounting for almost all sequenced in this genus), and also *B. pseudolongus*, *B. italicum* and several others, Figure 98, p. 285.

- Conversely, phylum *Verrucomicrobiota* was over-represented in CELL-fed animals, where it accounted for 13.5% of reads vs 0.11% in FOS-fed animals, p=0.052. *Akkermansia muciniphilia* accounted for almost all of this increase, Figure 99, p. 286.

- Phylum *Proteobacteria* accounted for 1.8% on reads in CELL fed animals but only 0.98% in FOS-fed, p=0.0008. Families within this phylum showing increased abundances in CELL-fed animals included *Enterobacteriaeceae*, *Neisseriaceae* and *Pasteurellaceae*.

- Abundances of a number of minor phyla were also increased in CELL-fed animals, including *Deferribacterota* (0.19% in CELL-fed vs <0.001% in FOS-fed, p=0.0002), *Spirochaetota* (0.1% vs 0.04%, p=0.048), *Patescibacteria* (0.06% vs 0.04%, p=0.027), *Syngergistota* (0.02% vs <0.0001%, p=0.0003) and others. No other taxa were significantly increased in FOS-fed animals beyond those mentioned above: *Actinobacterota* and the two *Firmicutes* sub-phyla.

Fermentable fibre, but not induction of experimental uraemia, has significant effects on the functional capacity of the gut microbiota

Analysis of the metabolic potential of the sequenced microbiota was carried out at a high functional level using COG identities (Clusters of Orthologous Genes), and then at the lower levels of KEGG orthologies and modules. In addition, because of the interest specifically in carbohydrate metabolism, CAZy (Carbohydrate Active enZYmes) categories were also compared between groups.

As with the bacterial composition of the microbiota, the presence of uraemia did not affect the metagenomic profile of the gut microbiota at all, but FOS- vs CELL-diet strongly did (Figure 100, p. 287).

When analysed by t-test with as the independent variable, none of the 24 major COG metabolic categories were different between control and uraemic animals whereas eight major COG metabolic categories were present in differential abundances between FOS and CELL diets. Most relevantly, genes involved in carbohydrate metabolism were increased in FOS-treated animals (diet accounting for 36.2% of variation in carbohydrate gene expression, p=0.029, uraemia vs control accounting for only 0.8% of variation, p=0.623), as were genes involved in lipid metabolism, including those involved in SCFA synthesis, Figure 101, p. 288.

Carbohydrate metabolism

Full analysis of individual metabolic pathways involved in carbohydrate metabolism is included in Appendix 6, p. 411. Briefly, samples from FOS-fed animals showed increases in various glycolytic pathways associated with release of simple sugars from complex carbohydrate polymers such as FOS, and also increases in a specific carbohydrate metabolism pathway, the fructose-6-phosphate division of the pentose phosphate pathway termed the 'bifid shunt' because of its centrality in carbohydrate metabolism in *Bifidobacteria*.

Lipid metabolism

Animals fed the FOS-diet had higher abundances of three of the four fatty acid metabolic modules represented in the database: M00082 (initiation of fatty acid synthesis), M00083 (elongation of fatty acids) and M00086 (beta-oxidation, acyl-CoA synthesis). Modules M00082

243

and M00083 are directly involved in synthesis of the short chain fatty acids acetate and butyrate

(Figure 102, p. 289).
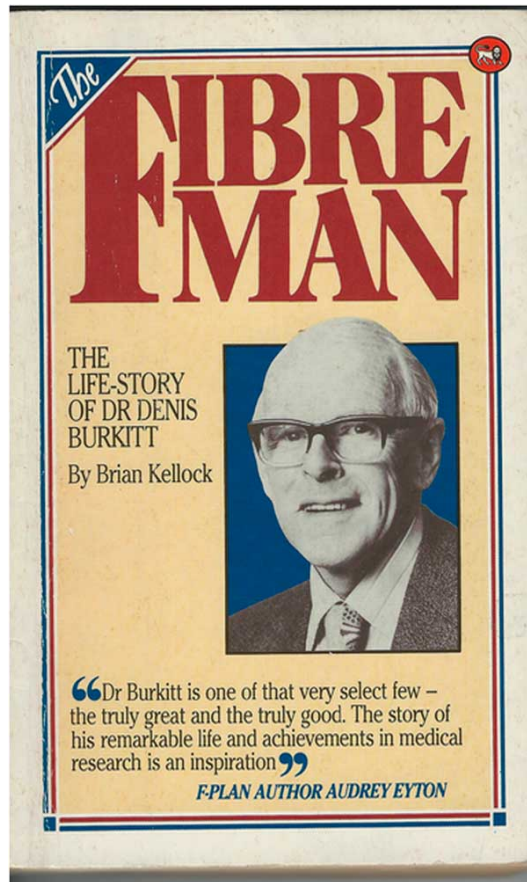
Figure 61: Denis Burkitt popularised the idea that a deficiency of dietary fibre was a common aetiological factor in many diseases highly prevalent in Western populations. *"In Africa, treating people who live largely off the land on vegetables they grow, I hardly ever saw cases of many of the most common diseases in the United States and England – including coronary heart disease, adult-onset diabetes, varicose veins, obesity, diverticulitis, appendicitis, gallstones, dental cavities, hemorrhoids, hiatal hernias and constipation. Western diets are so low on bulk and so dense in calories, that our intestines just don't pass enough volume to remain healthy."* [283]
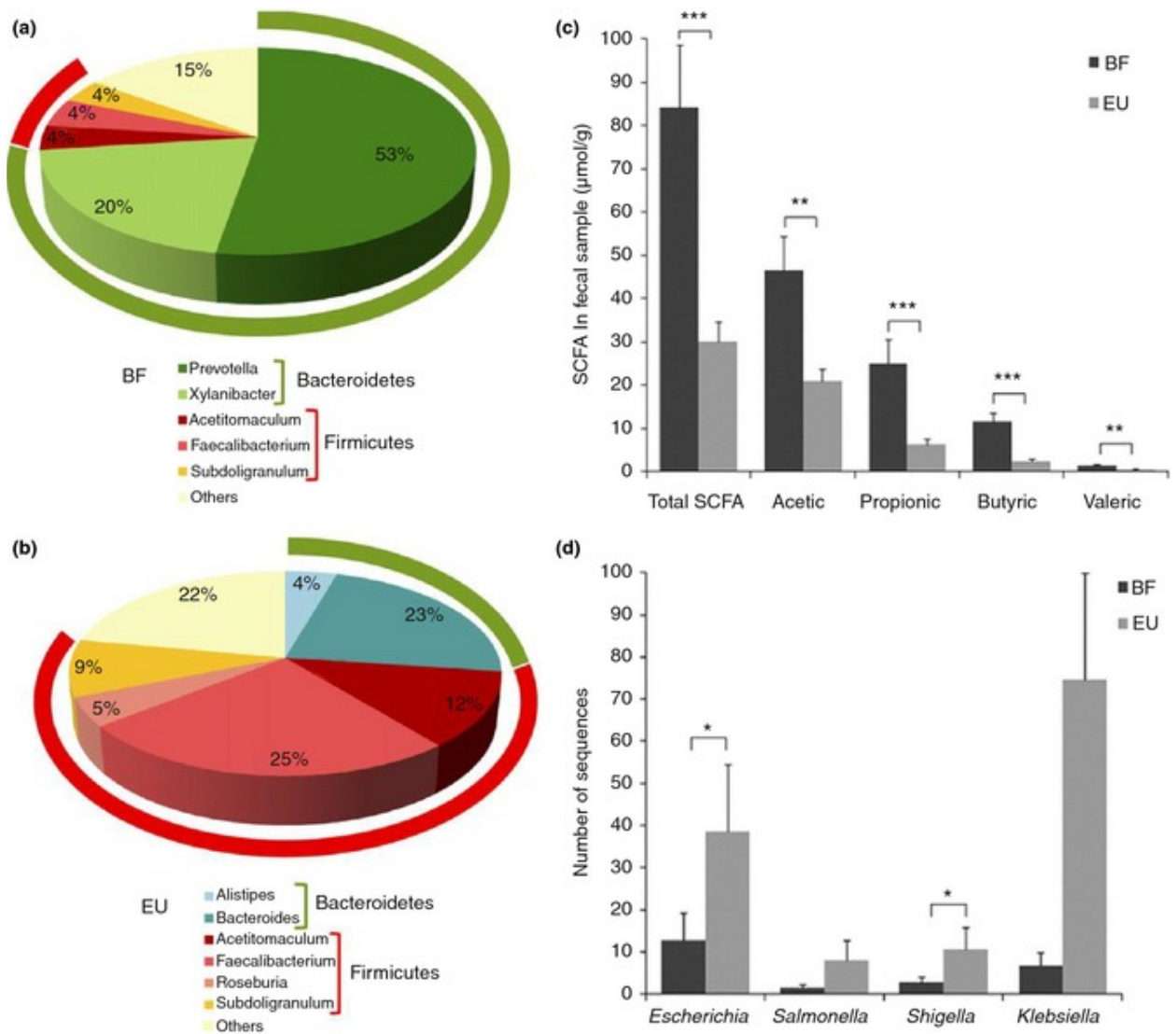
Figure 62: Differences in gut microbial populations between African (a) and European (b) children. African children had higher levels of faecal short chain fatty acids (c) and lower abundances of *Gammaproteobacteria* (d). From De Filippo et al, 2010. [278]
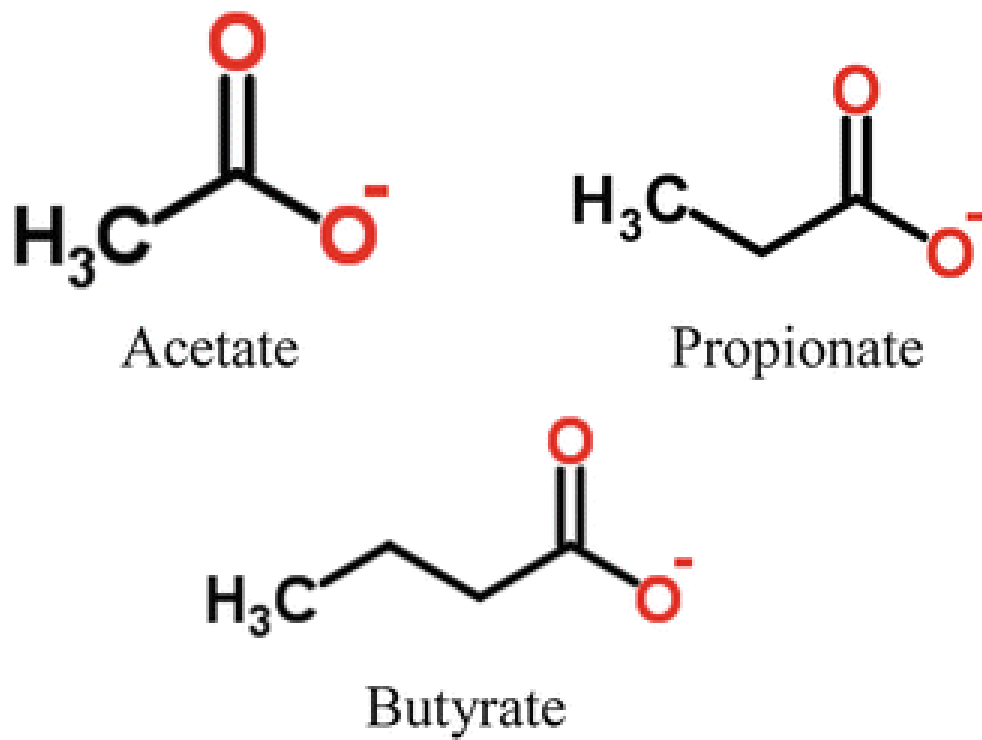
Figure 63: Molecular structure of the three commonest short chain fatty acids. Taken from Raman, 2016 [395].
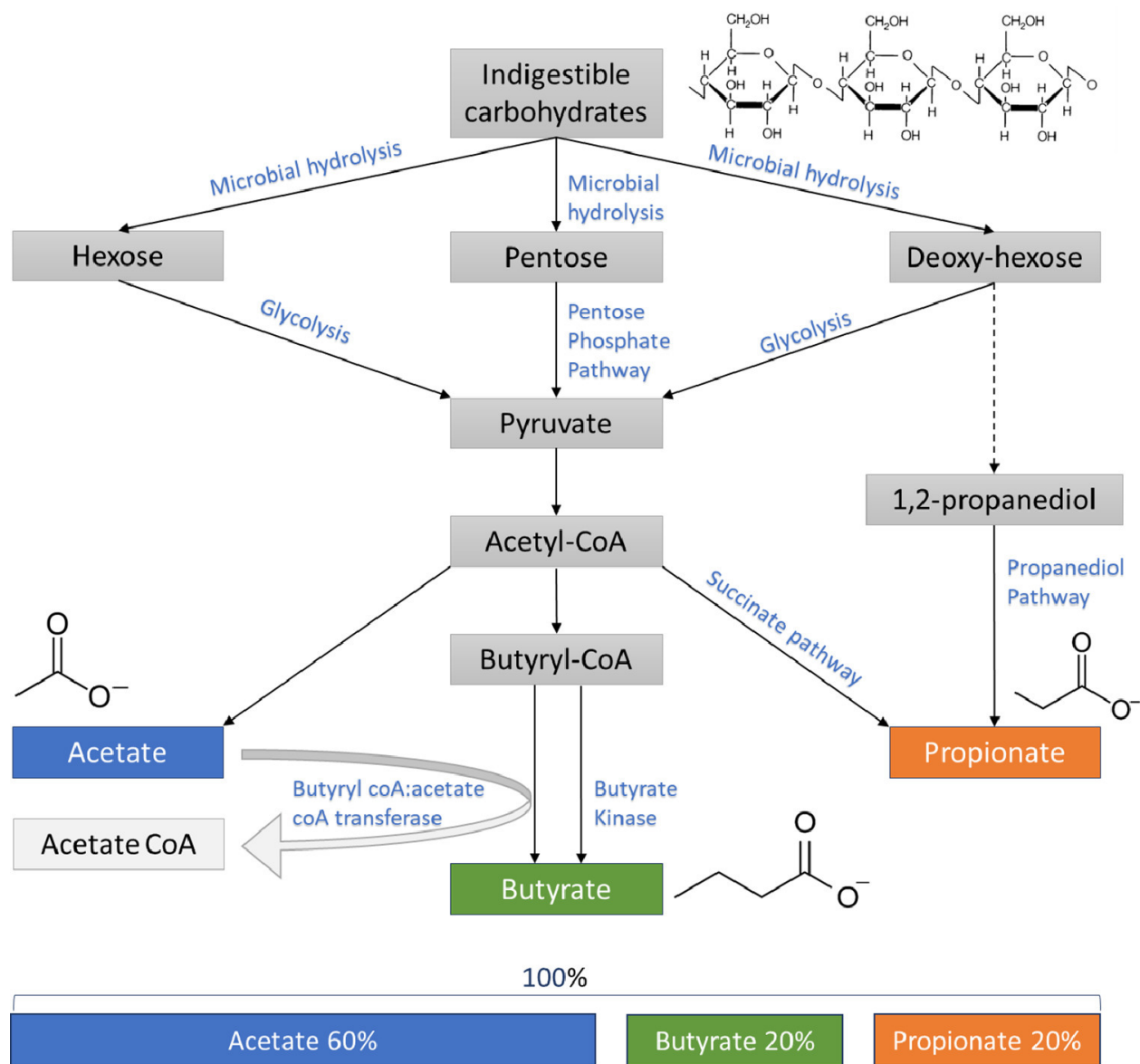
Figure 64: Principal routes of bacterial SCFA production. Taken from Deleu et al, 2021. [396]
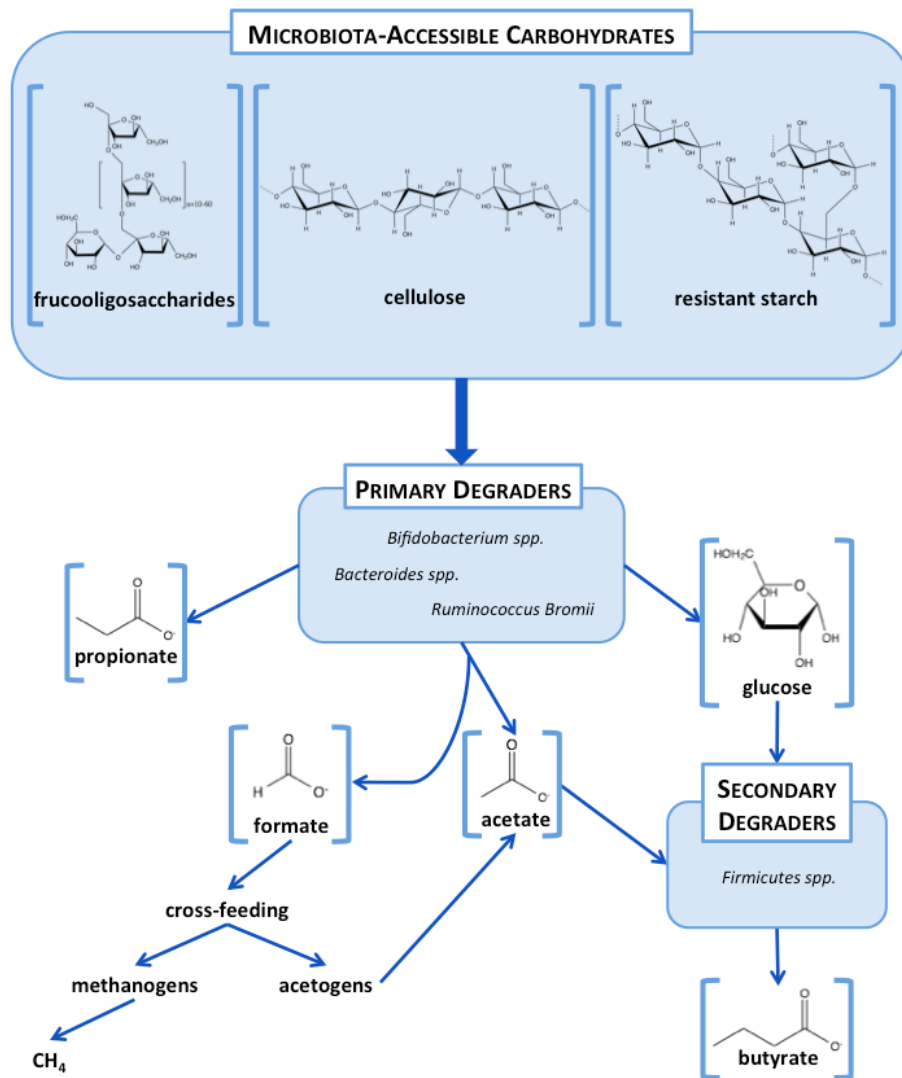
Figure 65: Primary and secondary fibre degrading organisms. Taken from https://sites.tufts.edu/absorption/carbdigestion/, last accessed 2nd February 2022.
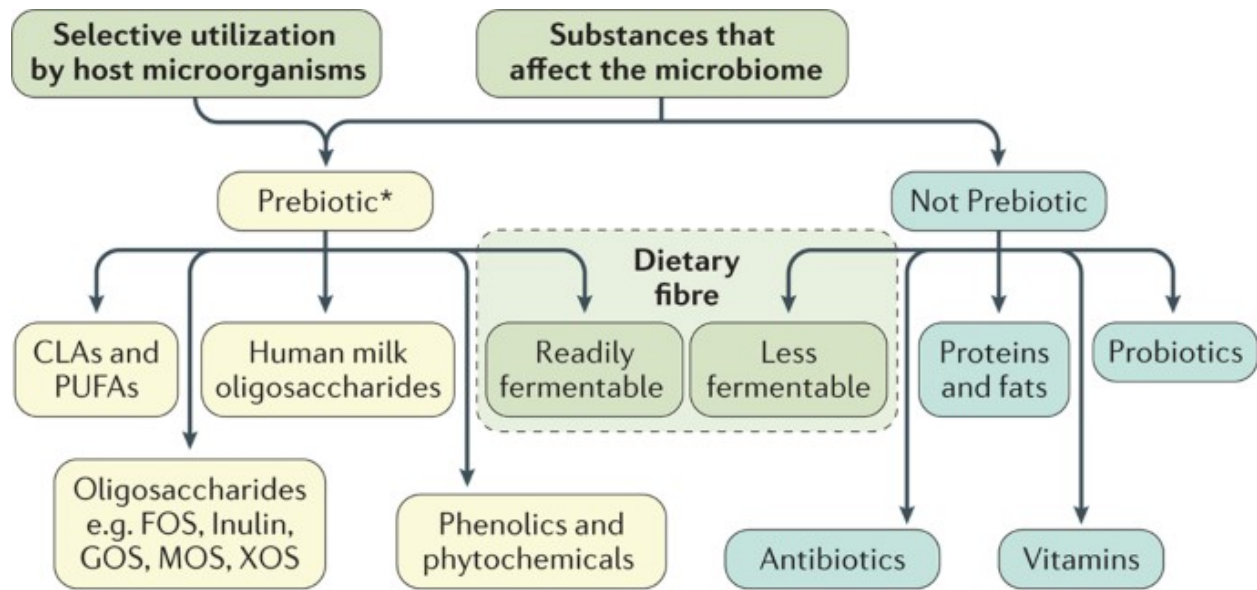
Nature Reviews | Gastroenterology & Hepatology

Figure 66: Dietary or therapeutic substances that may affect the microbiome. The relationships between the categories 'dietary fibre' and 'prebiotics' are illustrated. Taken from Gibson et al, 2017. [339]
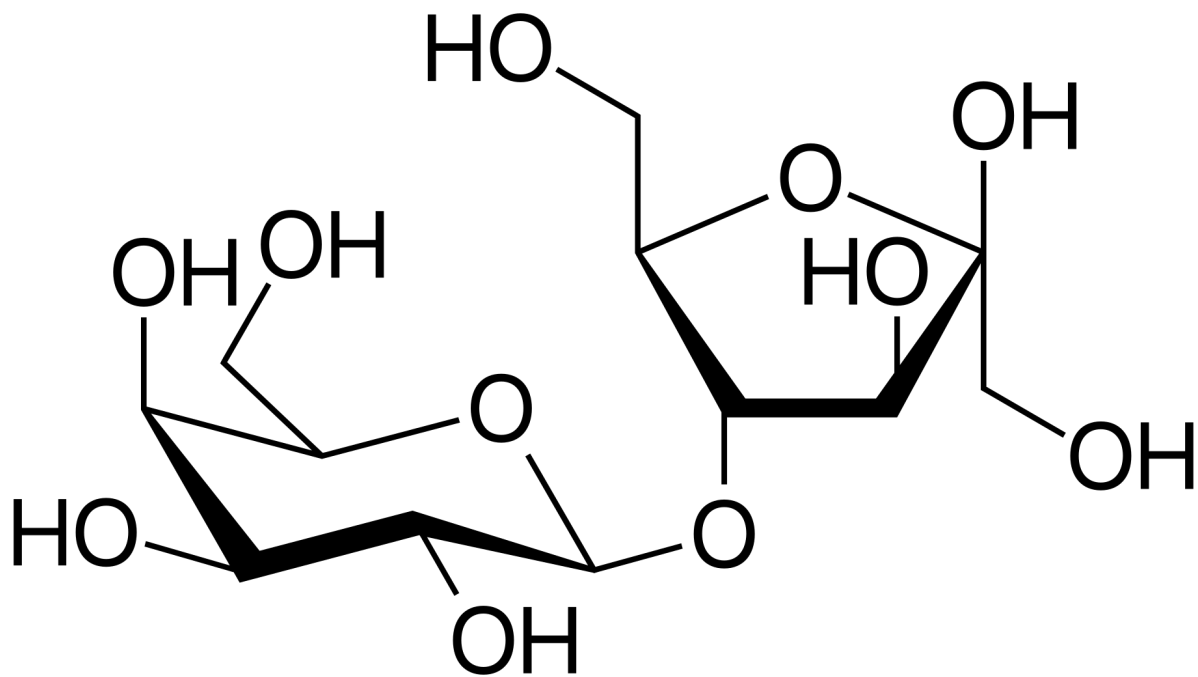
Figure 67: Lactulose is a disaccharide of galactose (left) and fructose (right). Taken from Wikimedia (Commons), downloaded from https://commons.wikimedia.org/wiki/File:Lactulose_structure.svg, last accessed 13th January 2022.
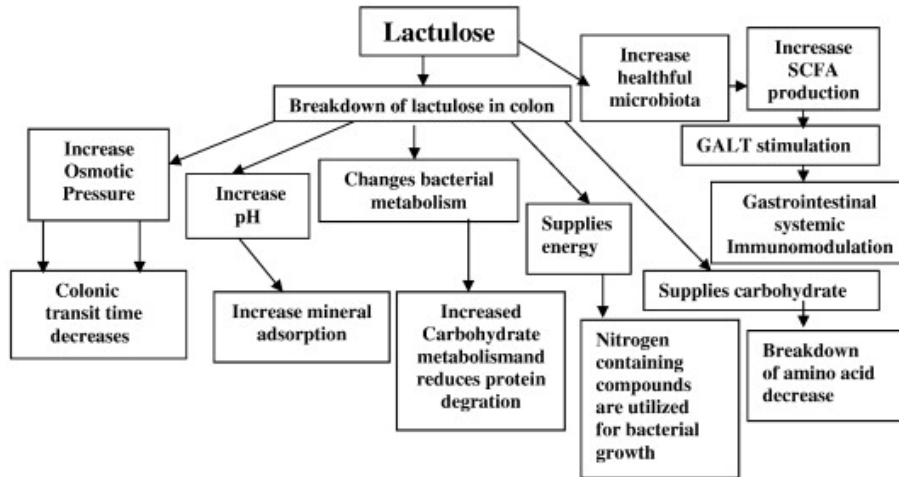
Figure 68: Beneficial effects of lactulose on gut transit time, nutrient absorption, the microbiome, protein versus carbohydrate metabolism and immune system function. One part of the figure is incorrect, in that lactulose fermentation decreases (not increases) gut pH. Taken from Panesar et al, 2011 [405]
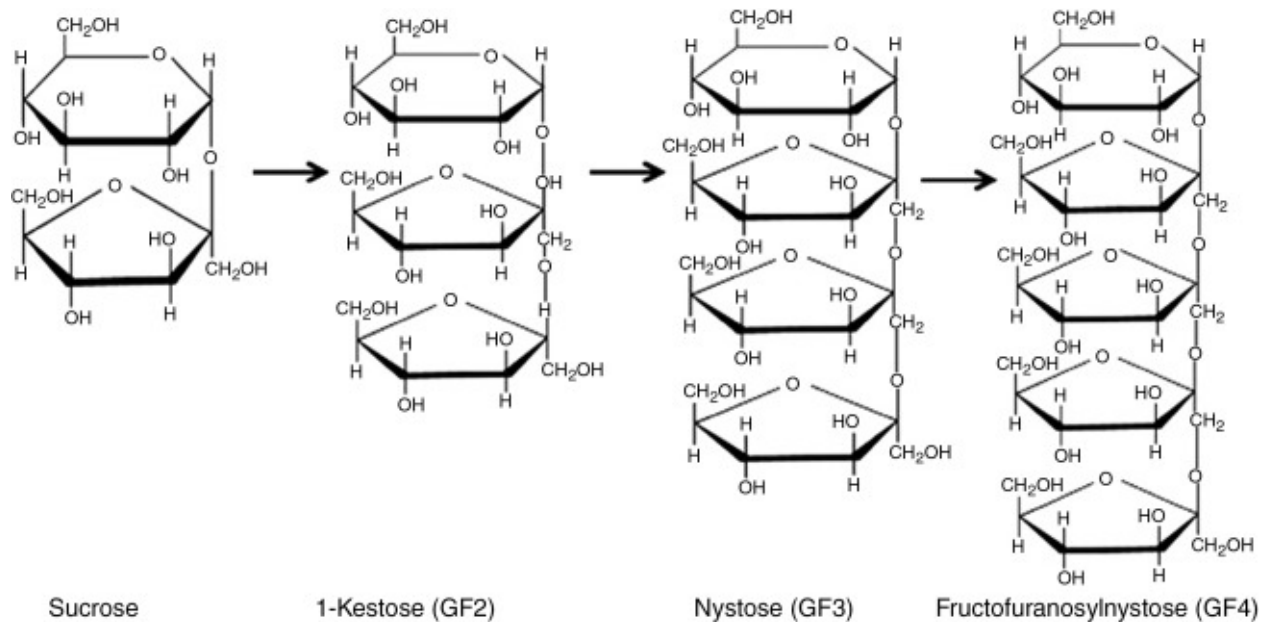
Figure 69: The molecular structure FOS polymers. Sucrose (left, not itself an examples of FOS) is a simple disaccharide of glucose and fructose; the FOS molecules 1-kestose (GF2), nystose (GF3) and fructofuranosylnystose (GF4) are the 2-, 3- and 4- fructose polymers which are the shortest degree of polymerisation FOS molecules; once the degree of polymerisation exceeds 10 the term FOS is no longer applied and molecules are instead referred to as inulins. Taken from Ahmad and Khalid, 2018. [397]
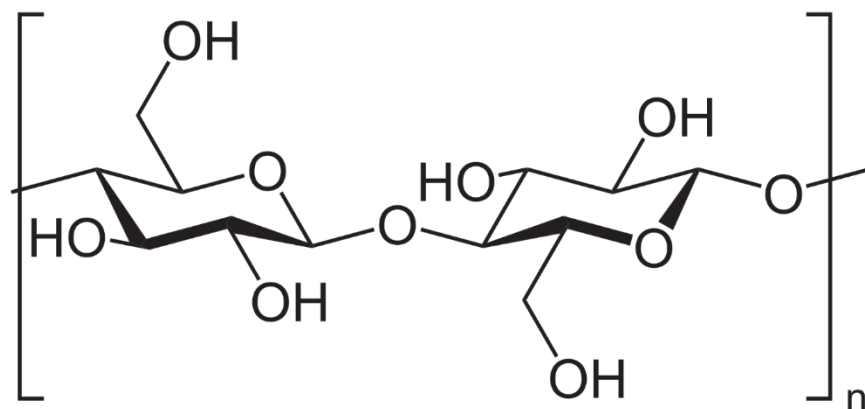
Figure 70: The chemical structure of cellulose. Taken from NeuroTIKER, Wikicommons, https://en.wikipedia.org/wiki/Cellulose#/media/File:Cellulose_Sessel.svg

Cohorts	Number	Uraemic intervention	Groups
1	32	Adenine-induced uraemia	Control, standard AIN, n=8
			Uraemic, standard AIN, n=8
			Uraemic, CELL diet, n=8
			Uraemic, FOS diet, n=8
2	28	Adenine-induced uraemia	Control, CELL diet, n=6
			Control, FOS diet, n=6
			Uraemic, CELL diet, n=8
			Uraemic, FOS diet, n=8
3	24	Subtotal nephrectomy	Control, CELL diet, n=6
			Control, FOS diet, n=6
			Uraemic, CELL diet, n=6
			Uraemic, FOS diet, n=6
4	13	Subtotal nephrectomy	Uraemic, CELL diet, n=6
			Uraemic, FOS diet, n=7

Table 7: Animal experiments carried out to assess the potential for FOS diets to ameliorate the phenotype of rat kidney disease. Cohorts 1 and 2 were administered either 0.75% adenine containing diet or control diet for 4 weeks to induce uraemia; after which they were switched to their experimental diet (AIN, FOS or CELL). Cohorts 3 and 4 underwent either subtotal nephrectomy or sham surgery, and then were switched to experimental diets (CELL or FOS) four weeks after surgery.

		Weeks 1&2	Weeks 3&4	Weeks 5&6	Weeks 7&8	Weeks 9&10	Weeks 11&12	Cull point
Cohort 1	n=8	Control diet		AIN diet				Start of week 9
	n=8	0.75% adenine		AIN diet				Start of week 9
	n=8	0.75% adenine		CELL diet				Start of week 9
	n=8	0.75% adenine		FOS diet				Start of week 9
Cohort 2	n=6	Control diet		CELL diet				Start of week 9
	n=6	Control diet		FOS diet				Start of week 9
	n=8	0.75% adenine		CELL diet				Start of week 9
	n=8	0.75% adenine		FOS diet				Start of week 9
Cohort 3	n=6	Sham	Control diet		CELL diet			Start of week 11
	n=6	Sham	Control diet		FOS diet			Start of week 11
	n=6	SNx	Control diet		CELL diet			Start of week 11
	n=6	SNx	Control diet		FOS diet			Start of week 11
Cohort 4	n=6	SNx	Control diet		CELL diet		Abx	Start of week 13
	n=7	SNx	Control diet		FOS diet		Abx	Start of week 13

Table 8: Experimental protocols for fibre experiment. Interventions rendering rats control (dark blue) or uraemic (red) preceded experimental diets; either standard AIN (brown), CELL (light blue) or FOS (green). Animals in cohort 4 had blood and urine collected at the start of week 11 (to allow direct comparison with cohort 3), and then were administered broad spectrum antibiotics for 10 days prior to sacrifice. Sham, sham surgery; SNX, subtotal nephrectomy; Abx, antibiotics.
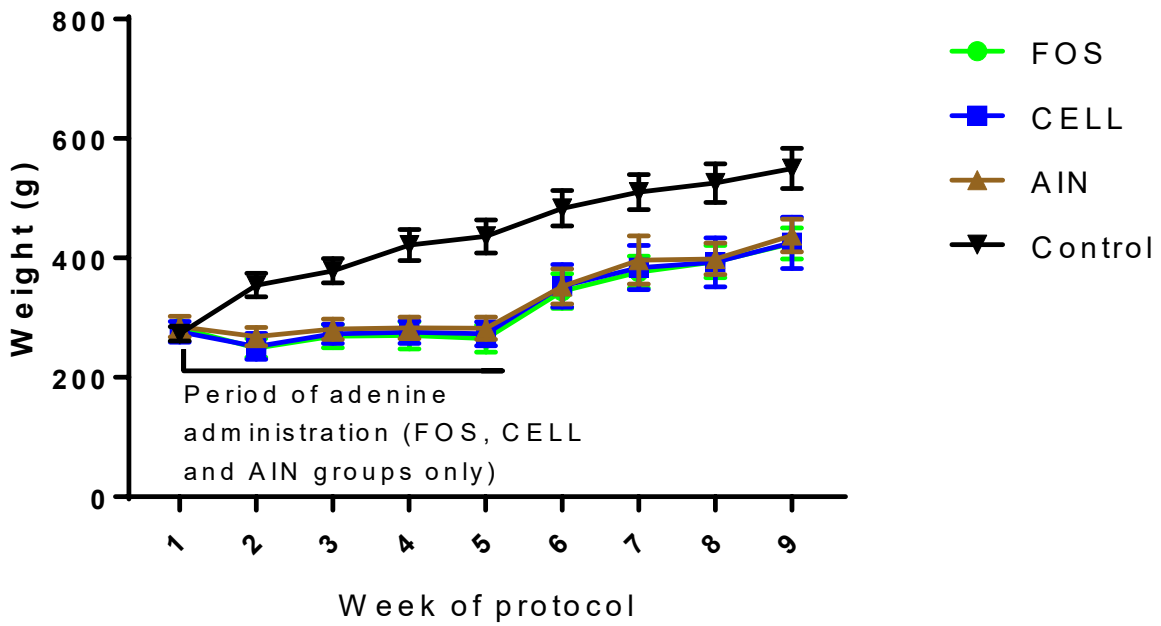
Figure 71: Rat weights by week of experimental protocol for animal in experimental cohort 1. Means and standard errors are shown, grouped according to diet. The control animals had normal renal function, all three other groups were rendered uraemic through a four-week period of adenine administration, before being started on different experimental diets.
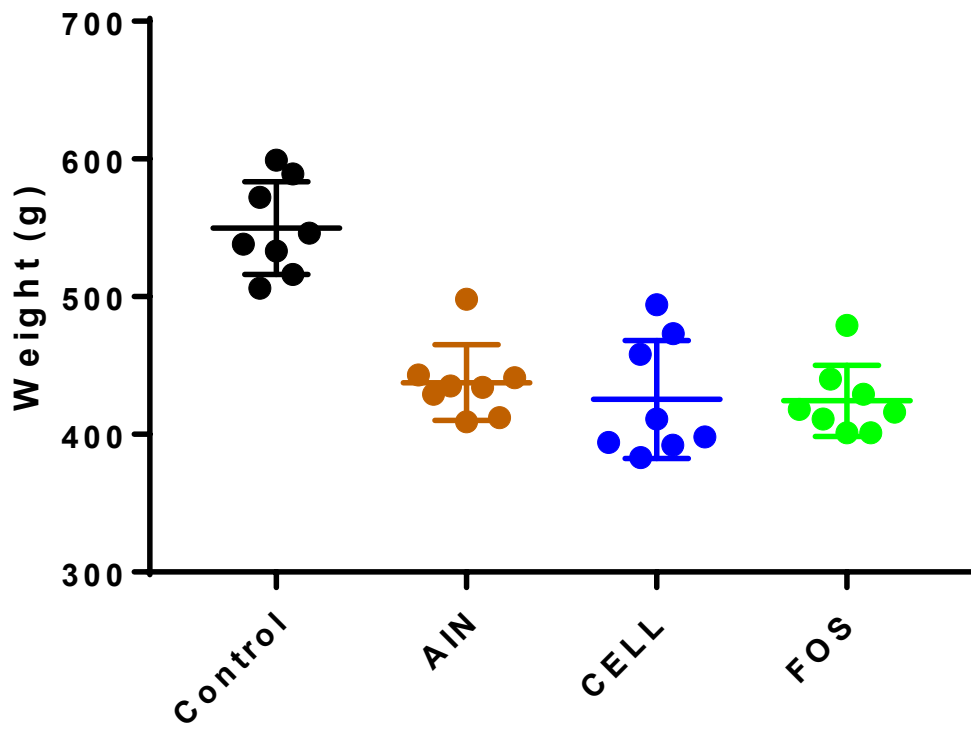
Figure 72: Weight at time of sacrifice according to the four experimental groups.
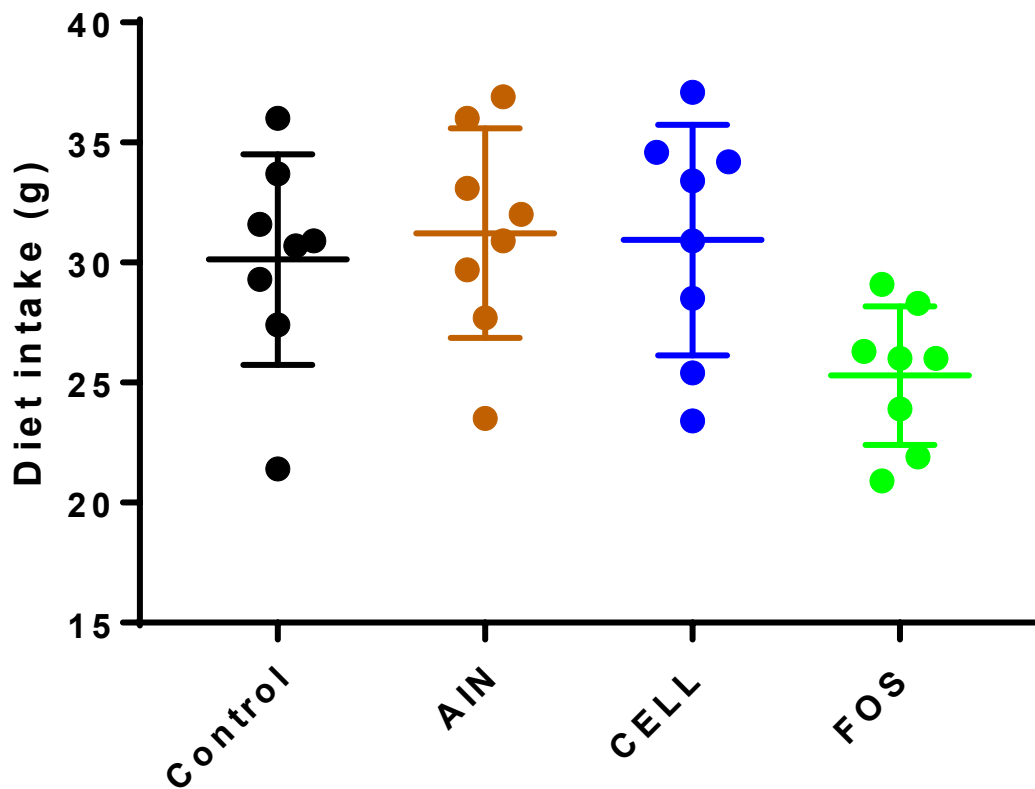
Figure 73: 24h diet consumption immediately prior to sacrifice according to the four experimental groups in cohort 1. One-way ANOVA demonstrated a significant difference among means (p=0.027), with the only significant difference between individual groups being that between animals receiving FOS diet compared to those receiving AIN diet (mean FOS consumption 25.3g vs mean AIN consumption 31.23g, p=0.039 by Tukey's post-hoc analysis).
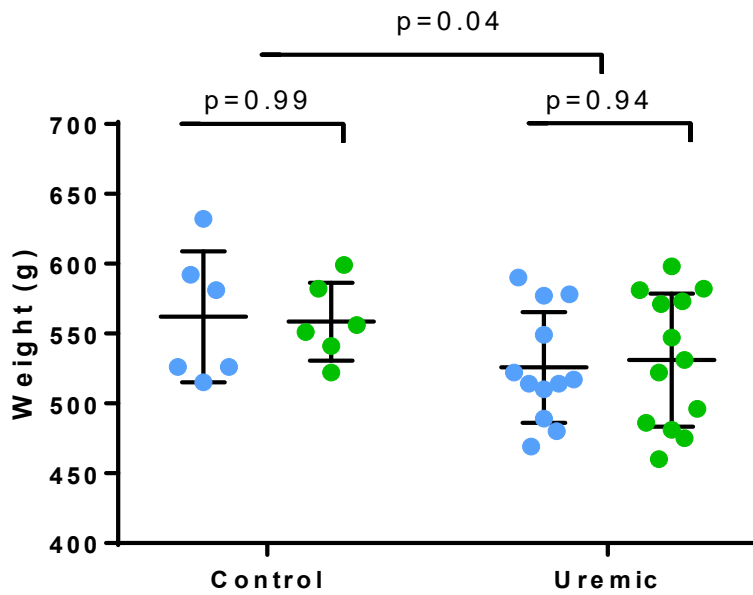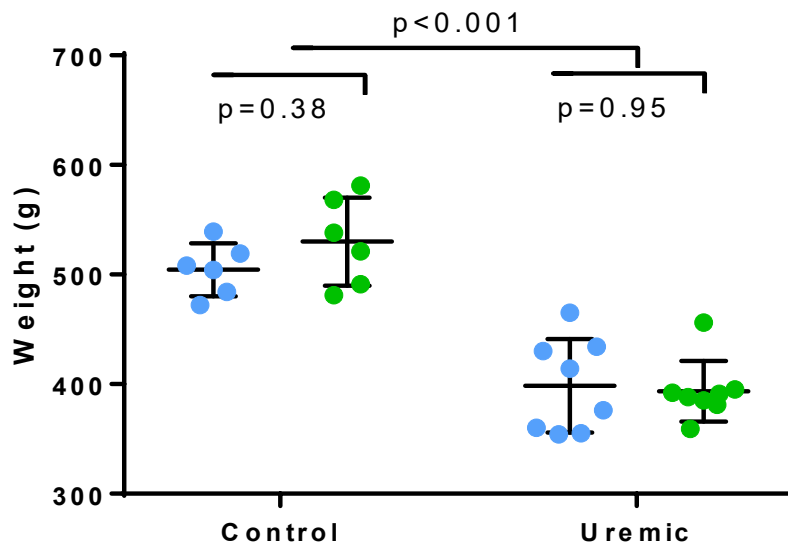
Figure 74: Weight at the time of sacrifice between control and uraemic animals on CELL (blue) and FOS (green) diets in chemically-induced uraemia (top) and surgically-induced uraemia (bottom) confirmatory cohorts.
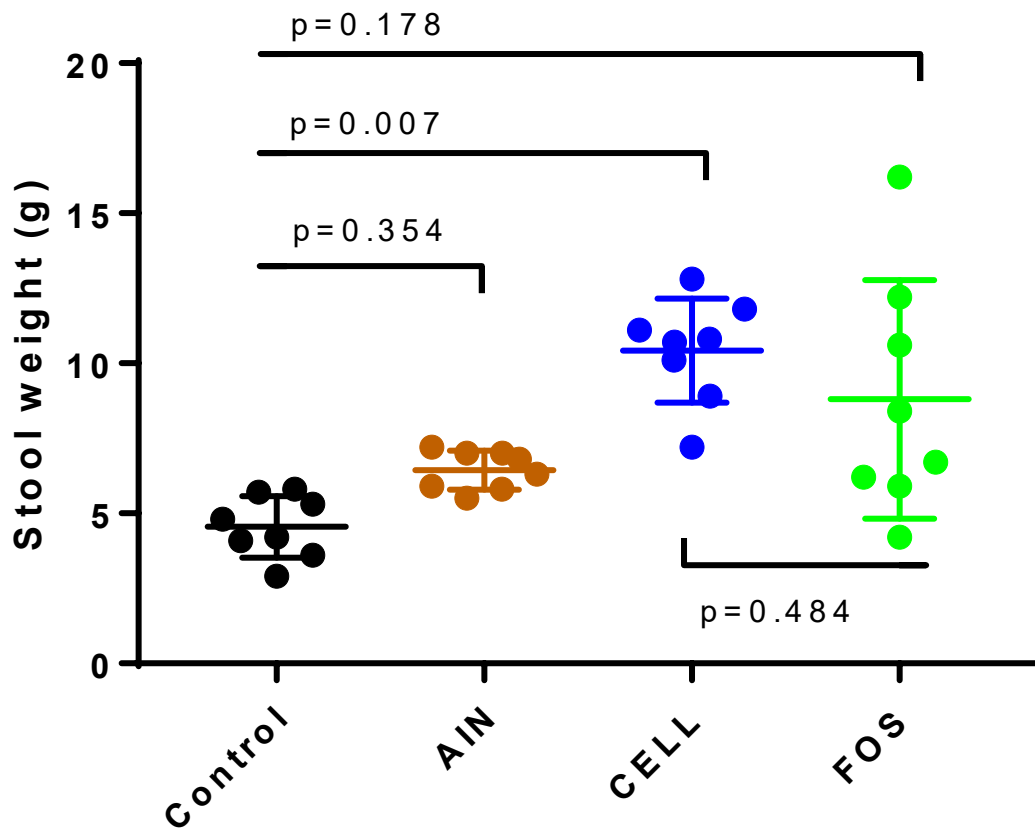
Figure 75: 24h stool weight between animals in cohort 1, grouped according to experimental intervention and diet. Significance is assessed by Tukey's post-hoc test following one-way ANOVA.

Control (AIN diet)	Uraemic, AIN diet
Uraemic, CELL diet	Uraemic, FOS diet

Figure 76: Selection of stool pellets from animals after 24h collection using metabolism cages. Pellets from animals fed the CELL diet were bulkier, paler and crumblier; pellets from animals fed the FOS diet were darker and softer.
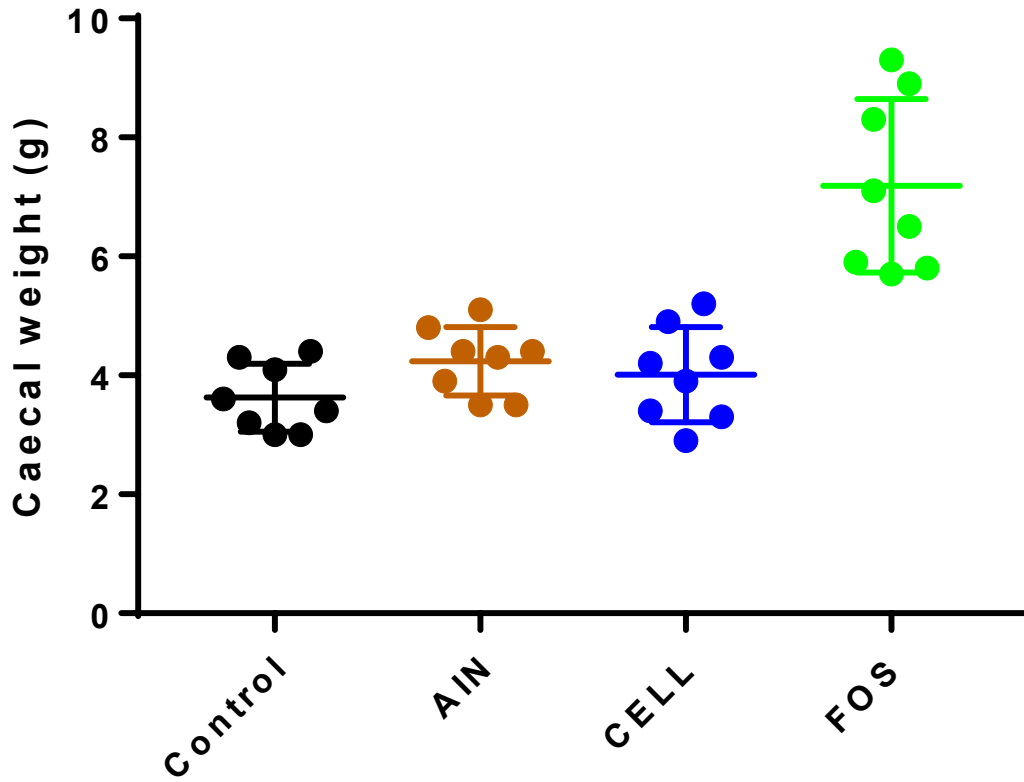
Figure 77: Caecal weight measured at the time of sacrifice between experimental groups.

| Control (AIN diet) | Uraemic, AIN diet | Uraemic, CELL diet | Uraemic, FOS diet |
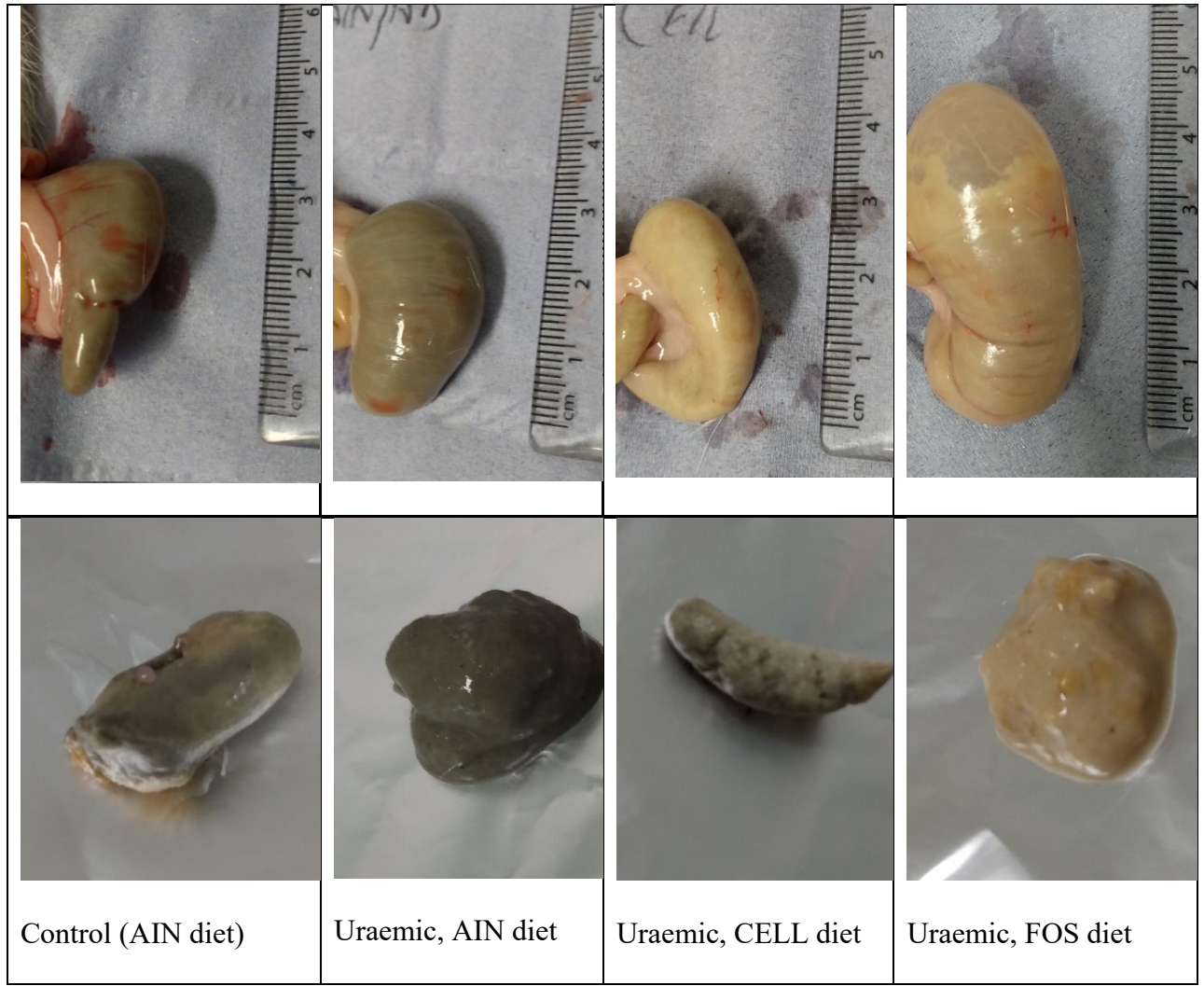
Figure 78: Caeca and caecal fluid from rats, photograph during specimen retrieval.

Figure 79: Colons from experimental rats, photograph during specimen retrieval.

| Control (AIN diet) | Uraemic, AIN diet | Uraemic, CELL diet | Uraemic, FOS diet |
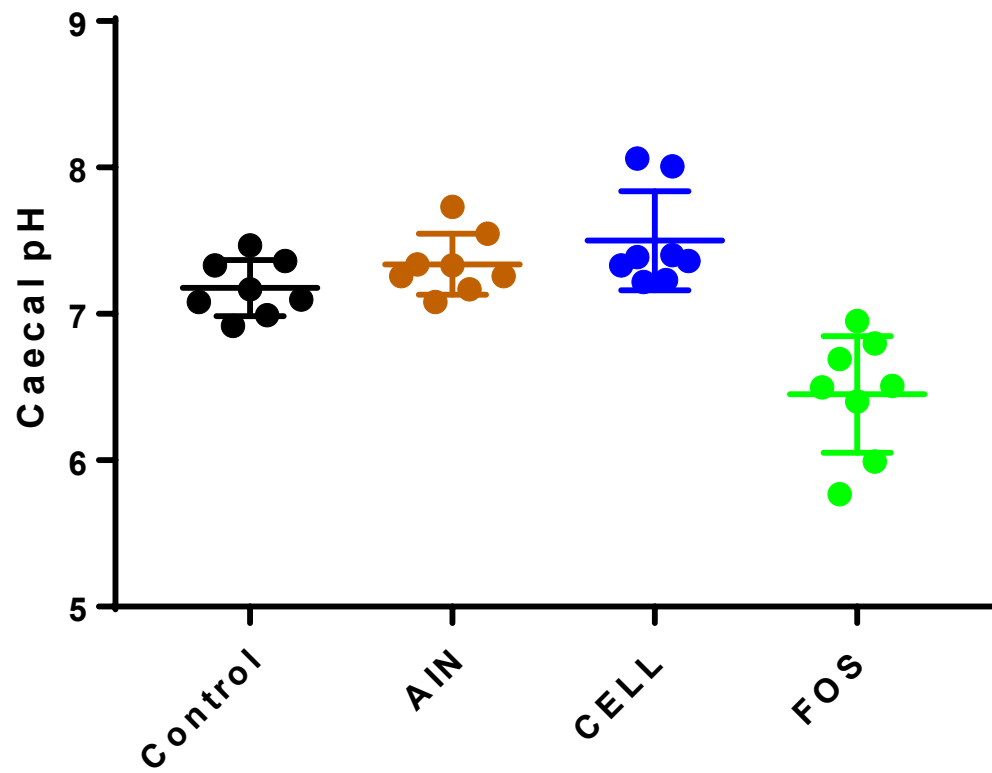
Figure 80: Caecal pH measured at the time of sacrifice between experimental groups.
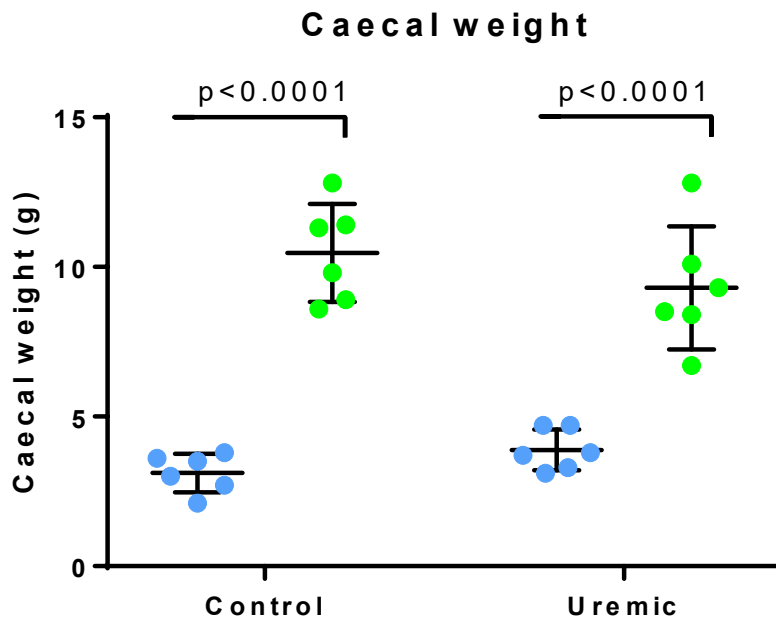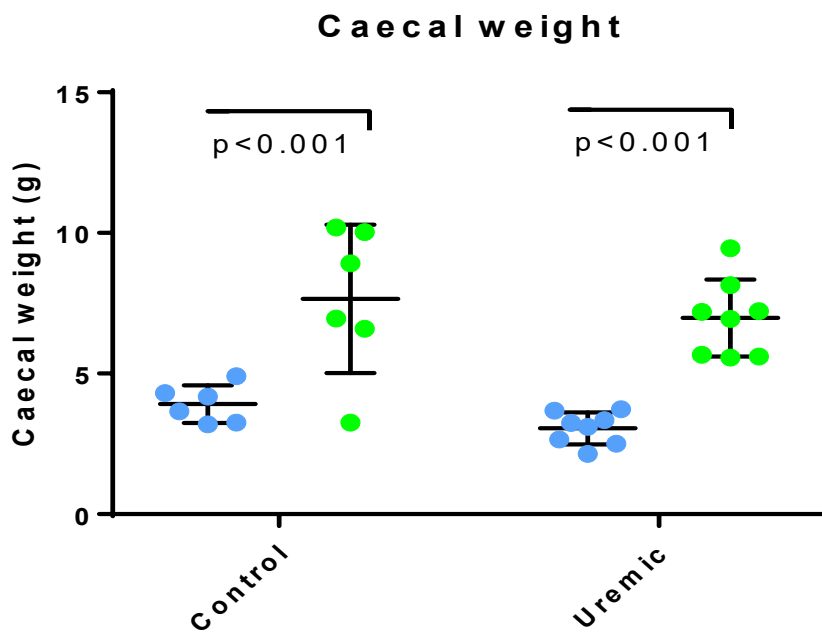
Figure 81: Confirmatory data: caecal weight at the time of sacrifice between control and uraemic animals on CELL and FOS diets in a second chemically-induced uraemia cohort (top) and a surgically-induced uraemia cohort (cohort 3, bottom). Animals receiving the CELL diet are shown in blue and animals receiving the FOS diet in green.
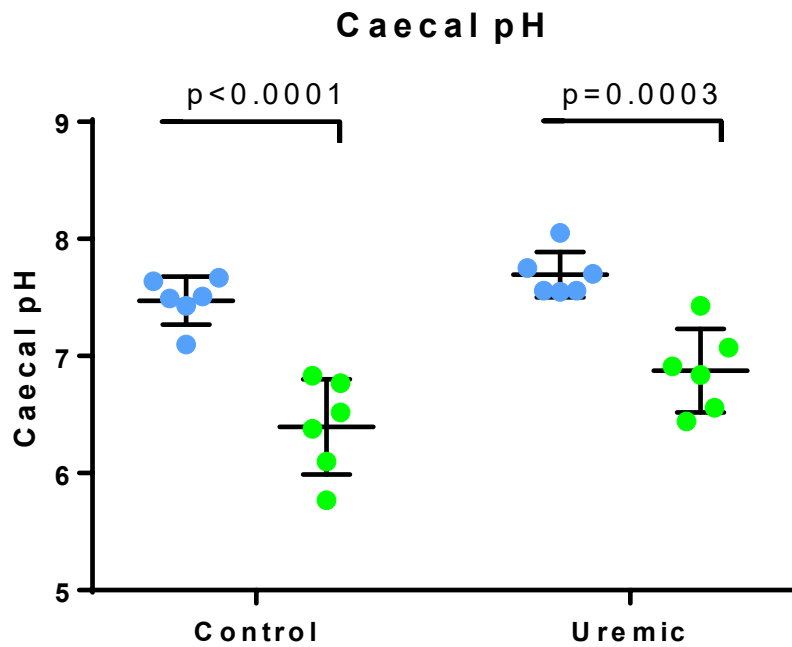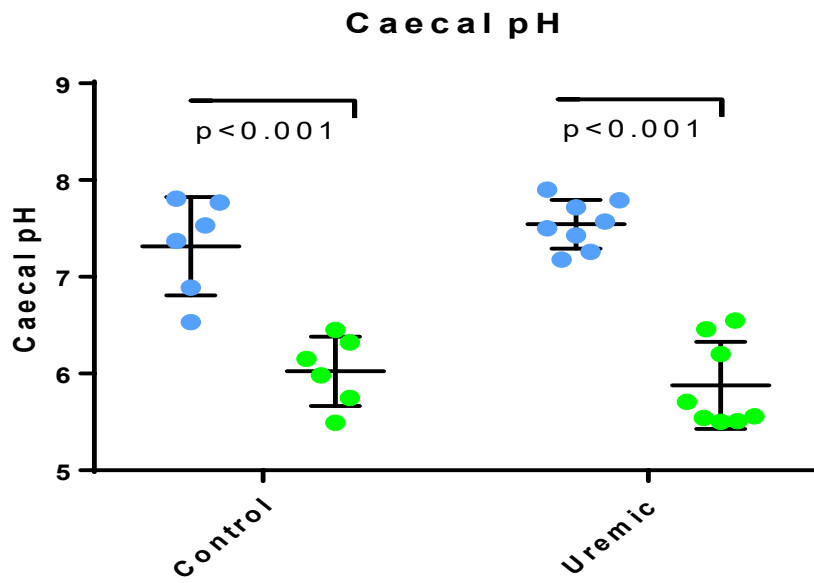
Figure 82: Confirmatory data: caecal pH at the time of sacrifice between control and uraemic animals on CELL and FOS diets in a second chemically-induced uraemia cohort (top) and a surgically-induced uraemia cohort (cohort 3, bottom). Animals receiving the CELL diet are shown in blue and animals receiving the FOS diet in green.
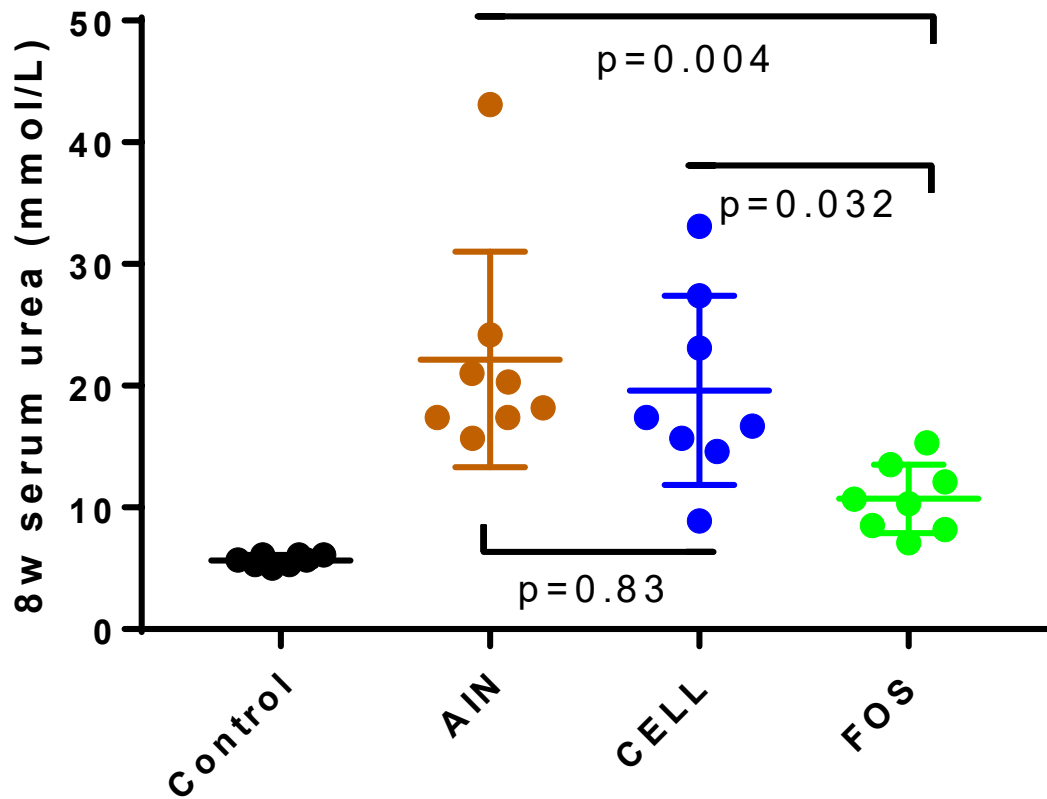
Figure 83: Serum urea at the time of sacrifice between control and uraemic animals. Significance is shown using Tukey's post-hoc test after 1-way ANOVA.
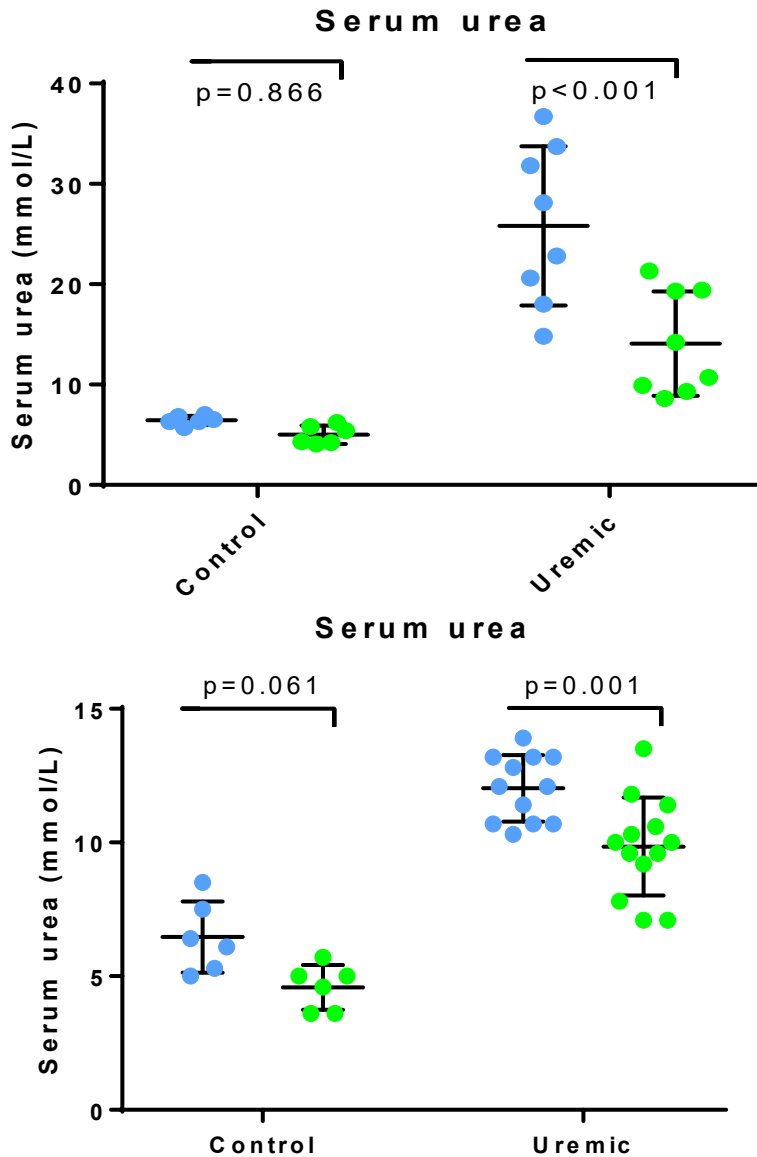
Figure 84: Confirmatory data: serum between control and uraemic animals on CELL and FOS diets in a second chemically-induced uraemia cohort (top) and both surgically-induced uraemia cohorts (cohorts 3&4). Animals receiving the CELL diet are shown in blue and animals receiving the FOS diet in green. Blood was taken at sacrifice from animals in cohort 3, and by venesection, immediately before commencing antibiotics, but after previously identical treatment to experiment 3 animals, from those in experiment 4.
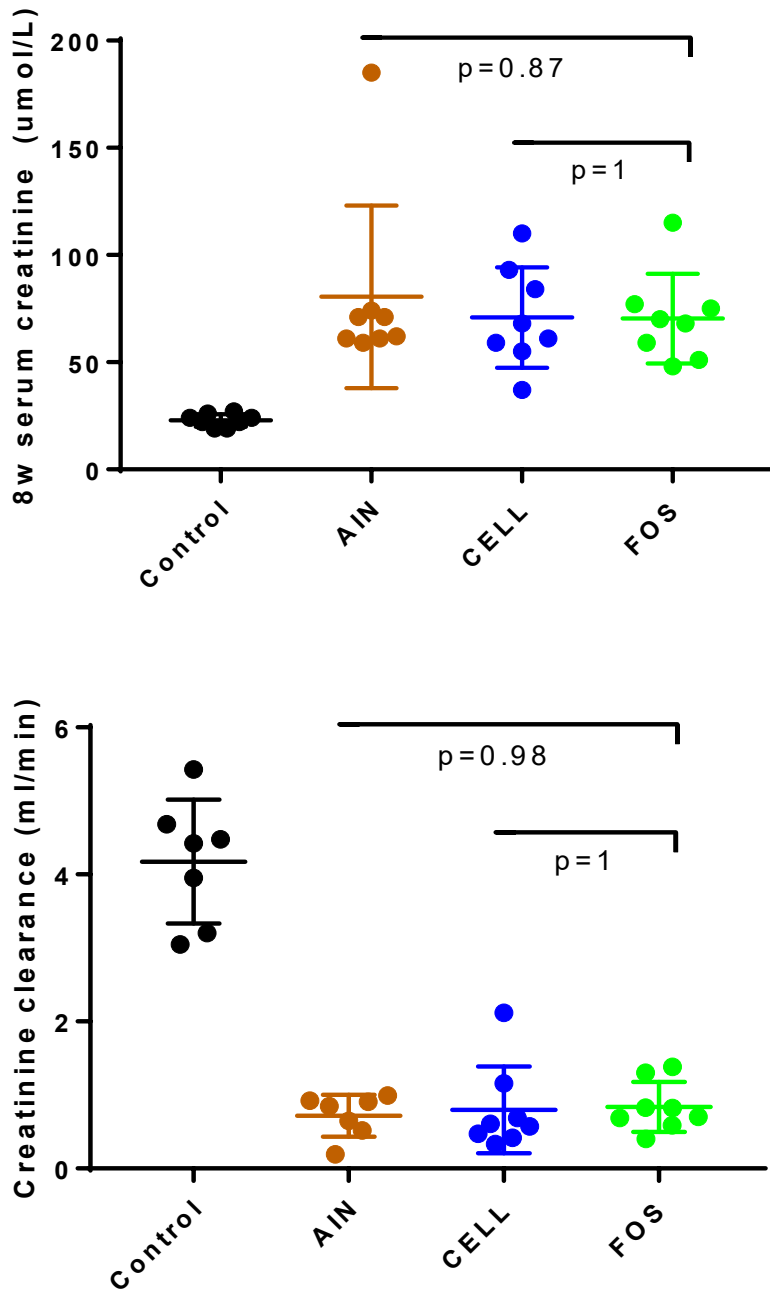
Figure 85: Serum creatinine and creatinine clearance at the time of sacrifice between control and uraemic animals. Significance is shown using Tukey's post-hoc test after 1-way ANOVA.
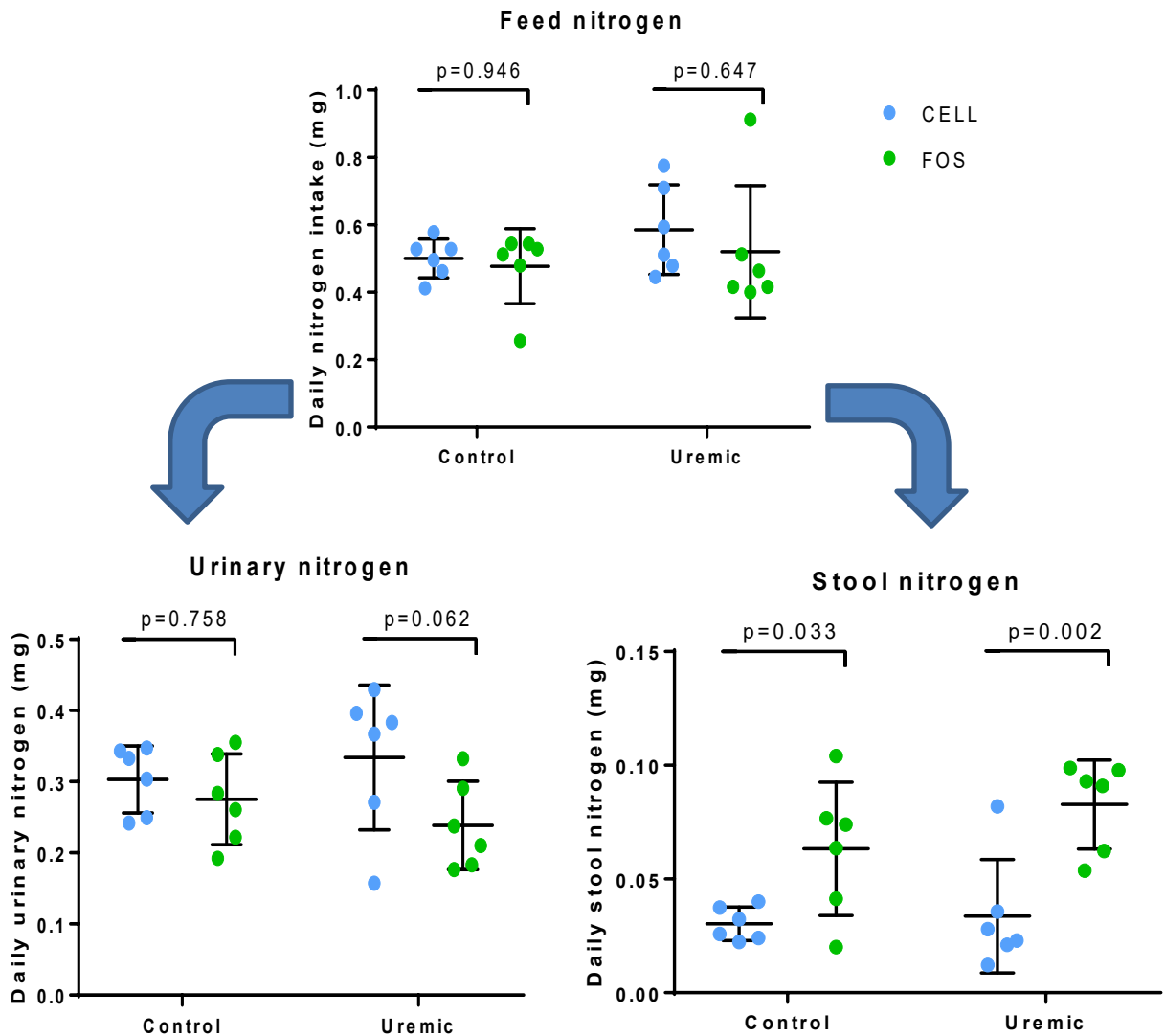
Figure 86: Total nitrogen balance in control and uraemic animals on CELL and FOS diets in the surgically-induced cohorts. Animals receiving the CELL diet are shown in blue and animals receiving the FOS diet in green. Significance is assessed using the Student t-test with Welch's correction.
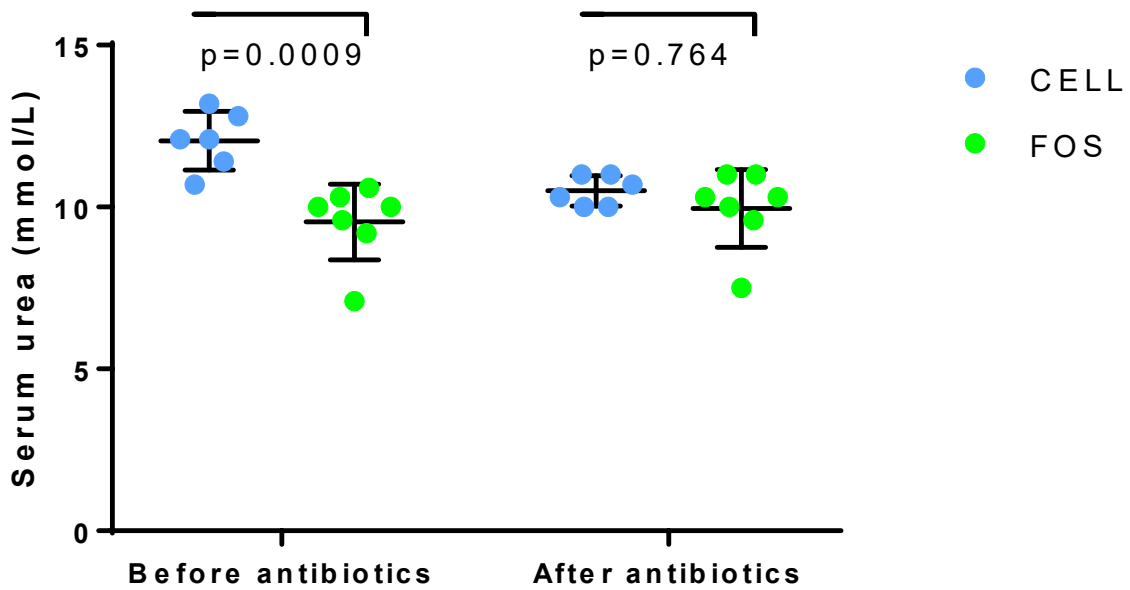
Figure 87: Serum urea in CELL- and FOS-fed animals, before and after a week of broad-spectrum antibiotics. Significance between groups is shown by Tukey's post-hoc analysis after two-way ANOVA. Antibiotic treatment abolished the urea-lowering effect of the FOS diet compared to the CELL diet.
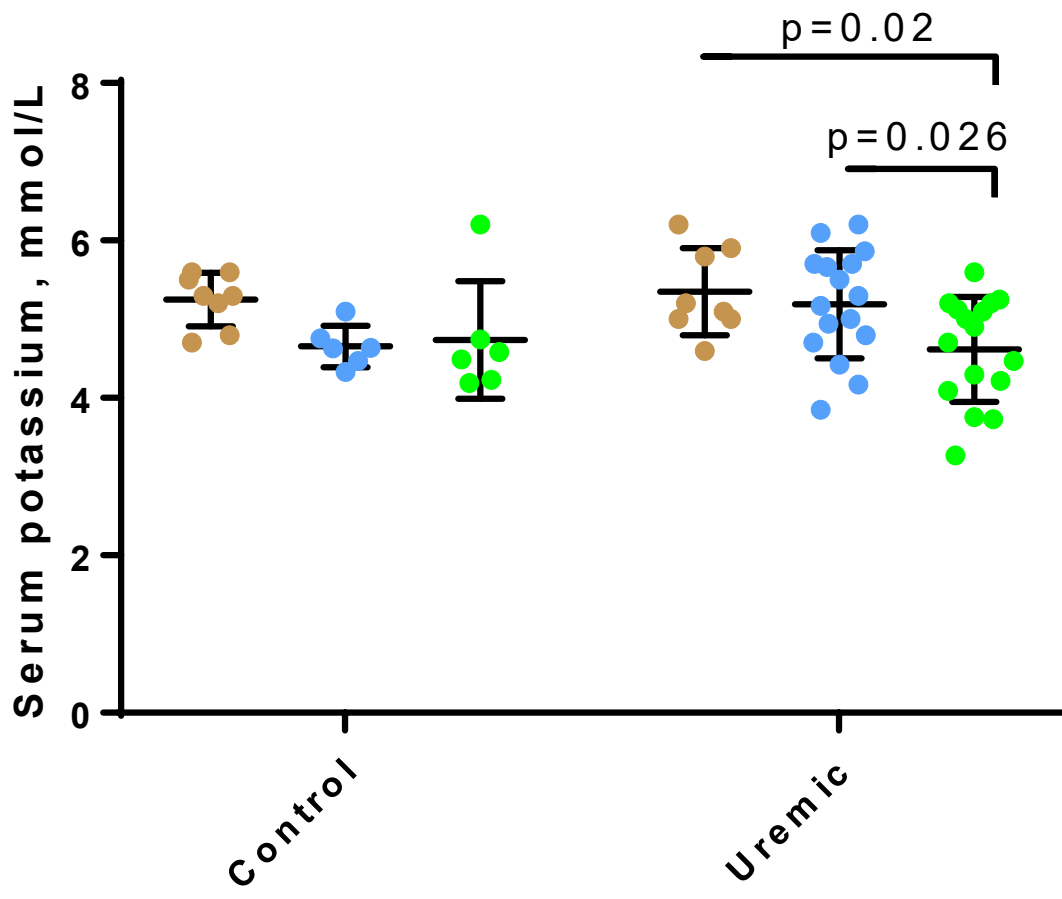
Figure 88: Serum potassium at the time of sacrifice between differently fed control and uraemic animals in experiments 1 and 2. Significance is shown using Tukey's post-hoc test after 2-way ANOVA.
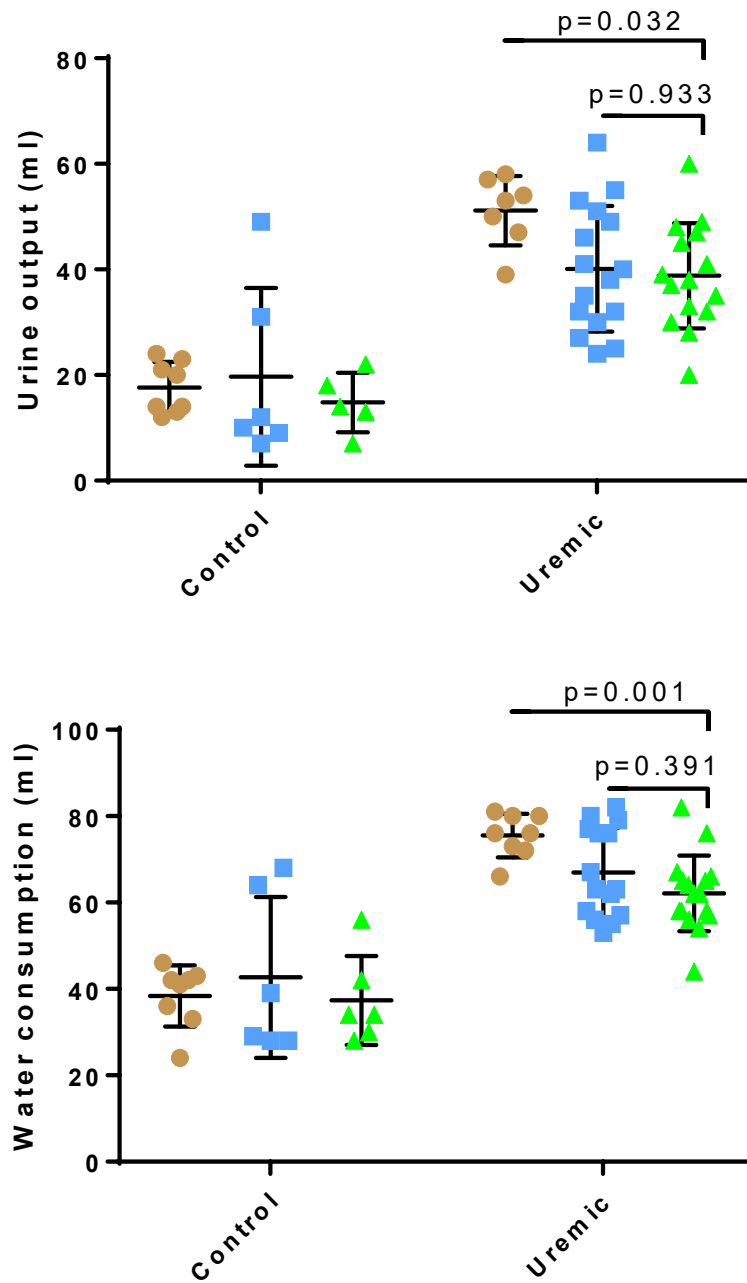
Figure 89: 24h urine output (top) and water consumption (bottom) between differently fed control and uraemic animals in experiments 1 and 2. Significance is shown using Tukey's post-hoc test after 2-way ANOVA. Brown, AIN diet; blue, CELL diet; green, FOS diet.
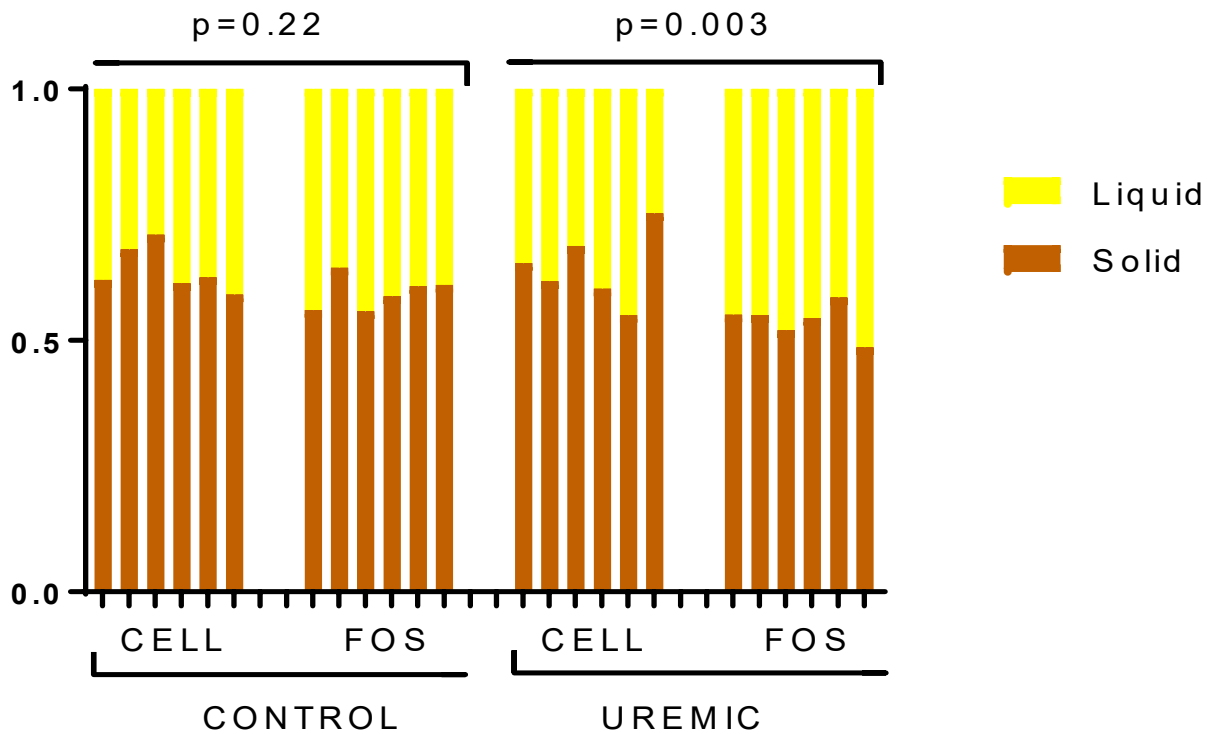
Figure 90: Composition of stool from control and uraemic animals fed CELL or FOS diet.

Results are from cohort 3 (surgically-induced uraemia). Among uraemic animals there was a

significant increase in the liquid component of stool, estimated by the difference in stool weight

before and after freeze drying. Significance is assessed by Sidak's multiple comparison test after

2-way ANOVA.
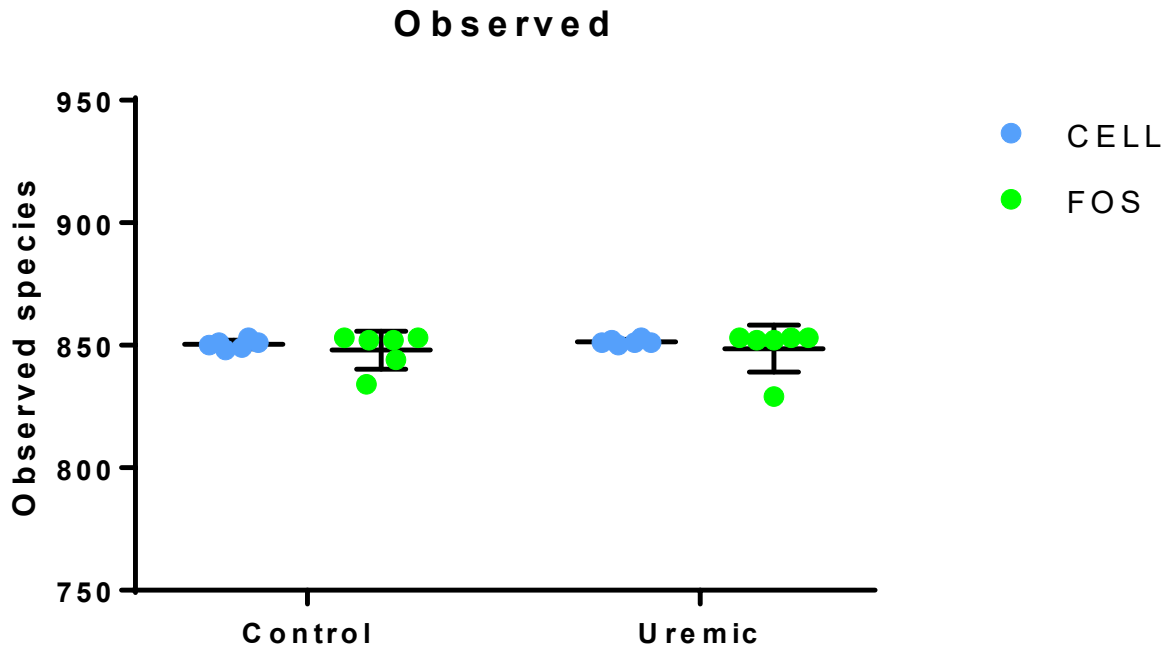
Figure 91: Observed species per sample, grouped by intervention type and diet. There were no significant differences between groups.
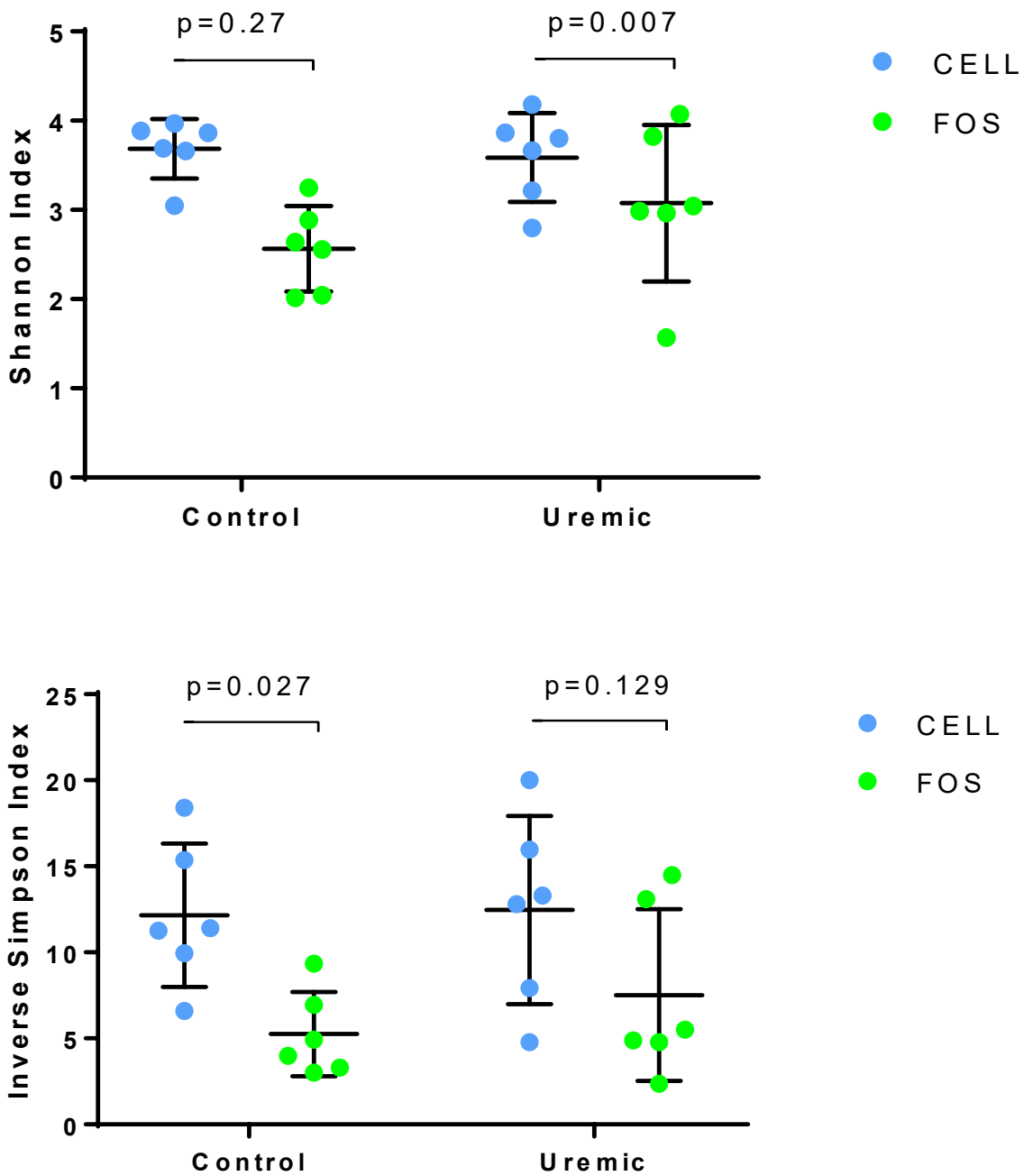
Figure 92: Alpha diversity assessed by the Shannon (top) and Inverse Simpson (bottom) indices between samples, grouped according to experimental intervention and diet. Significance is assessed using Sidak's post-hoc test after one-way ANOVA.
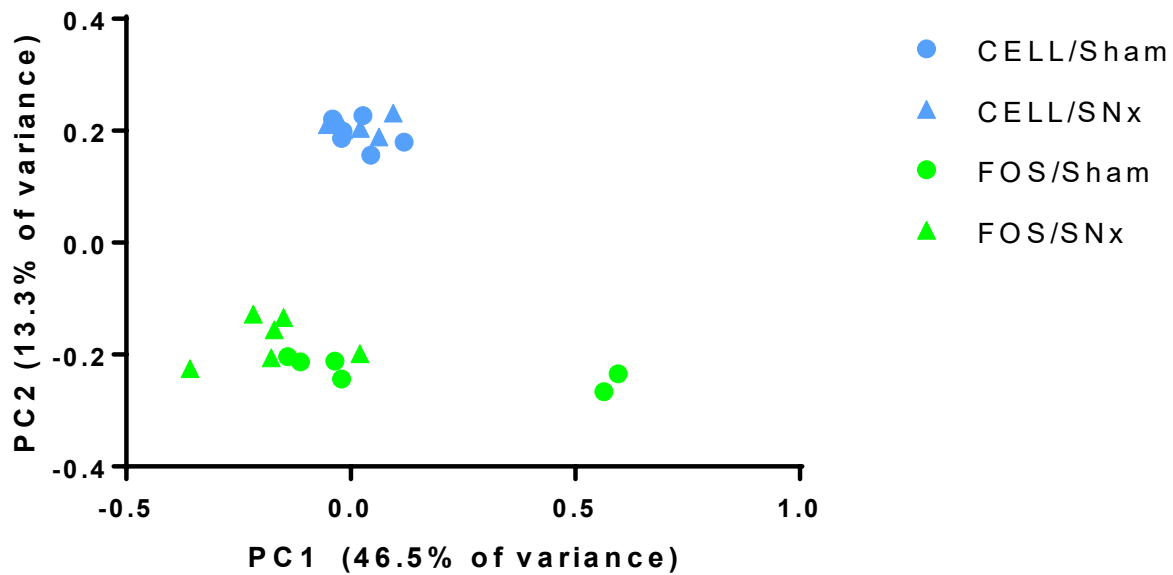
Figure 93: Principal coordinate plot of all samples based on species identity using a k-mers based approach. Each point represents the bacterial community of a particular animal subject, identified by diet (colour) and intervention (shape). The two outlying animals from the FOS group were both control animals and each had abnormally high abundances of (different but related) organisms seen only in tiny amounts in other samples; the bacterial composition of one had 52% of reads from genus *Turicibacter* and the bacterial composition of the other was 10.9% *Absiella*; although belonging to different families, these organisms share a common ancestry, both being from order *Erysipelotrichales,* class *Bacilli*. Despite these abnormalities, these samples otherwise shared similarities with other FOS-fed samples including high abundances of *Bifidobacterium*.
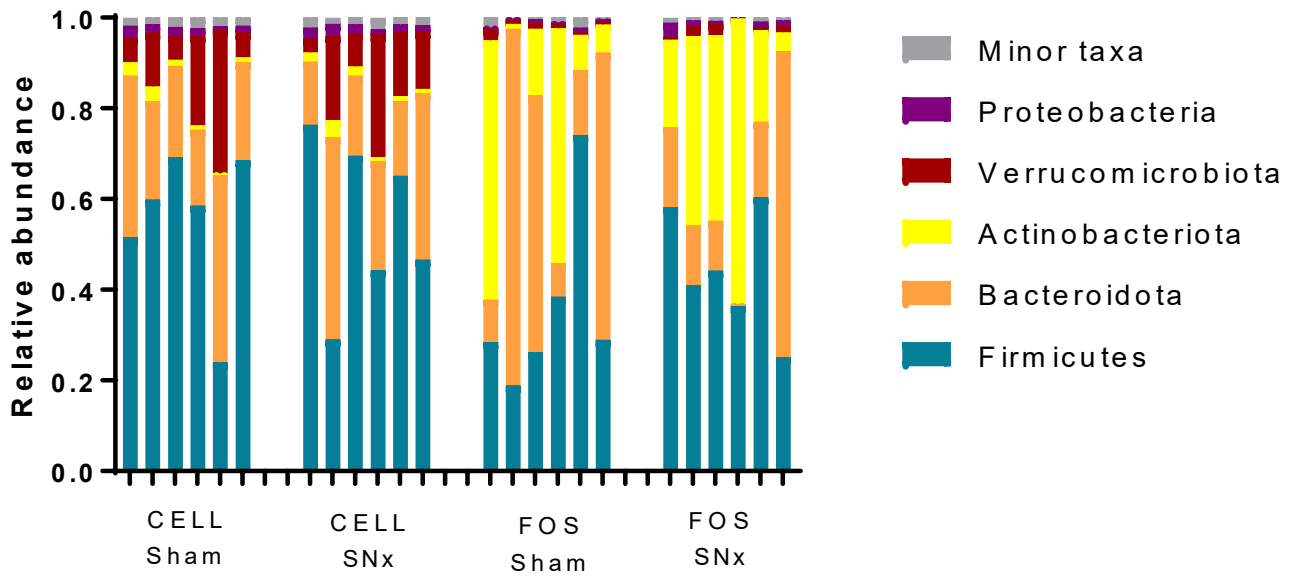
Figure 94: Composition of caecal microbiome at phylum level. Each bar represents the bacterial community of a particular animal subject, grouped by diet and intervention. The substantial proportional increases in *Actinobacteriota* in FOS-fed animals was almost entirely accounted for by an increase in genus *Bifidobacterium*.
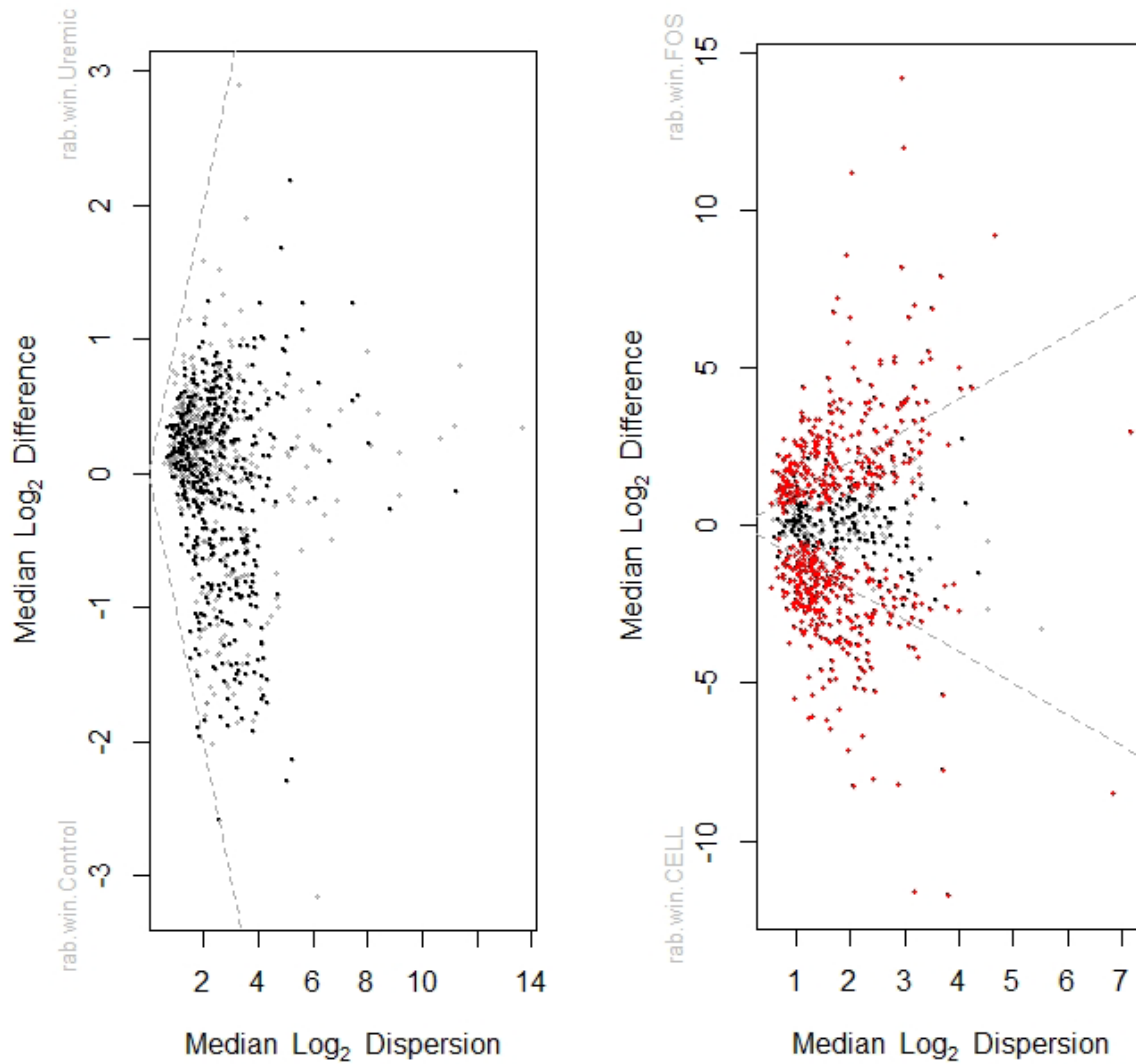
Figure 95: Dispersion plots showing the effect of left, intervention class (control vs uraemic), and right, diet (CELL vs FOS), on the differential abundance of all species present in the data set. Each point represents a different species; those in red showed significantly different proportional abundances after correction for multiple hypothesis testing and an alpha value of 0.05. Note the y-axis scales are different representing the far higher degree of variation between microbiota between samples according to diet than according to surgical intervention.

Lachnospiraceae

Proportional abundance

p=0.037   p=0.524

Control   Uremic

Marvinbryantia

Proportional abundance

p=0.17   p=0.014

Control   Uremic

UBA2882

Proportional abundance

p=0.011   p=0.062

Control   Uremic

Blautia_A

Proportional abundance

p=0.786   p=0.005

Control   Uremic

Eubacterium_F

Proportional abundance

p=0.019   p=0.013

Control   Uremic

Figure 96: Proportional abundances of family *Lachnospiraceae*, and four genera within this family. Of these genera, two (*Marvinbryantia* and *Blautia_A*) were increased in FOS-fed animals and two (unnamed genus *UBA2882* and *Eubacterium F*) were increased in CELL-fed animals. Significance is shown between FOS-fed (green) and CELL-fed (blue) animals within each intervention group (control or uraemic) using Sidak's post-test analysis following two-way ANOVA. Diet proved a highly significant determinant of abundances for each taxa shown, as documented in the text.
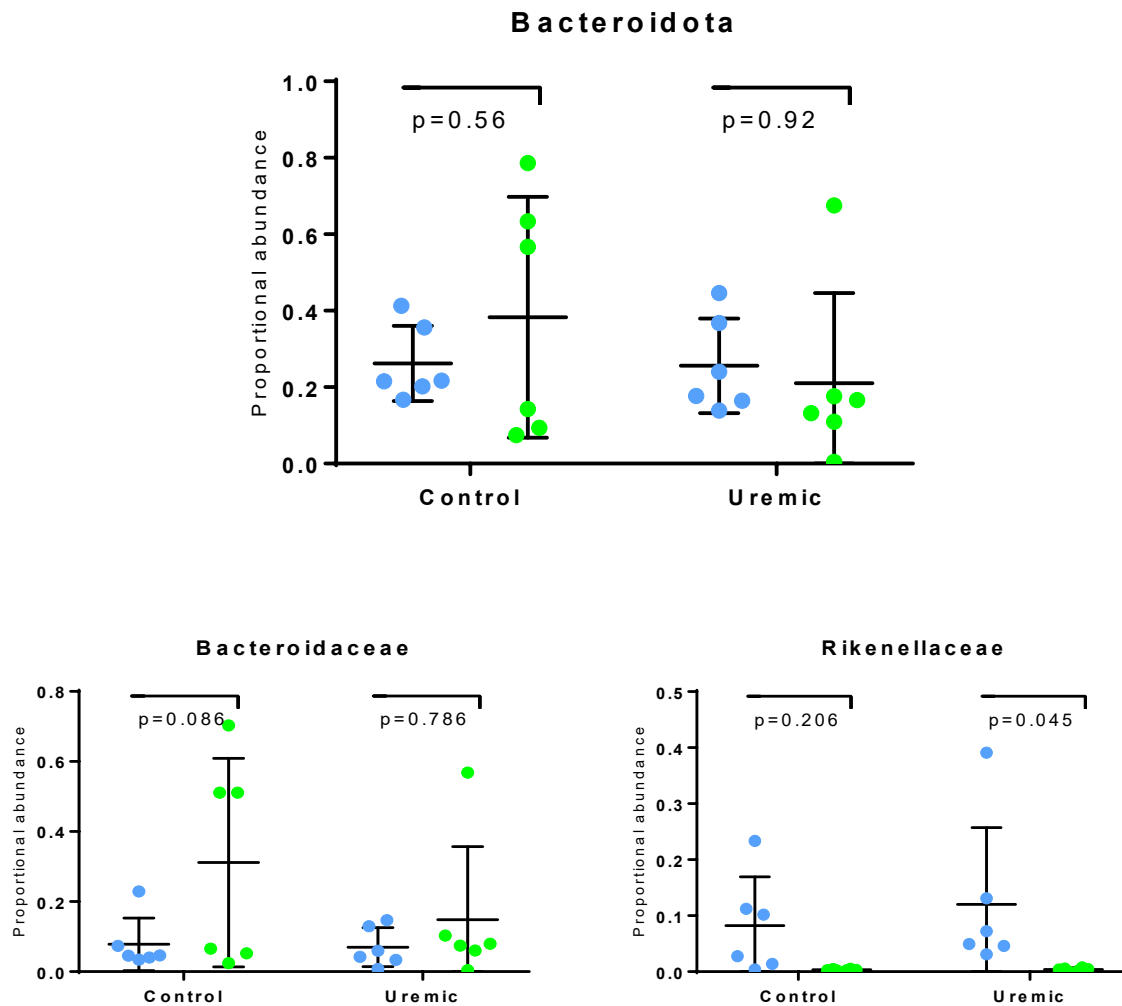
Figure 97: Proportional abundances of phylum *Bacteroidota* and of the two best-represented families within this phylum, *Bacteroidaceae* and *Rikenellaceae*. Significance is shown between FOS-fed (green) and CELL-fed (blue) animals within each intervention group (control or uraemic) using Sidak's post-test analysis following two-way ANOVA.
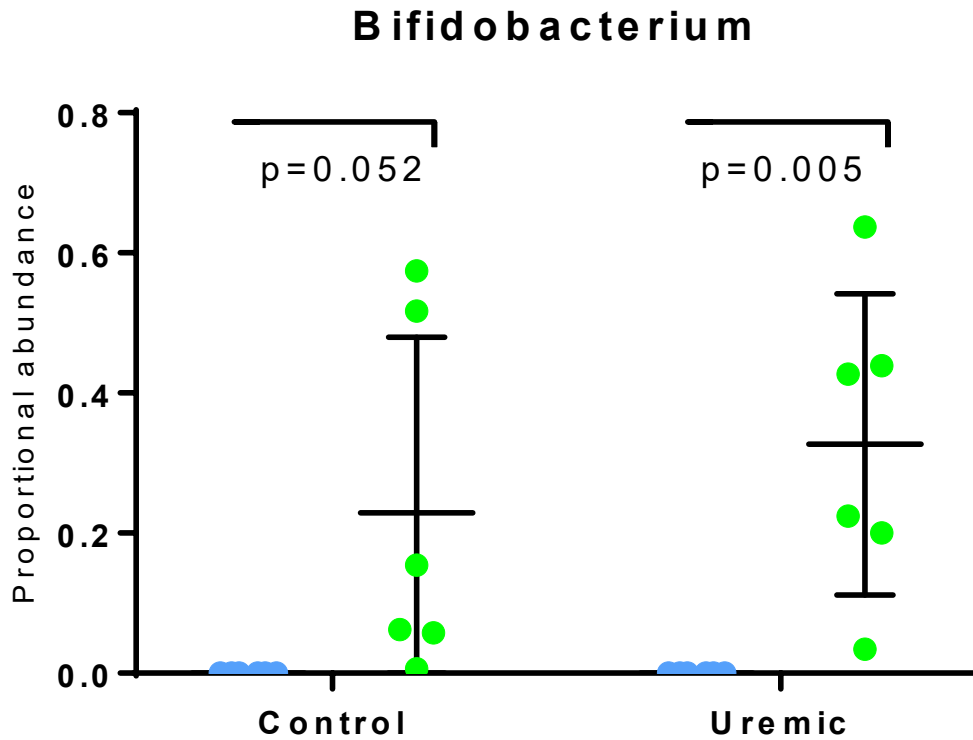
Bifidobacterium

Figure 98: Proportional abundances of the genus *Bifidobacterium*, which made up a substantial proportion of the microbiota of almost all FOS-fed animals in green but was barely present in those fed the CELL diet in blue. Significance is shown between FOS-fed and CELL-fed animals within each intervention group (control or uraemic) using Sidak's post-test analysis following two-way ANOVA.
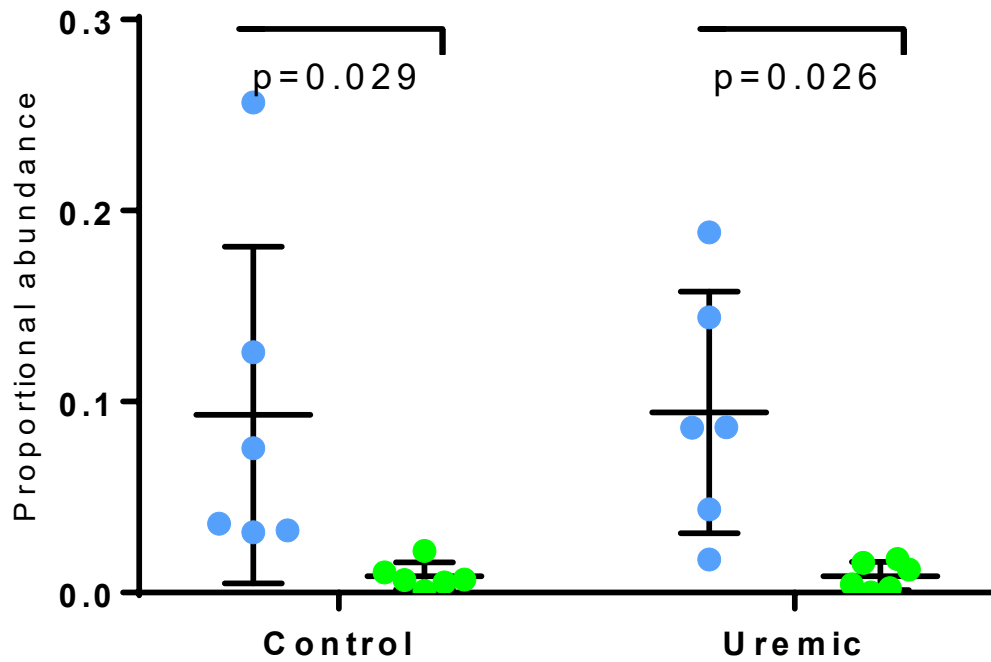
Figure 99: Proportional abundances of the phylum *Verrucomicrobiota*, which made up a substantial proportion of the microbiota of almost all CELL-fed animals but was barely present in those fed the FOS diet. Almost all of these differences were accounted for by genus *Akkermansia*. Significance is shown between FOS-fed in green and CELL-fed animals in blue within each intervention group (control or uraemic) using Sidak's post-test analysis following two-way ANOVA.
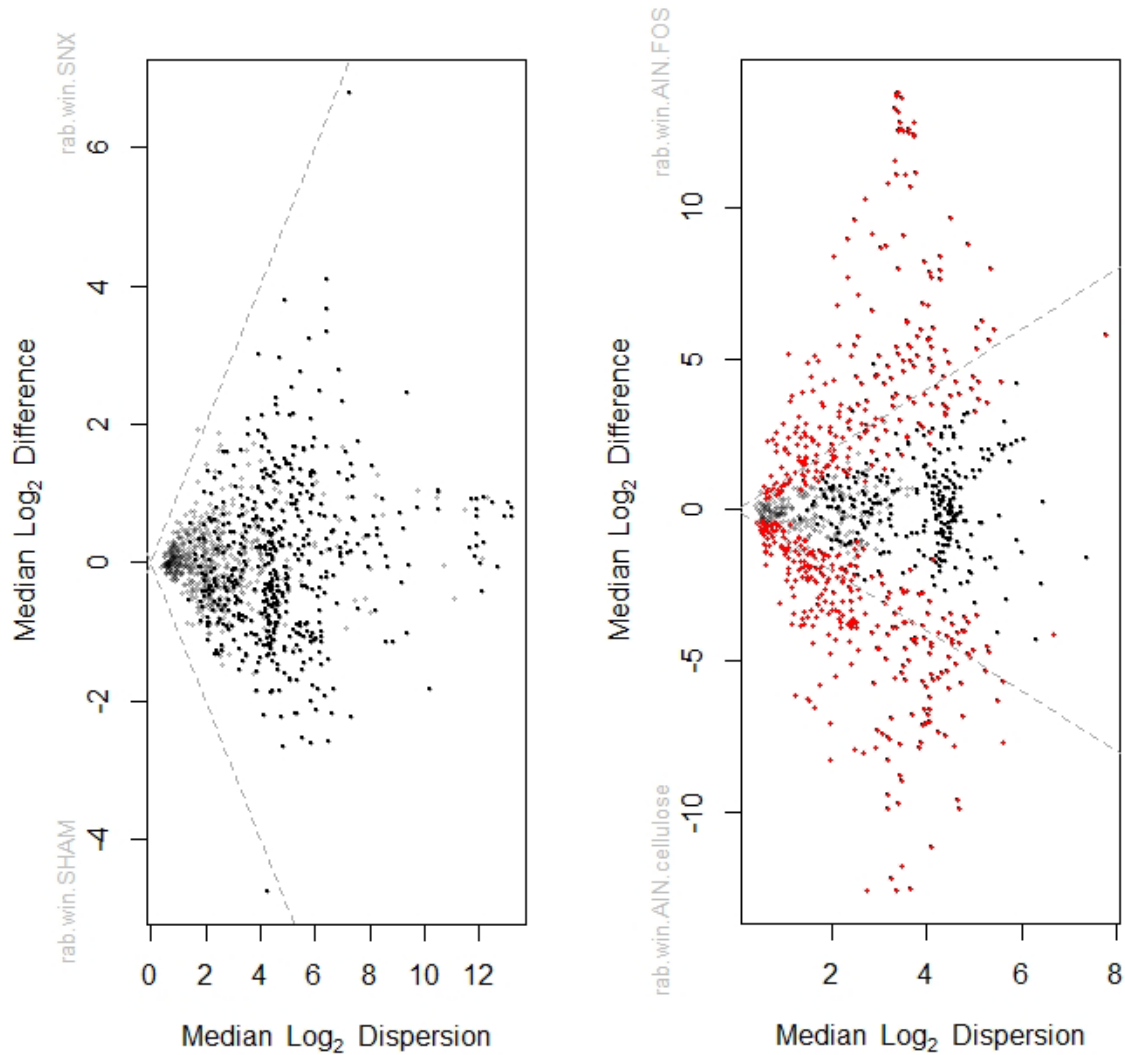
Figure 100: Dispersion plots showing the effect of, left, intervention class (control vs uraemic); and, right, diet (CELL vs FOS), on the differential abundance of all KEGG modules present in the data set. Each point represents a different KEGG module; those in red showed significantly different proportional abundances after correction for multiple hypothesis testing and an alpha value of 0.05. Note the difference in y-axis scales, confirming that diet had a far greater effect size than uraemia.
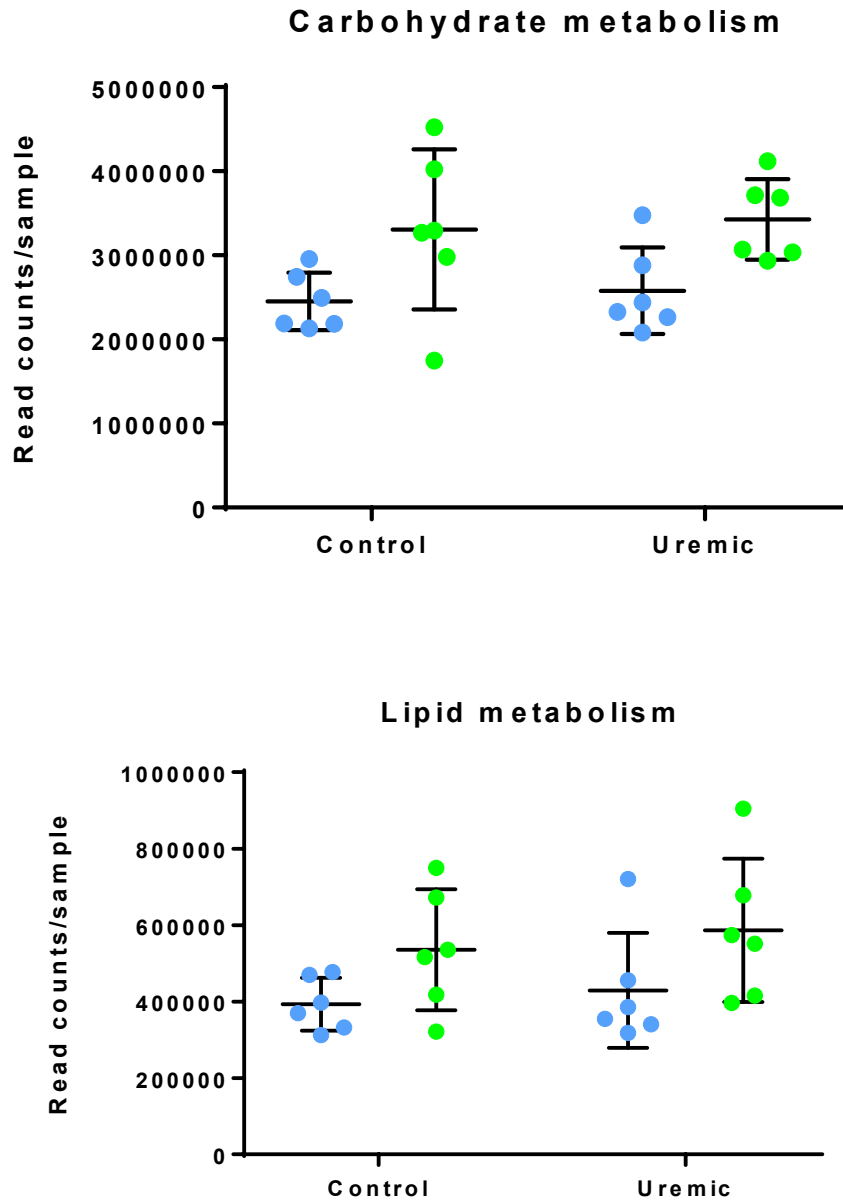
Figure 101: Read counts per sample of COG category G: carbohydrate metabolism (top) and category I: lipid metabolism (bottom). Means and standard deviations are shown. Diet significantly increased read counts in FOS-fed animals for carbohydrate metabolism (p=0.029 by two-way ANOVA) and lipid metabolism (p=0.022 by two-way ANOVA).

288

M00082: Fatty acid initiation

M00083: Fatty acid elongation
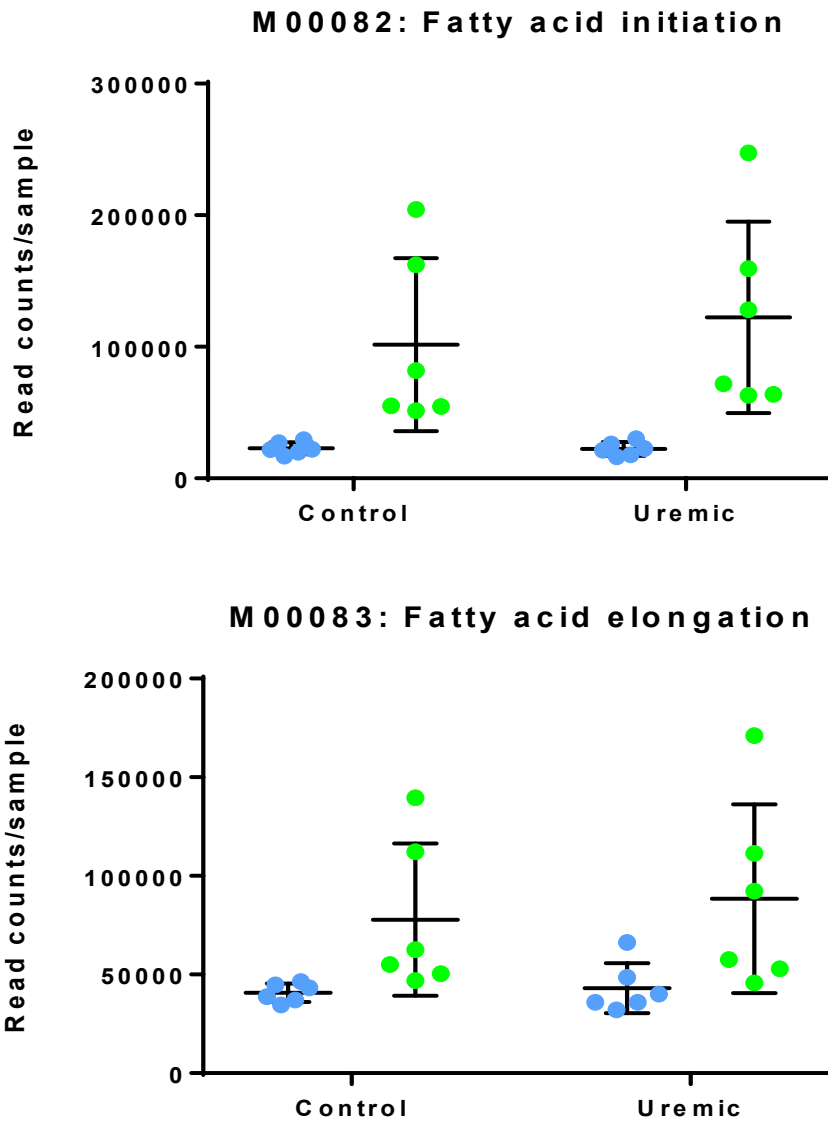
Figure 102: Count reads per sample of KEGG modules M00082 and M00083. These are the two modules involved in biosynthesis of short chain fatty acids (see **Error! Reference source not found.**, p. **Error! Bookmark not defined.**). Diet was a significant determinant of read counts for both modules (p=0.0002 for M00082 and p=0.004 for M00083) by two-way ANOVA.

Discussion

The results presented in the previous chapter (chapter 4) questioned whether uraemia exerted any reproducible effect at all on the gut microbiota. In contrast, here we demonstrate that fermentable fibre massively alters the bacterial composition of the caecal microbiome in a consistent way in both control and uraemic animals. The effect of the FOS diet dwarfs any potential effect of uraemia, and the results presented here are consistent with published research elsewhere documenting similar effects of fermentable fibre on the gut microbiota. [378, 380] It can confidently be stated that the gut microbiota in uraemic animals is not fixed, and may be modulated by administration of fermentable fibre: if these results can be reproduced in humans, the gut becomes a realistic therapeutic target to improve outcomes in patients with CKD, regardless of the baseline composition of their resident gut flora.

The results presented here also suggest that as well as modulating the gut microbiota, fermentable fibre may improve several aspects of the uraemic syndrome with potential benefit to patients. The commonest reasons why patients with advanced kidney start dialysis are typically recognised to be hyperkalaemia, acidosis, fluid overload and symptomatic uraemia (although acidosis is rarely a sole indication since it can generally be managed with oral base supplementation.) [398, 399] Fermentable fibre may potentially address each of these problems.

Disappointingly, we did not show any improvement in renal excretory function as measured by serum creatinine or creatinine clearance in these models. We had hoped that the anti-inflammatory properties of SCFAs might have reduced renal fibrosis. It is not clear whether this is simply a function of the particular models of uraemia we chose (SNx does not model

inflammatory renal disease, and the adenine model produces such severe renal inflammation that any anti-inflammatory effects of SCFA may have been overwhelmed), or whether SCFA generation does not offer a realistic prospect of reducing renal fibrosis in any setting. Use of a third model of renal injury (such as unilateral ureteric obstruction, a classic model of renal fibrosis), may be effective in answering this question.

Improvement in the uraemic syndrome

Potassium reduction: The FOS-diet lowered serum potassium by 0.6 mmol/L in uraemic rats compared to those receiving the unsupplemented AIN diet (p=0.02) and by 0.512mmol/L compared to those receiving a CELL-supplemented diet (0.026). The gut as a route for potassium excretion in individuals with CKD has been well established for many years, with older potassium exchanges resins being supplanted by newer agents in recent years with excellent evidence of efficacy. Compared to the 0.5-0.6mmol/L potassium lowering effects we have demonstrated using FOS-feed in rats, in human trials, the two most widely-used gut-acting potassium binders have been shown to achieve reductions in serum potassium of 0.75mEg/L (for patiromer [400]) and 1.1mEq/L (for zirconium, [401]).

The reason for the significant reduction in serum potassium is not immediately clear from this analysis, especially since in health almost all dietary potassium absorption occurs via passive transport in the small intestine. [402] Possible potassium-lowering mechanisms due to the effects of FOS include incorporation of luminal potassium into actively dividing bacteria, lowering

surrounding extracellular concentrations; pH dependent mechanisms in response to the massively increased intra-luminal SCFA production, or loss of potassium in the distal colon and rectum along with chloride as the colon secretes free water. [403] Another putative mechanism may be that reduced ammonium (NH_3) absorption leads to reduced urea generation in the liver; since urea generation from NH_3 generates bicarbonate from CO_2, [404, 405] reduced urea generation in the context of FOS administration may therefore contribute to higher systemic bicarbonate concentrations, metabolic alkalosis and an intracellular shift of potassium. One limitation of this work is that we did not measure serum bicarbonate concentration or pH, or faecal potassium, so the mechanism of the hypokalaemia seen in these animals remains hypothetical.

Whatever the mechanism, potassium-lowering effects of fermentable fibre may be especially important in humans with CKD. The renal diet suggested for such patients has been noted to be deficient in dietary fibre, partly because most forms of fibre come from fruit and vegetables that contain high amounts of potassium, making their consumption unsafe. [406] Dietary supplementation with synthetic or purified FOS, or other forms of fermentable fibre, may prove a safe way to increase dietary fibre with additional potassium-lowering effects.

Reduced urine output: The FOS diet led to a 24% reduction in mean urine output compared to AIN-treated animals (from 51.14ml/24h in AIN-fed to 38.8ml/24h in FOS-fed animals, p=0.032). Loss of the ability to concentrate urine is a well-recognised part of the phenotype of patients with advanced renal disease, often noticed by patients as thirst, and the need to pass urine overnight. Ultimately, patients approaching end-stage renal failure begin to develop

symptomatic fluid overload, manifested as peripheral and pulmonary oedema, as secondary hyperaldosteronism leads to retention of salt and water, despite patients passing increased volumes of dilute urine.

In these rats, despite there being no difference in renal excretory function as measured by creatinine clearance, the FOS diet was associated with reduced urinary volumes. A number of factors may have been at play, including increased gut clearance of water (as may be evidence from the increase liquid fraction of stool in these animals), reduced osmotic diuresis as a result of lower serum urea concentrations, and potentially preservation of the medullary osmotic gradient as a result of improved tubular function if it could be demonstrated there is less active inflammation in the renal interstitium as a result of the immunomodulatory functions of SCFA, although prior to histological examination of renal tissue this is impossible to say.

Either way, the demonstrated fractional increase in stool water may have a number of beneficial effects, including:

- Acting as an additional route of water excretion, allowing increased clearances of fluid volume for any given level of renal creatinine clearance,

- Reducing the energy demand on the renal tubules which is represented by the need to concentrate urine; studies in humans have shown that preservation of renal concentrating ability may predict better outcomes in CKD, [407]

- Softening stool. Constipation is a major problem affecting the majority of patients with CKD, and can be difficult to treat. [371] If fermentable fibre softens stool it may offer symptomatic benefit to patients.

Urea reduction: The FOS diet reduced serum urea by more than 50% in the severe, adenine-induced model of uraemia (from 22.2 to 10.7mmol/L, p=0.004), and by 18.2% in the milder, surgical model of uraemia (from 12.03 to 9.85mmol/L, p=0.001).

Results of total nitrogen analysis of feed, urine and stool suggest that the FOS diet does not affect dietary intake of nitrogen, but that it causes stool nitogen excretion to be significantly increased and urinary nitrogen excretion to be correspondingly reduced. Clearly, the guts of FOS-fed animals were macroscopically different from those of AIN or CELL-fed animals, with caeca and colons from FOS-fed animals being larger and containing softer contents, along with significant amounts of gas (probably methane and hydrogen from fermentation reactions), suggesting a high degree of metabolic activity. Importantly, the pH of the gut was significantly lower in FOS-fed animals, suggesting significant generation of short chain fatty acids which is crucial for the mechanism of gut elimination of nitrogen. Loss of the urea-lowering effect of the FOS-diet compared to the CELL-diet after a period of broad-spectrum antibiotic administration implies that the activity of the gut microbiota is crucial to the biological effects of FOS. It is clear that the FOS diet turns the colon into a major organ or nitrogen excretion.

Urea is produced by the urea cycle as the main end product of mammalian protein digestion, and the chief route of nitrogen excretion. [408] It accumulates in renal insufficiency as a result of impaired renal clearance (and disproportionately in the case of 'pre-renal azotaemia' as a result of increased tubular reabsorption due to low tubular flow rates).

Elevated serum urea levels are a key component of the clinical syndrome of 'uraemia', and yet the precise toxicity of urea has long been doubted, and it has instead been considered a biomarker (performing better than serum creatinine in both pre-dialysis and dialysis populations) for other toxins that accumulate in parallel with urea. [409] Historically, some animal studies have suggested that urea itself is not toxic when administered over short periods into experimental subjects, [410, 411] whilst others suggested that it may be associated over prolonged exposure with organ damage and increased mortality. [411, 412]

Healthy human subjects administered 2-3g of urea per kilogram of body weight, eight-hourly over a 24 hour period exhibited non-specific neurological toxicity at serum concentrations over around 25mmol/L. [413] Conversely, patients with established renal disease tolerated lower doses of oral urea, but exhibited a conditioning response, becoming extremely symptomatic only at concentrations >50mmol/L. [414] Accidental ingestion of urea instead of salt caused 80 people to be hospitalised in South Africa in 1961, although all patients subsequently recovered. [415]

Despite largely reassuring evidence of the safety of modestly increased urea concentrations in the short or medium term, concern has emerged that chronically elevated urea concentrations may be responsible for other 'degenerative' aspects of the CKD phenotype. [416-418] In vitro evidence has suggested that high urea concentrations may cause vascular inflammation and

calcification, [419, 420] adipocyte dysfunction driven by reactive-oxygen species, contributing to insulin resistance, [421, 422] leaky gut tight junctions and systemic inflammation [53] and protein carbamylation leading to anaemia, atherosclerosis, inflammation and a prematurely aged phenotype. [423-425]

Historically, low protein diets (<0.6g/kg/d) have been advocated as a way of staving off symptoms of uraemia and delaying the initiation of renal replacement therapy. [426, 427] However, because of concerns that these may compromise the nutritional status of patients (who may already be avoiding high-potassium, high-sodium and high-phosphate foods), recent guidance has steered away from their routine use in CKD, despite some evidence that when supervised closely they can be safe and efficacious. [428, 429]

Although the evidence for the toxicity of urea, as discreet from other 'uraemic toxins' for which it may act as a biomarker, is incomplete, there is nevertheless accumulating evidence both of its chronic toxicity and of the benefits of lowering dietary protein intake in prolonging the time before renal replacement therapy is required in the pre-dialysis context. Therefore, use of fermentable dietary fibre potentially offers benefit in this regard by reducing serum urea without requiring dietary protein restriction.

Modulation of the gut microbiome

The metagenomic whole-genome sequencing data was consistent with a dramatic transformation of the composition and function of the gut microbiota in FOS-fed animals.

Microbial communities in the gut display a crucial phenomenon that has been explored in the past decade and termed 'cross-feeding'. [430] According to this phenomenon, species possessing different metabolic pathways can thrive in co-culture by exchanging metabolites; this behaviour when investigated between *Bacteroides* and *Bifidobacteria* subspecies was so reliable that it could be predicted using computer models based on monoculture and co-culture data. [431]

A classic example of cross-feeding is seen in how bacterial communities process complex carbohydrates such as FOS. When communities are exposed to this type of fibre, cross-feeding may occur between species described as primary fermenters, which possess hydrolases capable of digesting long oligomers into simple sugars and subsequently metabolising them into simple fatty acids such as formate, acetate and propionate; and secondary fermenters capable of using acetate to produce butyrate, Figure 65, p. 249.

We demonstrated expansion of three key taxa involved in the primary degradation of dietary fibre: genus *Bifidobacteria* (which has been shown to reproducibly increase in abundance in response to dietary supplementation by fermentable fibre in various systematic reviews, [436, 437]), genus *Bacteroides*, and the subspecies *Ruminoclostridium Bromii_B*.

Genus *Bifidobacterium* was by far the most abundant taxon in FOS-fed animals. It has long been regarded as a health-associated genus, and strains have been used in a number of trials as a probiotic in adult and paediatric populations. [169, 438, 439] They are among the first organisms to colonise the gut of newborn infants, because of their unique abilities to degrade the human breast milk oligosaccharides. [440] These properties chiefly centre on a unique metabolic pathway, termed the 'bifid shunt' (or the fructose-6-phosphate phosphoketolase pathway), which

allows *Bifidobacteria* both to generate ATP from a range of 6-carbon sugars including fructose and glucose, but also to produce short-chain fatty acids, chiefly acetate, Figure 120. [441, 442] At the level of KEGG modules, we demonstrated significant increases in the bifid shunt and in other carbohydrate metabolism pathways in FOS-fed animals which is consistent with the dramatic increase in *Bifidobacterium* abundance, and a shift towards a more saccharolytic microbial phenotype (see additional data in appendix 6, p. 411). Acetate production both alters the gut luminal pH, offering a barrier to infection by pathogenic organisms, [443] but also provides a substrate for secondary fermenters. [444]

Most secondary degraders are from the family *Lachnospiraceae*, within the phylum *Firmicutes*. This is a highly abundant family (accounting for just over 30% of reads per sample on average), and one in which its constituent genera display highly variable metabolic potential. [445, 446] Despite the CELL-fed animals having higher proportional abundances of *Lachnospiraceae* overall, this was chiefly driven by unnamed genera including *UBA2882* and *CAG-95* which have relatively poorly described metabolic activity, and overall genes involved in carbohydrate metabolism and SCFA synthesis were decreased in CELL-fed animals.

The dramatic reduction in *Akkermansia municiphilia* from the microbiota of FOS-fed animals was unexpected. These are widely regarded as health-associated bacteria, [432, 433] and are known producers of short chain fatty acids. [434, 435] *A. muciniphilia* is known to be closely associated with the mucous layer in the colon, and to generate SCFA via degradation of mucins, rather than primarily from dietary oligosaccharides. Therefore it is possible that its relative

absence in FOS-fed animals may relate to changes in the mucin layer in these animals, relative to those being fed the CELL-diet; or to the organism simply being outcompeted by *Bifidobacteria*.

The advantage of having undertaken WGS metagenomics is that regardless of changes in individual species abundances, we are able to say with confidence that genes involved in the initiation (M00082), elongation (M00083) and acyl-CoA synthesis of fatty acids (M00086, which can also be used in reverse to degrade SCFAs as an energy source), were increased in the gut microbiota of animals consuming the FOS diet. A number of organisms well described as SCFA producers were increased in these animals (eg *Marvinbryantia*, [449, 450] *Dorea* [451] and *Blautia*; [293, 452]); regardless of which species are involved, it is clear that a genotype shift has occurred in the gut population of these animals in keeping with increased generation of all three main SCFAs. Further metabolomic work is needed to confirm that this increase in genetic potential does indeed lead to increase faecal, serum and urine SCFA concentrations.

Conclusion

The results presented in this chapter demonstrate that it is possible to modulate the gut microbiome to achieve desired therapeutic effects in the host organism.

We have additionally shown a prebiotic preparation of fermentable dietary fibre to:

- increase faecal elimination of nitrogen, associated with significant lowering of serum urea concentrations,

- reduce serum potassium concentrations,

- reduce polyuria, possibly by increasing the fluid fraction of stool.

Although not yet quantified, it is likely these effects are mediated through generation of large amounts of short chain fatty acids (and this is suggested by a large decrease in caecal pH). In addition to the effects described above, SCFA have a range of other well-described benefits to health.

The results of further work is awaited, including:

- measuring faecal, serum and urine SCFA levels,

- establishing whether the FOS diet reduces the degree of fibrosis or active inflammation in the kidneys of adenine-treated animals,

- using a different model of renal impairment (unilateral ureteric obstruction) to establish whether the FOS-diet reduces fibrosis in this (shorter duration) model.

It is unclear how these benefits may translate into a clinical context, but similar prebiotic preparations have demonstrated good tolerability and safety profiles in trials.

The way is clear to attempt clinical trials to establish whether fermentable fibre may benefit patients, including:

- Assessing whether fermentable fibre may delay the initiation of renal replacement therapy in the pre-dialysis population,

- Assessing whether fermentable fibre may slow or even prevent the decline in renal function at earlier stages of CKD,

- Assessing the potential for fermentable fibre to produce beneficial effects on other aspects of the uraemic syndrome in individuals living with CKD – such as by improving indices of anaemia or CKD mineral and bone disease,

- Assessing whether the shifts in gut microbiota seen in this experiment associate with reduced generation of well-describe uraemic toxins (for example, indoxyl sulphate, p-cresyl sulphate or trimethyl oxide),

- Assessing whether fermentable fibre may offer improved quality or length of life in patients with advanced CKD who opt to receive supportive care rather than dialysis,

- Assessing whether fermentable fibre may allow patients receiving maintenance haemodialysis to reduce the amount of treatment they receive,

- Assessing whether fermentable fibre may improve outcomes for renal transplant recipients – especially given the potential for SCFAs to reduce inflammation and promote immune tolerance. There is already some experimental work suggesting that both fibre and direct SCFA supplementation may reduce intestinal dysbiosis after kidney transplantation and induce donor-specific tolerance in mice.[453]

Summary

- **Administration of fermentable fibre, in the form of FOS-supplemented feed, can transcend the minimal effects of uraemia to produce substantial effects on the gut microbiota of both control and uraemic animals.**

- **A fermentable fibre-enriched diet increased SCFA-producing organisms, and increased the abundance of bacterial metabolic pathways involved in carbohydrate metabolism, and in the initiation and elongation of SCFAs.**

- **A fermentable fibre-enriched diet increased the volume of caecal contents and decreased its pH, transforming the gut into an organ of nitrogen excretion.**

- **A fermentable fibre-enriched diet led to improvements in aspects of the uraemic syndrome including by reducing serum urea, reducing polyuria and reducing serum potassium.**

Conclusion: Fermentable fibre produces substantial and similar changes in the gut microbiome in both control and uraemic animals. These results suggest that fermentable fibre supplements may offer significant benefits to human subjects with CKD if this research can be translated into clinical practice.

Chapter 6

Conclusions and plans for further work

The gut microbiota of a 90kg adult human male have been estimated to weigh approximately 900g and to constitute roughly 1% of a human's biomass. [454, 455] This compares to 2% for the liver, 1.8% for the brain, 0.35% for both kidneys and 0.18% for the spleen. [456]

By comparison, the hundred trillion bacteria believed to colonise the guts of each adult contain a metagenome roughly one hundred times the size of the host genome, [457] with the total genetic diversity of bacteria discovered across multiple human hosts dwarfing human genetic diversity one hundred and fifty times. [458]

As such, the gut microbiome deserves to be treated as of equivalent importance to the host organism as other major metabolically-active organs. Unlike host organs, though, its genetic

composition can be significantly altered by environmental factors, disease and therapeutic strategies; and it can exert negative or beneficial effects on the host as a result.

This thesis has presented a large volume of work exploring the relationship between bacterial communities in the mouth and gut and their host organisms, in the context of experimental uraemia. The main findings are summarised below.

Periodontal disease and the oral microbiome

Both rats and mice with experimental uraemia are shown to have an increased distance between the alveolar bone ridge and the cemento-enamel junction. There is histological evidence of a failure of bone formation at the growing edge of alveolar bone, although with limited evidence of frank periodontal inflammation. The oral microbiota of uraemic animals is altered, with a reduction in counts of cultivatable bacteria, significant reductions in *Streptococcus* and *Rothia* species and an increase in Gram-negative anaerobic species. *In vitro* evidence suggests that increasing salivary urea may exert a selective pressure on bacterial populations favouring the growth of organisms associated with periodontal disease. Evidence from co-caging and oral microbial transfer experiments suggests that changes in the oral microbiome may transmit or modify the periodontal phenotype in recipient host organisms.

Conclusion: uraemia may induce oral dysbiosis that subsequently affects bone formation at the alveolar bone ridge, causing periodontal disease.

Uraemia, the gut microbiome and the constraints of experimental techniques

A substantial heterogeneity exists between the gut microbiotas of animals in different experimental batches that eclipses any observable effect of uraemia. Untargeted ^{1}H-NMR spectroscopy further revealed that batch effects outweigh the effects of uraemia even in the urinary metabolome. The findings were validated by performing a meta-analysis of all available datasets studying the effect of experimental uraemia on the rodent gut microbiome in online repositories, where again batch variation dramatically exceeds that of uraemia. Broad trends were elicited which were present in some or all datasets, and that suggested certain taxa may be more or less competitive in the context of the uraemic gut, despite wide variations between groups.

Conclusions:

1) Contrary to what has been widely asserted, there is limited evidence that uraemia disrupts the composition of the gut microbiota. Gut dysbiosis attributable directly to uraemia probably does not play a major role in the aetiology of CKD. It is possible that other factors in humans with CKD may drive intestinal dysbiosis, such as dietary restrictions or use of antimicrobial or gut-acting medications.

2) Evidence of a high degree of variability between the gut microbiomes of animals from different experimental batches poses major challenges to all forms of animal research, and may underlie the difficulties experienced in reproducing experimental research in some fields.

Fermentable fibre and the ability to manipulate the gut microbiome to achieve therapeutic effects

Results in this thesis demonstrate that a diet high in fermentable fibre not only causes dramatic changes in the composition and metabolic potential gut microbiome, but also in the physical appearance and chemical environment of the gut itself. Supplementation with fermentable fibre leads to reductions in serum urea, serum potassium and polyuria, leading to improvements in the disease phenotype of the host organism itself.

Conclusion: these results suggest that fermentable fibre supplements may offer significant benefits to human subjects with CKD if this research can be translated into clinical practice.

Opportunities for further research arising from the findings in this thesis would include:

- *Establishing the role for dental screening and treatment in addressing periodontal disease in patients with CKD.* It may be that they benefit from standard non-surgical periodontal treatment, which has demonstrated efficacy in PD in the general population; it may be that such treatment might improve aspects of systemic disease such as chronic inflammation, cardiovascular disease and malnutrition. Alternatively, it may be that there are ways of addressing particular features of uraemic periodontal disease that are less

relevant in periodontal disease in the general population: for instance, dysbiosis caused by high salivary urea concentrations.

- *Establishing ways of addressing the problems of batch variation in animal research.* Because the implications of batch variation between the microbiomes of experimental animals are potentially so broad, affecting biological processes not directly associated with the gut microbiota, achieving standards to ensure that this variability is minimised hold the promise of improving the reproducibility of research across the board. Minimum standards should be developed for documenting the origins, husbandry, diet and caging or experimental animals; researchers should be encouraged to perform studies in several batches of animals and to document whether effects are seen uniformly between groups. In specific microbiome studies, using animals as their own controls, comparing microbiota before and after a given intervention may prove more effective than the traditional approach of comparing the microbiotas of different control and intervention animals.

- *Developing the use of meta-analysis in basic sciences research.* The use of online repositories so that results can easily be compared between similar experiments conducting in diverse settings – such as the meta-analysis included in this thesis – allow more confident conclusions to be reached without a substantial increase in animal use by all groups.

- *Completing experimental work around the effect of fermentable fibre in experimental uraemia, including assessing the effects on SCFA generation and renal fibrosis.* In particular, confirming that fermentable fibre-enriched diets do increase SCFA concentrations, and establishing whether this affects histological evidence of kidney fibrosis or inflammation are obvious next steps.

- *Performing clinical trials to assess the efficacy of fermentable fibre in ameliorating the uraemic phenotype in patients with CKD.* Fermentable fibre is not a magic bullet, and CKD is likely for most to remain a progressive illness requiring renal replacement therapy for most patients. But if this point can be delayed, if the effectiveness of renal replacement therapy can be supplemented, if the systemic effects of renal failure can be minimised, then dietary fibre has the potential to be of significant benefit to patients.

Rather than regard the gut as a toxic reservoir of potential pathogens, the results presented in this thesis show the potential for bacterial activity to be utilised to provide significant benefit to the host. The challenge now is to build on what has been achieved here and try to deliver tangible benefits for patients.

References

1.   Mishima, E., et al., *Evaluation of the impact of gut microbiota on uremic solute accumulation by a CE-TOFMS-based metabolomics approach.* Kidney Int, 2017. **92**(3): p. 634-645.

2.   Jang, H.R., et al., *Early exposure to germs modifies kidney damage and inflammation after experimental ischemia-reperfusion injury.* American journal of physiology. Renal physiology, 2009. **297**(5): p. F1457-F1465.

3.   Einheber, A. and D. Carter, *The role of the microbial flora in uremia. I. Survival times of germfree, limited-flora, and conventionalized rats after bilateral nephrectomy and fasting.* J Exp Med, 1966. **123**(2): p. 239-50.

4.   Emal, D., et al., *Depletion of Gut Microbiota Protects against Renal Ischemia-Reperfusion Injury.* J Am Soc Nephrol, 2017. **28**(5): p. 1450-1461.

5.   Aronov, P.A., et al., *Colonic contribution to uremic solutes.* J Am Soc Nephrol, 2011. **22**(9): p. 1769-76.

6.   Devlin, A.S., et al., *Modulation of a Circulating Uremic Solute via Rational Genetic Manipulation of the Gut Microbiota.* Cell Host Microbe, 2016. **20**(6): p. 709-715.

7.   Wong, J., et al., *Expansion of urease- and uricase-containing, indole- and p-cresol-forming and contraction of short-chain fatty acid-producing intestinal microbiota in ESRD.* Am J Nephrol, 2014. **39**(3): p. 230-237.

8.   Wang, X., et al., *Aberrant gut microbiota alters host metabolome and impacts renal failure in humans and rodents.* Gut, 2020: p. gutjnl-2019-319766.

9.   Porter, R., *The greatest benefit to mankind : a medical history of humanity from antiquity to the present.* 1999, London: FontanaPress.

10.   Sonnenborn, U., *100 years of E. coli strain Nissle 1917.* 2017, OUPBlog: Academic Insights for the Thinking World.

11.   Turnbaugh, P.J., et al., *An obesity-associated gut microbiome with increased capacity for energy harvest.* Nature, 2006. **444**(7122): p. 1027-31.

12.   Prescott, S.L., *History of medicine: Origin of the term microbiome and why it matters.* Human Microbiome Journal, 2017. **4**: p. 24-25.

13.   Arumugam, M., et al., *Enterotypes of the human gut microbiome.* Nature, 2011. **473**(7346): p. 174-80.

14.   *Structure, function and diversity of the healthy human microbiome.* Nature, 2012. **486**(7402): p. 207-14.

15.   Kadooka, Y., et al., *Effect of Lactobacillus gasseri SBT2055 in fermented milk on abdominal adiposity in adults in a randomised controlled trial.* Br J Nutr, 2013. **110**(9): p. 1696-703.

16.   Kostic, A.D., et al., *Fusobacterium nucleatum potentiates intestinal tumorigenesis and modulates the tumor-immune microenvironment.* Cell Host Microbe, 2013. **14**(2): p. 207-15.

17.   Smith, M.I., et al., *Gut microbiomes of Malawian twin pairs discordant for kwashiorkor.* Science, 2013. **339**(6119): p. 548-54.

18.   Juul, F.E., et al., *Fecal Microbiota Transplantation for Primary Clostridium difficile Infection.* N Engl J Med, 2018. **378**(26): p. 2535-2536.

19.   Sender, R., S. Fuchs, and R. Milo, *Are We Really Vastly Outnumbered? Revisiting the Ratio of Bacterial to Host Cells in Humans.* Cell, 2016. **164**(3): p. 337-40.

20.   Luckey, T.D., *Introduction to intestinal microecology.* Am J Clin Nutr, 1972. **25**(12): p. 1292-4.

21.   Sender, R., S. Fuchs, and R. Milo, *Revised Estimates for the Number of Human and Bacteria Cells in the Body.* PLoS Biol, 2016. **14**(8): p. e1002533.

22.   Sedghi, L., et al., *The oral microbiome: Role of key organisms and complex networks in oral health and disease.* Periodontology 2000, 2021. **87**(1): p. 107-131.

23.   Harris, M.A., C.A. Reddy, and G.R. Carter, *Anaerobic bacteria from the large intestine of mice.* Appl Environ Microbiol, 1976. **31**(6): p. 907-12.

24.   Claesson, M.J., et al., *Comparative analysis of pyrosequencing and a phylogenetic microarray for exploring microbial community structures in the human distal intestine.* PLoS One, 2009. **4**(8): p. e6669.

25.   Hisada, T., K. Endoh, and K. Kuriki, *Inter- and intra-individual variations in seasonal and daily stabilities of the human gut microbiota in Japanese.* Arch Microbiol, 2015. **197**(7): p. 919-34.

26.   Donaldson, G.P., S.M. Lee, and S.K. Mazmanian, *Gut biogeography of the bacterial microbiota.* Nat Rev Microbiol, 2016. **14**(1): p. 20-32.

27.   Kim, C.H., *Immune regulation by microbiome metabolites.* Immunology, 2018. **154**(2): p. 220-229.

28.   Francino, M.P., *Early development of the gut microbiota and immune health.* Pathogens, 2014. **3**(3): p. 769-90.

29.   Krajmalnik-Brown, R., et al., *Effects of gut microbes on nutrient absorption and energy regulation.* Nutr Clin Pract, 2012. **27**(2): p. 201-14.

30.   Riedl, R.A., et al., *The Gut Microbiome, Energy Homeostasis, and Implications for Hypertension.* Curr Hypertens Rep, 2017. **19**(4): p. 27.

31.   Biesalski, H.K., *Nutrition meets the microbiome: micronutrients and the microbiota.* Ann N Y Acad Sci, 2016. **1372**(1): p. 53-64.

32.   Zhang, N. and Q.S. He, *Commensal Microbiome Promotes Resistance to Local and Systemic Infections.* Chin Med J (Engl), 2015. **128**(16): p. 2250-5.

33.   *Global, regional, and national burden of chronic kidney disease, 1990-2017: a systematic analysis for the Global Burden of Disease Study 2017.* Lancet, 2020. **395**(10225): p. 709-733.

34.   Liyanage, T., et al., *Worldwide access to treatment for end-stage kidney disease: a systematic review.* Lancet, 2015. **385**(9981): p. 1975-82.

35.   Coresh, J., *Update on the Burden of CKD.* Journal of the American Society of Nephrology, 2017. **28**(4): p. 1020.

36.   Klarenbach, S.W., et al., *Economic evaluation of dialysis therapies.* Nat Rev Nephrol, 2014. **10**(11): p. 644-52.

37. Laupacis, A., et al., *A study of the quality of life and cost-utility of renal transplantation.* Kidney Int, 1996. **50**(1): p. 235-42.

38. Levin, A., et al., *KDIGO 2012 clinical practice guideline for the evaluation and management of chronic kidney disease.*, K.d.I.g.o.K.C.w. group., Editor. 2012: Kidney International Supplements. p. 1-150.

39. Meisinger, C., A. Döring, and H. Löwel, *Chronic kidney disease and risk of incident myocardial infarction and all-cause and cardiovascular disease mortality in middle-aged men and women from the general population.* Eur Heart J, 2006. **27**(10): p. 1245-50.

40. Thompson, S., et al., *Cause of Death in Patients with Reduced Kidney Function.* Journal of the American Society of Nephrology, 2015. **26**(10): p. 2504.

41. Wolfe, R.A., et al., *Comparison of mortality in all patients on dialysis, patients on dialysis awaiting transplantation, and recipients of a first cadaveric transplant.* N Engl J Med, 1999. **341**(23): p. 1725-30.

42. Tonelli, M., et al., *Systematic review: kidney transplantation compared with dialysis in clinically relevant outcomes.* Am J Transplant, 2011. **11**(10): p. 2093-109.

43. Levey, A.S. and G. Eknoyan, *Cardiovascular disease in chronic renal disease.* Nephrol Dial Transplant, 1999. **14**(4): p. 828-33.

44. Townsend, R.R., *Arterial Stiffness in CKD: A Review.* Am J Kidney Dis, 2019. **73**(2): p. 240-247.

45. Hassan, N.A., et al., *The risk for medial arterial calcification in CKD.* Clin J Am Soc Nephrol, 2012. **7**(2): p. 275-9.

46. Moran, A., et al., *Left ventricular hypertrophy in mild and moderate reduction in kidney function determined using cardiac magnetic resonance imaging and cystatin C: the multi-ethnic study of atherosclerosis (MESA).* Am J Kidney Dis, 2008. **52**(5): p. 839-48.

47. van der Zee, S., et al., *Cardiovascular risk factors in patients with chronic kidney disease.* Nat Rev Cardiol, 2009. **6**(9): p. 580-9.

48. Hung, S.C., et al., *Volume overload and adverse outcomes in chronic kidney disease: clinical observational and animal studies.* J Am Heart Assoc, 2015. **4**(5).

49. Heine, G.H., M. Nangaku, and D. Fliser, *Calcium and phosphate impact cardiovascular risk.* Eur Heart J, 2013. **34**(15): p. 1112-21.

50. Fitts, M.K., et al., *Hemodynamic Shear Stress and Endothelial Dysfunction in Hemodialysis Access.* Open Urol Nephrol J, 2014. **7**(Suppl 1 M5): p. 33-44.

51. Linden, E., et al., *Endothelial dysfunction in patients with chronic kidney disease results from advanced glycation end products (AGE)-mediated inhibition of endothelial nitric oxide synthase through RAGE activation.* Clin J Am Soc Nephrol, 2008. **3**(3): p. 691-8.

52. Evenepoel, P., et al., *Uremic toxins originating from colonic microbial metabolism.* Kidney International, 2009. **76**: p. S12-S19.

53. Vaziri, N.D., et al., *Disintegration of colonic epithelial tight junction in uremia: a likely cause of CKD-associated inflammation.* Nephrol Dial Transplant, 2012. **27**(7): p. 2686-93.

54. Meijers, B., et al., *Intestinal Barrier Function in Chronic Kidney Disease.* Toxins (Basel), 2018. **10**(7).

55. Tan, J., et al., *The role of short-chain fatty acids in health and disease.* Adv Immunol, 2014. **121**: p. 91-119.

56.   Garza, D.R., et al., *Towards predicting the environmental metabolome from metagenomics with a mechanistic model.* Nature Microbiology, 2018. **3**(4): p. 456-460.

57.   Streicher, M.H., *Experimental Uremia. Uremic Enteritis.* Proceedings of the Society for Experimental Biology and Medicine, 1928. **26**(2): p. 171-172.

58.   Sloan, H., *Production of experimental uremia by sodium tetrathionate.* Proc Soc Exp Biol Med, 1951. **76**(2): p. 344-6.

59.   Christensen, S. and P.D. Ottosen, *Lithium-induced uremia in rats - a new model of chronic renal failure.* Pflugers Arch, 1983. **399**(3): p. 208-12.

60.   Mandal, A., et al., *In vivo assessment of bacteriotherapy on acetaminophen-induced uremic rats.* J Nephrol, 2013. **26**(1): p. 228-36.

61.   Diwan, V., et al., *Adenine-induced chronic kidney and cardiovascular damage in rats.* J Pharmacol Toxicol Methods, 2013. **68**(2): p. 197-207.

62.   Yokozawa, T., et al., *Animal model of adenine-induced chronic renal failure in rats.* Nephron, 1986. **44**(3): p. 230-4.

63.   Yokozawa, T., H. Oura, and F. Koizumi, *2,8-Dihydroxyadenine urolithiasis induced by dietary adenine in rats.* Nihon Jinzo Gakkai Shi, 1985. **27**(3): p. 371-8.

64.   Verma, R., et al., *Dihydroxyadenine crystal-induced nephropathy presenting with rapidly progressive renal failure.* Kidney Res Clin Pract, 2018. **37**(3): p. 287-291.

65.   Rahman, A., et al., *A novel approach to adenine-induced chronic kidney disease associated anemia in rodents.* PLoS One, 2018. **13**(2): p. e0192531.

66.   Claramunt, D., et al., *Chronic kidney disease induced by adenine: a suitable model of growth retardation in uremia.* Am J Physiol Renal Physiol, 2015. **309**(1): p. F57-62.

67.   Ali, B.H., et al., *New model for adenine-induced chronic renal failure in mice, and the effect of gum acacia treatment thereon: comparison with rats.* J Pharmacol Toxicol Methods, 2013. **68**(3): p. 384-93.

68.   Ormrod, D. and T. Miller, *Experimental uremia. Description of a model producing varying degrees of stable uremia.* Nephron, 1980. **26**(5): p. 249-54.

69.   Wang, X., et al., *A Mouse 5/6th Nephrectomy Model That Induces Experimental Uremic Cardiomyopathy.* J Vis Exp, 2017(129).

70.   Chow, K.-M., Z.-C. Liu, and T.M.-S. Chang.

71.   Mishima, E., et al., *Alteration of the Intestinal Environment by Lubiprostone Is Associated with Amelioration of Adenine-Induced CKD.* Journal of the American Society of Nephrology, 2015. **26**(8): p. 1787-1794.

72.   Okada, H., et al., *Reversibility of adenine-induced renal failure in rats.* Clinical and Experimental Nephrology, 1999. **3**(2): p. 82-88.

73.   Morrison, A.B., *Experimentally induced chronic renal insufficiency in the rat.* Lab Invest, 1962. **11**: p. 321-32.

74.   Chow, K.-M., Z.-C. Liu, and T.M.-S. Chang, *Animal Remnant Kidney Model of Chronic Renal Failure Revisited.* Hong Kong Journal of Nephrology, 2003. **5**(2): p. 57-64.

75.   Chesser, A.M., et al., *Myocardial bioenergetic abnormalities in experimental uremia.* Int J Nephrol Renovasc Dis, 2016. **9**: p. 129-37.

76.   Byrne, C.J., et al., *Ischemic conditioning protects the uremic heart in a rodent model of myocardial infarction.* Circulation, 2012. **125**(10): p. 1256-65.

77. Dreyer, G., et al., *Ergocalciferol improves endothelial vasodilatory and vasoconstrictor function in an in vivo model of mild uraemia.* Biosci Rep, 2019. **39**(12).

78. Kieswich, J.E., et al., *A novel model of reno-cardiac syndrome in the C57BL/ 6 mouse strain.* BMC Nephrol, 2018. **19**(1): p. 346.

79. Yi, P. and L. Li, *The germfree murine animal: An important animal model for research on the relationship between gut microbiota and the host.* Veterinary Microbiology, 2012. **157**(1): p. 1-7.

80. Nicklas, W., L. Keubler, and A. Bleich, *Maintaining and Monitoring the Defined Microbiota Status of Gnotobiotic Rodents.* ILAR Journal, 2015. **56**(2): p. 241-249.

81. Fontaine, C.A., et al., *How free of germs is germ-free? Detection of bacterial contamination in a germ free mouse unit.* Gut Microbes, 2015. **6**(4): p. 225-233.

82. Kennedy, E.A., K.Y. King, and M.T. Baldridge, *Mouse Microbiota Models: Comparing Germ-Free Mice and Antibiotics Treatment as Tools for Modifying Gut Bacteria.* Frontiers in Physiology, 2018. **9**: p. 1534.

83. Lagier, J.C., et al., *Culture of previously uncultured members of the human gut microbiota by culturomics.* Nat Microbiol, 2016. **1**: p. 16203.

84. Wade, W., *Unculturable bacteria--the uncharacterized organisms that cause oral infections.* J R Soc Med, 2002. **95**(2): p. 81-3.

85. He, X., et al., *Cultivation of a human-associated TM7 phylotype reveals a reduced genome and epibiotic parasitic lifestyle.* Proc Natl Acad Sci U S A, 2015. **112**(1): p. 244-9.

86. Almeida, A., et al., *A new genomic blueprint of the human gut microbiota.* Nature, 2019. **568**(7753): p. 499-504.

87. Singhal, N., et al., *MALDI-TOF mass spectrometry: an emerging technology for microbial identification and diagnosis.* Front Microbiol, 2015. **6**: p. 791.

88. Bosshard, P.P., et al., *16S rRNA gene sequencing versus the API 20 NE system and the VITEK 2 ID-GNB card for identification of nonfermenting Gram-negative bacteria in the clinical laboratory.* Journal of clinical microbiology, 2006. **44**(4): p. 1359-1366.

89. Lane, D.J., et al., *Rapid determination of 16S ribosomal RNA sequences for phylogenetic analyses.* Proceedings of the National Academy of Sciences, 1985. **82**(20): p. 6955-6959.

90. Woese, C.R. and G.E. Fox, *Phylogenetic structure of the prokaryotic domain: the primary kingdoms.* Proceedings of the National Academy of Sciences, 1977. **74**(11): p. 5088-5090.

91. Kuczynski, J., et al., *Experimental and analytical tools for studying the human microbiome.* Nat Rev Genet, 2011. **13**(1): p. 47-58.

92. Klindworth, A., et al., *Evaluation of general 16S ribosomal RNA gene PCR primers for classical and next-generation sequencing-based diversity studies.* Nucleic Acids Res, 2013. **41**(1): p. e1.

93. Quast, C., et al., *The SILVA ribosomal RNA gene database project: improved data processing and web-based tools.* Nucleic Acids Res, 2013. **41**(Database issue): p. D590-6.

94. Yilmaz, P., et al., *The SILVA and "All-species Living Tree Project (LTP)" taxonomic frameworks.* Nucleic Acids Res, 2014. **42**(Database issue): p. D643-8.

95. DeSantis, T.Z., et al., *Greengenes, a chimera-checked 16S rRNA gene database and workbench compatible with ARB.* Appl Environ Microbiol, 2006. **72**(7): p. 5069-72.

96. Johnson, M., et al., *NCBI BLAST: a better web interface.* Nucleic Acids Res, 2008. **36**(Web Server issue): p. W5-9.

97. Ghyselinck, J., et al., *The effect of primer choice and short read sequences on the outcome of 16S rRNA gene based diversity studies.* PLoS One, 2013. **8**(8): p. e71360.

98. Darwish, N., et al., *Choice of 16S ribosomal RNA primers affects the microbiome analysis in chicken ceca.* Scientific Reports, 2021. **11**(1): p. 11848.

99. Tremblay, J., et al., *Primer and platform effects on 16S rRNA tag sequencing.* Frontiers in Microbiology, 2015. **6**: p. 771.

100. Langille, M.G., et al., *Predictive functional profiling of microbial communities using 16S rRNA marker gene sequences.* Nat Biotechnol, 2013. **31**(9): p. 814-21.

101. Iwai, S., et al., *Piphillin: Improved Prediction of Metagenomic Content by Direct Inference from Human Microbiomes.* PLoS One, 2016. **11**(11): p. e0166104.

102. Ranjan, R., et al., *Analysis of the microbiome: Advantages of whole genome shotgun versus 16S amplicon sequencing.* Biochem Biophys Res Commun, 2016. **469**(4): p. 967-77.

103. Mascarenhas, R., et al., *Integrating Computational Methods to Investigate the Macroecology of Microbiomes.* Frontiers in Genetics, 2020. **10**.

104. Hird Sarah, M., *Microbiomes, Community Ecology, and the Comparative Method.* mSystems. **4**(3): p. e00112-19.

105. Shampo, M.A., R.A. Kyle, and D.P. Steensma, *Isidor Rabi-1944 Nobel laureate in physics.* Mayo Clinic proceedings, 2012. **87**(2): p. e11-e11.

106. Emwas, A.-H., et al., *NMR Spectroscopy for Metabolomics Research.* Metabolites, 2019. **9**(7): p. 123.

107. Haug, K., et al., *MetaboLights: a resource evolving in response to the needs of its scientific community.* Nucleic Acids Res, 2020. **48**(D1): p. D440-d444.

108. Commins, J., C. Toft, and M.A. Fares, *Computational biology methods and their application to the comparative genomics of endocellular symbiotic bacteria of insects.* Biol Proced Online, 2009. **11**: p. 52-78.

109. Hajishengallis, G. and R.J. Lamont, *Beyond the red complex and into more complexity: the polymicrobial synergy and dysbiosis (PSD) model of periodontal disease etiology.* Mol Oral Microbiol, 2012. **27**(6): p. 409-19.

110. Hienz, S.A., S. Paliwal, and S. Ivanovski, *Mechanisms of Bone Resorption in Periodontitis.* J Immunol Res, 2015. **2015**: p. 615486.

111. Listgarten, M.A., *The role of dental plaque in gingivitis and periodontitis.* J Clin Periodontol, 1988. **15**(8): p. 485-7.

112. Dahlen, G., O. Fejerskov, and F. Manji, *Current concepts and an alternative perspective on periodontal disease.* BMC Oral Health, 2020. **20**(1): p. 235.

113. Liang, S., et al., *The C5a receptor impairs IL-12-dependent clearance of Porphyromonas gingivalis and is required for induction of periodontal bone loss.* J Immunol, 2011. **186**(2): p. 869-77.

114.   Park, Y.D., et al., *Porphyromonas gingivalis lipopolysaccharide regulates interleukin (IL)-17 and IL-23 expression via SIRT1 modulation in human periodontal ligament cells.* Cytokine, 2012. **60**(1): p. 284-93.

115.   Bartold, P.M. and T.E. Van Dyke, *Periodontitis: a host-mediated disruption of microbial homeostasis. Unlearning learned concepts.* Periodontol 2000, 2013. **62**(1): p. 203-17.

116.   Bui, F.Q., et al., *Association between periodontal pathogens and systemic disease.* Biomed J, 2019. **42**(1): p. 27-35.

117.   Chen, Y.-C., et al., *Association of pocket epithelial cell proliferation in periodontitis with TLR9 expression and inflammatory response.* Journal of the Formosan Medical Association, 2014. **113**(8): p. 549-556.

118.   Holtfreter, B., et al., *Epidemiology of periodontal diseases in the Study of Health in Pomerania.* J Clin Periodontol, 2009. **36**(2): p. 114-23.

119.   König, J., B. Holtfreter, and T. Kocher, *Periodontal health in Europe: future trends based on treatment needs and the provision of periodontal services--position paper 1.* Eur J Dent Educ, 2010. **14 Suppl 1**: p. 4-24.

120.   Norderyd, O. and A. Hugoson, *Risk of severe periodontal disease in a Swedish adult population. A cross-sectional study.* J Clin Periodontol, 1998. **25**(12): p. 1022-8.

121.   Baelum, V., et al., *Periodontal conditions among adults in Southern Thailand.* J Periodontal Res, 2003. **38**(2): p. 156-63.

122.   Loos, B.G. and T.E. Van Dyke, *The role of inflammation and genetics in periodontal disease.* Periodontol 2000, 2020. **83**(1): p. 26-39.

123.   Laine, M.L., B.G. Loos, and W. Crielaard, *Gene polymorphisms in chronic periodontitis.* Int J Dent, 2010. **2010**: p. 324719.

124.   Wang, F., et al., *Mendelian randomization analysis identified genes potentially pleiotropically associated with periodontitis.* Saudi Journal of Biological Sciences, 2021. **28**(7): p. 4089-4095.

125.   de Carvalho, F.M., et al., *Aggressive periodontitis is likely influenced by a few small effect genes.* Journal of clinical periodontology, 2009. **36**(6): p. 468-473.

126.   Dewhirst, F.E., et al., *The human oral microbiome.* J Bacteriol, 2010. **192**(19): p. 5002-17.

127.   Hajishengallis, G., et al., *Low-abundance biofilm species orchestrates inflammatory periodontal disease through the commensal microbiota and complement.* Cell Host Microbe, 2011. **10**(5): p. 497-506.

128.   Wade, W.G., *The oral microbiome in health and disease.* Pharmacol Res, 2013. **69**(1): p. 137-43.

129.   Solbiati, J. and J. Frias-Lopez, *Metatranscriptome of the Oral Microbiome in Health and Disease.* J Dent Res, 2018. **97**(5): p. 492-500.

130.   Loe, H., E. Theilade, and S.B. Jensen, *EXPERIMENTAL GINGIVITIS IN MAN.* J Periodontol, 1965. **36**: p. 177-87.

131.   Socransky, S.S., et al., *Microbial complexes in subgingival plaque.* J Clin Periodontol, 1998. **25**(2): p. 134-44.

132.   Marsh, P.D., *Microbial ecology of dental plaque and its significance in health and disease.* Adv Dent Res, 1994. **8**(2): p. 263-71.

133. Holt, S.C., et al., *Implantation of Bacteroides gingivalis in nonhuman primates initiates progression of periodontitis.* Science, 1988. **239**(4835): p. 55-7.

134. Shi, M., et al., *The Subgingival Microbiome of Periodontal Pockets With Different Probing Depths in Chronic and Aggressive Periodontitis: A Pilot Study.* Front Cell Infect Microbiol, 2018. **8**: p. 124.

135. Lamont, R.J. and G. Hajishengallis, *Polymicrobial synergy and dysbiosis in inflammatory disease.* Trends Mol Med, 2015. **21**(3): p. 172-83.

136. Oxford University, P., *Oxford English dictionary.* 2002, [Oxford, England]: Oxford University Press.

137. Ruospo, M., et al., *Prevalence and severity of oral disease in adults with chronic kidney disease: a systematic review of observational studies.* Nephrol Dial Transplant, 2014. **29**(2): p. 364-75.

138. Akar, H., et al., *Systemic consequences of poor oral health in chronic kidney disease patients.* Clin J Am Soc Nephrol, 2011. **6**(1): p. 218-26.

139. Anuradha, B.R., et al., *Oral and salivary changes in patients with chronic kidney disease: A clinical and biochemical study.* J Indian Soc Periodontol, 2015. **19**(3): p. 297-301.

140. Lasisi, T.J., Y.R. Raji, and B.L. Salako, *Salivary creatinine and urea analysis in patients with chronic kidney disease: a case control study.* BMC Nephrol, 2016. **17**: p. 10.

141. Romero, A.C., et al., *Salivary Alterations in Rats with Experimental Chronic Kidney Disease.* PLoS One, 2016. **11**(2): p. e0148742.

142. Guzeldemir, E., et al., *Oral health-related quality of life and periodontal health status in patients undergoing hemodialysis.* J Am Dent Assoc, 2009. **140**(10): p. 1283-93.

143. Gürkan, A., T. Köse, and G. Atilla, *Oral health status and oral hygiene habits of an adult Turkish population on dialysis.* Oral Health Prev Dent, 2008. **6**(1): p. 37-43.

144. Chambrone, L., et al., *Periodontitis and chronic kidney disease: a systematic review of the association of diseases and the effect of periodontal treatment on estimated glomerular filtration rate.* J Clin Periodontol, 2013. **40**(5): p. 443-56.

145. Sharma, P., et al., *The periodontal health component of the Renal Impairment In Secondary Care (RIISC) cohort study: a description of the rationale, methodology and initial baseline results.* J Clin Periodontol, 2014. **41**(7): p. 653-61.

146. Ioannidou, E. and H. Swede, *Disparities in periodontitis prevalence among chronic kidney disease patients.* J Dent Res, 2011. **90**(6): p. 730-4.

147. Dietrich, T., et al., *Age-dependent associations between chronic periodontitis/edentulism and risk of coronary heart disease.* Circulation, 2008. **117**(13): p. 1668-74.

148. Xu, F. and B. Lu, *Prospective association of periodontal disease with cardiovascular and all-cause mortality: NHANES III follow-up study.* Atherosclerosis, 2011. **218**(2): p. 536-42.

149. Sharma, P., et al., *Association between periodontitis and mortality in stages 3-5 chronic kidney disease: NHANES III and linked mortality study.* J Clin Periodontol, 2016. **43**(2): p. 104-13.

150. Zhang, J., et al., *Association between periodontal disease and mortality in people with CKD: a meta-analysis of cohort studies.* BMC Nephrol, 2017. **18**(1): p. 269.

151. Chen, L.P., et al., *Does periodontitis reflect inflammation and malnutrition status in hemodialysis patients?* Am J Kidney Dis, 2006. **47**(5): p. 815-22.

152. Buhlin, K., et al., *Oral health and pro-inflammatory status in end-stage renal disease patients.* Oral Health Prev Dent, 2007. **5**(3): p. 235-44.

153. Epstein, S.R., I. Mandel, and I.W. Scopp, *Salivary composition and calculus formation in patients undergoing hemodialysis.* J Periodontol, 1980. **51**(6): p. 336-8.

154. De Rossi, S.S. and M. Glick, *Dental considerations for the patient with renal disease receiving hemodialysis.* The Journal of the American Dental Association, 1996. **127**(2): p. 211-219.

155. Tomas, I., et al., *Changes in salivary composition in patients with renal failure.* Arch Oral Biol, 2008. **53**(6): p. 528-32.

156. Marinoski, J., et al., *Oral mucosa and salivary findings in non-diabetic patients with chronic kidney disease.* Arch Oral Biol, 2019. **102**: p. 205-211.

157. Honarmand, M., et al., *Oral manifestation and salivary changes in renal patients undergoing hemodialysis.* J Clin Exp Dent, 2017. **9**(2): p. e207-e210.

158. Kho, H.S., et al., *Oral manifestations and salivary flow rate, pH, and buffer capacity in patients with end-stage renal disease undergoing hemodialysis.* Oral Surg Oral Med Oral Pathol Oral Radiol Endod, 1999. **88**(3): p. 316-9.

159. Marsh, P.D., *Are dental diseases examples of ecological catastrophes?* Microbiology (Reading), 2003. **149**(Pt 2): p. 279-294.

160. Gaal Kovalcikova, A., et al., *Urea and creatinine levels in saliva of patients with and without periodontitis.* Eur J Oral Sci, 2019.

161. Damasiewicz, M.J. and T.L. Nickolas, *Rethinking Bone Disease in Kidney Disease.* JBMR Plus, 2018. **2**(6): p. 309-322.

162. Bosworth, C. and I.H. de Boer, *Impaired vitamin D metabolism in CKD.* Semin Nephrol, 2013. **33**(2): p. 158-68.

163. Wahl, P. and M. Wolf, *FGF23 in chronic kidney disease.* Adv Exp Med Biol, 2012. **728**: p. 107-25.

164. Erben, R.G., *Physiological Actions of Fibroblast Growth Factor-23.* Frontiers in Endocrinology, 2018. **9**.

165. *UK Renal Registry 19th Annual Report: Appendix J Laboratory Conversion Factors.* Nephron, 2017. **137 Suppl 1**: p. 403-404.

166. Evenepoel, P., et al., *Bone biopsy practice patterns across Europe: the European renal osteodystrophy initiative—a position paper.* Nephrology Dialysis Transplantation, 2017. **32**(10): p. 1608-1613.

167. Sherrard, D.J., et al., *The spectrum of bone disease in end-stage renal failure--an evolving disorder.* Kidney Int, 1993. **43**(2): p. 436-42.

168. Miller, P.D., *The role of bone biopsy in patients with chronic renal failure.* Clinical journal of the American Society of Nephrology : CJASN, 2008. **3 Suppl 3**(Suppl 3): p. S140-S150.

169. Allen, S.J., et al., *Lactobacilli and bifidobacteria in the prevention of antibiotic-associated diarrhoea and Clostridium difficile diarrhoea in older inpatients (PLACIDE): a randomised, double-blind, placebo-controlled, multicentre trial.* Lancet, 2013. **382**(9900): p. 1249-57.

170. Lee, M.M., et al., *Characterization of mandibular bone in a mouse model of chronic kidney disease.* J Periodontol, 2010. **81**(2): p. 300-9.

171.   Ferrario, V.F., et al., *Facial changes in adult uremic patients on chronic dialysis: possible role of hyperparathyroidism.* Int J Artif Organs, 2005. **28**(8): p. 797-802.
172.   Silva, N., et al., *Host response mechanisms in periodontal diseases.* J Appl Oral Sci, 2015. **23**(3): p. 329-55.
173.   Hajishengallis, G., *Aging and its Impact on Innate Immunity and Inflammation: Implications for Periodontitis.* J Oral Biosci, 2014. **56**(1): p. 30-37.
174.   Rossaint, J., et al., *FGF23 signaling impairs neutrophil recruitment and host defense during CKD.* J Clin Invest, 2016. **126**(3): p. 962-74.
175.   Anding, K., et al., *The influence of uraemia and haemodialysis on neutrophil phagocytosis and antimicrobial killing.* Nephrol Dial Transplant, 2003. **18**(10): p. 2067-73.
176.   Sczepanik, F.S.C., et al., *Periodontitis is an inflammatory disease of oxidative stress: We should treat it that way.* Periodontol 2000, 2020. **84**(1): p. 45-68.
177.   Su, H., C.T. Lei, and C. Zhang, *Interleukin-6 Signaling Pathway and Its Role in Kidney Disease: An Update.* Front Immunol, 2017. **8**: p. 405.
178.   Bandach, I., Y. Segev, and D. Landau, *Experimental modulation of Interleukin 1 shows its key role in chronic kidney disease progression and anemia.* Sci Rep, 2021. **11**(1): p. 6288.
179.   Kikuchi, K., et al., *Gut microbiome-derived phenyl sulfate contributes to albuminuria in diabetic kidney disease.* Nature Communications, 2019. **10**(1): p. 1835.
180.   Cobo, G., B. Lindholm, and P. Stenvinkel, *Chronic inflammation in end-stage renal disease and dialysis.* Nephrol Dial Transplant, 2018. **33**(suppl_3): p. iii35-iii40.
181.   Kato, S., et al., *Aspects of immune dysfunction in end-stage renal disease.* Clin J Am Soc Nephrol, 2008. **3**(5): p. 1526-33.
182.   Hajishengallis, G., et al., *Immune and regulatory functions of neutrophils in inflammatory bone loss.* Semin Immunol, 2016. **28**(2): p. 146-58.
183.   Preshaw, P.M. and S.M. Bissett, *Periodontitis and diabetes.* British Dental Journal, 2019. **227**(7): p. 577-584.
184.   Preshaw, P.M., et al., *Periodontitis and diabetes: a two-way relationship.* Diabetologia, 2012. **55**(1): p. 21-31.
185.   Macedo Paizan, M.L. and J.F. Vilela-Martin, *Is there an association between periodontitis and hypertension?* Curr Cardiol Rev, 2014. **10**(4): p. 355-61.
186.   Brasil-Oliveira, R., et al., *Corticosteroid Use and Periodontal Disease: A Systematic Review.* Eur J Dent, 2020. **14**(3): p. 496-501.
187.   Najeeb, S., et al., *The Role of Nutrition in Periodontal Health: An Update.* Nutrients, 2016. **8**(9).
188.   Guthrie, G.D. and S. Bell, *Deprivation and kidney disease-a predictor of poor outcomes*, in *Clin Kidney J.* 2020, © The Author(s) 2019. Published by Oxford University Press on behalf of ERA-EDTA. p. 128-132.
189.   Bello, A.K., et al., *Socioeconomic status and chronic kidney disease at presentation to a renal service in the United Kingdom.* Clin J Am Soc Nephrol, 2008. **3**(5): p. 1316-23.
190.   Hakeem, F.F. and W. Sabbah, *Is there socioeconomic inequality in periodontal disease among adults with optimal behaviours.* Acta Odontol Scand, 2019. **77**(5): p. 400-407.

191. Bonfim, M.d.L.C., et al., *Social determinants of health and periodontal disease in Brazilian adults: a cross- sectional study.* BMC Oral Health, 2013. **13**.

192. Hu, J., et al., *Location-Specific Oral Microbiome Possesses Features Associated With CKD.* Kidney Int Rep, 2018. **3**(1): p. 193-204.

193. Duan, X., et al., *Salivary microbiome in patients undergoing hemodialysis and its associations with the duration of the dialysis.* BMC Nephrology, 2020. **21**(1): p. 414.

194. Deschamps-Lenhardt, S., et al., *Association between periodontitis and chronic kidney disease: Systematic review and meta-analysis.* Oral Dis, 2019. **25**(2): p. 385-402.

195. Lertpimonchai, A., et al., *Periodontitis as the risk factor of chronic kidney disease: Mediation analysis.* J Clin Periodontol, 2019. **46**(6): p. 631-639.

196. Martin, K.J. and E.A. González, *Metabolic bone disease in chronic kidney disease.* J Am Soc Nephrol, 2007. **18**(3): p. 875-85.

197. Lemesch, S., et al., *Mode of renal replacement therapy determines endotoxemia and neutrophil dysfunction in chronic kidney disease.* Sci Rep, 2016. **6**: p. 34534.

198. Klausen, B., R.T. Evans, and C. Sfintescu, *Two complementary methods of assessing periodontal bone level in rats.* Scand J Dent Res, 1989. **97**(6): p. 494-9.

199. Fernandes, M.I., et al., *Comparison of histometric and morphometric analyses of bone height in ligature-induced periodontitis in rats.* Braz Oral Res, 2007. **21**(3): p. 216-21.

200. Schneider, C.A., W.S. Rasband, and K.W. Eliceiri, *NIH Image to ImageJ: 25 years of image analysis.* Nat Methods, 2012. **9**(7): p. 671-5.

201. Baker, P.J., M. Dixon, and D.C. Roopenian, *Genetic control of susceptibility to Porphyromonas gingivalis-induced alveolar bone loss in mice.* Infect Immun, 2000. **68**(10): p. 5864-8.

202. Dempster, D.W., et al., *Standardized nomenclature, symbols, and units for bone histomorphometry: a 2012 update of the report of the ASBMR Histomorphometry Nomenclature Committee.* Journal of bone and mineral research : the official journal of the American Society for Bone and Mineral Research, 2013. **28**(1): p. 2-17.

203. Davis, G.R., A.N. Evershed, and D. Mills, *Quantitative high contrast X-ray microtomography for dental research.* J Dent, 2013. **41**(5): p. 475-82.

204. Flancman, R., A. Singh, and J.S. Weese, *Evaluation of the impact of dental prophylaxis on the oral microbiota of dogs.* PLoS One, 2018. **13**(6): p. e0199676.

205. Kato, M., et al., *Visualization of junctional epithelial cell replacement by oral gingival epithelial cells over a life time and after gingivectomy.* Sci Rep, 2019. **9**(1): p. 7640.

206. Fujita, T., et al., *Regulation of defensive function on gingival epithelial cells can prevent periodontal disease.* Jpn Dent Sci Rev, 2018. **54**(2): p. 66-75.

207. Moutsopoulos, N.M., et al., *Defective neutrophil recruitment in leukocyte adhesion deficiency type I disease causes local IL-17-driven inflammatory bone loss.* Sci Transl Med, 2014. **6**(229): p. 229ra40.

208. Cafiero, C., et al., *Inflammation induces osteoclast differentiation from peripheral mononuclear cells in chronic kidney disease patients: crosstalk between the immune and bone systems.* Nephrol Dial Transplant, 2018. **33**(1): p. 65-75.

209. Bajwa, N.M., et al., *Cortical and trabecular bone are equally affected in rats with renal failure and secondary hyperparathyroidism.* BMC Nephrol, 2018. **19**(1): p. 24.

210. Marchesan, J., et al., *An experimental murine model to study periodontitis.* Nat Protoc, 2018. **13**(10): p. 2247-2267.

211. Hyde, E.R., et al., *Characterization of the rat oral microbiome and the effects of dietary nitrate.* Free Radic Biol Med, 2014. **77**: p. 249-57.

212. Sulyanto, R.M., et al., *The Predominant Oral Microbiota Is Acquired Early in an Organized Pattern.* Scientific Reports, 2019. **9**(1): p. 10550.

213. van Winkelhoff, A.J., et al., *Non-oral gram-negative facultative rods in chronic periodontitis microbiota.* Microb Pathog, 2016. **94**: p. 117-22.

214. J, W., et al., *Comparison of oral microbiome in stable vs declining kidney function in renal transplant recipients [abstract].* 2014: Am J Transplant. p. D633-D642.

215. Araújo, M.V., et al., *End stage renal disease as a modifier of the periodontal microbiome.* BMC Nephrol, 2015. **16**: p. 80.

216. Li, B., et al., *Oral bacteria colonize and compete with gut microbiota in gnotobiotic mice.* Int J Oral Sci, 2019. **11**(1): p. 10.

217. Payne, M.A., et al., *Horizontal and Vertical Transfer of Oral Microbial Dysbiosis and Periodontal Disease.* J Dent Res, 2019. **98**(13): p. 1503-1510.

218. Caruso, R., et al., *Dynamic and Asymmetric Changes of the Microbial Communities after Cohousing in Laboratory Mice.* Cell Rep, 2019. **27**(11): p. 3401-3412.e3.

219. Abusleme, L., et al., *Establishment and Stability of the Murine Oral Microbiome.* J Dent Res, 2020. **99**(6): p. 721-729.

220. I, N., A. A, and L. P. *Analysis of organic acids produced by lactic acid bacteria.* in *IOP Conf. Ser.: Earth Environ Sci.* 2019.

221. Hou, Y., et al., *Risk factors of periodontal disease in maintenance hemodialysis patients.* Medicine (Baltimore), 2017. **96**(35): p. e7892.

222. Ramezani, A. and D.S. Raj, *The gut microbiome, kidney disease, and targeted interventions.* J Am Soc Nephrol, 2014. **25**(4): p. 657-70.

223. Vaziri, N.D., et al., *Chronic kidney disease alters intestinal microbial flora.* Kidney Int, 2013. **83**(2): p. 308-15.

224. Mandal, S., et al., *Analysis of composition of microbiomes: a novel method for studying microbial composition.* Microb Ecol Health Dis, 2015. **26**: p. 27663.

225. Washburne, A.D., et al., *Phylogenetic factorization of compositional data yields lineage-level associations in microbiome datasets.* PeerJ, 2017. **5**: p. e2969.

226. Andersen, K., et al., *Intestinal Dysbiosis, Barrier Dysfunction, and Bacterial Translocation Account for CKD-Related Systemic Inflammation.* J Am Soc Nephrol, 2017. **28**(1): p. 76-83.

227. Chen, Y.-Y., et al., *Microbiome–metabolome reveals the contribution of gut–kidney axis on kidney disease.* Journal of Translational Medicine, 2019. **17**(1): p. 5.

228. Das, T., et al., *Alterations in the gut bacterial microbiome in people with type 2 diabetes mellitus and diabetic retinopathy.* Scientific Reports, 2021. **11**(1): p. 2738.

229. Chaves, L.D., et al., *Chronic kidney disease, uremic milieu, and its effects on gut bacterial microbiota dysbiosis.* American Journal of Physiology-Renal Physiology, 2018. **315**(3): p. F487-F502.

230. Lun, H., et al., *Altered gut microbiota and microbial biomarkers associated with chronic kidney disease.* Microbiologyopen, 2019. **8**(4): p. e00678.

231. Uchiyama, K., et al., *Contribution of uremic dysbiosis to insulin resistance and sarcopenia.* Nephrology Dialysis Transplantation, 2020. **35**(9): p. 1501-1517.

232. Nanto-Hara, F., et al., *The guanylate cyclase C agonist linaclotide ameliorates the gut-cardio-renal axis in an adenine-induced mouse model of chronic kidney disease.* Nephrol Dial Transplant, 2020. **35**(2): p. 250-264.

233. Kikuchi, M., et al., *Uremic Toxin-Producing Gut Microbiota in Rats with Chronic Kidney Disease.* Nephron, 2017. **135**(1): p. 51-60.

234. Randall, D.W., et al., *Batch effect exerts a bigger influence on the rat urinary metabolome and gut microbiota than uraemia: a cautionary tale.* Microbiome, 2019. **7**(1): p. 127.

235. Al-Asmakh, M., et al., *The Effects of Gum Acacia on the Composition of the Gut Microbiome and Plasma Levels of Short-Chain Fatty Acids in a Rat Model of Chronic Kidney Disease.* Front Pharmacol, 2020. **11**: p. 569402.

236. Collins, F.S. and L.A. Tabak, *Policy: NIH plans to enhance reproducibility.* Nature, 2014. **505**(7485): p. 612-3.

237. Stappenbeck, T.S. and H.W. Virgin, *Accounting for reciprocal host-microbiome interactions in experimental science.* Nature, 2016. **534**(7606): p. 191-9.

238. Parker, K.D., et al., *Microbiome Composition in Both Wild-Type and Disease Model Mice Is Heavily Influenced by Mouse Facility.* Front Microbiol, 2018. **9**: p. 1598.

239. Heintz-Buschart, A. and P. Wilmes, *Human Gut Microbiome: Function Matters.* Trends Microbiol, 2018. **26**(7): p. 563-574.

240. Pallister, T., et al., *Hippurate as a metabolomic marker of gut microbiome diversity: Modulation by diet and relationship to metabolic syndrome.* Sci Rep, 2017. **7**(1): p. 13670.

241. Tang, W.H., et al., *Intestinal microbial metabolism of phosphatidylcholine and cardiovascular risk.* N Engl J Med, 2013. **368**(17): p. 1575-84.

242. Qi, J., et al., *Circulating trimethylamine N-oxide and the risk of cardiovascular diseases: a systematic review and meta-analysis of 11 prospective cohort studies.* J Cell Mol Med, 2018. **22**(1): p. 185-194.

243. Stubbs, J.R., et al., *Serum Trimethylamine-N-Oxide is Elevated in CKD and Correlates with Coronary Atherosclerosis Burden.* J Am Soc Nephrol, 2016. **27**(1): p. 305-13.

244. Tamanai-Shacoori, Z., et al., *Roseburia spp.: a marker of health?* Future Microbiol, 2017. **12**: p. 157-170.

245. Ohkawara, S., et al., *Oral administration of butyrivibrio fibrisolvens, a butyrate-producing bacterium, decreases the formation of aberrant crypt foci in the colon and rectum of mice.* J Nutr, 2005. **135**(12): p. 2878-83.

246. Eeckhaut, V., et al., *The Probiotic Butyricicoccus pullicaecorum Reduces Feed Conversion and Protects from Potentially Harmful Intestinal Microorganisms and Necrotic Enteritis in Broilers.* Front Microbiol, 2016. **7**: p. 1416.

247. Bradley, P.H. and K.S. Pollard, *Proteobacteria explain significant functional variability in the human gut microbiome.* Microbiome, 2017. **5**(1): p. 36.

248. Gryp, T., et al., *Gut microbiota generation of protein-bound uremic toxins and related metabolites is not altered at different stages of chronic kidney disease.* Kidney Int, 2020. **97**(6): p. 1230-1242.

249. Rossi, M., D.W. Johnson, and K.L. Campbell, *The Kidney-Gut Axis: Implications for Nutrition Care.* J Ren Nutr, 2015. **25**(5): p. 399-403.

250. Lees, H., et al., *Age and microenvironment outweigh genetic influence on the Zucker rat microbiome.* PLoS One, 2014. **9**(9): p. e100916.

251. Ericsson, A.C., et al., *Effects of vendor and genetic background on the composition of the fecal microbiota of inbred mice.* PLoS One, 2015. **10**(2): p. e0116704.

252. Hildebrand, F., et al., *Inflammation-associated enterotypes, host genotype, cage and inter-individual effects drive gut microbiota variation in common laboratory mice.* Genome Biol, 2013. **14**(1): p. R4.

253. Swann, J.R., et al., *Variation in antibiotic-induced microbial recolonization impacts on the host metabolic phenotypes of rats.* J Proteome Res, 2011. **10**(8): p. 3590-603.

254. Bidot, W.A., A.C. Ericsson, and C.L. Franklin, *Effects of water decontamination methods and bedding material on the gut microbiota.* PLoS One, 2018. **13**(10): p. e0198305.

255. Xiao, L., et al., *A catalog of the mouse gut metagenome.* Nat Biotechnol, 2015. **33**(10): p. 1103-8.

256. (NICE)., N.I.f.H.a.C.E., *Developing NICE guidelines: the manual.* 2014, Process and Methods [PMG20].

257. Medicine., O.C.f.E.-B., *Levels of Evidence.* 2009.

258. Mikolajewicz, N. and S.V. Komarova, *Meta-Analytic Methodology for Basic Research: A Practical Guide.* Frontiers in Physiology, 2019. **10**.

259. Sauvant, D., et al., *Meta-analyses of experimental data in animal nutrition.* Animal, 2008. **2**(8): p. 1203-14.

260. Al-Obaide, M.A.I., et al., *Gut Microbiota-Dependent Trimethylamine-N-oxide and Serum Biomarkers in Patients with T2DM and Advanced CKD.* J Clin Med, 2017. **6**(9).

261. Xu, K.Y., et al., *Impaired renal function and dysbiosis of gut microbiota contribute to increased trimethylamine-N-oxide in chronic kidney disease patients.* Sci Rep, 2017. **7**(1): p. 1445.

262. Li, F., et al., *Alterations to the Gut Microbiota and Their Correlation With Inflammatory Factors in Chronic Kidney Disease.* Front Cell Infect Microbiol, 2019. **9**: p. 206.

263. Stadlbauer, V., et al., *Structural and functional differences in gut microbiome composition in patients undergoing haemodialysis or peritoneal dialysis.* Sci Rep, 2017. **7**(1): p. 15601.

264. Li, Y., et al., *Dysbiosis of the gut microbiome is associated with CKD5 and correlated with clinical indices of the disease: a case-controlled study.* J Transl Med, 2019. **17**(1): p. 228.

265. De Angelis, M., et al., *Microbiota and metabolome associated with immunoglobulin A nephropathy (IgAN).* PLoS One, 2014. **9**(6): p. e99006.

266. Wang, F., et al., *Gut bacterial translocation contributes to microinflammation in experimental uremia.* Dig Dis Sci, 2012. **57**(11): p. 2856-62.

267. Jiang, S., et al., *Alteration of the gut microbiota in Chinese population with chronic kidney disease.* Sci Rep, 2017. **7**(1): p. 2870.

268. Jiang, S., et al., *A reduction in the butyrate producing species Roseburia spp. and Faecalibacterium prausnitzii is associated with chronic kidney disease progression.* Antonie Van Leeuwenhoek, 2016. **109**(10): p. 1389-96.

269.   Tao, S., et al., *Understanding the gut-kidney axis among biopsy-proven diabetic nephropathy, type 2 diabetes mellitus and healthy controls: an analysis of the gut microbiota composition.* Acta Diabetol, 2019. **56**(5): p. 581-592.

270.   Shi, K., et al., *Gut bacterial translocation may aggravate microinflammation in hemodialysis patients.* Dig Dis Sci, 2014. **59**(9): p. 2109-17.

271.   Markowiak-Kopeć, P. and K. Śliżewska, *The Effect of Probiotics on the Production of Short-Chain Fatty Acids by Human Intestinal Microbiome.* Nutrients, 2020. **12**(4): p. 1107.

272.   Wallen, Z.D., et al., *Characterizing dysbiosis of gut microbiome in PD: evidence for overabundance of opportunistic pathogens.* npj Parkinson's Disease, 2020. **6**(1): p. 11.

273.   Yamaguchi, Y., et al., *Association of Intestinal Microbiota with Metabolic Markers and Dietary Habits in Patients with Type 2 Diabetes.* Digestion, 2016. **94**(2): p. 66-72.

274.   Zeng, M.Y., N. Inohara, and G. Nuñez, *Mechanisms of inflammation-driven bacterial dysbiosis in the gut.* Mucosal Immunology, 2017. **10**(1): p. 18-26.

275.   Alhmoud, T., et al., *Investigating intestinal permeability and gut microbiota roles in acute coronary syndrome patients.* Human Microbiome Journal, 2019. **13**: p. 100059.

276.   Lagkouvardos, I., et al., *Sequence and cultivation study of Muribaculaceae reveals novel species, host preference, and functional potential of this yet undescribed family.* Microbiome, 2019. **7**(1): p. 28.

277.   Turnbaugh, P.J., et al., *A core gut microbiome in obese and lean twins.* Nature, 2009. **457**(7228): p. 480-4.

278.   De Filippo, C., et al., *Impact of diet in shaping gut microbiota revealed by a comparative study in children from Europe and rural Africa.* Proc Natl Acad Sci U S A, 2010. **107**(33): p. 14691-6.

279.   Lin, A., et al., *Distinct distal gut microbiome diversity and composition in healthy children from Bangladesh and the United States.* PLoS One, 2013. **8**(1): p. e53838.

280.   Ou, J., et al., *Diet, microbiota, and microbial metabolites in colon cancer risk in rural Africans and African Americans.* Am J Clin Nutr, 2013. **98**(1): p. 111-20.

281.   Russell, W.M.S., et al., *The principles of humane experimental technique.* 2005.

282.   Burkitt, D.P., *Epidemiology of cancer of the colon and rectum.* Cancer, 1971. **28**(1): p. 3-13.

283.   Burkitt, D.P., *Are our commonest diseases preventable?* Prev Med, 1977. **6**(4): p. 556-9.

284.   Cummings, J.H. and A. Engineer, *Denis Burkitt and the origins of the dietary fibre hypothesis.* Nutr Res Rev, 2018. **31**(1): p. 1-15.

285.   Yatsunenko, T., et al., *Human gut microbiome viewed across age and geography.* Nature, 2012. **486**(7402): p. 222-7.

286.   Turnbaugh, P.J., et al., *The effect of diet on the human gut microbiome: a metagenomic analysis in humanized gnotobiotic mice.* Sci Transl Med, 2009. **1**(6): p. 6ra14.

287.   Devkota, S., et al., *Dietary-fat-induced taurocholic acid promotes pathobiont expansion and colitis in Il10-/- mice.* Nature, 2012. **487**(7405): p. 104-8.

288.   Martinez-Medina, M., et al., *Western diet induces dysbiosis with increased E coli in CEABAC10 mice, alters host barrier function favouring AIEC colonisation.* Gut, 2014. **63**(1): p. 116-24.

289. De Vuyst, L., et al., *Summer Meeting 2013: growth and physiology of bifidobacteria.* J Appl Microbiol, 2014. **116**(3): p. 477-91.

290. Egan, M., et al., *Cross-feeding by Bifidobacterium breve UCC2003 during co-cultivation with Bifidobacterium bifidum PRL2010 in a mucin-based medium.* BMC Microbiol, 2014. **14**: p. 282.

291. Egan, M., et al., *Metabolism of sialic acid by Bifidobacterium breve UCC2003.* Appl Environ Microbiol, 2014. **80**(14): p. 4414-26.

292. Turroni, F., et al., *Deciphering bifidobacterial-mediated metabolic interactions and their impact on gut microbiota by a multi-omics approach.* Isme j, 2016. **10**(7): p. 1656-68.

293. Louis, P. and H.J. Flint, *Formation of propionate and butyrate by the human colonic microbiota.* Environmental Microbiology, 2017. **19**(1): p. 29-41.

294. Hernández, M.A.G., et al., *The Short-Chain Fatty Acid Acetate in Body Weight Control and Insulin Sensitivity.* Nutrients, 2019. **11**(8): p. 1943.

295. Schütze, A., et al., *The Impact of ackA, pta, and ackA-pta Mutations on Growth, Gene Expression and Protein Acetylation in Escherichia coli K-12.* Frontiers in Microbiology, 2020. **11**: p. 233.

296. Reichardt, N., et al., *Phylogenetic distribution of three pathways for propionate production within the human gut microbiota.* Isme j, 2014. **8**(6): p. 1323-35.

297. Duncan, S.H., et al., *Growth requirements and fermentation products of Fusobacterium prausnitzii, and a proposal to reclassify it as Faecalibacterium prausnitzii gen. nov., comb. nov.* Int J Syst Evol Microbiol, 2002. **52**(Pt 6): p. 2141-2146.

298. Louis, P., et al., *Diversity of human colonic butyrate-producing bacteria revealed by analysis of the butyryl-CoA:acetate CoA-transferase gene.* Environ Microbiol, 2010. **12**(2): p. 304-14.

299. Baxter, N.T., et al., *Dynamics of Human Gut Microbiota and Short-Chain Fatty Acids in Response to Dietary Interventions with Three Fermentable Fibers.* mBio, 2019. **10**(1): p. e02566-18.

300. Chung, W.S., et al., *Modulation of the human gut microbiota by dietary fibres occurs at the species level.* BMC Biol, 2016. **14**: p. 3.

301. Walker, A.W., et al., *pH and peptide supply can radically alter bacterial populations and short-chain fatty acid ratios within microbial communities from the human colon.* Appl Environ Microbiol, 2005. **71**(7): p. 3692-700.

302. Cummings, J.H., et al., *Short chain fatty acids in human large intestine, portal, hepatic and venous blood.* Gut, 1987. **28**(10): p. 1221.

303. Bloemen, J.G., et al., *Short chain fatty acids exchange across the gut and liver in humans measured at surgery.* Clin Nutr, 2009. **28**(6): p. 657-61.

304. van der Beek, C.M., et al., *Hepatic Uptake of Rectally Administered Butyrate Prevents an Increase in Systemic Butyrate Concentrations in Humans.* J Nutr, 2015. **145**(9): p. 2019-24.

305. Verbeke, K., et al., *Influence of the type of indigestible carbohydrate on plasma and urine short-chain fatty acid profiles in healthy human volunteers.* European Journal of Clinical Nutrition, 2010. **64**(7): p. 678-684.

306. Macfarlane, G.T., G.R. Gibson, and J.H. Cummings, *Comparison of fermentation reactions in different regions of the human colon.* J Appl Bacteriol, 1992. **72**(1): p. 57-64.

307. Kirat, D., et al., *Monocarboxylate transporter 1 (MCT1) plays a direct role in short-chain fatty acids absorption in caprine rumen.* The Journal of physiology, 2006. **576**(Pt 2): p. 635-647.

308. Sivaprakasam, S., et al., *Short-Chain Fatty Acid Transporters: Role in Colonic Homeostasis.* Comprehensive Physiology, 2017. **8**(1): p. 299-314.

309. Thangaraju, M., et al., *GPR109A is a G-protein-coupled receptor for the bacterial fermentation product butyrate and functions as a tumor suppressor in colon.* Cancer research, 2009. **69**(7): p. 2826-2832.

310. Kobayashi, M., et al., *Short-chain fatty acids, GPR41 and GPR43 ligands, inhibit TNF-α-induced MCP-1 expression by modulating p38 and JNK signaling pathways in human renal cortical epithelial cells.* Biochem Biophys Res Commun, 2017. **486**(2): p. 499-505.

311. Willemsen, L.E.M., et al., *Short chain fatty acids stimulate epithelial mucin 2 expression through differential effects on prostaglandin E(1) and E(2) production by intestinal myofibroblasts.* Gut, 2003. **52**(10): p. 1442-1447.

312. Peng, L., et al., *Butyrate enhances the intestinal barrier by facilitating tight junction assembly via activation of AMP-activated protein kinase in Caco-2 cell monolayers.* The Journal of nutrition, 2009. **139**(9): p. 1619-1625.

313. Rivière, A., et al., *Bifidobacteria and Butyrate-Producing Colon Bacteria: Importance and Strategies for Their Stimulation in the Human Gut.* Frontiers in Microbiology, 2016. **7**: p. 979.

314. Roediger, W.E., *Role of anaerobic bacteria in the metabolic welfare of the colonic mucosa in man.* Gut, 1980. **21**(9): p. 793-8.

315. Schönfeld, P. and L. Wojtczak, *Short- and medium-chain fatty acids in energy metabolism: the cellular perspective.* J Lipid Res, 2016. **57**(6): p. 943-54.

316. Bergman, E.N., *Energy contributions of volatile fatty acids from the gastrointestinal tract in various species.* Physiol Rev, 1990. **70**(2): p. 567-90.

317. Cani, P.D. and C. Knauf, *How gut microbes talk to organs: The role of endocrine and nervous routes.* Mol Metab, 2016. **5**(9): p. 743-52.

318. Frost, G., et al., *The short-chain fatty acid acetate reduces appetite via a central homeostatic mechanism.* Nat Commun, 2014. **5**: p. 3611.

319. Nogal, A., et al., *Circulating Levels of the Short-Chain Fatty Acid Acetate Mediate the Effect of the Gut Microbiome on Visceral Fat.* Frontiers in Microbiology, 2021. **12**: p. 1943.

320. Wu, M., et al., *Associations between disordered gut microbiota and changes of neurotransmitters and short-chain fatty acids in depressed mice.* Translational Psychiatry, 2020. **10**(1): p. 350.

321. van de Wouw, M., et al., *Short-chain fatty acids: microbial metabolites that alleviate stress-induced brain–gut axis alterations.* The Journal of Physiology, 2018. **596**(20): p. 4923-4944.

322. Jiang, H., et al., *Altered fecal microbiota composition in patients with major depressive disorder.* Brain Behav Immun, 2015. **48**: p. 186-94.

323. Zheng, P., et al., *Gut microbiome remodeling induces depressive-like behaviors through a pathway mediated by the host's metabolism.* Mol Psychiatry, 2016. **21**(6): p. 786-96.

324. Chen, J.J., et al., *Divergent Urinary Metabolic Phenotypes between Major Depressive Disorder and Bipolar Disorder Identified by a Combined GC-MS and NMR Spectroscopic Metabonomic Approach.* J Proteome Res, 2015. **14**(8): p. 3382-9.

325. Skonieczna-Żydecka, K., et al., *Faecal Short Chain Fatty Acids Profile is Changed in Polish Depressive Women.* Nutrients, 2018. **10**(12).

326. Caspani, G., et al., *Gut microbial metabolites in depression: understanding the biochemical mechanisms.* Microbial cell (Graz, Austria), 2019. **6**(10): p. 454-481.

327. Rutsch, A., J.B. Kantsjö, and F. Ronchi, *The Gut-Brain Axis: How Microbiota and Host Inflammasome Influence Brain Physiology and Pathology.* Frontiers in Immunology, 2020. **11**: p. 3237.

328. Milazzo, G., et al., *Histone Deacetylases (HDACs): Evolution, Specificity, Role in Transcriptional Complexes, and Pharmacological Actionability.* Genes, 2020. **11**(5).

329. Chriett, S., et al., *Prominent action of butyrate over β-hydroxybutyrate as histone deacetylase inhibitor, transcriptional modulator and anti-inflammatory molecule.* Scientific Reports, 2019. **9**(1): p. 742.

330. Davie, J.R., *Inhibition of histone deacetylase activity by butyrate.* J Nutr, 2003. **133**(7 Suppl): p. 2485s-2493s.

331. Kobayashi, H., E.M. Tan, and S.E. Fleming, *Sodium butyrate inhibits cell growth and stimulates p21WAF1/CIP1 protein in human colonic adenocarcinoma cells independently of p53 status.* Nutr Cancer, 2003. **46**(2): p. 202-11.

332. Vaziri, C., L. Stice, and D.V. Faller, *Butyrate-induced G1 arrest results from p21-independent disruption of retinoblastoma protein-mediated signals.* Cell Growth Differ, 1998. **9**(6): p. 465-74.

333. Kim, M.H., et al., *Short-chain fatty acids activate GPR41 and GPR43 on intestinal epithelial cells to promote inflammatory responses in mice.* Gastroenterology, 2013. **145**(2): p. 396-406.e1-10.

334. Sun, M., et al., *Microbiota-derived short-chain fatty acids promote Th1 cell IL-10 production to maintain intestinal homeostasis.* Nature Communications, 2018. **9**(1): p. 3555.

335. Li, M., et al., *The Anti-inflammatory Effects of Short Chain Fatty Acids on Lipopolysaccharide- or Tumor Necrosis Factor α-Stimulated Endothelial Cells via Activation of GPR41/43 and Inhibition of HDACs.* Frontiers in Pharmacology, 2018. **9**: p. 533.

336. Park, J., et al., *Short-chain fatty acids induce both effector and regulatory T cells by suppression of histone deacetylases and regulation of the mTOR–S6K pathway.* Mucosal Immunology, 2015. **8**(1): p. 80-93.

337. Bhaskaran, N., et al., *Role of Short Chain Fatty Acids in Controlling T(regs) and Immunopathology During Mucosal Infection.* Frontiers in microbiology, 2018. **9**: p. 1995-1995.

338. Cheplin, H.A. and L.F. Rettger, *Studies on the Transformation of the Intestinal Flora, with Special Reference to the Implantation of Bacillus Acidophilus: II. Feeding Experiments on Man.* Proceedings of the National Academy of Sciences of the United States of America, 1920. **6**(12): p. 704-705.

339.   Gibson, G.R., et al., *Expert consensus document: The International Scientific Association for Probiotics and Prebiotics (ISAPP) consensus statement on the definition and scope of prebiotics.* Nature Reviews Gastroenterology & Hepatology, 2017. **14**(8): p. 491-502.

340.   Consultation., F.a.A.O.a.W.H.O.E., *Evaluation of health and nutritional properties of powder milk and live lactic acid bacteria.*   . 2001: Córdoba, Argentina: Food and Agriculture Organization of the United Nations and World Health Organization.

341.   Peng, M., et al., *Effectiveness of probiotics, prebiotics, and prebiotic-like components in common functional foods.* Comprehensive Reviews in Food Science and Food Safety, 2020. **19**(4): p. 1908-1933.

342.   Perraudeau, F., et al., *Improvements to postprandial glucose control in subjects with type 2 diabetes: a multicenter, double blind, randomized placebo-controlled trial of a novel probiotic formulation.* BMJ Open Diabetes Res Care, 2020. **8**(1).

343.   Cunningham, M., et al., *Shaping the Future of Probiotics and Prebiotics.* Trends Microbiol, 2021. **29**(8): p. 667-685.

344.   Alves-Santos, A.M., et al., *Prebiotic effect of dietary polyphenols: A systematic review.* Journal of Functional Foods, 2020. **74**: p. 104169.

345.   Vijay, A., et al., *The prebiotic effects of omega-3 fatty acid supplementation: A six-week randomised intervention trial.* Gut Microbes, 2021. **13**(1): p. 1863133.

346.   Sabater-Molina, M., et al., *Dietary fructooligosaccharides and potential benefits on health.* J Physiol Biochem, 2009. **65**(3): p. 315-28.

347.   Azizi, N.F., et al., *Kefir and Its Biological Activities.* Foods (Basel, Switzerland), 2021. **10**(6): p. 1210.

348.   Hong, K.B., et al., *Evaluation of Prebiotic Effects of High-Purity Galactooligosaccharides in vitro and in vivo.* Food Technol Biotechnol, 2016. **54**(2): p. 156-163.

349.   Stewart, M.L., D.A. Timm, and J.L. Slavin, *Fructooligosaccharides exhibit more rapid fermentation than long-chain inulin in an in vitro fermentation system.* Nutr Res, 2008. **28**(5): p. 329-34.

350.   Kobayashi, T., et al., *Comparison of Chain-Length Preferences and Glucan Specificities of Isoamylase-Type α-Glucan Debranching Enzymes from Rice, Cyanobacteria, and Bacteria.* PLOS ONE, 2016. **11**(6): p. e0157020.

351.   Smiricky-Tjardes, M.R., et al., *In vitro fermentation characteristics of selected oligosaccharides by swine fecal microflora1.* Journal of Animal Science, 2003. **81**(10): p. 2505-2514.

352.   Childs, C.E., et al., *Xylo-oligosaccharides alone or in synbiotic combination with Bifidobacterium animalis subsp. lactis induce bifidogenesis and modulate markers of immune function in healthy adults: a double-blind, placebo-controlled, randomised, factorial cross-over study.* British Journal of Nutrition, 2014. **111**(11): p. 1945-1956.

353.   Chen, H.L., et al., *Effects of isomalto-oligosaccharides on bowel functions and indicators of nutritional status in constipated elderly men.* J Am Coll Nutr, 2001. **20**(1): p. 44-9.

354.   Thomson, P., D.A. Medina, and D. Garrido, *Human milk oligosaccharides and infant gut bifidobacteria: Molecular strategies for their utilization.* Food Microbiol, 2018. **75**: p. 37-46.

355. Buffie, C.G. and E.G. Pamer, *Microbiota-mediated colonization resistance against intestinal pathogens.* Nat Rev Immunol, 2013. **13**(11): p. 790-801.

356. Lawson, M.A.E., et al., *Breast milk-derived human milk oligosaccharides promote Bifidobacterium interactions within a single ecosystem.* The ISME Journal, 2020. **14**(2): p. 635-648.

357. Bircher, J., et al., *Treatment of chronic portal-systemic encephalopathy with lactulose.* Lancet, 1966. **1**(7443): p. 890-2.

358. Gluud, L.L., H. Vilstrup, and M.Y. Morgan, *Non-absorbable disaccharides versus placebo/no intervention and lactulose versus lactitol for the prevention and treatment of hepatic encephalopathy in people with cirrhosis.* Cochrane Database Syst Rev, 2016. **4**: p. Cd003044.

359. Dahlqvist, A. and J.D. Gryboski, *Inability of the human small-intestinal lactase to hydrolyze lactulose.* Biochimica et Biophysica Acta (BBA) - Enzymology and Biological Oxidation, 1965. **110**(3): p. 635-636.

360. Hoffmann, K., et al., *Untersuchungen über die Wirkungsweise der Lactulose (ß-Galactosido-Fructose) im Darm.* Klinische Wochenschrift, 1964. **42**(3): p. 126-130.

361. Ito, Y., et al., *Effect of lactulose on short-chain fatty acids and lactate production and on the growth of faecal flora, with special reference to Clostridium difficile.* J Med Microbiol, 1997. **46**(1): p. 80-4.

362. Agostini, L., et al., *Faecal ammonia and pH during lactulose administration in man: comparison with other cathartics.* Gut, 1972. **13**(11): p. 859-66.

363. Rottiers, R., et al., *Cirrhosis, hyperammonemia and Lactulose.* Tijdschr Gastroenterol, 1968. **11**(2): p. 123-39.

364. Weber, F.L., Jr., et al., *Nitrogen in fecal bacterial, fiber, and soluble fractions of patients with cirrhosis: effects of lactulose and lactulose plus neomycin.* J Lab Clin Med, 1987. **110**(3): p. 259-63.

365. Bates, R.G. and G.D. Pinching, *Dissociation Constant of Aqueous Ammonia at 0 to 50° from E. m. f. Studies of the Ammonium Salt of a Weak Acid.* Journal of the American Chemical Society, 1950. **72**(3): p. 1393-1396.

366. Elkington, S.G., *Lactulose.* Gut, 1970. **11**(12): p. 1043-8.

367. Sarangi, A.N., et al., *Faecal bacterial microbiota in patients with cirrhosis and the effect of lactulose administration.* BMC Gastroenterol, 2017. **17**(1): p. 125.

368. Wang, J.Y., et al., *Lactulose improves cognition, quality of life, and gut microbiota in minimal hepatic encephalopathy: A multicenter, randomized controlled trial.* J Dig Dis, 2019. **20**(10): p. 547-556.

369. Chae, J.P., et al., *Revealing the combined effects of lactulose and probiotic enterococci on the swine faecal microbiota using 454 pyrosequencing.* Microbial Biotechnology, 2016. **9**(4): p. 486-495.

370. Zhai, S., et al., *Effect of lactulose intervention on gut microbiota and short chain fatty acid composition of C57BL/6J mice.* MicrobiologyOpen, 2018. **7**(6): p. e00612-e00612.

371. Ikee, R., K. Yano, and T. Tsuru, *Constipation in chronic kidney disease: it is time to reconsider.* Renal Replacement Therapy, 2019. **5**(1): p. 51.

372. Niittynen, L., K. Kajander, and R. Korpela, *Galacto-oligosaccharides and bowel function*, in *Scand J Food Nutr*. 2007, © 2007 Taylor & Francis. p. 62-6.

373. Tayebi Khosroshahi, H., et al., *Lactulose for reduction of nitrogen products in patients with chronic kidney disease.* Iran J Kidney Dis, 2014. **8**(5): p. 377-81.

374. Tayebi-Khosroshahi, H., et al., *The effect of lactulose supplementation on fecal microflora of patients with chronic kidney disease; a randomized clinical trial.* J Renal Inj Prev, 2016. **5**(3): p. 162-7.

375. Miura, M., Y. Nomoto, and H. Sakai, *Short term effect of lactulose therapy in patients with chronic renal failure.* Tokai J Exp Clin Med, 1989. **14**(1): p. 29-34.

376. Miyazaki, M., K. Aoyagi, and S. Tojo, *Lactulose Therapy for Chronic Renal Failure.* The Japanese Journal of Nephrology, 1984. **26**(8): p. 1091-1098.

377. Lorenzoni, A.S.G., et al., *Fructooligosaccharides synthesis by highly stable immobilized β-fructofuranosidase from Aspergillus aculeatus.* Carbohydrate Polymers, 2014. **103**: p. 193-197.

378. Mao, B., et al., *Effects of Different Doses of Fructooligosaccharides (FOS) on the Composition of Mice Fecal Microbiota, Especially the Bifidobacterium Composition.* Nutrients, 2018. **10**(8): p. 1105.

379. Li, S., et al., *Lean rats gained more body weight from a high-fructooligosaccharide diet.* Food Funct, 2015. **6**(7): p. 2315-21.

380. Liu, F., et al., *Fructooligosaccharide (FOS) and Galactooligosaccharide (GOS) Increase Bifidobacterium but Reduce Butyrate Producing Bacteria with Adverse Glycemic Metabolism in healthy young population.* Scientific Reports, 2017. **7**(1): p. 11789.

381. Le Blay, G.l., et al., *Prolonged Intake of Fructo-Oligosaccharides Induces a Short-Term Elevation of Lactic Acid-Producing Bacteria and a Persistent Increase in Cecal Butyrate in Rats.* The Journal of Nutrition, 1999. **129**(12): p. 2231-2235.

382. Tanno, H., et al., *Characterization of fructooligosaccharide metabolism and fructooligosaccharide-degrading enzymes in human commensal butyrate producers.* Gut Microbes, 2021. **13**(1): p. 1869503.

383. Tsukahara, T., et al., *Stimulation of Butyrate Production in the Large Intestine of Weaning Piglets by Dietary Fructooligosaccharides and Its Influence on the Histological Variables of the Large Intestinal Mucosa.* Journal of Nutritional Science and Vitaminology, 2003. **49**(6): p. 414-421.

384. Whelan, K., et al., *Fructooligosaccharides and fiber partially prevent the alterations in fecal microbiota and short-chain fatty acid concentrations caused by standard enteral formula in healthy humans.* J Nutr, 2005. **135**(8): p. 1896-902.

385. Singh, R.P., et al., *High-Fat Diet Induced Alteration of Mice Microbiota and the Functional Ability to Utilize Fructooligosaccharide for Ethanol Production.* Frontiers in Cellular and Infection Microbiology, 2020. **10**: p. 376.

386. McCay, C.M., et al., *Cellulose in the Diet of Rats and Mice: Two Figures.* The Journal of Nutrition, 1934. **8**(4): p. 435-447.

387. Johnson, R.B., D.A. Peterson, and B.M. Tolbert, *Cellulose Metabolism in the Rat.* The Journal of Nutrition, 1960. **72**(3): p. 353-356.

388. Hsu, J.C. and M.H. Penner, *Influence of cellulose structure on its digestibility in the rat.* J Nutr, 1989. **119**(6): p. 872-8.

389. Lewis, G., et al., *Dietary Fiber-Induced Microbial Short Chain Fatty Acids Suppress ILC2-Dependent Airway Inflammation.* Frontiers in Immunology, 2019. **10**: p. 2051.

390.   Slavin, J.L., et al., *Production of Short-Chain Fatty Acids (SCFA) During in vitro Fermentation of Fibers.* Journal of the American Dietetic Association, 1999. **99**(9, Supplement): p. A97.

391.   Harris, H.C., D.J. Morrison, and C.A. Edwards, *Impact of the source of fermentable carbohydrate on SCFA production by human gut microbiota in vitro - a systematic scoping review and secondary analysis.* Critical Reviews in Food Science and Nutrition, 2020: p. 1-12.

392.   Stark, A.H. and Z. Madar, *In Vitro Production of Short-Chain Fatty Acids by Bacterial Fermentation of Dietary Fiber Compared with Effects of Those Fibers on Hepatic Sterol Synthesis in Rats.* The Journal of Nutrition, 1993. **123**(12): p. 2166-2173.

393.   Reeves, P.G., F.H. Nielsen, and G.C. Fahey, Jr., *AIN-93 purified diets for laboratory rodents: final report of the American Institute of Nutrition ad hoc writing committee on the reformulation of the AIN-76A rodent diet.* J Nutr, 1993. **123**(11): p. 1939-51.

394.   Fernandes, A.D., et al., *Unifying the analysis of high-throughput sequencing datasets: characterizing RNA-seq, 16S rRNA gene sequencing and selective growth experiments by compositional data analysis.* Microbiome, 2014. **2**(1): p. 15.

395.   Raman, M., P. Ambalam, and M. Doble, *Short-Chain Fatty Acids*, in *Probiotics and Bioactive Carbohydrates in Colon Cancer Management*, M. Raman, P. Ambalam, and M. Doble, Editors. 2016, Springer India: New Delhi. p. 97-115.

396.   Deleu, S., et al., *Short chain fatty acids and its producing organisms: An overlooked therapy for IBD?* EBioMedicine, 2021. **66**: p. 103293.

397.   Ahmad, A. and S. Khalid, *Chapter 3 - Therapeutic Aspects of Probiotics and Prebiotics*, in *Diet, Microbiome and Health*, A.M. Holban and A.M. Grumezescu, Editors. 2018, Academic Press. p. 53-91.

398.   Christopher W, M. and B. James O, *Dialysis.* The BMJ, 2014. **348**: p. bmj.g2.

399.   Chen, W. and M.K. Abramowitz, *Treatment of metabolic acidosis in patients with CKD.* American journal of kidney diseases : the official journal of the National Kidney Foundation, 2014. **63**(2): p. 311-317.

400.   Bushinsky, D.A., et al., *Patiromer induces rapid and sustained potassium lowering in patients with chronic kidney disease and hyperkalemia.* Kidney Int, 2015. **88**(6): p. 1427-1433.

401.   Kosiborod, M., et al., *Effect of sodium zirconium cyclosilicate on potassium lowering for 28 days among outpatients with hyperkalemia: the HARMONIZE randomized clinical trial.* Jama, 2014. **312**(21): p. 2223-33.

402.   Agarwal, R., R. Afzalpurkar, and J.S. Fordtran, *Pathophysiology of potassium absorption and secretion by the human intestine.* Gastroenterology, 1994. **107**(2): p. 548-71.

403.   Rajendran, V.M. and G.I. Sandle, *Colonic Potassium Absorption and Secretion in Health and Disease.* Compr Physiol, 2018. **8**(4): p. 1513-1536.

404.   Häussinger, D., R. Steeb, and W. Gerok, *Ammonium and bicarbonate homeostasis in chronic liver disease.* Klin Wochenschr, 1990. **68**(3): p. 175-82.

405.   Atkinson, D.E. and E. Bourke, *Metabolic aspects of the regulation of systemic pH.* Am J Physiol, 1987. **252**(6 Pt 2): p. F947-56.

406. Chiavaroli, L., et al., *Dietary fiber effects in chronic kidney disease: a systematic review and meta-analysis of controlled feeding trials.* European Journal of Clinical Nutrition, 2015. **69**(7): p. 761-768.

407. Lee, M.J., et al., *Urine Osmolality and Renal Outcome in Patients with Chronic Kidney Disease: Results from the KNOW-CKD.* Kidney and Blood Pressure Research, 2019. **44**(5): p. 1089-1100.

408. Wright, P.A., *Nitrogen excretion: three end products, many physiological roles.* J Exp Biol, 1995. **198**(Pt 2): p. 273-81.

409. Mehrotra, R., et al., *Evidence that urea is a better surrogate marker of uremic toxicity than creatinine.* Asaio j, 1997. **43**(5): p. M858-61.

410. Balestri, P.L., P. Rindi, and M. Biagini, *Chronic urea intoxication in dogs.* Experientia, 1971. **27**(7): p. 811-2.

411. Fleischman, R.W., et al., *Carcinogenesis bioassay of acetamide, hexanamide, adipamide, urea and P-tolylurea in mice and rats.* J Environ Pathol Toxicol, 1980. **3**(5-6): p. 149-70.

412. Hart, E.B., et al., *The utilization of the nitrogen of urea and ammonium bicarbonate by growing calves.* Journal of Animal Science, 1938. **1938**(1): p. 333-336.

413. Crawford, H. and J.F. McIntosh, *THE USE OF UREA AS A DIURETIC IN ADVANCED HEART FAILURE.* Archives of Internal Medicine, 1925. **36**(4): p. 530-541.

414. Johnson, W.J., et al., *Effects of urea loading in patients with far-advanced renal failure.* Mayo Clin Proc, 1972. **47**(1): p. 21-9.

415. Steyn, D.G., *A outbreak of urea poisonlng among bantu farms labourers in the porgietersrust distric, transvaal.* 1961. **35**(9).

416. Lau, W.L. and N.D. Vaziri, *Urea, a true uremic toxin: the empire strikes back.* Clin Sci (Lond), 2017. **131**(1): p. 3-12.

417. Verdier, V., C.O. Soulage, and L. Koppe, *New clinical evidence for urea toxicity.* Nephrology Dialysis Transplantation, 2022. **37**(1): p. 1-4.

418. Kalim, S., et al., *Protein carbamylation and chronic kidney disease progression in the Chronic Renal Insufficiency Cohort Study.* Nephrology Dialysis Transplantation, 2022. **37**(1): p. 139-147.

419. Moeslinger, T., et al., *Urea induces macrophage proliferation by inhibition of inducible nitric oxide synthesis.* Kidney Int, 1999. **56**(2): p. 581-8.

420. Chang, J.-F., et al., *Uremic Vascular Calcification Is Correlated With Oxidative Elastic Lamina Injury, Contractile Smooth Muscle Cell Loss, Osteogenesis, and Apoptosis: The Human Pathobiological Evidence.* Frontiers in Medicine, 2020. **7**: p. 78.

421. D'Apolito, M., et al., *Urea-induced ROS generation causes insulin resistance in mice with chronic renal failure.* J Clin Invest, 2010. **120**(1): p. 203-13.

422. Xie, Y., et al., *Higher blood urea nitrogen is associated with increased risk of incident diabetes mellitus.* Kidney International, 2018. **93**(3): p. 741-752.

423. Pietrement, C., et al., *Chronic increase of urea leads to carbamylated proteins accumulation in tissues in a mouse model of CKD.* PLoS One, 2013. **8**(12): p. e82506.

424. Sun, S., et al., *Inhibition of protein carbamylation in urea solution using ammonium-containing buffers.* Anal Biochem, 2014. **446**: p. 76-81.

425. Velasquez, M.T., A. Ramezani, and D.S. Raj, *Urea and protein carbamylation in ESRD: surrogate markers or partners in crime?* Kidney Int, 2015. **87**(6): p. 1092-4.

426. Giovannetti, S. and Q. Maggiore, *A LOW-NITROGEN DIET WITH PROTEINS OF HIGH BIOLOGICAL VALUE FOR SEVERE CHRONIC URAEMIA.* Lancet, 1964. **1**(7341): p. 1000-3.

427. Wright, P.L., P.J. Brereton, and D.E.M. Snell, *Effectiveness of modified Giovannetti diet compared with mixed low-protein diet.* Metabolism, 1970. **19**(3): p. 201-213.

428. Baragetti, I., et al., *The low-protein diet for chronic kidney disease: 8 years of clinical experience in a nephrology ward.* Clinical Kidney Journal, 2020. **13**(2): p. 253-260.

429. Ko, G.J., et al., *Dietary protein intake and chronic kidney disease.* Curr Opin Clin Nutr Metab Care, 2017. **20**(1): p. 77-85.

430. Goyal, A., et al., *Ecology-guided prediction of cross-feeding interactions in the human gut microbiome.* Nature Communications, 2021. **12**(1): p. 1335.

431. Van Wey, A.S., et al., *Monoculture parameters successfully predict coculture growth kinetics of Bacteroides thetaiotaomicron and two Bifidobacterium strains.* Int J Food Microbiol, 2014. **191**: p. 172-81.

432. Depommier, C., et al., *Supplementation with Akkermansia muciniphila in overweight and obese human volunteers: a proof-of-concept exploratory study.* Nature Medicine, 2019. **25**(7): p. 1096-1103.

433. Cani, P.D. and W.M. de Vos, *Next-Generation Beneficial Microbes: The Case of Akkermansia muciniphila.* Frontiers in Microbiology, 2017. **8**: p. 1765.

434. Parada Venegas, D., et al., *Short Chain Fatty Acids (SCFAs)-Mediated Gut Epithelial and Immune Regulation and Its Relevance for Inflammatory Bowel Diseases.* Frontiers in Immunology, 2019. **10**: p. 277.

435. Earley, H., et al., *The abundance of Akkermansia muciniphila and its relationship with sulphated colonic mucins in health and ulcerative colitis.* Scientific Reports, 2019. **9**(1): p. 15683.

436. Jefferson, A. and K. Adolphus, *The Effects of Intact Cereal Grain Fibers, Including Wheat Bran on the Gut Microbiota Composition of Healthy Adults: A Systematic Review.* Frontiers in Nutrition, 2019. **6**: p. 33.

437. Makki, K., et al., *The Impact of Dietary Fiber on Gut Microbiota in Host Health and Disease.* Cell Host & Microbe, 2018. **23**(6): p. 705-715.

438. Costeloe, K., et al., *A randomised controlled trial of the probiotic Bifidobacterium breve BBG-001 in preterm babies to prevent sepsis, necrotising enterocolitis and death: the Probiotics in Preterm infantS (PiPS) trial.* Health Technol Assess, 2016. **20**(66): p. 1-194.

439. Zaharuddin, L., et al., *A randomized double-blind placebo-controlled trial of probiotics in post-surgical colorectal cancer.* BMC Gastroenterology, 2019. **19**(1): p. 131.

440. Sakanaka, M., et al., *Varied Pathways of Infant Gut-Associated Bifidobacterium to Assimilate Human Milk Oligosaccharides: Prevalence of the Gene Set and Its Correlation with Bifidobacteria-Rich Microbiota Formation.* Nutrients, 2019. **12**(1).

441. Devika, N.T. and K. Raman, *Deciphering the metabolic capabilities of Bifidobacteria using genome-scale metabolic models.* Scientific Reports, 2019. **9**(1): p. 18222.

442. O'Callaghan, A. and D. van Sinderen, *Bifidobacteria and Their Role as Members of the Human Gut Microbiota.* Front Microbiol, 2016. **7**: p. 925.

443. Fukuda, S., et al., *Bifidobacteria can protect from enteropathogenic infection through production of acetate.* Nature, 2011. **469**(7331): p. 543-7.

444. Duncan, S.H., et al., *Contribution of acetate to butyrate formation by human faecal bacteria.* Br J Nutr, 2004. **91**(6): p. 915-23.

445. Stackebrandt, E., *The Family Lachnospiraceae*, in *The Prokaryotes: Firmicutes and Tenericutes*, E. Rosenberg, et al., Editors. 2014, Springer Berlin Heidelberg: Berlin, Heidelberg. p. 197-201.

446. Vacca, M., et al., *The Controversial Role of Human Gut Lachnospiraceae.* Microorganisms, 2020. **8**(4).

447. Schwiertz, A., et al., *Influence of resistant starch on the SCFA production and cell counts of butyrate-producing Eubacterium spp. in the human intestine.* J Appl Microbiol, 2002. **93**(1): p. 157-62.

448. Parks, D.H., et al., *A standardized bacterial taxonomy based on genome phylogeny substantially revises the tree of life.* Nat Biotechnol, 2018. **36**(10): p. 996-1004.

449. Rey, F.E., et al., *Dissecting the in vivo metabolic potential of two human gut acetogens.* J Biol Chem, 2010. **285**(29): p. 22082-90.

450. Hu, Y., et al., *Manipulation of the gut microbiota using resistant starch is associated with protection against colitis-associated colorectal cancer in rats.* Carcinogenesis, 2016. **37**(4): p. 366-375.

451. Bang, S.J., et al., *The influence of in vitro pectin fermentation on the human fecal microbiome.* AMB Express, 2018. **8**(1): p. 98.

452. Ozato, N., et al., *Blautia genus associated with visceral fat accumulation in adults 20–76 years of age.* npj Biofilms and Microbiomes, 2019. **5**(1): p. 28.

453. Wu, H., et al., *Gut Microbial Metabolites Induce Donor-Specific Tolerance of Kidney Allografts through Induction of T Regulatory Cells by Short-Chain Fatty Acids.* Journal of the American Society of Nephrology, 2020. **31**(7): p. 1445.

454. Riedl, R.A., et al., *Gut Microbiota Represent a Major Thermogenic Biomass.* Function, 2021. **2**(3): p. zqab019.

455. Turnbaugh, P.J., et al., *The human microbiome project.* Nature, 2007. **449**(7164): p. 804-10.

456. Molina, D.K. and V.J. DiMaio, *Normal organ weights in men: part II-the brain, lungs, liver, spleen, and kidneys.* Am J Forensic Med Pathol, 2012. **33**(4): p. 368-72.

457. Qin, J., et al., *A human gut microbial gene catalogue established by metagenomic sequencing.* Nature, 2010. **464**(7285): p. 59-65.

458. Ley, R.E., D.A. Peterson, and J.I. Gordon, *Ecological and evolutionary forces shaping microbial diversity in the human intestine.* Cell, 2006. **124**(4): p. 837-48.

459. Caporaso, J.G., et al., *QIIME allows analysis of high-throughput community sequencing data*, in *Nat Methods*. 2010. p. 335-6.

460. Schloss, P.D., et al., *Introducing mothur: open-source, platform-independent, community-supported software for describing and comparing microbial communities.* Appl Environ Microbiol, 2009. **75**(23): p. 7537-41.

461. Callahan, B.J., et al., *DADA2: High-resolution sample inference from Illumina amplicon data.* Nat Methods, 2016. **13**(7): p. 581-3.

462. McMurdie, P.J. and S. Holmes, *phyloseq: an R package for reproducible interactive analysis and graphics of microbiome census data.* PLoS One, 2013. **8**(4): p. e61217.

463. Pollock, J., et al., *The Madness of Microbiome: Attempting To Find Consensus "Best Practice" for 16S Microbiome Studies.* Appl Environ Microbiol, 2018. **84**(7).

464. Schloss, P.D., *Identifying and Overcoming Threats to Reproducibility, Replicability, Robustness, and Generalizability in Microbiome Research.* mBio, 2018. **9**(3).

465. Salter, S.J., et al., *Reagent and laboratory contamination can critically impact sequence-based microbiome analyses.* BMC Biol, 2014. **12**: p. 87.

466. Eisenhofer, R., et al., *Contamination in Low Microbial Biomass Microbiome Studies: Issues and Recommendations.* Trends Microbiol, 2019. **27**(2): p. 105-117.

467. Martin, M., *Cutadapt removes adapter sequences from high-throughput sequencing reads.* 2011, 2011. **17**(1): p. 3.

468. Davis, N.M., et al., *Simple statistical identification and removal of contaminant sequences in marker-gene and metagenomics data.* Microbiome, 2018. **6**(1): p. 226.

469. Tierney, B.T., et al., *The Landscape of Genetic Content in the Gut and Oral Human Microbiome.* Cell Host Microbe, 2019. **26**(2): p. 283-295.e8.

470. Reese, A.T. and R.R. Dunn, *Drivers of Microbiome Biodiversity: A Review of General Rules, Feces, and Ignorance.* mBio, 2018. **9**(4).

471. McMurdie, P.J. and S. Holmes, *Waste not, want not: why rarefying microbiome data is inadmissible.* PLoS Comput Biol, 2014. **10**(4): p. e1003531.

472. Weiss, S., et al., *Normalization and microbial differential abundance strategies depend upon data characteristics.* Microbiome, 2017. **5**(1): p. 27.

473. Gloor, G.B., et al., *Microbiome Datasets Are Compositional: And This Is Not Optional.* Front Microbiol, 2017. **8**: p. 2224.

474. Silverman, J.D., et al., *A phylogenetic transform enhances analysis of compositional microbiota data.* Elife, 2017. **6**.

475. Simpson, E.H., *Measurement of Diversity.*

476. Shannon, C.E., *A Mathematical Theory of Communication.* Bell System Technical Journal, 1948. **27**(3): p. 379-423.

477. Mosca, A., M. Leclerc, and J.P. Hugot, *Gut Microbiota Diversity and Human Diseases: Should We Reintroduce Key Predators in Our Ecosystem?* Front Microbiol, 2016. **7**: p. 455.

478. Ai, D., et al., *Integrated metagenomic data analysis demonstrates that a loss of diversity in oral microbiota is associated with periodontitis.* BMC Genomics, 2017. **18**(1): p. 1041.

479. Bray, J.R. and J.T. Curtis, *An Ordination of the Upland Forest Communities of Southern Wisconsin.* Ecological Monographs, 1957. **27**(4): p. 325-349.

480. Jaccard, P.

481. Lozupone, C.A., et al., *Quantitative and qualitative beta diversity measures lead to different insights into factors that structure microbial communities.* Appl Environ Microbiol, 2007. **73**(5): p. 1576-85.

482. Anderson, M.J. and J. Santana-Garcon, *Measures of precision for dissimilarity-based multivariate analysis of ecological communities.* Ecology letters, 2015. **18**(1): p. 66-73.

483.   Thévenot, E.A., et al., *Analysis of the Human Adult Urinary Metabolome Variations with Age, Body Mass Index, and Gender by Implementing a Comprehensive Workflow for Univariate and OPLS Statistical Analyses.* J Proteome Res, 2015. **14**(8): p. 3322-35.

484.   Anderson, M.J., *Distance-based tests for homogeneity of multivariate dispersions.* Biometrics, 2006. **62**(1): p. 245-53.

485.   Hall, T.A. *BIOEDIT: A USER-FRIENDLY BIOLOGICAL SEQUENCE ALIGNMENT EDITOR AND ANALYSIS PROGRAM FOR WINDOWS 95/98/ NT*. 1999.

486.   Huang, X. and A. Madan, *CAP3: A DNA sequence assembly program.* Genome Res, 1999. **9**(9): p. 868-77.

487.   Joseph, S., et al., *A 16S rRNA Gene and Draft Genome Database for the Murine Oral Bacterial Community.* mSystems, 2021. **6**(1).

488.   Cole, J.R., et al., *Ribosomal Database Project: data and tools for high throughput rRNA analysis.* Nucleic Acids Res, 2014. **42**(Database issue): p. D633-42.

489.   Kumar, S., et al., *MEGA X: Molecular Evolutionary Genetics Analysis across Computing Platforms.* Mol Biol Evol, 2018. **35**(6): p. 1547-1549.

490.   Revell, L.J., *phytools: an R package for phylogenetic comparative biology (and other things).* Methods in Ecology and Evolution, 2012. **3**(2): p. 217-223.

491.   Oksanen, J., et al.

492.   Gibbs, R.A., et al., *Genome sequence of the Brown Norway rat yields insights into mammalian evolution.* Nature, 2004. **428**(6982): p. 493-521.

493.   Havlak, P., et al., *The Atlas genome assembly system.* Genome Res, 2004. **14**(4): p. 721-32.

494.   H., L., *Aligning sequence reads, clone sequences and assembly contigs with BWA-MEM. .* 2013: arXiv. . p. 1303.3997.

495.   Li, D., et al., *MEGAHIT v1.0: A fast and scalable metagenome assembler driven by advanced methodologies and community practices.* Methods, 2016. **102**: p. 3-11.

496.   Hoyles, L., et al., *Molecular phenomics and metagenomics of hepatic steatosis in non-diabetic obese women.* Nature Medicine, 2018. **24**(7): p. 1070-1080.

497.   Hyatt, D., et al., *Prodigal: prokaryotic gene recognition and translation initiation site identification.* BMC Bioinformatics, 2010. **11**(1): p. 119.

498.   Rognes, T., et al., *VSEARCH: a versatile open source tool for metagenomics.* PeerJ, 2016. **4**: p. e2584.

499.   Steinegger, M. and J. Söding, *MMseqs2 enables sensitive protein sequence searching for the analysis of massive data sets.* Nat Biotechnol, 2017. **35**(11): p. 1026-1028.

500.   Huerta-Cepas, J., et al., *Fast Genome-Wide Functional Annotation through Orthology Assignment by eggNOG-Mapper.* Mol Biol Evol, 2017. **34**(8): p. 2115-2122.

501.   Huerta-Cepas, J., et al., *eggNOG 5.0: a hierarchical, functionally and phylogenetically annotated orthology resource based on 5090 organisms and 2502 viruses.* Nucleic Acids Research, 2019. **47**(D1): p. D309-D314.

502.   Wood, D.E., J. Lu, and B. Langmead, *Improved metagenomic analysis with Kraken 2.* Genome Biology, 2019. **20**(1): p. 257.

503.   Méric, G., et al., *Correcting index databases improves metagenomic studies.* bioRxiv, 2019: p. 712166.

504.   Le Chatelier, E., et al., *Richness of human gut microbiome correlates with metabolic markers.* Nature, 2013. **500**(7464): p. 541-546.

505.   Qin, N., et al., *Alterations of the human gut microbiome in liver cirrhosis.* Nature, 2014. **513**(7516): p. 59-64.

506.   Committee, J.F., *British National Formulary (online).* London: BMJ Group and Pharmaceutical Press <http://www.medicinescomplete.com>

507.   Matsuoka, Y., et al., *[Effects of lactulose on intestinal functions in mice and rats].* Nihon Yakurigaku Zasshi, 1990. **96**(6): p. 301-6.

508.   Fan, J.G., Z.J. Xu, and G.L. Wang, *Effect of lactulose on establishment of a rat non-alcoholic steatohepatitis model.* World J Gastroenterol, 2005. **11**(32): p. 5053-6.

509.   Taskin, B., et al., *Antifibrotic Effect of Lactulose on a Methotrexate-Induced Liver Injury Model.* Gastroenterol Res Pract, 2017. **2017**: p. 7942531.

510.   Juśkiewicz, J. and Z. Zduńczyk, *Lactulose-induced diarrhoea in rats: effects on caecal development and activities of microbial enzymes.* Comp Biochem Physiol A Mol Integr Physiol, 2002. **133**(2): p. 411-7.

Appendix 1 – Acknowledgement of the work of others

Below is a list of all experimental work completed, identifying and acknowledging the contributions of others.

Animal work

The primary responsibility for all animal work belonged to Julius Kieswich, who carried out all purchasing, surgery, diet administration and basic husbandry. David Randall was involved in overseeing the experimental design of all experiments, specifying experimental diets, carrying out observations relating to metabolic caging (eg making up and measuring 24h urine volumes, water consumption, diet intake etc), and carrying out most observations at the time of cull, including caecal weights and pH measurements, taking photographs, and retrieving, processing and storing most samples.

Analysis of bone loss

David Randall completed chemical and manual defleshing of all rodent heads. Monometric determination of bone loss was carried out by Asil Alsam using a dissecting microscope and ImageJ software. Statistical analysis was carried out by David Randall.

Preparation of jaw samples for light microscopy and immunohistochemistry

David Randall developed a method for decalcifying rat jaws using formic acid, and subsequently completed this work. Decalcified samples were them embedded by Asil Alsam before being sectioned at the Barts Cancer Institute (BCI), or by Steve Cannon at the Blizard Institute. Asil Alsam carried out the immunohistochemistry.

Measurement of rat serum PTH concentration

This was carried out jointly by David Randall and Julius Kieswich.

Micro computed tomography

David supplied defleshed samples to the micro-CT department at Queen Mary University of London, Mile End campus. Scanning was carried out by David Mills, with parameters set by Graham Davies. Analysis of images was carried out by David Randall using TomCat software developed by Graham Davies.

Scanning electron microscopy

David Randall supplied sectioned and whole (wet) jaw samples to Alan Boyde. They were prepared for examination by Alan Boyde and Maureen Aurora and scanned by Alan Boyde.

Cultural microbiology

All cultural microbiology was carried out by David Randall, including DNA extraction and 16S PCR from isolated organisms. John's transport medium had been produced by Susan Joseph and Joe Aduse-Opoku at the Blizard Institute and later the Department of Oral Health, Dentistry and Orofacial Sciences at King's College London. All additional in vitro work (urease activity, urea tolerance) was also carried out by David Randall.

NGS sequencing of oral swabs

David Randall completed all steps, including DNA extraction, PCR, library preparation and quantification of DNA for sequencing.

Analysis of saliva

David Randall supervised saliva collection carried out jointly with Julius Kieswich, based on a protocol from Gordon Proctor and Guy Carpenter. David Randall qualified serum and salivary urea using colorimetric analysis.

NGS sequencing of DNA from stool samples of first two rat cohorts

David Randall extracted the DNA, which was transferred to Lesley Hoyles for quantification. It was then sent to a third party provider for library preparation, PCR and sequencing. Lesley Hoyles completed early parts of the subsequent data processing, including trimming of sequencing reads, assembly of reads and assignment of taxonomic identities. All subsequent data analysis of these samples was carried out by David Randall.

NGS sequencing of subsequent rat and mouse stool samples

All steps, including DNA extraction, PCR, library preparation and quantification of DNA for sequencing, were carried out by David Randall.

Analysis of all NGS bioinformatic data

This was entirely carried out by David Randall.

H₁-NMR spectroscopy of urine samples

A first batch of samples were prepared for analysis by Jonathan Swann at Imperial College. A second batch were prepared for analysis by David Randall. All analysis of spectra, identification of metabolites, relative quantification and statistical analysis of both batches was carried out by David Randall.

Metaanalysis

All aspects of data retrieval and analysis were completed by David Randall.

Whole genome sequencing

David Randall collected and processed caecal fluid samples and extracted, purified and quantified DNA. Sequencing was carried out by Macrogen. Early steps of data analysis including assembly of genomes and functional attribution, which required high-performance computing, was carried out by Lesley Hoyles. All subsequent steps were carried out by David Randall.

Total nitrogen quantification

David Randall conveyed samples to the Department of Geography at QMUL, where total nitrogen was quantified under the supervision of Michelle Day. David Randall analysed the data in the context of total water, feed, stool and urine quantities.

Appendix 2: Extra microbiological methods

Processing NGS sequencing data

Outputs from MiSeq sequencing providers are generally supplied de-multiplexed (ie, reads are grouped into individual FASTQ format files for each sample). However, several steps are required before the data is in a form in which can be used to perform analyses, and often these steps require considerable computing power and memory space. A number of 'pipelines' have been developed to help semi-automate this process, including QIIME/QIIME2 [459], Mothur [460] and DADA2 [461]. The steps presented below are based on the DADA2 pipeline but are illustrative of the approaches taken in other sequencing pathways.

Assessing sequence quality

This is a step unique to the DADA2 pathway. The FASTQ file format is shown in Figure 103, p. 368, and includes for each sequence (typically many thousand for gut samples, fewer in lower biomass samples), an initial identifier code (beginning with '@'), followed by the genetic sequence (second line), followed by '+', followed by quality data (based on ASCII scale with, generally, punctuation and numbers representing low quality and capitals and lower case letters representing the highest), corresponding to each individual base of the genetic sequence.

The DADA2 pipeline is unique among the NGS pipelines in making use of this quality data in order to delineate true sample variants (which can be identified as such when they differ from other sequences in high-quality regions of sequencing), from variants due to sequencing artefacts

(differences in low-quality regions) [461]. The DADA2 algorithm can plot forward and reverse quality plots (eg Figure 104, p. 369 these are shown for sequencing data from two of rat oral samples presented in chapter three). The x-axis represents the position along the sequence read (up to ~250bp), the y axis is logarithmic representing the quality score at each position: 20 indicates a 1:100 chance of the assigned base being incorrect, 30 a 1:1000 chance. The green line represents the median quality score across all reads in the sample at any individual point in the sequence, and the orange lines the inter-quartile range. As expected, quality is much better for forward than for reverse reads, which is taken into account during further data processing as outlined below.

Filter and trim

On the basis of the quality plots, decisions can be made about where to trim sequences (for example, based on the quality plots above, a decision may be made to aim for a median quality score of >1:1000, and forward reads were trimmed to 230bp length, and reverse reads to 140bp). A trade-off must sometimes be made between trimming to eliminate lower quality reads, whilst maintaining sufficient overlap (>20bp) to allow forward and reverse reads to be correctly aligned. Further decisions can be made within the DADA2 algorithm on the number of errors that are accepted in order to maintain alignment quality whilst not rejecting too much sample data.

Dereplication

Identical reads are then grouped together into unique amplicon sequence variants (ASVs), maintaining abundance data to allow for subsequent analysis.

345

Merging paired reads

Based on a minimum 20bp overlap, forward and reverse reads are combined to form full length (in the case of the V1-V2 amplicon, approximately 320bp), denoised sequences.

Constructing a sequence table

The earlier-stored abundance data is now used to construct a sequence table indicating the frequency by which each individual sequence was seen in each sample.

Removing chimeras

Any misassembled sequences (that can be exactly assembled by partial reads from two more-abundant 'parent' sequences) are removed.

Assigning taxonomy

Each unique sequence are assigned a taxonomic identity using a publicly available bacterial database such as SILVA [93], using a naive Bayesian clustering method.

Further pre-processing

The output of the DADA2 pipeline is a sequence table, with assigned taxonomy for each of the sequences included. Further data processing can be carried out using other software, for instance the R package *phyloseq* [462]. A number of further decisions must be made, and no consensus exists on 'best practice' in a number of key areas [463], leading to significant concerns about the reproducibility of poorly-conducted microbiome research [464].

Treatment of negative 'kitome' control samples

Published evidence suggests that contamination of laboratory reagents and equipment by DNA from environmental bacteria is ubiquitous and highly variable between reagent batches, making the use of negative 'kitome' controls obligatory in amplicon sequencing experiments [465, 466]. Several software packages can be used in order to remove contaminating bacterial sequences from datasets, including the *Cutadapt* package in QIIME, [467] or the *Decontam* package in R, [468] built to work with *phyloseq* objects. The latter offers options to remove contaminants based on the frequency with which they occur adjusted to the DNA concentration in raw DNA samples, or based simply on their presence in negative control samples.

Removal of low abundance bacterial taxa

Several authors suggest removal of low abundance bacterial taxa, including 'singletons' or sequences that are present in only one sample, prior to microbiome analysis, in order to avoid implicating spurious diversity to variants that actually simply represent sequencing artefacts or low level contaminants (for instance this is the approach advocated by McMurdie and Holmes [462]). However other studies suggest that singletons and low abundance taxa may actually be crucial in understanding microbial variance [469], and that the DADA2 formula, by incorporating sequencing quality data, offers the potential to tell true from spurious variation [461].

Rarefying data

Differences in sequencing depth can lead to false assumptions about diversity and the differential abundance of individual taxa [470]. Rarefaction (where all samples are subsampled at random to

347

the same number of reads, Figure 105, p. 370) offers a solution from environmental ecology to even up between-sample differences in sampling depth. However, its use has been characterised as wasteful [471] and insufficient in controlling for the problems of depth variation. [97, 472] In view of the various new compositional statistical techniques now available (reviewed below), rarefying data is increasingly viewed as an outmoded form of data analysis, although it can be used to give confidence that sequencing has been performed to an adequate depth, and as a measure of the alpha diversity of samples.

Statistical approaches to amplicon sequencing data

Compositional data analysis (CoDA)

Next generation sequencing data from microbial communities is unlike much other biological data because it represents a (hopefully representative) compositional subset of a larger bacterial community, and has a 'sum to one' character that renders many standard statistical methods inappropriate. [473] For example, an observed rise in the abundance of one species, A, will necessarily lead to an observed corresponding fall in other species; it is impossible to tell whether these results arise from an absolute increase in species A or an absolute decrease in the other species. [472]

Although technically insoluble, a number of approaches have been developed to handle the complexities of compositional data analysis, most based around log-ratio transformation of raw data, without requiring rarefaction or other normalisation of data counts. The *ANCOM* [224] and

philr [474] algorithms are each examples of this kind of approach (both requiring pseudocounts to be added throughout the sequence table, to deal with the problem of zeroes), and allow the following fundamental exploratory tools of ecological analysis to be undertaken.

Alpha diversity

This is a measure of intra-sample variation, which may be thought of conceptually as the probability, if two features are drawn at random from a given population, that they will be of different species. In environmental ecology, a field sown with wheat has a low alpha diversity whilst a rainforest has high alpha diversity. A number of methods are available for measuring alpha diversity, ranging from the raw number of species present within a sample, to indexes assessing the relative distribution of species abundance within samples, such as the Simpson [475] or Shannon [476] indices. Interestingly, different patterns have emerged in diversity-disease association studies between the oral microbiome and the gut microbiome: whereas in the gut, many disease states are associated with reduced alpha diversity [477]; in the mouth the opposite seems to be the case in experimental models, with periodontitis often associating with increased alpha diversity, [217] although real-world clinical data suggests that patients with stable periodontal disease may show reductions in alpha diversity. [478]

Beta diversity

This is a measure of between-sample variation, and can be calculated using a variety of formulae that produce distance matrices between individual samples, such as the Bray-Curtis dissimilarity [479] or the Jaccard similarity [480] scores. Phylogenetic distance can be used instead of simple presence/absence or abundance data, for instance to calculate the UniFrac distance. [481] Although some of these methods are not valid for use with compositional data, the *philr* algorithm used in tandem with a phylogenetic tree allows construction of a dissimilarity matrix in Euclidean space, with subsequent plotting of ordination to assess sample clustering.

Beta diversity scores can be used to construct a distance matrix, which describes how dissimilar samples are from each other. Such matrices can be used to construct ordination models using various methods, typically employing multiple dimensions, that can then be plotted to give a visual representation of how closely related different samples are, to identify outliers, and to detect patterns of differential clustering. Advanced statistical techniques such as permutational analysis of variance (PerMANOVA) [482] or orthogonal projection to latent squares discriminant analysis (OPLS-DA) [483] can be used to assess the degree of variance explained by independent experimental variables, and to estimate the significance of any associations. Homogeneity of dispersion within groups can be used to assess whether a particular experimental condition causes individual samples to disperse from each other using different beta diversity indices. [484]

Abundance changes in individual taxa

Using inbuilt functionality in microbiome data processing tools such as *Phyloseq*, relative abundance data can be agglomerated at higher taxonomic levels (genus, family, class, order and phylum), and abundance differences can be assessed using the ANCOM tool, which uses a variety of conventional statistical parametric and non-parametric tests in log-ratio transformed data with correction for multiple-hypothesis testing using the Benjamini-Hochberg method. [224]

Analysis of the oral microbiota using bacterial culture

Analysis of the oral microbiome

Oral swabs were taken from animals by agitating sterile cotton swabs against the molars of rats or mice being held in the scruff position for a period of 30 seconds [127]. Swabs were then placed into 100µl of John's transport medium and transferred directly to the laboratory, where they were vortexed for 30 seconds to mobilize cells and 30µl was removed for culture. The remaining transport medium and swab was frozen at -80ºC for subsequent DNA extraction.

John's transport media was made and autoclaved in-house from the following ingredients:

- Yeast Extract 0.5g 100ml-1
- Protease Peptone 0.1g 100ml-1
- Sodium Chloride 0.85g 100ml-1

- Cysteine Hydrochloride 0.05g 100ml-1

- Sodium Hydrogen Phosphate 0.085g 100ml-1

- Tween 80 0.1ml 100ml-1

- Glycerol 15ml 100ml-1

- De-ionised water 85ml 100ml-1

The pH was adjusted to pH7.0 +/- 0.1 with 1M Sodium Hydroxide. The media was then autoclaved and decanted into sterile universal pots and stored at 4º C.

Culture analysis

Transport medium withdrawn for culture was serially diluted and spread onto blood agar plates containing 5% defibrinated horse blood (TCS Biosciences, UK) before being incubated under both aerobic and anaerobic conditions (80% N_2, 10% H_2 and 10% CO_2) for 48 hours at 37ºC. After this, colonies were counted according to morphology and grown to purity on new blood agar plates. DNA was extracted using the GenElute Bacterial Genomic DNA extraction kit (Sigma Aldrich, UK). PCR products were cleaned up using the NucleoSpin® Gel and PCR clean-up kit (Machery-Nagel, Germany), and then identified using Sanger sequencing of the whole 16S rRNA gene (Eurofins Scientific, Luxembourg), using the widely-used 27F-1492R primer pair. Consensus sequences of forward and reverse reads were assembled using the BioEdit Sequence Alignment Editor [485], full length 16S rRNA gene sequences were assembled from forward and reverse reads using the CAP3 Contig Assembly Programme [486] available online via the Pôle Rhône-Alpes de Bioinformatique Site

(http://doua.prabi.fr/software/cap3, last accessed 13th January 2022). All consensus sequences were >1400 base pairs in length and the mean length was 1456bp.

All full-length 16S sequences have been supplied to curators of the rodent oral microbiome database where they formed part of the founding collection. [487]

Isolates were identified by comparing their 16S rRNA gene sequences with reference datasets using both the NCBI Nucleotide BLAST database (https://blast.ncbi.nlm.nih.gov/Blast.cgi last accessed 13th January 2022), and the Ribosomal Database Project (RDP) [488] online search tool (https://rdp.cme.msu.edu/index.jsp last accessed 13th January 2022). In many cases these tools agreed on a species level identification for the isolate, but in some cases agreement between the two was only at higher taxonomic levels (such as in the case of different species of *Streptococcus* or *Enterobacteriaceae*). Thus, for all isolates, full-length reference 16S rRNA gene sequences for all species within the genus identified by BLAST and RDP search were downloaded from the RDP Hierarchy Browser. These reference sequences were aligned with the sequences from our research isolates, trimmed to a uniform length and used to construct a maximum likelihood tree, using MEGA [489] version 7. Pairwise distances between all isolates within a particular genus and all references sequences within that genus were calculated and used to generate a distance matrix.

Species level identification was determined when possible at >98.5% sequence identity. Isolates that failed to obtain any match at this level were treated as potential novel species. One was a *Streptococcus* species (4 isolates) with a closest proximity to *S. danieliae* at 97.33% and another was a *Pasteurella* species (closes match being *P. pneumotropica* at 94.7%).

For the purposes of subsequent *in vitro* microbiological work (urease testing and calculation of the mean inhibitory concentration of urea), where more than one isolate was assigned to a particular species identity, differences in in vitro characteristics were resolved for subsequent analysis by treating all isolates assigned to one species as urease positive if one isolate of that species was urease positive, and all isolates within a single species identification as possessing the highest urea tolerance of any isolate in that species.

Analysis of cultured microbiome data

Once assigned a species identity, the abundance of each isolate (log_{10} of colony forming units/ml) was carried out using Microsoft Excel and GraphPad Prism, using the Student t-test with Welch's correction to assess difference between growth in uraemic animals and growth in controls. Comparisons were made at species level and then aggregated to allow comparisons at higher taxonomic levels.

Additional in vitro bacterial work

In vitro assessment of urease activity and tolerance of variable urea concentrations were assessed for all bacterial isolates after they were grown to purity on 5% blood agar plates under standard aerobic or anaerobic conditions.

Measurement of urease activity: Urease activity was assessed in all isolates by culturing under either aerobic or anaerobic conditions on Christensen's urea agar (Sigma-Aldrich) at 37ºC. A

positive urease result was recorded if there was a colour change to purple, and the sample was re-grown if there was no discernible growth on the top of the agar.

Calculation of mean inhibitory concentration of urea: Two broths were used to assess bacterial growth at different concentrations of urea: Iso-sensitest broth (ThermoFisher Scientific) and Brain-Heart Infusion (BHI) broth (SigmaAldrich). The BHI broth was used for some samples after they could not be grown after several attempts in Iso-sensitest broth. One isolate (eventually identified as *Haemophilus parainfluenzae*) did not grow in either broth and after researching its specific growth requirements in the published literature, eventually grew well after filter-sterilized hemin and nicotinamide adenine dinucleotide were added to the growth medium.

Preparations of both broths were prepared at variably stronger concentrations than the manufacturer's instructions would suggest so that when diluted with different concentrations of filter-sterilized 60% urea solution, broths with eventual concentrations of 0%, 4%, 8%, 12%, 18% and 24% urea ensued.

Bacteria grown to purity on blood agar were then transferred into 2ml sterile phosphate buffered saline (PBS). A 1ml aliquot was assessed using a spectrophotometer at 600nm and the remainder of the bacterial solution further diluted with sterile PBS to achieve a standard turbidity of 0.5 McFarland units, equating to a concentration of bacteria of 1.5×10^8 colony forming units/ml (cfu/ml). These solutions were further diluted 50-fold to achieve an approximate concentration of 3×10^6 cfu/ml, and then 34µl of this bacterial preparation were added to 200µl of varying concentrations of urea broth in a 96-well plate, to achieve 234µl incubations each containing

approximately 5×10^5 cfu bacteria in eventual urea concentrations of 0%, 3.3%, 6.6%, 10%, 15% and 20%.

These plates were then incubated at 37° in either aerobic or anaerobic conditions for 24 hours before being read on a plate reader at 620nm. The mean inhibitory concentration was defined for each organism as the urea concentration at which the optical density of the solution was decreased to less than 10% of the difference between 0% urea and control (non-inoculated) wells. One isolate did not achieve sufficient growth to allow calculation of MIC.

Analysis of the oral microbiota via next-generation sequencing

A number of proprietary kit-based methods are available, and we began by using the FastDNA$^{©}$ kit from MP Bio, which uses mechanical and chemical means to degrade cell walls and release DNA (through bead beating at 24,000 rpm and use of their CLS-TC cell lysis buffer), followed by centrifugation to remove complexed protein and cellular debris. DNA is then isolated and purified using a silica-based DNA binding matrix, before DNA elution.

Initial attempts at DNA extraction and PCR were straightforward for oral samples; but from the stool samples proved challenging, as despite high concentrations of DNA being extracted, the samples amplified poorly due to the presumed presence of PCR inhibitors such as bile acids. In response to this we switched technique to use the PowerSoil© kit from Qiagen (formerly MoBio), which although otherwise similar to the FastDNA$^{©}$ kit has patented inhibitor-removal technology, and samples purified using this kit subsequently amplified well (Figure 106, p. 371).

All subsequent oral and gut samples were extracted using this kit, and negative 'kitome' control [465] were included for all steps of sample extraction for each different reagent batch used.

Primer choice for NGS sequencing

The Illumina MiSeq sequencing platform is able to generate paired-end reads of up to 300bp, meaning that a target region within the 16S gene must be chosen for sequencing. PCR was carried out using barcoded 27F/338R primer pairs, targeting the V1/V2 hypervariable region of the 16S rRNA gene, which performs well in identifying most common oral and gut bacteria, although may bias against the identification of minor phyla such as *Verrucomicrobia* and *Tenericutes* [97].

Library preparation for PCR

To allow massive parallel sequencing of the eluted DNA, a library was constructed using PCR with barcoded primers unique to each sample, targeting the V1/V2 hypervariable region of the bacterial 16S gene. Primers are shown in Figure 107, p. 372.

PCR was then carried out in a sterile 96-well plate using Phusion Green Hot Start II High Fidelity PCR Master Mix (ThermoFisher Scientific), using an initial denaturation step for 5 mins at 98°C followed by 25 cycles of 98°C for 10s, 53°C for 30s, 72°C for 45s and a final extension of 72°C for 10 min. The plate was prepared as shown in Figure 108, p. 373.

Amplicon sequencing

Normalisation of DNA concentrations was carried out using SequalPrep™ Normalisation Plates (ThermoFisher) and DNA was quantified using either the Quant-iT® PicoGreen™ dsDNA Quantitation Kit (ThermoFisher Scientific) or a Qubit® 4 Fluorometer (also ThermoFisher). The samples were pooled and sequenced at the Barts & the London Genome Centre, QMUL using an Illumina MiSeq 2 x 250 flow cell for paired-end sequencing.

Analysis of NGS data

The DADA2 2 sequencing pipeline was used according to the available online tutorial (available online at https://benjjneb.github.io/dada2/tutorial_1_6.html, last accessed 2nd Feb 2022), and default parameters, adjusting filter parameters to achieve maximum quality scores whilst achieving sufficient overlap between forward and reverse reads. Subsequent analysis was carried out in R using the *Phyloseq* package. Sequences were aligned against the Silva v128 dataset [93], and this database was also used to assign taxonomy. Eukaryotic sequences, and those not assigned at phylum level, were expunged, but because of the robustness of the DADA2 algorithm in delineating true from artefactual sequence variation, no pruning of singletons or low-abundance taxa was carried out. Sequence variants were manually removed from all samples at the levels found in negative controls from all samples extracted using the same kit using Microsoft Excel, and then samples with fewer than 500 reads/sample were excluded from subsequent analysis (reflecting the fact that oral rodent samples are typically low biomass).

The *philr* package was then used to adjust all sequence abundance data to composition form, using isometric log-ratio transformation. A pseudocount of 0.001 was added to all OTU abundances to avoid calculating log-ratios involving zeros. A phylogenetic tree was generated using MEGA v7.0 [489], and rooted to a random node using the R package *phytools* [490].

Alpha diversity for each sample was calculated for the compositional data using the 'estimate_richness' function in *Phyloseq*, and differences between groups were assessed for significance using Student's t-test with Welch's correction for unequal variance. Ordination was carried out using the 'ordinate' function in *Phyloseq* to calculate Euclidean distances in *philr* space.

Permutational analysis of variance (PerMANOVA) and the PERMDISP test for homogeneity of variance [484], were carried out using the R package *vegan* [491]. Alpha diversity was assessed using *Phyloseq.*

Differences between groups in the relative abundances of different taxa were calculated at various taxonomic levels by using the 'tax_glom' function in *Phyloseq* to produce new phyloseq objects with sequence abundance data agglomerated at genus, family, class, order and phylum level. The *Analysis of Composition Of Microbiomes (ANCOM)* methodology [224] was used to assess the significance of abundance differences between groups in the compositional data, which has built-in correction for multiple hypothesis testing using the Benjamini-Hochberg method. Code for ANCOM analysis in R is kindly made available by the author from her own web-page (https://sites.google.com/site/siddharthamandal1985/research, accessed 26th August 2019).

Analysis of the gut microbiome

Sample collection

For all cohorts, this was carried out using caecal fluid obtained at the time of animal sacrifice. The caecum was externalized, perforated and drained of fluid onto squares of clean aluminium foil which were directly flash frozen in liquid nitrogen, and subsequently stored at -80^0.

Processing of caecal samples for first two rat cohorts in chapter four

DNA was extracted from samples of caecal fluid using the DNeasy PowerSoil kit from QIAGEN, used according to the manufacturer's instructions. All samples were processed using the same kit, and a negative 'kitome' control was also included with samples. DNA diluted to 10 ng/μL (in 10 mM Tris HCl pH 8.5) was submitted to the Centre for Genomic Research at the University of Liverpool for library preparation and sequencing of the V3 hypervariable region of the 16S rRNA gene.

Initial analysis of this sequencing data was carried out using QIIME v1.9. Paired-end data were joined using join_paired_ends.py, and primer sequences removed from split library files using cutadapt. OTUs were picked using 99% BLAST identity using usearch; from these, a representative set of OTUs was selected. Sequences were aligned (PyNAST) against Silva v128 [33], and this database was also used to assign taxonomy. Singletons, mitochondria-,

cyanobacteria- and control-associated OTUs were removed from the OTU table, as were OTUs unaffiliated with any taxonomic group.

Raw sequences were subsequently downloaded from the NCBI Short Reads Archive, and imported into R for in-house re-analysis using the DADA2 and *phyloseq* packages. A phylogenetic tree was generated using MEGA v7.0 and rooted to a random node using the R package *phytools*. A pseudocount of 0.001 was added to all OTU abundances to avoid calculating log-ratios involving zeros, and then data was then made compositional through isometric log-ratio transformation using the R package *philr*. Ordination was carried out using the 'ordinate' function in *Phyloseq*, based on Euclidean distances in philr space. Permutational analysis of variance (PERMANOVA) was carried out using the ADONIS command in the R package *vegan*. OPLS-DA models were built using the *ropls* package in R. Alpha diversity was assessed using *Phyloseq*. Compositional analysis of the microbiota at six taxonomic levels was based on isometric log-ratio transformation of raw sequence abundances and adjusted for multiple testing using the Benjamini-Hochberg method, carried out using the *ANCOM* statistical framework in R.

Processing of caecal samples and downloaded microbiome data for subsequent rat and mouse cohorts in chapter four, including the meta-analysis

DNA from caecal fluid was extracted using the PowerSoil© kit from Qiagen. PCR was carried out in house using barcoded 27F/338R primer pairs, targeting the V1/V2 hypervariable region of the 16S rRNA gene. PCR was carried out in a sterile 96-well plate using Phusion Green Hot Start

II High Fidelity PCR Master Mix (ThermoFisher Scientific), using an initial denaturation step for 5 mins at 98°C followed by 25 cycles of 98°C for 10s, 53°C for 30s, 72°C for 45s and a final extension of 72°C for 10 min. Normalisation of DNA concentrations was carried out using SequalPrep™ Normalisation Plates (ThermoFisher) and DNA was quantified using a Qubit® 4 Fluorometer (also ThermoFisher). Pooled samples were then sent for next generation sequencing at the DNA Sequencing Facility, Department of Biochemistry, University of Cambridge.

Raw sequences from this analysis were combined with additional sequences downloaded from the NCBI Short Reads Archive, to complete the meta-analysis. Datasets downloaded from the SRA were converted into fastq format using the fastq-dump software from the SRA toolkit. Raw sequences were analysed in R version 3.6.1, using the DADA2 pipeline, [461] with each dataset pre-processed separately because of differences in primer pairs and sequencing quality, with filtering and trim parameters being optimised for each dataset. One dataset (Al-Asmakh2020) used widely separated primer pairs (337F/805R) which meant that after adjusting for quality, only a very small proportion of reads could be successfully merged, and so for this dataset the decision was made to include only forward reads to avoid bias. Two datasets (Mishima2015 and Kikuchi2017) used 454 pyrosequencing instead of Illumina paired-end sequencing, and so only longer, forward reads were available for these datasets.

Amplicon sequencing variants (ASVs) were aligned against Silva v138 to assign taxonomy. Raw abundance data of ASVs were used with taxonomic assignments and sample metadata to create phyloseq objects for each sequencing run. These phyloseq objects were retained for

analysis within each dataset at the level of individual ASVs, but then agglomerated at family level and merged to allow analysis of the whole dataset as described below.

Phylochip data for the Vaziri2013 dataset was substantially different in nature from the sequencing data of all the other datasets; partly because of the nature of the data acquisition (consisting of fluoroscopic intensity scores for each of several thousand probes on the chip, rather than simply those sequences present in the sample), and partly because the taxonomic identities attributed to the different 25-mer probes on the phylochip are incommensurable with the modern Silva taxonomy. Thus, OTU table, taxonomic and meta-data were combined for this dataset to allow it to be individually analysed in phyloseq in parallel with the other datasets, but this dataset was not agglomerated and merged into the whole-dataset object for combined analysis.

Combined analysis of the whole chapter four metaanalysis dataset

A combined dataset was constructed to permit comparison between microbial communities from all samples (excluding the Vaziri2013 dataset), irrespective of the sequencing methodologies and primer pairs used.

To allow this, taxa from the individual cohort phyloseq objects were agglomerated to family level (the lowest taxonomic level at which all sequencing variants received a confident taxonomic identity), using the tax_glom function in *phyloseq*. Taxa were manually renamed across datasets to allow comparison of like with like between cohorts; then a combined

taxonomy, meta-data and ASV table were used to construct a phyloseq object incorporating all samples.

This data was rendered compositional using centred log-ratio transformation via the transform function in the R package *microbiome*, and redundancy analysis (RDA) was carried out using the ordinate function in *phyloseq* which was plotted using the plot_ordination function. Scores and loadings were extracted from the RDA model and used to calculate spatial means and the vector between control and uraemic samples within each cohort on the combined RDA axes. The ADONIS function in R package *vegan* was used for PerMANOVA calculations.

Each cohort was then analysed independently at the level of individual ASVs, without agglomeration at higher taxonomic levels. Redundancy analysis and PerMANOVA were carried out using the same methods as for the combined dataset. Additionally, alpha diversity analyses were carried out on log-ratio transformed datasets using the estimate_richness function in *phyloseq*, and beta dispersion was calculated for control and uraemic groups using the betadisper function in *vegan*. Abundance data from the combined phyloseq object were aggregated to phylum level and rendered compositional before being used to generate the bar charts demonstrating compositional community abundance.

To reflect the composition nature of microbiome datasets, and to allow for multiple hypothesis correction, testing for ASVs displaying differential abundances according to uraemia was carried out for all cohorts using the *ANCOM* statistical framework. Code for ANCOM 2v1 was obtained from GitHub (https://github.com/FrederickHuangLin/ANCOM, last accessed 2nd February 2022) and used according to default parameters. ANCOM analysis was carried using data agglomerated

at family, order, class and phylum levels to pick out differences between control and uraemic samples at each of these levels. For the data presented in supplementary Table 18, only taxa detected at a cut-off of 0.7 were included as significant, and at each level the differentially-abundant taxa were listed in descending order according to their W score. Also, on this table to allow a crude comparison of the significance of association is the 2-sample t-test; in some cases this is higher than the set alpha of 0.05, but these all actually had an adjusted significance of <0.05 after multiple hypothesis correction. A simple ratio between mean abundance in uraemic animals and mean abundance in control animals is presented to show whether uraemic animals had increased or decreased abundance relative to controls.

Processing of whole genome metagenomic caecal samples for rat samples in chapter five

Samples of caecal fluid were taken from one cohort of rats (those treated by subtotal nephrectomy) for microbiome analysis. Samples were collected and stored as previously, and DNA was extracted for analysis using the PowerSoil© kit from Qiagen. No PCR step was carried out, but rather the extracted DNA was sent to Macrogen Inc. for whole-genome metagenomic sequencing.

Sequence data were generated by Macrogen Inc. (Illumina Novaseq 4000; paired-end; 150 bp), with the library prepared using the TruSeq Nano DNA kit according to the manufacturer's instructions. Macrogen-supplied data were checked using fastQC v0.11.9 (https://www.bioinformatics.babraham.ac.uk/projects/fastqc/, last accessed 13th January 2022), with an average of 7.23 Gb (± 0.90 Gb) sequence data generated for each sample. No trimming

of data was required. These files were uploaded to the Sequence Read Archive and are available under BioProject PRJNA682232, and used for all subsequent analyses.

Rat DNA within samples was detected by mapping reads against the rat genome (Rnor_6.0) [492, 493] using bwa mem v0.7.17-r1188 [494]. Non-rat DNA was extracted from read files using samtools v1.3.1 (http://www.htslib.org/, last accessed 13th January 2022), leaving total read pairs in each dataset representing 7.03 Gb (± 0.90 Gb) sequence data. Megahit v1.2.9 [495] was used to assemble sequence data for each of the 24 datasets, with only contigs ≥500 nt retained. Unassembled reads were then pooled and subjected to a second round of assembly to improve the representation of low-abundance sequences [496]. Genes (nucleotide and protein sequences) in assemblies were predicted using Prodigal v2.6.3 (default settings), with a total of 7,676,260 genes predicted across all samples [497]. Protein sequences were sorted using VSEARCH v2.15.1 [498], then clustered using MMseqs2 v12.113e3 [499] with 90 % coverage and a 90 % cut-off identity. Centroid sequences from each cluster were used to generate a non-redundant gene catalogue (n=1,491,110) for determination of gene abundances and functional predictions. Gene abundances in each sample were determined as described previously [496]. The command-line version of eggNOG-mapper v2 (eggNOG 5.0) was used (default settings) to generate functional predictions for the dataset [500, 501]: the non-redundant gene catalogue was associated with 7,334 KEGG orthologies, 1,065 KEGG modules,152 COG terms and 176 CAZy terms. Taxonomic abundance and read count data for archaea and bacteria were generated using Kraken2 2.0.7-beta [502] and the pre-compiled Kraken2 GTBD_r89_54k index (downloaded on 24 November 2020; available from https://bridges.monash.edu/articles/GTDB_r89_54k/8956970?file=16378295) [503].

Measures of alpha and beta diversity were determined using Phyloseq v1.34.0 [462], with species-level data (where counts had ≥1 % relative abundance in each metagenome) rarefied to 7,663,923 reads prior to analysis. Non-rarefied count data for taxonomic (where counts had ≥1 % relative abundance in each metagenome) and functional metrics were subject to analyses using ALDex2 v.1.18.0 [394].

Microbial gene richness was determined as described previously [496, 504, 505]. Data were downsized to adjust for sequencing depth and technical variability by randomly selecting 30 million reads mapped to the merged gene catalogue (of 1,491,110 genes for each sample and then computing the mean number of genes over 30 random drawings).

@M00527:100:000000000-BFHC7:1:1101:14912:1598 1:N:0:

GATGAACGCTGGCGGCGTGCCTAATACATGCAAGTAGAACGCTGAAGGAAGTGC...

+

>A?FF@ABBDFCEGGAEE2GFFE5F3FFHBEFGFGFBDED1AEGHHHHHFHHFBBGB...

Figure 103: The FASTQ format. The first line identifies the sample, the second line contains the genetic sequence, the fourth line contains quality codes for each base in the genetic sequence.
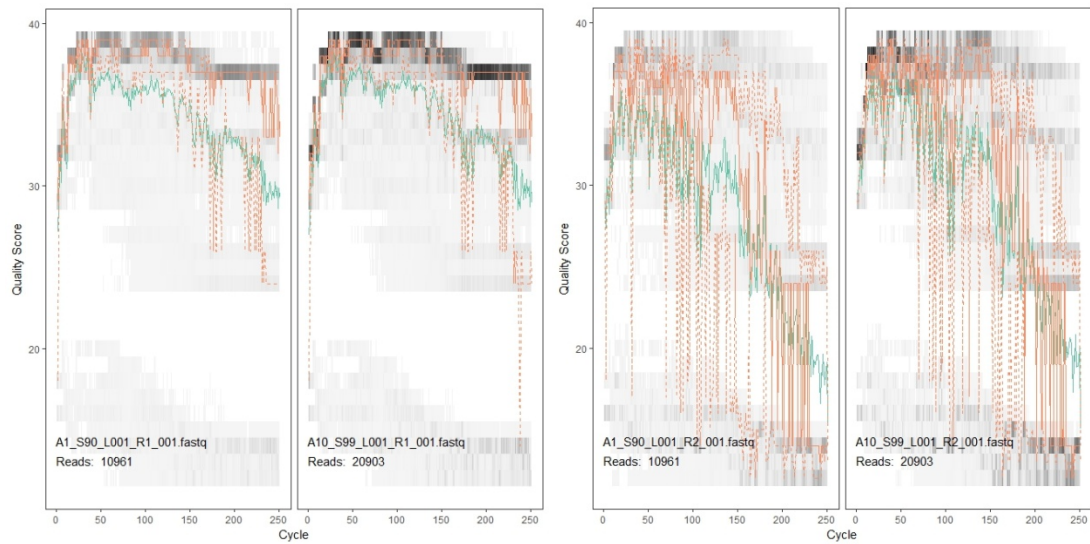
Figure 104: Quality scoring of next generation sequencing data. The x axis indicates the position along the gene and the y axis the log$_{10}$ quality score.
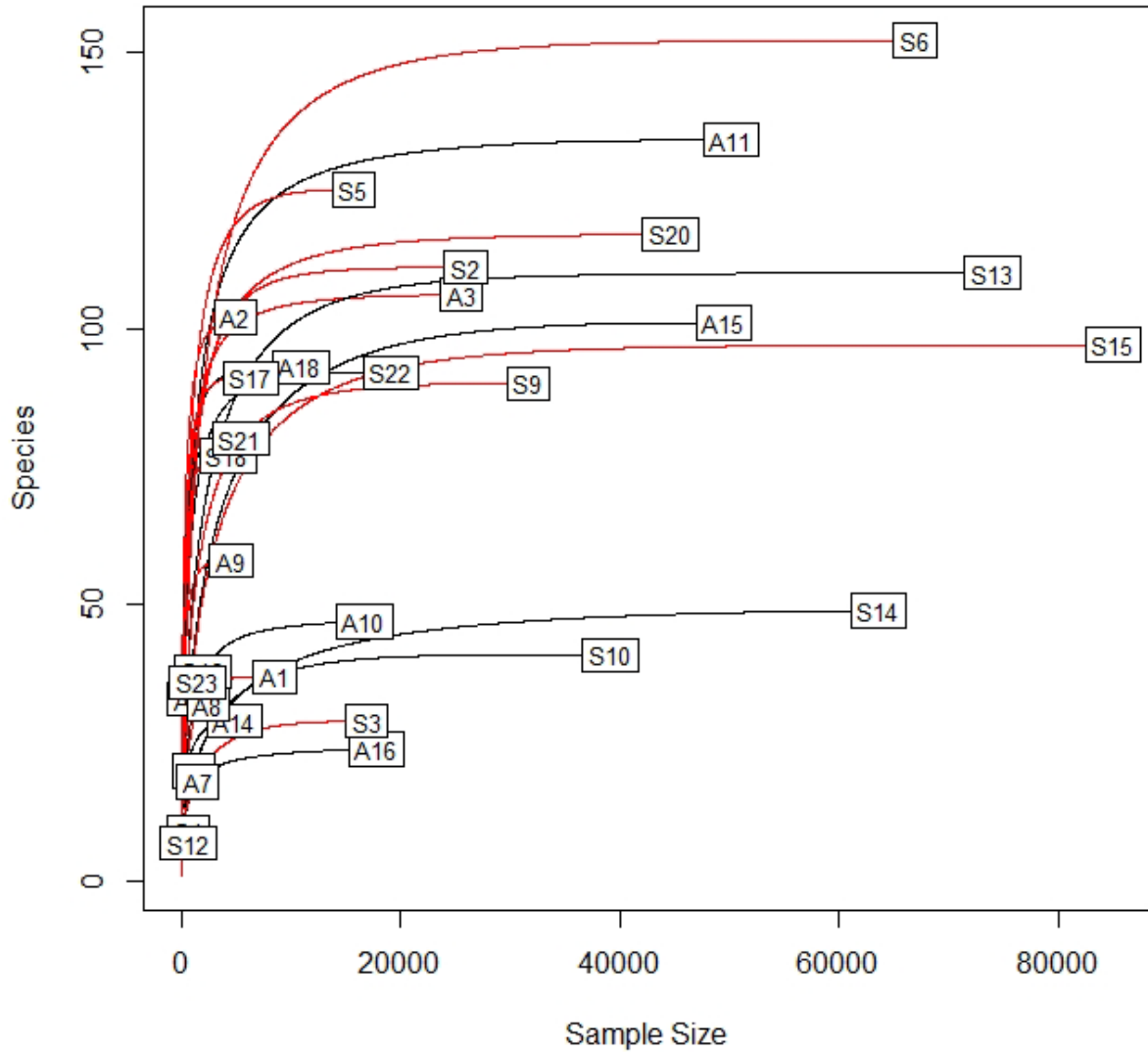
Figure 105: Rarefaction curve of next generation sequencing of the 16S amplicon from DNA extracted from oral swabs. Samples from uraemic animals are shown in red generally had higher numbers of species (sequence variants) per sample. Such rarefaction curves can be used to assess the adequacy of sequencing depth, with lines flattening to horizontal indicating that further sequencing is unlikely to reveal further bacterial diversity.
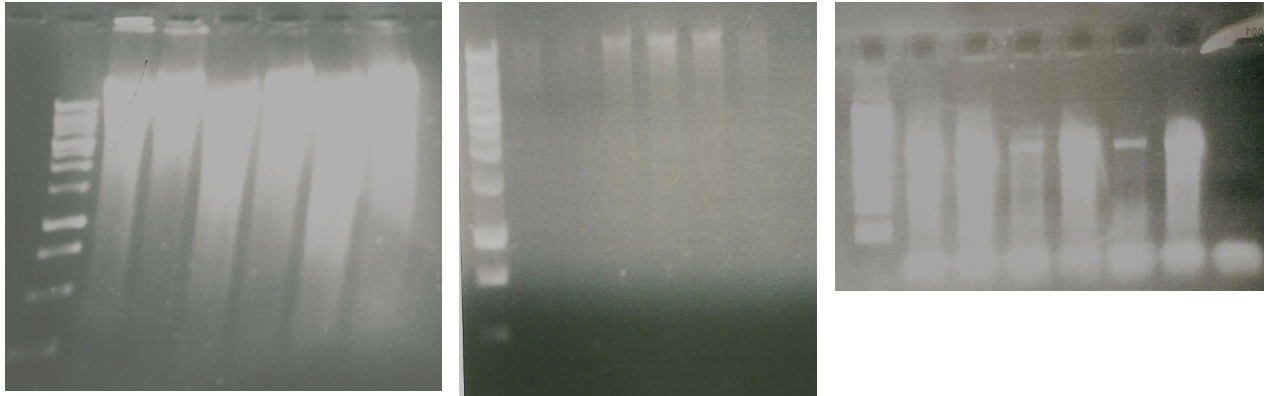
Figure 106: DNA extraction from stool for next-generation sequencing. The 1% agarose gels in each picture are loaded in a similar order: (from left to right) DNA ladder, 2 caecal samples from chemically-induced uraemic animals, 2 caecal samples from SNx animals, 2 caecal samples from sham-operated (control) animals, negative control. A: DNA freshly extracted before PCR, showing large amounts of DNA were easily extracted from these caecal samples (corresponding DNA concentrations measured using a DeNovix spectrophotometer were 210-325ng/µL). B Post-PCR using DNA extracted using the FastDNA$^©$ kit from MP Bio. Note the poor amplification in all samples of the desired band, and especially in samples 1, 2 and 6. C: Post-PCR using DNA extracted using the PowerSoil$^©$ kit from Mobio (now Qiagen). A clear band is seen in all samples, although a significant amount of shearing has occurred during the experimental procedure.

Forward PCR primer - 27F-YM

5'-

AATGATACGGCGACCACCGAGATCTACACXXXXXXXXAGTCAGTCTGTCAGAGTTTGATYMTGGCTC

AG- 3'

Reverse PCR primer - 338R-R

5'- CAAGCAGAAGACGGCATACGAGATXXXXXXXXTATGGTAATTCATGCTGCCTCCCGTAGRAGT -3'

Figure 107: Barcoded primer design for high throughput pooled sequencing. The primers included an adapter sequence (purple) for attachment to the Illumina flow cell; an eight base barcode (red) unique to each sample for identification of reads to a particular animal; a 10-base primer pad (blue) to alter the Tm of the primer, improving specificity at the expense of product; and a 2 base linker sequence (green). The black primer binding sequences are complementary to the 27F and 338R sequences of the 16S gene, with the inclusion of a degenerate base (orange) in the reverse primer to accommodate a common polymorphism seen in certain species oral bacteria and reduce bias against these organisms.

Plate C	REVERSE	1	2	3	4	5	6	7	8	9	10	11	12
FORWARD		SB-701	SB-702	SB-703	SB-704	SB-705	SB-706	SB-707	SB-708	SB-709	SB-710	SB-711	SB-712
A	SA-501												
B	SA-502												
C	SA-503												
D	SA-504												
E	SA-505												
F	SA-506												
G	SA-507												
H	SA-508												

Figure 108: Plate layout for next-generation sequencing. Forward (SA501 - SA508) and reverse (SB701 – SB712) barcoded primers were used in rows and columns, and DNA extracted from up to 96 individual samples was added to each well such that each had a unique combination of forward and reverse barcodes. For example, reads from the sample placed in the top left hand well would be identified by forward reads beginning with the SA-501 barcode and reverse reads beginning with the SB-701 barcode. Three other plates using different combinations of primers can be created, with the products normalized and pooled allowing DNA from up to 384 samples to be sequenced in parallel.

Appendix 3: Detailed microbiological analysis of sequencing data from chapter 4

This appendix describes detailed analysis of NGS sequencing data from the caecal fluid analyses in chapter 4, assessed using the *PhyloFactor* and *ANCOM* methodologies.

The microbial effects of uraemia on individual cohorts of animals are subtle and variable

Each cohort was examined independently, in non-aggregated datasets based on individual ASVs, using phylogentic techniques with log-ratio transformed abundance data.

No differences in alpha diversity were observed between control and uraemic animals in any of the cohorts when assessed using a range of measures including the Simpson and Shannon indices. Differences between samples in different cohorts when assessed using the Shannon index are explained by differences in sequencing depth between sequencing runs, Figure 109, p. 379.

Some degree of differential clustering between control and uraemic microbiotas was seen in several of the cohorts; this proved significant based on PerMANOVA in rat cohort 2 and mouse cohort 1; significance was not achieved despite the observed separation of samples owing to the small sample size in mouse cohort 2, Figure 110, p. 380.

Phylogenetic factorisation using the R package *PhyloFactor* was used to determine which taxonomic balances in relative abundance best served to distinguish between control and uraemic animals. The top three discriminatory factors for each cohort are described in Table 9, p. 382, and represented in Figure 111, p. 381; they generally separated small monophyletic clades or single taxa from the rest of the dataset. These splits in the taxonomic tree explained relatively small proportions of the total variance (an average of 0.78%, 0.52% and 0.44% of total variance, or 1.71% taking the top three discriminant factors together across all five cohorts), and the groups split off from the main dataset accounted for small but significant proportions of the total abundance data (those split off by the first, second and third factors averaging 3.44%, 1.09% and 2.18% of the total sequencing data, respectively, meaning that these top three factors accounted for an average of 6.71% of all reads across all cohorts).

The identity of taxa within the groups distinct from the main dataset by these discriminatory factors were assessed to determine common patterns across the cohorts, using published full length 16S rRNA gene sequences from the Ribosomal Database Project (RDP) and National Centre for Biotechnology Information (NCBI) databases alongside the SILVA database identities.

A complex and inconsistent picture emerged between different cohorts, in which different phylogenetically-defined sub-taxa responded differently to the effects of uraemia. All groups split off from the main dataset in the top three factors in rat cohorts 1 and 2 belonged to the family *Lachnospiraceae*; four of these groups (representing 11 individual taxa across both

cohorts) belonged to the NK4A136 group at genus level, while the remaining two groups (which together accounted for five taxa) belonged to the UCG-001 group.

In rat cohort 1, the five taxa split off in factor 1 were from the NK4A136 group that displayed close sequence homology (>98.5%) with each other and identified closely (at >98.5 and in some cases >99% sequence similarity) with published 16S rRNA gene sequences from the closely related genera *Hungatella*, *Lachrimispora* and *Enterocloster*. The factor 2 group comprised two taxa from the UCG-001 group, which were near identical to each other and most closely matched (although at only 96.2% homology) with the 16S rRNA gene sequence for *Dorea longicatena*. Factor 3 split off a single taxon also from the NK4A136 group, which showed 94.5% sequence similarity to *Blautia wexlerae*. Taxa in each of these groups showed significant decreases in isometric log ratio (ILR) balances in uraemic animals (ILR balance 0.148 in uraemic animals, p=0.003; balance 0.048, p=0001; and balance 0.016, p=001, respectively).

In rat cohort 2, only two of the top three factors splitting the dataset proved significant, reveal a complex pattern of association. Factor 1 split off a disparate group of *Lachnospiraceae* (sharing only 95.5% similarity between members) which demonstrated decreased abundances in uraemic animals (ILR balance 0.59 in uraemic animals, p=0.001), whereas factor two split off a single taxon of *Lachnospiraceae*, which actually increased in abundance in uraemic animals (ILR balance 54.2, p<0.001), despite showing greatest similarity with the *Hungatella*, *Lachrimispora* and *Enterocloster* cluster which decreased in abundance in uraemic animals in cohort 1.

Rat cohort 3 showed the least influence of uraemia on the microbiota, with only one factor (a single taxon most closely identified with *Ruminococcus champanellensis*) showing differential

abundance between treatment groups, with increased ILR balances in uraemic animals (ILR balance in uraemic animals 0.85, p=0.047).

In contrast, in mouse cohort 1, multiple factors showed a strong statistical significance in ILR balances between treatment groups, splitting off clades that accounted for significant proportions of the total amount of sequenced reads. Factors 1 and 2 described taxonomic splits located in the phylum *Bacteroidota*, and centering on family *Muribaculaceae*, with both clades split off showing significantly increased abundances in uraemic animals (ILR balance 13.9 in uraemic animals, p<0.001; and balance 158.8, p<0.001; respectively). Factor 3 split off a single taxon from the family *Lachnospiraceae* from the rest of the dataset, which again was significantly elevated in uraemic samples (ILR balance 8.29, p<0.001); this had closest sequence homology with isolates from the NK4A136 group including 95% sequence similarity with three *Blautia* isolates and others from genera *Eisenbergiella*, *Bariatricus* and *Tyzerella*.

The method of phylogenetic factorisation does not easily permit adjustment of significance in the light of multiple hypothesis testing; therefore, as an additional measure, the ANalysis of the COMposition of microbiotas (ANCOM) methodology was used at the level of individual ASVs to determine whether any were differentially abundant between control and uraemic animals. A similarly inconsistent pattern emerged between cohorts: there were no ASVs differentially abundant between treatment groups after multiple-hypothesis testing in three of the cohorts; whereas in rat cohort 2 there were four and in mouse cohort 1 there were 19 (Table 10, p. 384). No obvious pattern could be discerned that would predict why certain bacterial taxa were likely to be over- or under-represented in uraemic animals compared to controls; although for many of

the isolates, confident identification was possible only at the level of family meaning selective differences at genus, species or strain level may have been relevant.
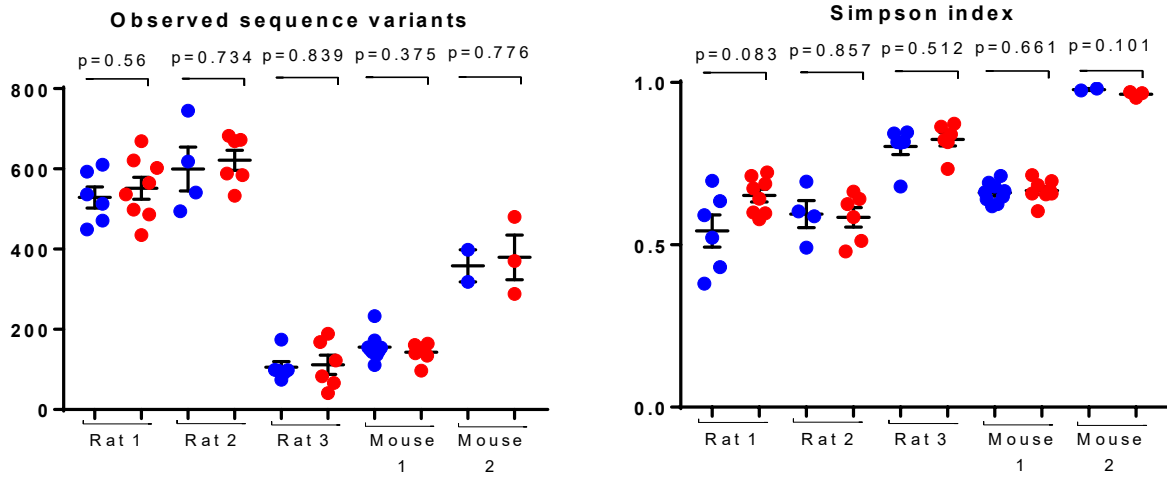
Figure 109: Alpha diversity as assessed by the number of observed sequencing variants per samples, and the Simpson index. Each point represents an individual microbial community, grouped according to cohort and with control samples shown in blue and uraemic samples in red.
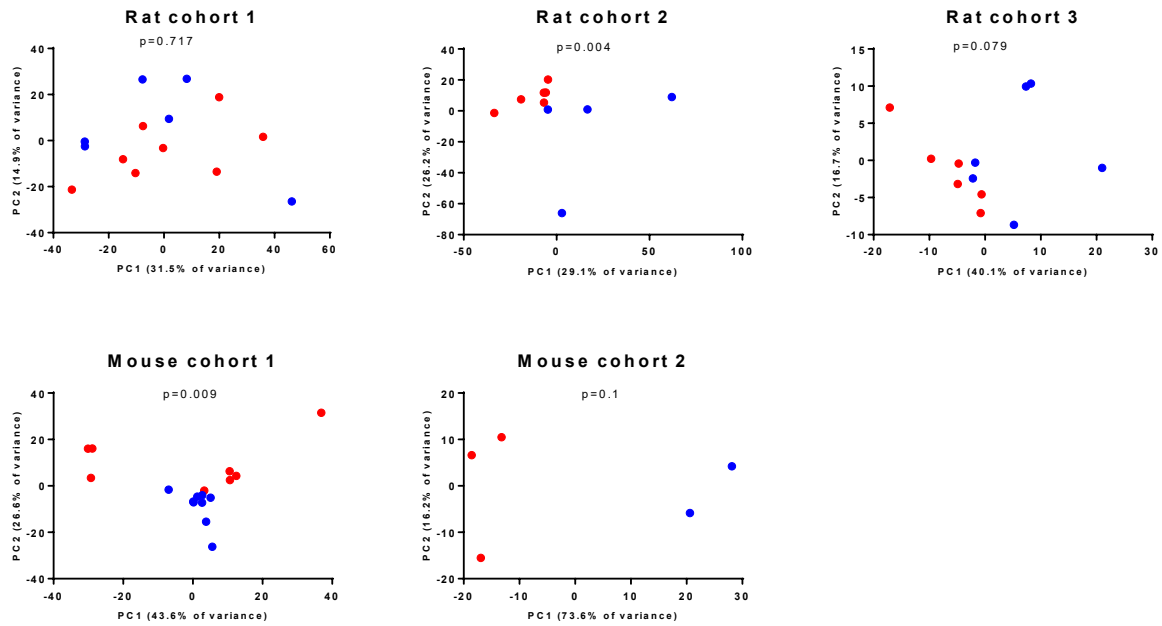
Figure 110: Ordination plots of log-ratio transformed, phylogenetically ordered sequence abundance data plotted in Euclidean space. Each point represents the gut microbiota of a single animal, coloured blue for controls and red for uraemic. The p value reflects the significance of differential clustering as determined by PerMANOVA and the contribution of the first and second principal components to explaining total overall variance are indicated on the x and y axes respectively.

A
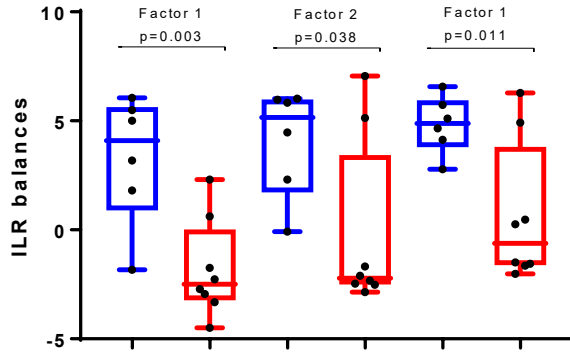
B
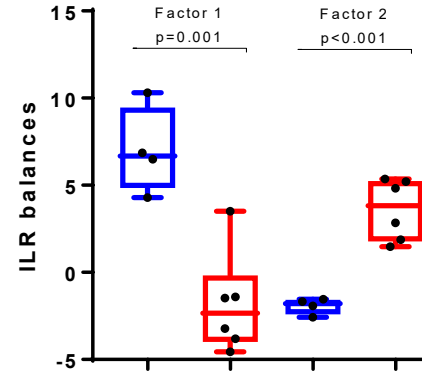
C
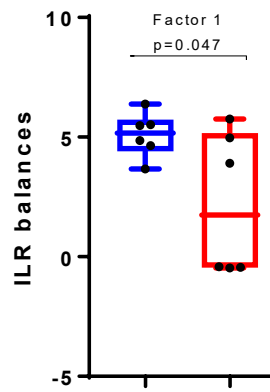
D
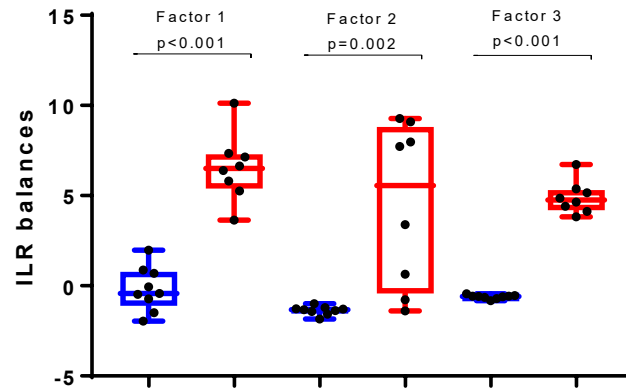
Figure 111: Discriminant ILR balances between control (blue) and uraemic (red) animals in four of the experimental datasets. A, rat cohort 1; B, rat cohort 2; C, rat cohort 3; D, mouse cohort 1.

Factor number	Number group 1	Number group 2	Variance explained	p	group % uraemic animals	group % controls	Smaller group Family
Rat cohort 1							
1	5	1324	0.002	0.003	0.134	6.569	Lachnospiraceae gp NK4A136
2	2	1322	0.001	0.038	0.132	0.271	Lachnospiraceae gp UGC-001
3	1	1321	0.0013	0.011	0.233	0.776	Lachnospiraceae gp NK4A136
Rat cohort 2							
1	4	1222	0.006	0.001	0.109	6.181	Lachnospiraceae gp NK4A136
2	1	1221	0.002	0.0003	0.487	0	Lachnospiraceae gp NK4A136
3	3	1218	0.002	0.01	6.017	2.625	Lachnospiraceae gp UGC-001
Rat cohort 3							
1	5	706	0.003	0.073	8.44	0.554	Erysipelotrichaceae;Turicibacter
2	1	705	0.002	0.074	0	6.268	Ruminococcaceae;Ruminococcus
3	1	704	0.002	0.047	4.51	1.967	Ruminococcaceae;Ruminococcus
Mouse cohort 1							
1	20	963	0.007	<0.001	9.184	2.236	Prevotellaceae/Bacteroidaceae/Muribaculaceae
2	5	958	0.005	<0.001	2.189	0	Muribaculaceae
3	1	957	0.005	<0.001	2.174	0	Lachnospiraceae gp NK4A136
Mouse cohort 2							
1	5	961	0.021	0.001	0.121	4.19	Erysipelotrichaceae;Faecalibaculum
2	17	944	0.014	0.002	0.005	2.054	Clostridia UCG-014
3	4	940	0.01	0.004	2.516	0.052	Muribaculaceae

Table 9: Discriminatory ILR balances between control and uraemic animals in different cohorts. For each cohort, the most strongly discriminatory isometric log ratio (ILR) balances distinguishing control from uraemic samples are shown. Columns B and C describe, respectively, the number of individual taxa within the smaller group split off from the main tree, and the number of taxa remaining in the tree, after the division. Columns D and E detail the amount of variance explained by the balance and the p value. Columns F and G describe the average sum relative abundance of all taxa in control samples in that cohort and uraemic samples in that cohort. Finally, column H locates the level at which the division occurs in the taxonomic tree; which samples are cleaved off in the smaller group.

Highest abundance cut-off	Relative abundance in control	Relative abundance in uraemic	Proportional increase or decrease in uraemia	Phylum	Genus
Rat cohort 1					
None					
Rat cohort 2					
Increased in controls					
0.8	4.576855	0.052634	0.011	Firmicutes	Lachnospiraceae NK4A136 group
0.7	0.053008	0	Absent in uraemic	Firmicutes	Colidextribacter
Increased in uraemic animals					
0.8	0	0.486741	Absent in control	Firmicutes	Lachnospiraceae NK4A136 group
0.6	0.003879	0.095228	23.79	Firmicutes	Lachnoclostridium
Rat cohort 3					
None					
Mouse cohort 1					
Increased in controls					
0.7	0.679957	0	Absent in uraemic	Firmicutes	Oscillobacter
0.7	0.231264	0	Absent in uraemic	Firmicutes	Unclassified, f. Lachnospiraceae
0.8	0.535346	0	Absent in uraemic	Firmicutes	Unclassified, o. Clostridia
0.7	2.33424	0.624557	0.268	Bacteroidota	Unclassified, f. Muribaculaceae
Increased in uraemic animals					
0.9	0.052669	1.935047	36.75	Firmicutes	Unclassified, f. Lachnospiraceae
0.8	0.032908	0.613343	18.64	Firmicutes	Oscillobacter
0.6	0	0.495447	Absent in control	Bacteroidota	Unclassified, f. Muribaculaceae
0.8	0	1.083519	Absent in control	Bacteroidota	Unclassified, f. Muribaculaceae
0.6	0.05452	0.43393		Firmicutes	Lachnoclostridium
0.8	0	0.770804	Absent in control	Firmicutes	Unclassified, f. Lachnospiraceae
0.6	0	0.642868	Absent in control	Bacteroidota	Unclassified, f. Muribaculaceae
0.9	0	2.174041	Absent in	Firmicutes	Lachnospiraceae

			control		NK4A136 group
0.6	0	0.45587	Absent in control	Firmicutes	Lachnospiraceae UCG-001 group
0.8	0	0.723112	Absent in control	Bacteroidota	Unclassified, f. Muribaculaceae
0.7	0	0.22762	Absent in control	Firmicutes	Incertae Sedis
0.6	0.035253	0.262314	7.44	Actinobacteriota	Enterorhabdus
0.9	0.135813	2.265105	16.68	Bacteroidota	Unclassified, f. Muribaculaceae
0.7	0	0.324163	Absent in control	Bacteroidota	Unclassified, f. Muribaculaceae
0.6	0	0.485751	Absent in control	Bacteroidota	Muribaculum
Mouse cohort 2					
None					

Table 10: Amplicon sequencing variants (ASVs) showing discriminant abundance differences between control and uraemic animals in each cohort. The ANCOM methodology is used with multiple hypothesis correction and a significance cutoff of 0.6. For each ASV the highest abundance cut-off (a crude signifier of the strength of association), and proportional abundance in control and in uraemic animals is shown, along with the identification at phylum and genus level.

Appendix four: Pilot data using lactulose to modulate the gut microbiome

Methods

Animal work: Twenty-seven wild-type outbred Wister IGS rats were obtained from Charles Rivers and rendered uraemic using the subtotal nephrectomy model as described previously. Prior to surgery, rats were swapped between cages each day for a week in order to heterogenise resident microbiota. Seventeen underwent SNx and ten underwent sham procedures. Four weeks after surgery, lactulose was administered mixed into drinking water to eight SNx animals and six controls, with the remaining animals in each group continuing to receive tap water. Details of the lactulose administration and the rationale for dosing are given below. Animals were then sacrificed four weeks later, eight weeks after the completion of surgical procedures, after 24-hour individual metabolism caging to allow urine and stool collection. Serum samples were obtained at the time of sacrifice and sent for routine biochemical analysis (Idexx, Germany).

Lactulose dosing: Lactulose is available over the counter in the UK at a concentration of 10g/15ml. Therapeutic doses of lactulose in humans is up to 100g daily in divided dose for ammonia reduction in hepatic encephalopathy, with individual dose adjustments being made to target 2-3 bowel openings per day of soft stool, or a faecal pH <5.0. [506] In rats, an effective dose (ED50) of 3.8g/kg/day has been shown to produce soft stool, with 5.4g/kg/day as a

sufficient dose for significant reductions in the insoluble concentration of caecal contents. [507] The maximum tolerated dose is 18g/kg/day and the calculated lethal dose 31g/kg/day in male Wistar rats. Recent studies investigating the role of lactulose in rodent models used twice daily oral gavage (at doses of 2.4g/kg/day [508] or 5g/kg/day [509]), or lactulose mixed with food pellets [510], in the case of the oral gavage studies for only a short period of time. In order to allow a longer period of treatment to allow for full transformation of gut bacterial communities and for the longer-term effects of short chain fatty acid generation to have systemic effects, and also because uraemic animals may eat less food as a result of uraemia, lactulose was administered in the drinking water, targeting administration of 5g/kg/day, based on mean weekly measurements of rat weights. This was then used to calculate the dilution of the 10g/15ml lactulose solution in the drinking water for that week.

Analysis of the caecal microbiota: Caecal fluid obtained at the time of sacrifice was loaded directly into bead-beating tubes from the ZymoBIONICS^{TM} DNA/RNA Mini Kit, and stored at -80ºC. DNA was extracted according to manufacturers instructions and in-house library preparation and PCR of the V1/V2 hypervariable region of the 16S rRNA genes was carried out as described earlier. MiSeq sequencing was carried out at the DNA Sequencing Facility, Department of Biochemistry, University of Cambridge.

Results

Experimental observations reveal significant problems with the method of lactulose administration

Unfortunately significant problems emerged with using lactulose added to drinking water. Due to presumed bacterial overgrowth in the sugary water, the solutions rapidly became brackish and discoloured, despite being changed three times per week.

Basic observations of the experimental animals revealed that for both control and uraemic animals, those administered lactulose had lower body weight than those receiving tap water (Figure 112, p. 391).

Urine output was lower in uraemic animals receiving lactulose compared to those receiving water, although as expected all animals in the uraemic group were polyuric compared with controls, as a result of the loss of urinary concentrating ability which is observed in chronic renal insufficiency (Figure 113, p. 392).

Lactulose administration may lower serum urea

Whilst there was no significant difference in creatinine concentration between groups (means serum creatinine 96.33umol/L in water treated uraemic animals vs 89.5umol/L in lactulose treated animals, p=0.437 by Welch's t-test); the serum urea was lower in lactulose treated

uraemic animals compared to those receiving water (24.9mmol/L in water treated vs 19.8mmol/L in lactulose treated; p=0.003, Figure 114, p. 393).

Analysis of gut microbiome

Samples with fewer than 5000 reads per samples were excluded from subsequent analysis, meaning that in the smallest of the experimental groups (sham/lactulose, n=4), only two samples remained, meaning that confident conclusions could not be drawn from data from these animals. Because of the previously described problems with the experimental method, only a brief analysis of the caecal microbiota was conducted in order to establish trends which might inform future work.

Samples from animals treated with lactulose displayed reduced alpha diversity compared to those with pure tap water, a trend seen in both control and uraemic animals when analysed by both Simpson and Shannon alpha diversity indices, Figure 115, p. 394.

Uraemic samples were extracted from the dataset and used to ascertain whether lactulose administration caused differential clustering. Principal coordinate analysis (PCA) suggested that despite some overlap, there may be a difference associated with lactulose administration in axis 2, although the differential clustering was not significant when assessed by PerMANOVA ($R^2 = 0.124$, p=0.075), Figure 116, p. 395.

A brief analysis of community composition was conducted using the ANCOM methodology as described earlier, at all taxonomic levels from individual amplicon sequencing variants up to phylum level.

Differential abundance was clear between lactulose and water treated animals as high a class level, with an increase in *Actinobacteria*, and specifically in ASVs representing the species *Bifidobacterium animalis*, which was substantially over-represented in samples from lactulose-treated animals. At genus level, a genus from family *Lachnospiraceae*, which are known to contain many species with high metabolic activity including SCFA production, were over-represented in lactulose-treated animals whilst a genus from family *Ruminococcaceae* were over-represented in water-treated animals. This is reflected in compositional bar charts represented in Figure 117, p. 396.

Discussion

Addition of lactulose to the drinking water of experimental animal in this pilot experiment was methodologically flawed, because of obvious subsequent bacterial contamination of the drinking water. This likely led to reduced water intake (based on reduced urine output of lactulose treated animals), and reduced body weight. This prevented any robust conclusions to be drawn from the reduction in serum urea in these animals, or from subsequent microbiological analysis of their caecal fluid.

However, a reduction in serum urea is an expected effect of lactulose treatment, and so the reduction seen would be in keeping with the anticipated effect. Likewise a significant increase in *Bifidobacteria* and a genus within family *Lachnospiraceae* are associated with an increase in carbohydrate fermenting organisms, typical of animals fed a prebiotic diet.

Thus, although suggesting that prebiotic treatment may have beneficial effects on the biochemical and microbiological profile of animals with experimental uraemia, this pilot work was clearly compromised by the method of prebiotic administration chosen, and no firm conclusions of efficacy could be drawn.

Options for further work were either to choose a different method of lactulose administration (eg by oral gavage, as reported in other studies [508-510]), or to use a different method type of prebiotic. The decision to proceed using an alternative type of prebiotic was made because it was desirable to achieve a longer period of prebiotic administration (4 weeks) than is really feasible by twice daily gavage, and secondly because other forms of prebiotic are associated with production of a broader range of SCFA that lactulose, which really only causes production of acetate and lactate.

Thus, we decided instead to proceed with further experiments based around therapeutic administration of diets enriched with fructo-oligosaccharide (FOS).
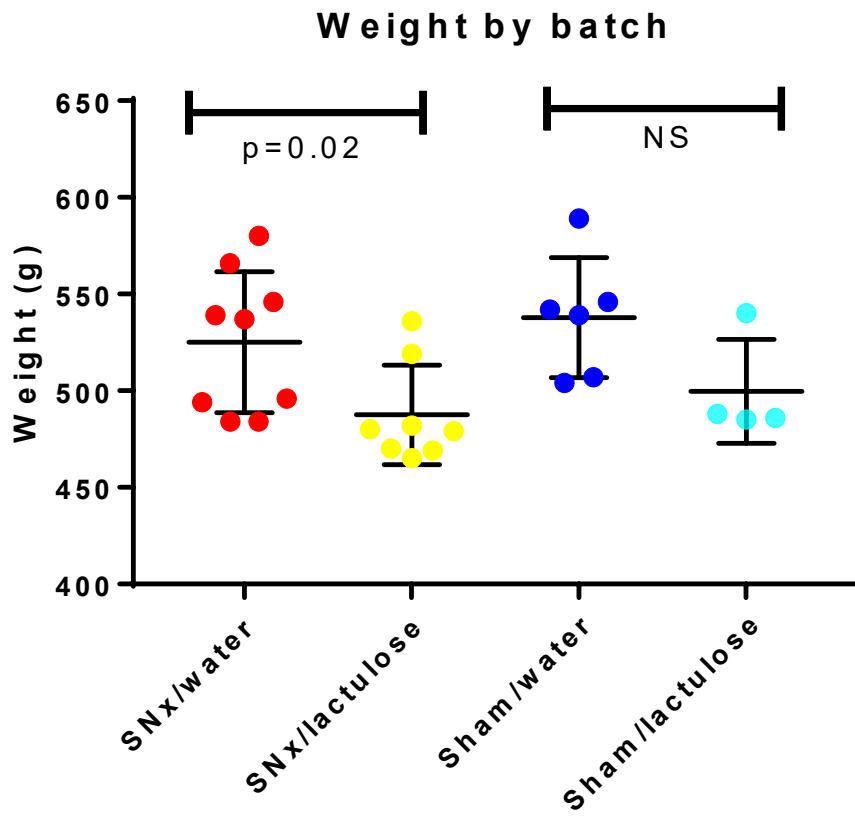
Figure 112: Weight at time of sacrifice according to experimental interventions.
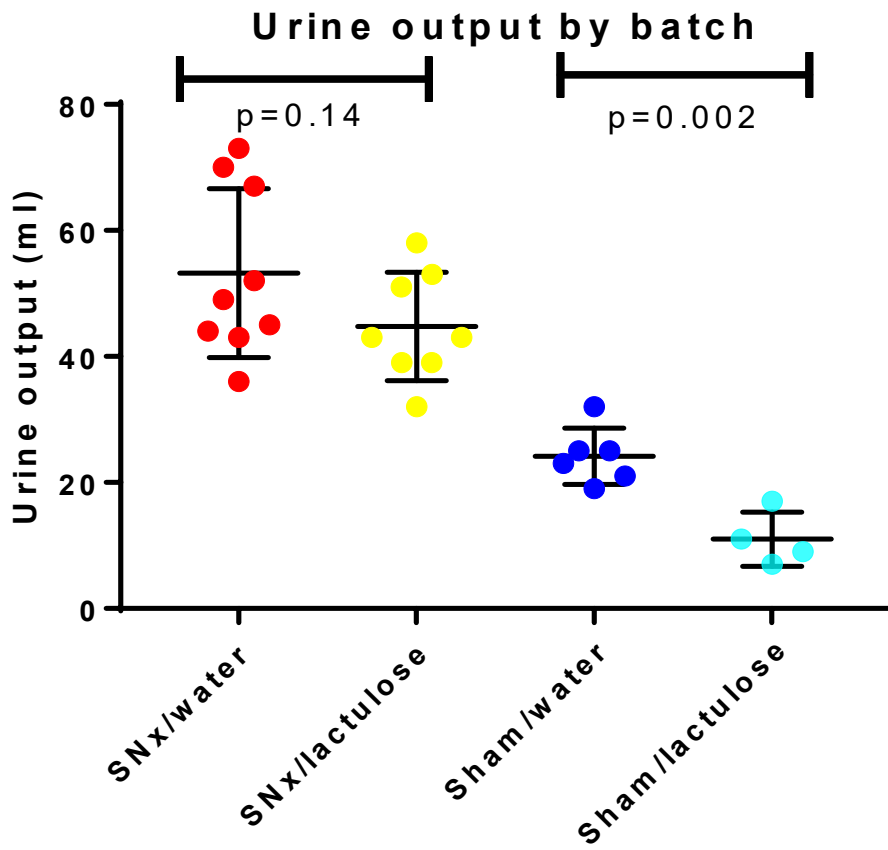
Figure 113: 24-hour urine collection immediately prior to sacrifice according to experimental interventions.
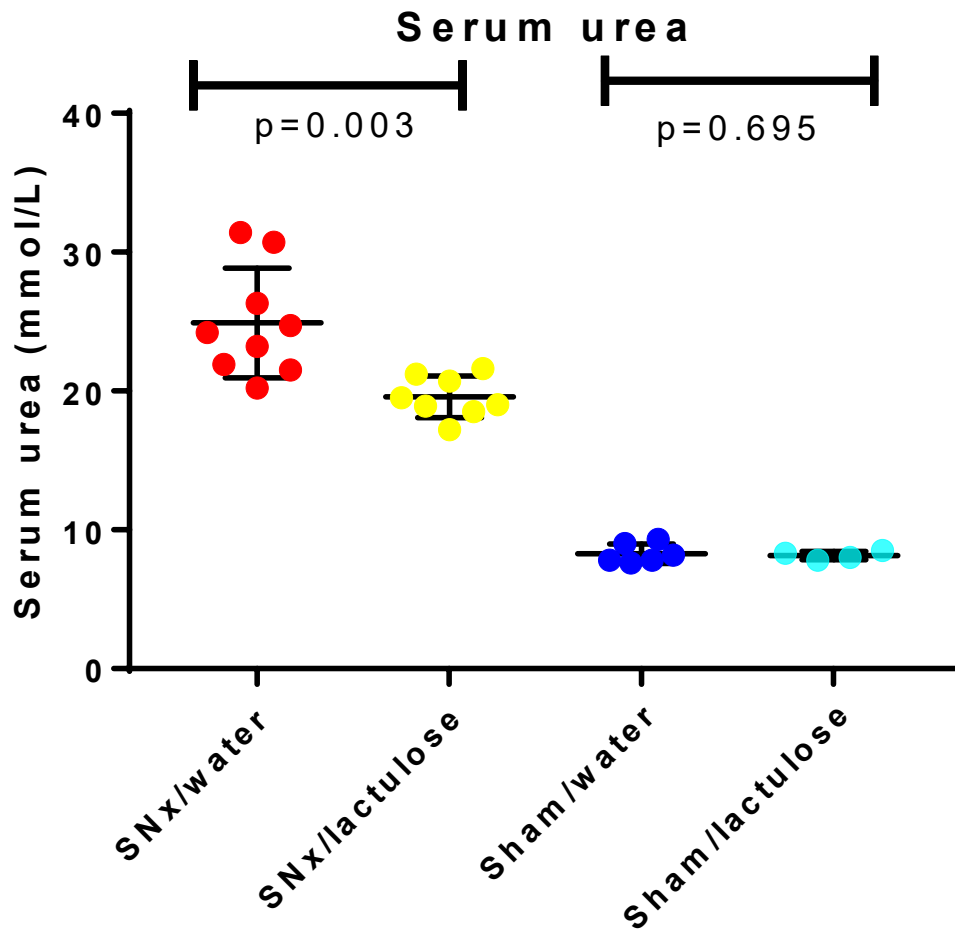
Figure 114: Serum urea according to experimental interventions.
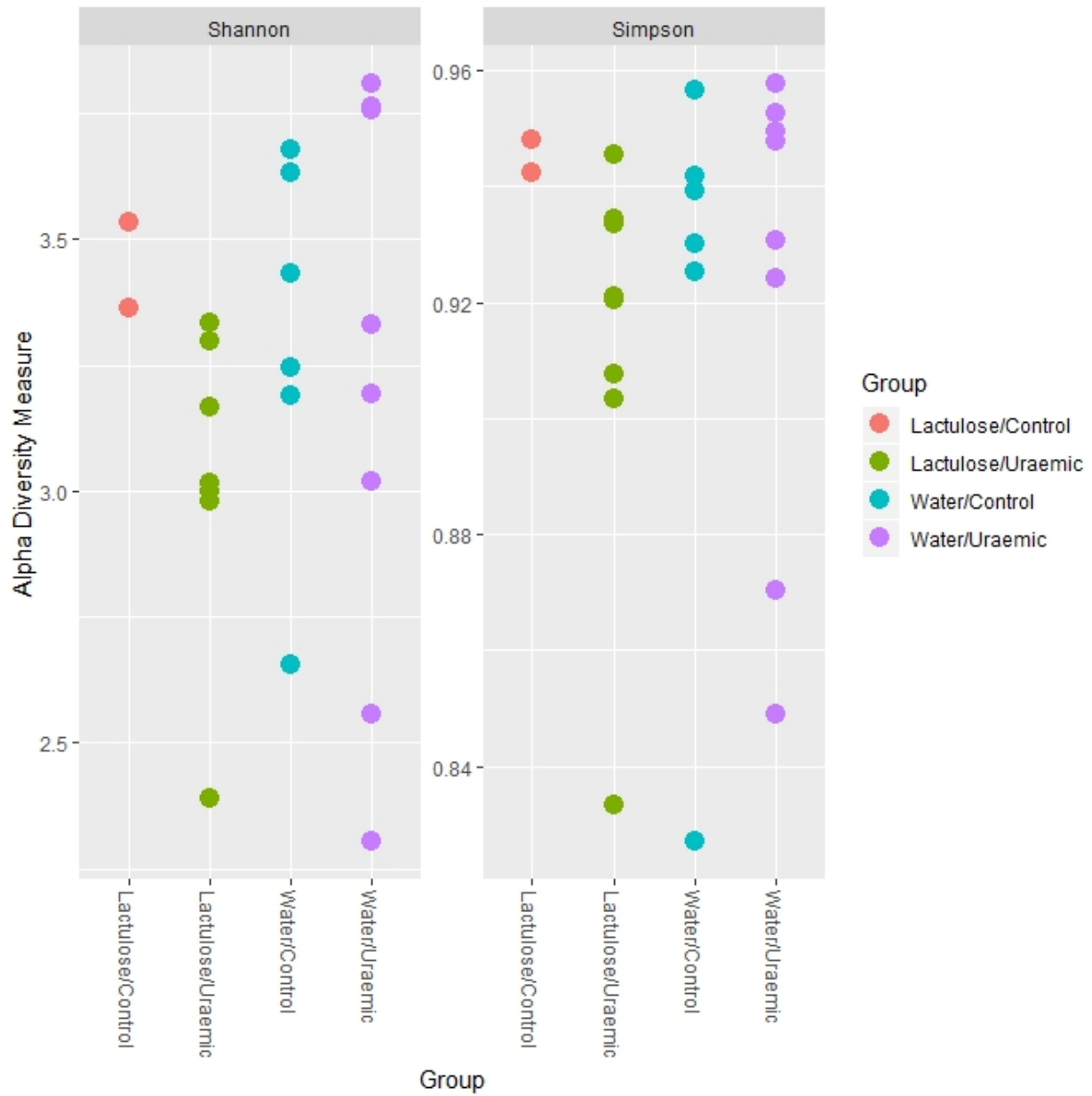
Figure 115: Alpha diversity measured using Shannon and Simpson indices according to experimental interventions. Each point represents an individual sample.
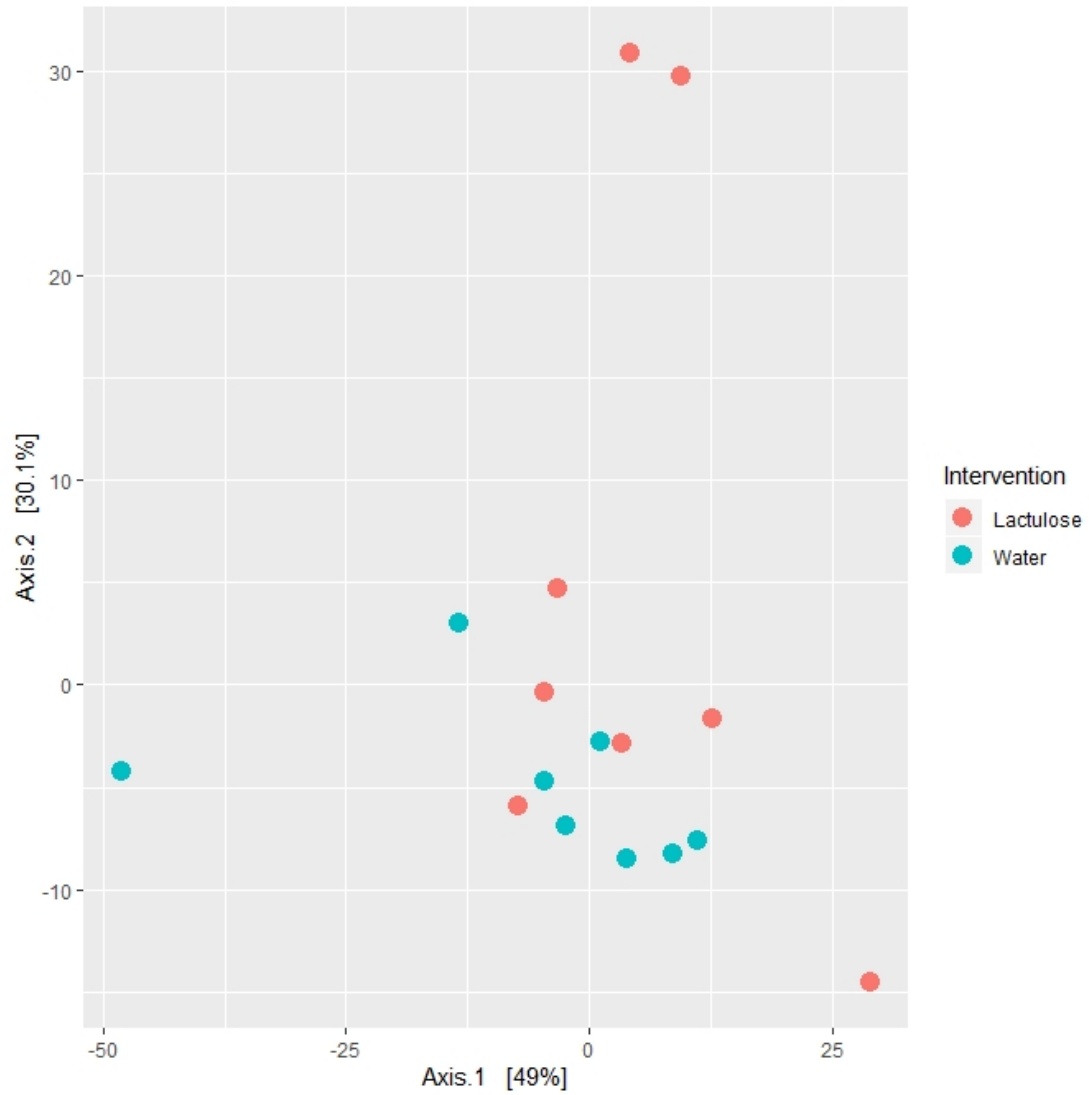
Figure 116: Principal coordinate analysis (PCA) of uraemic samples, coloured according to lactulose administration. Each point represents an individual sample.
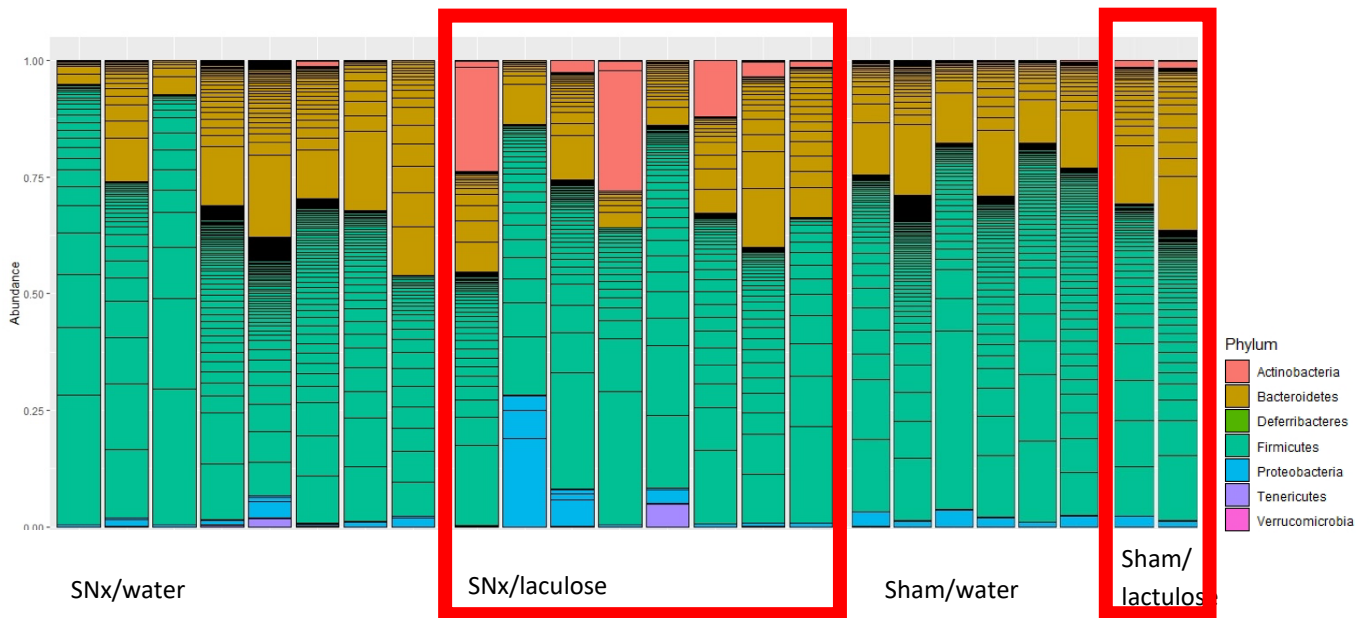
Figure 117: Proportional composition of the caecal microbiome of experimental animals. Each bar represents the total caecal bacterial community of an individual animal. Horizontal divisions are according to subtaxa, coloured by phylum identity.

Appendix 5: Supplementary tables

	Surgically-induced uraemia		Chemically-induced uraemia	
	Control	**Uraemic**	**Control**	**Uraemic**
	-0.0025	-0.08221	0.039521	-0.119470029
	-0.05962	-0.09504	-0.01958	-0.147320906
	-0.00041	-0.11127	0.021319	-0.156970029
	0.009783	-0.17684	0.056736	-0.21431652
	-0.01401	-0.15502	-0.04897	-0.128790205
	0.013182	-0.08441	-0.00445	-0.126158626
	-0.00842	-0.03967	0.054982	-0.108943713
	0.066801	-0.06467	-0.00543	-0.109272661
	-0.0048	-0.02476	-0.02528	-0.121772661
			-0.06885	-0.136100146
				-0.081641082
				-0.119141082
				-0.090084064
Mean	6.66667E-07	-0.092654444	-6.1E-17	-0.127690902
p	0.000367808		5.99247E-07	

Table 11: Periodontal bone loss in rats. Each point represents the average of multiple measurements over the buccal and lingual surfaces of all molar roots in a single rat, expressed relative to the average amount of bone loss in all control animals. Means are calculated for each group, and significance assessed by the Student t-test with Welch's correction.

Rat	Treatment	8 minute salivary volume (ml)	pH	Salivary urea	Serum urea
1	Uraemic	89	8.1	2.247584	6.11388
2	Uraemic	71	8.06	5.839821	17.04461
3	Uraemic	59	7.72	4.010985	10.5611
4	Uraemic	35	8.58	4.996166	7.43922
5	Uraemic		8.34	3.995001	7.577415
12	Uraemic	64	8.27	2.596235	8.772885
13	Uraemic	38	8.28	2.390108	7.657335
6	Control	42	7.89	1.542123	3.64635
7	Control	97	8.09	1.471361	3.341655
8	Control	23	8.5	1.522976	3.17349
9	Control	26	8.27	1.757075	4.713615
10	Control	57	8.3	1.806692	3.494835
11	Control	40	8.33	1.634031	4.547115
	Ur mean	59.33333	8.192857	3.725129	9.309492
	Ct mean	47.5	8.23	1.622376	3.81951
	p	0.415177	0.786144	0.006809	0.007129

Table 12: Rat saliva. Means are calculated for each group, and significance assessed by the Student t-test with Welch's correction.

Animal	Treatment	Acetate	Lactate	3-Hydroxyisovalerate	Acetoin	Succinate	Dimethyl sulphone	Glycerol	Formate
1	Uremic	92.75913	43.57964	31.7378	13.38607	11.73828	9.197662	67.34918	4.230157
2	Uremic	75.81494	48.00739	37.18551	13.47971	8.766325	13.43784	158.3737	2.038419
3	Uremic	78.36038	38.72408	32.14409	11.90122	7.097108	8.297988	824.1796	1.289339
4	Uremic	86.01184	55.7325	20.89384	7.569663	12.32688	5.46744	540.3971	1.56307
5	Uremic	120.4372	28.77564	24.5643	11.77292	8.721744	11.89906	628.3289	2.525976
12	Uremic	70.30469	37.49793	29.61918	12.62755	8.419812	7.851297	117.9882	0.63884
13	Uremic	100.0675	177.1647	34.60687	14.4181	9.699386	11.45069	140.1344	0.334284
6	Control	123.3265	105.0295	46.37138	15.01217	8.248937	6.291064	536.3801	1.659812
7	Control	99.41525	179.3148	46.47522	16.68206	13.93438	8.358535	53.31192	2.937516
8	Control	152.7733	105.7513	19.74186	8.822669	8.973874	3.01561	536.8972	1.662941
9	Control	136.6578	51.87838	29.16875	10.78286	7.487479	6.303263	102.3334	1.785663
10	Control	96.50084	135.2961	23.65266	9.704137	6.664695	2.193621	443.8807	1.22179
11	Control	124.4744	123.5818	22.65013	10.1792	9.933598	4.561678	77.06765	1.295597
	Uremic mean	89.10795	61.35455	30.10737	12.16503	9.538505	9.657425	353.8216	1.802869
	Control mean	122.1914	116.8086	31.34334	11.86385	9.20716	5.120628	291.6452	1.760553
	p	0.013495	0.056231	0.824833	0.850656	0.799956	0.007944	0.686922	0.941025

Table 13: Salivary metabolites measured using ^{1}H-NMR spectroscopy. Significance is calculated between control and uraemic animals using Student's t-test and Welch's correction.

Cage	Mouse	Treatment	Periodontal bone loss
1	1	Uraemic	-0.01997
	2	Uraemic	-0.01565
	3	Uraemic	-0.03222
	4	Uraemic	-0.01798
	5	Uraemic	-0.012
2	6	Uraemic	-0.01321
	7	Uraemic	-0.01134
	8	Uraemic	-0.01395
	9	Uraemic	-0.02677
	10	Uraemic	-0.00407
			0.64393
3	11	Control	0.011774
	12	Control	0.007064
	13	Control	-0.01146
	14	Control	0.003214
	15	Control	0.013359
4	16	Control	-0.00494
	17	Control	-0.00035
	18	Control	0.003758
	19	Control	-0.00938
	20	Control	-0.01304
			0.532454
			-0.01672
			-1.00E-07
			0.000504

Table 14: Periodontal bone loss in mice. Each point represents the average of multiple measurements over the buccal and lingual surfaces of all molar roots in a single mouse, expressed relative to the average amount of bone loss in all control animals. Means are calculated for each group, and significance assessed by Student's t-test with Welch's correction.

Mouse	Cage	Donor mouse	Treatment	Periodontal bone loss
1	1	11	Control recipient	0.009821
2			Control recipient	-0.0051
3		12	Control recipient	-0.00345
4	2	13	Control recipient	0.005246
5			Control recipient	-0.01101
6		14	Control recipient	0.006469
7			Control recipient	-0.00069
8	3	1	Uraemic recipient	-0.05503
9			Uraemic recipient	-0.03443
10		2	Uraemic recipient	-0.04711
11			Uraemic recipient	-0.03383
12	4	3	Uraemic recipient	-0.02578
13			Uraemic recipient	-0.05436
14		4	Uraemic recipient	-0.04004
15			Uraemic recipient	-0.04887
			Control recipients	0.000183714
			Uraemic recipients	-0.04243125
			p	7.16882E-07

Table 15: Each point represents the average of multiple measurements over the buccal and lingual surfaces of all molar roots in a single mouse, expressed relative to the average amount of bone loss in all control animals. Means are calculated for each group, and significance is assessed using Welch's t-test for unequal variances.

		Trimethylamine (TMA)	Trimethylamine-N-oxide (TMAO)	Indoxyl sulphate	Acetate	Propionate	Butyrate	Lactate	Acetoin	Benzoate	Hippurate
Rat 1	Control	0.03	0.43	0.02	1.77	0.01	0.12	2.65	3.43	0.56	0.04
	Uraemic	0.08	0.53	0.02	2.00	0.01	0.13	3.06	3.93	0.55	0.04
	p	0.26	0.36	0.92	0.73	0.01	0.62	0.72	0.70	0.82	0.84
Rat 2	Control	0.06	0.43	0.02	0.61	0.01	0.09	0.82	1.26	0.20	0.40
	Uraemic	0.34	0.25	0.02	1.32	0.02	0.10	0.81	1.46	0.26	0.28
	p	0.03	0.02	0.96	0.03	0.06	0.45	0.95	0.42	0.35	0.48
Rat 3	Control	0.01	0.39	0.01	0.27	0.01	0.10	0.33	0.01	0.12	0.21
	Uraemic	0.04	0.25	0.02	0.70	0.02	0.13	0.59	0.03	0.15	0.12
	p	0.25	0.00	0.00	0.12	0.00	0.23	0.19	0.00	0.50	0.19
Mouse 1	Control	4.61	1.77	0.07	21.97	0.10	0.30	11.05	0.21	0.31	0.22
	Uraemic	2.42	2.72	0.09	19.73	0.11	0.17	7.11	0.34	0.37	0.33
	p	0.09	0.06	0.05	0.79	0.44	0.00	0.31	0.47	0.69	0.48
All rat	Control	0.03	0.41	0.02	0.80	0.01	0.10	1.13	1.35	0.27	0.21
	Uraemic	0.13	0.34	0.02	1.31	0.02	0.12	1.51	1.76	0.32	0.13
	p	0.02	0.15	0.13	0.09	0.00	0.12	0.44	0.52	0.48	0.21
All samples	Control	1.40	0.82	0.03	7.15	0.04	0.16	4.11	1.01	0.28	0.22
	Uraemic	0.83	1.06	0.04	6.89	0.05	0.14	3.21	1.33	0.33	0.19
	p	0.35	0.38	0.32	0.94	0.40	0.26	0.57	0.50	0.42	0.72
Rat ANOVA	Batch effect	21.02	19.70	3.87	43.58	3.66	6.69	51.03	63.34	74.03	46.40
	p	0.00	0.00	0.24	<0.0001	0.52	0.28	<0.0001	<0.0001	<0.0001	<0.0001
	Treatment effect	14.08	5.46	3.07	6.25	8.72	6.85	0.55	0.37	0.41	4.11
	p	0.01	0.07	0.57	0.05	0.08	0.11	0.52	0.52	0.44	0.11
ANOVA, samples	Batch effect	67.22	60.04	74.02	42.87	63.42	65.73	55.09	64.96	33.09	20.05
	p	<0.0001	<0.0001	<0.0001	<0.0001	<0.0001	<0.0001	<0.0001	<0.0001	0.00	0.01
	Treatment effect	1.36	0.64	1.09	0.01	0.69	1.52	0.66	0.35	0.46	0.26
all	p	0.16	0.25	0.04	0.95	0.30	0.08	0.41	0.43	0.57	0.69

Table 16: Relative abundances of ten bacterial metabolites in the urine of experimental rodents determined by 1HNMH spectroscopy. For each metabolite listed, the mean metabolite:creatinine ratio for control and uraemic groups in shown for each cohort followed by the significance, assessed using the Student t test with Welch's correction. The same analyses to all rat samples analysed as a single group, and then to all samples including rats and mice. At the bottom, the results of a two way ANOVA for rat samples only, and then all samples together are presented, with each 2-way ANOVA analysis including the effect on the dependent variable (metabolite:creatinine ratio) of two independent variables; batch effect (ie the difference between cohorts), and treatment effect (control vs uraemic animals). The amount of variance (%) explained by the independent variable is followed by the significance of the association.

Samples		Observed	Chao1	ACE	Shannon	Simpson	InvSimpson	Fisher
All	Control	264.2727	276.7979	275.3142	4.218349	0.960381	50.06054	48.34638
	Uraemic	310.2167	323.2466	321.5804	4.48433	0.967609	58.18471	54.64726
	p	0.241869	0.258507	0.257115	0.071008	0.237533	0.320681	0.442636
All	Rat	338.1639	348.3587	347.4597	4.418917	0.964652	52.91533	54.19312
	Mouse	231.8519	247.5703	245.2234	4.287315	0.963588	55.86254	48.74272
	p	0.005922	0.01358	0.011582	0.374035	0.86245	0.723185	0.519674
All rat	Control	304.4815	313.3404	312.5974	4.134649	0.951707	40.73592	48.33108
	Uraemic	364.9118	376.1674	375.1445	4.644659	0.974931	62.58722	58.84826
	p	0.268216	0.246968	0.249008	0.011485	0.010399	0.012118	0.181531
All mouse	Control	225.5	241.5605	239.3626	4.299059	0.968745	59.05213	48.36114
	Uraemic	238.6923	254.0423	251.535	4.274668	0.958033	52.42759	49.15365
	p	0.809216	0.838598	0.840086	0.913894	0.23955	0.638785	0.958414
Al-Asmakh2020	Control	97.5	97.5	97.5	3.135402	0.914613	14.29764	11.95862
	Uraemic	215.8333	215.8333	215.8333	4.822523	0.986176	84.84954	28.13348
	p	6.15E-05	6.15E-05	6.15E-05	0.000518	0.005946	0.002882	4.36E-05
Kikuchi2017	Control	286.2	332.498	328.9492	4.937353	0.98775	84.71603	81.62513
	Uraemic	287.125	333.7404	329.3856	4.958876	0.988051	89.3964	83.00479
	p	0.943912	0.954696	0.982363	0.817995	0.866277	0.682319	0.789598
Mishima2015	Control	594.1667	661.5233	652.7835	5.630914	0.993499	162.2519	155.0729
	Uraemic	590.1667	643.808	635.7291	5.506364	0.990052	116.6685	143.4158
	p	0.887316	0.584555	0.568712	0.277395	0.145511	0.088232	0.311609
Kikuchi2015	Control	138.2	138.5	138.5587	4.312634	0.977377	45.81849	21.2936
	Uraemic	123	123	123.0408	4.245583	0.978734	47.23175	18.3392
	p	0.02145	0.024108	0.022356	0.343012	0.550787	0.784561	0.018107
Nanto-Hara2020	Control	82.375	86.1317	85.62427	3.397298	0.944038	18.13115	11.67478
	Uraemic	129.2857	137.7861	136.3981	3.255075	0.895321	10.15815	19.57703
	p	0.007956	0.010202	0.009521	0.222875	0.003342	4.78E-05	0.008374
Randall2019a	Control	528.8333	528.8333	528.8333	4.58483	0.965273	41.0663	68.26556
	Uraemic	551.875	551.875	551.875	4.733444	0.975732	49.25629	70.72847
	p	0.557495	0.557495	0.557495	0.505193	0.307658	0.560928	0.669956
Randall2019b	Control	599.5	599.5	599.5	4.896129	0.981281	62.42806	76.51418
	Uraemic	621.6667	621.6667	621.6667	4.98459	0.983421	66.72698	80.73599
	p	0.73058	0.73058	0.73058	0.684303	0.71	0.787519	0.592132
Randall2021a	Control	105.6667	106.95	106.5639	3.507143	0.925483	15.73231	18.2353
	Uraemic	111.6667	113.2949	113.3049	3.589526	0.936636	18.21413	19.62634
	p	0.834565	0.830248	0.81921	0.766181	0.596245	0.498627	0.771918
Randall2021b	Control	155.4444	157	156.407	4.205179	0.969409	33.97849	24.86759
	Uraemic	143.125	145.3438	144.4432	4.26122	0.975954	44.48003	23.59562
	p	0.374689	0.404173	0.387341	0.603385	0.082514	0.034534	0.53427

Table 17: Alpha diversity in meta-analysis datasets. The range of measures used including observed ASVs per sample, and the Chao1, ACE, Shannon, Simpson, Inverse Simpson and Fisher indices are listed. Means for individual groups are listed and significance calculated for between group differences using Student's t test with Welch's correction, in all samples between control and uraemic animals and between rats and mice; and then within each individual cohort between control and uraemic animals.

Cohort			Increased in uraemia	Decreased in uraemia
Al-Asmakh2020	**Order**		*Enterobacterales*	
			Corynebacteriales	
			Bifidobacteriales	
	Family		*Atopobiaceae*	
			Enterobacteriaceae	
			Bifidobacteriaceae	
			Aerococcaceae	
			Clostridiaceae	
	Genus		*Klebsiella*	
			Coriobacteriaceae UCG-002	
			Faecalibaculum	
			Aerococcus	
	Species:			
	Lactobacillus			10
	Enterococcus			4
	Klebsiella		4	
	Atopobiaeceae		3	
	Pseudomonas		5	
	Peptostreptococcus			1
	Atlantibaculum		1	
	Desulfovibrio		1	
	Bifidobacterium		1	
Kikuchi2017			None	None
Kikuchi2019	**Family**		*Peptostreptococcaceae*	*Lachnospiraceae*
	Genus		*Romboutsia*	*Lachnospiraceae NK4A136 group*
	Species:			
	Atlantibaculum			2
	Turicibacter			1
	Klebsiella			1
	Eschericia			1
	Clostridium sensu stricta			1
	Lactobacillus			1
	Peptostreptococcus		1	
	Bifidobacterium		1	
	Enterobacteriaceae		1	
	Clostridium		1	

Mishima2015	**Class**	*Actinobacteria*	
	Order	*Bifidobacteriales*	
		Erysipelotrichales	
	Family	*Bifidobacteriaceae*	
		Erysipelotrichaceae	
	Genus	*Bifidobacterium*	
		Dubosiella	
	Species:		
	Lactobacillus	11	
	Bifidobacterium	4	
	Dubosiella	8	
	Muribaculaceae	3	
	Parabacteroides	1	
Nanto-Hara2020	**Family**	*Prevotellaceae*	
	Genus	*Alloprevotella*	
	Species:		
	Muribaculaceae	15	9
	Alloprevotella	1	
	Lachnospiraceae group NK4A136	2	
	Bacteroides caecimuris		1
	Lachnoclostridium	1	
	Lactobacillus	3	
Randall2019a		None	None
Randall2019b	**Species:**		
	Lachnospiraceae group NK4A136	1	1
	Colidextribacter		1
Randall2021a		None	None
Randall2021b	**Species:**		
	Lachnospiraceae	3	
	Muribaculaceae	2	
	Clostridia		1
	Oscillobacter	1	
Vaziri2013	**Phylum**	*NC10*	*Verrucomicrobia*
		TM7	*SPAM*
		Chlorobi	
	Class	*Chthonomonadetes*	*Verrucomicrobiae*
		12-24	
		TM7-3	

		Ignavibacteria	
	Order	*Chthonomonadales*	*Lactobacillales*
		MIZ17	*Verrucomicrobiales*
		CW040	
		Ignavibacteriales	
	Family	*Chthonomonadaceae*	*Lactobacillaceae*
		Unclassified, o. MIZ17	*Verrucomicrobiaceae*
		F16	
		Peptostreptococcaceae	
		Ignavibacteriaceae	
	Genus	*Chthonomonas*	*Pseudanabaena*
		Unclassified, f. F16	*Unclassified, f. Planococcaceae*
		Unclassified, o. MIZ17	*Pediococcus*
		Bacteroides	*Prevotella*
		Peptostresptococcus	*Solibacillus*
		Unclassified, o. Bacillales	*Lactobacillus*
			Akkermansia
	Species:		
	Corynebacteria	1	2
	Chthonomonas	1	
	Bacteroides		2
	Parabacteroides		1
	Porphyromonas		1
	Prevotella		24
	Rikenellaceae	9	6
	YS2/4	3	
	Pseudanabaena		1
	Planococcus		1
	Staphylococcus		3
	Lactobacillus		89
	Pediococcus		3
	Streptococcus		3
	Turicibacter		2
	Clostridium	3	
	Blautia	2	
	Butyrivibrio		1
	Coprococcus	2	12
	Eubacterium		1

	Moryella	1	
	Roseburia	2	1
	Ruminococcus	17	1
	Lachnospiraceae	40	3
	Peptostreptococcus	1	
	Oscillospirar	1	
	Veillonella	1	
	MIZ17	1	
	Aquabacter		1
	Eschaericia	1	
	Shigella	2	
	Enterobacteriaceae	8	
	Allobaculum		1
	p-75-a5		1
	RF39	1	
	F16/17	2	
	Akkermansia		72
	CV106		1

Table 18: Bacterial taxa showing significant differences in abundance between control and uraemic samples at each taxonomic level within each cohort. All significantly differentially abundant taxa at an ANCOM cut-off of 0.7 are included; at species level these are aggregated at genus level.

Appendix 6: Metagenomic analysis of carbohydrate metabolism in animals fed fermentable fibre

The non-redundant gene catalogue from metagenomic sequencing described in chapter 5 was compared to the CAZy (Carbohydrate Active enZYmes) database to interrogate further the nature of the observed increases in carbohydrate metabolic pathways. The genes set was associated with 89 agglomerated categories, including:

- One auxiliary activity (AA) molecule family,

- Five carbohydrate binding (CBM) modules,

- Two carbohydrate esterase (CE) families

- 48 glycoside hydrolase (GH) families

- 26 glycosyltransferase (GT) families

- Five polysaccharide lyase (PL) families.

The auxiliary activity family (AA10) was increased in samples from CELL-treated animals (p=0.012 by Kruskal Wallis). This family includes a range of copper-dependent molecules with roles in cleaving complex polysaccharides including cellulose.

Similarly, two of the carbohydrate binding families (CBM6 and CBM73) which were increased in abundances in CELL-treated animals have described functions in binding long molecules such as cellulose and chitin.

Glycoside hydrolase molecules provide the vast bulk of cellular machinery for breaking down complex sugars. Of the 48 molecules in this class associated with the dataset, 21 were present in significantly increased abundances in FOS-treated animals compared to three in CELL-treated animals when assessed by two-way Kruskal-Wallis.

The 21 GH families increased in FOS-fed animals included a number of major families (GH3, GH4, GH13, GH15) with well-described roles in the reduction of complex polysaccharides. Enzymes from the GH13 family are the major GH family acting on the alpha-glucosidic bonds such as those joining the terminal glucose molecule onto FOS molecules (in association with GH15 enzymes which hydrolyse the non-reducing end residues of this metabolism). Conversely, GH3 is a major family acting on beta-glycosidic bonds such as those in the backbone of FOS molecules. The GH32 family has specific activity against fructans and inulins with a broad overlap for FOS fibre; a number of other families increased in FOS-fed animals (eg GH95, GH121 and GH127) are core parts of the metabolic machinery of genus *Bifidobacteria*, Figure 118, p. 415.

Of the three GH families increased in CELL-fed animals, at least one (GH94) has a specialist role in cellulose degradation; the two others included a carrageenase (GH82) and an alpha-galactosidase (GH27).

Ten of the 26 associated glycosyltransferase (GT) molecules were significantly over-represented in CELL-fed animals whilst 8 were over-represented in FOD-fed. GTs may fulfil both synthetic and catalytic functions, by molecules that transfer a carbohydrate residue from a donor molecule (often a nucleotide) to an acceptor: thus they may be involved in digestion or in synthesis of new molecules.

The GT families increased in CELL-fed were predominant synthetic, including those synthesising cellulose for extra-cellular transport (eg the GT2 family), and those involved in lipopolysaccharide (LPS) production: the GT8, GT9 and GT25 families. Conversely, a number of the GT families increased in FOS-fed animals had wider metabolic roles including the GT1 family (fulfilling a wide range of glucoryl transferase activities), and families involved in energy storage such as GT4, GT5, GT35 and GT51 which each contain enzymes involved in starch, glucan and glycogen storage.

To better understand these metabolic changes at the level of individual metabolic pathways, 237 KEGG modules were compared; 112 were differentially abundant according to diet by Kruskal-Wallis adjusted for multiple hypothesis testing, with 68 being increased in FOS-fed and 44 increased in CELL-fed animals.

Analysis of individual modules revealed extensive differences between FOS-fed and CELL-fed animals, consistent with a substantial shift in energy pathways and metabolites utilisation.

In FOS fed animals, pathways involved in extraction of simple sugars from complex carbohydrate fibres were significantly more abundant than in CELL-fed animals, including KEGG modules M00061 (D-glucuronate degradation), M00081 (pectin degradation) and

M00631 (D-galacturonate degradation); each consistent with an increase in bacterial metabolic machinery for degrading plant-based fibres.

There was a significant increase in the two pathways used for glucose reduction in some bacteria in preference to glycolysis: the Entner Doudoroff pathway (both its non-phosphorylative form, M00008; and the semi-phosphorylative pathway, M00633); and the fructose-6-phosphate division of the pentose phosphate pathway (M00007, which has been termed the 'bifid shunt', Figure 119 and Figure 120; p. 416 & 417), and subsequent PRPP synthesis pathway (M00005). By contrast, the reductive pentose phosphate cycle (M00166) was over-represented in CELL-fed animals. Taken together, these are suggestive of the increased abundance of simple sugars in the gut lumen for direct utilisation by bacteria with the correct metabolic pathways.

FOS-treated animals also showed an increase in metabolic pathways to use short chain fatty acids as an energy source, including the methylaspartate cycle (M00740) that produces glycoxylate from acetate, and the glycoxylate cycle that utilises glycoxylate for energy generation (M00012); and propanoyl-CoA metabolism that allows propionate to enter the Krebs cycle via conversion to methylmalonate and succinate (M00741).
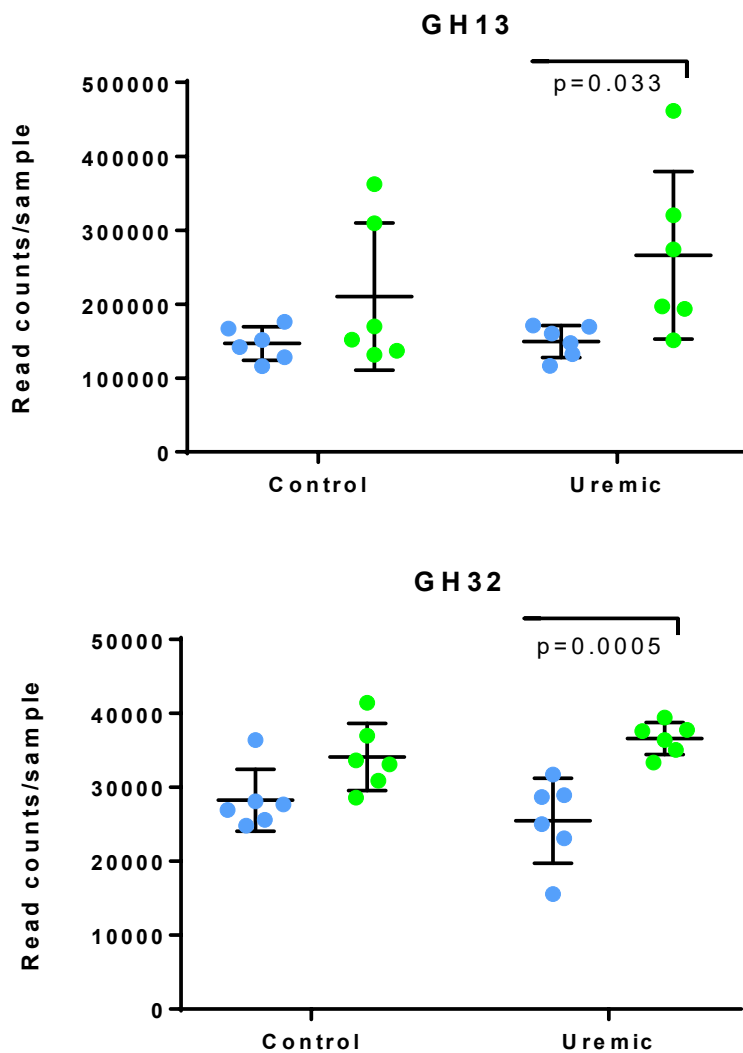
Figure 118: Count reads per sample of the glycosyl hydrolase 13 and 32 families. The GH13 is the major family acting on alpha-glucosidic bonds such as those linking the terminal glucose to the fructose residues in FOS fibres; the GH32 family acts specifically to degrade inulins and fructans. Significance is shown between FOS-fed (green) and CELL-fed (blue) animals within each intervention group (control or uraemic) using Sidak's post-test analysis following two-way ANOVA.
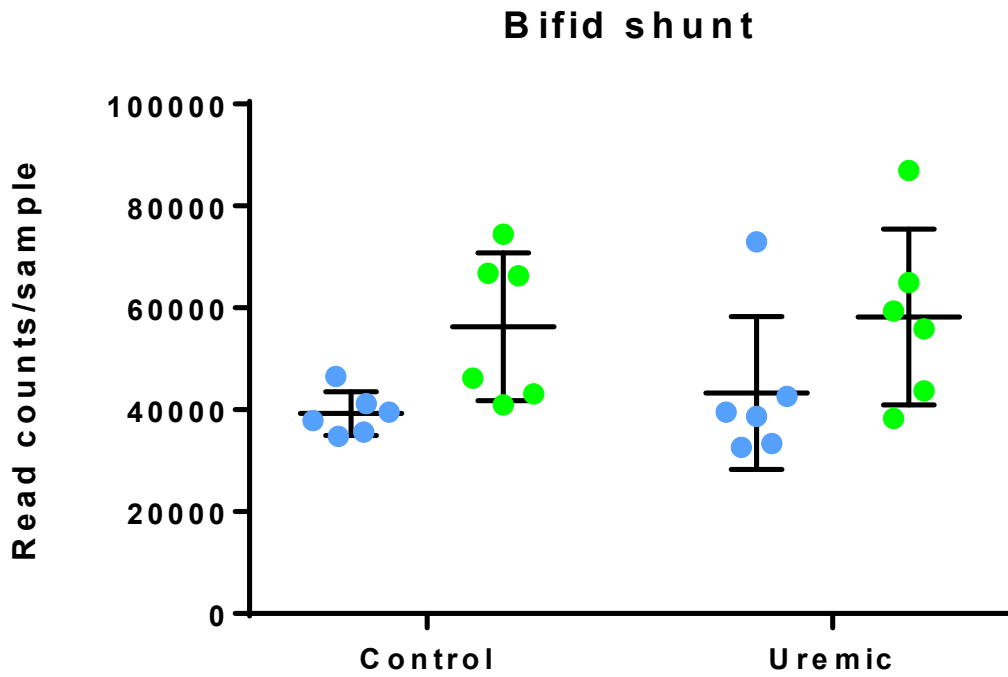
Figure 119: Read counts per sample for genes associated with the 'bifid shunt'; the fructose-6-phosphate division of the pentose phosphate pathway. Diet was significant (p=0.01) by two-way ANOVA. Blue, CELL diet; green, FOS diet.

Figure 120: The 'bifid shunt'. Taken from O'Callaghan and van Sinderen, 2016. [442] This pathway, unique to genus *Bifidobacterium*, allows these organisms to thrive in environments with high supply of carbohydrate oligomers, such as in the gut of prebiotic supplemented rats.